Model-based sizing of building energy systems with renewable sources

Thèse N° 9560

Présentée le 5 juillet 2019

à la Faculté des sciences et techniques de l'ingénieur
Groupe SCI STI FM
Programme doctoral en énergie

pour l'obtention du grade de Docteur ès Sciences

par

Paul Michael STADLER

Acceptée sur proposition du jury

Prof. D. Dujic, président du jury
Prof. F. Maréchal, directeur de thèse
Prof. N. Shah, rapporteur
Prof. M. Baldea, rapporteur
Dr J. Van Herle, rapporteur

2019

ÉCOLE POLYTECHNIQUE
FÉDÉRALE DE LAUSANNE

Acknowledgements

Un grand merci à mes collègues de bureau des groupes IPESE et GEM qui ont dus me supporter durant ces quatre dernières années, vous avez vraiment rendu cette période super agréable. Il est vrai qu'avec une bonne équipe, ça fait toujours beaucoup plus plaisir de se lever chaque matin pour aller au boulot!

Merci à tous ceux qui m'ont épaulé durant ces années et permis de conserver un bon équilibre de vie; les membres du DPS Vevey, particulièrement les sections N03 et J02 avec qui nous avons effectuées de nombreuses interventions au fil de ces années dont, occasionnellement, des vraiment comiques. Merci aux équipes de Châtel et du Pierrier à Clarens pour tous les bons moments que nous avons passés ensemble: sur les terrains de Fribourg, dans le bac à sable au bord du' et bien sûr, lors des quelques célébrations de victoires acharnées. Merci à mes vieux amies et amis de la Riviera (et maintenant d'ailleurs aussi) pour les nombreuses vacances, soirées et excursions tant chaleureuses que drôles. Vivez votre vie vinaigrette!

Bien sûr, je remercie toute ma famille, mes parents Susanne et Richard, ma sœur Sabine, mon frère Christian ainsi que mon oncle Wolf pour m'avoir soutenu durant tout ce temps.

Finalement, je désire remercier Francesca pour son soutien inébranlable, dans les meilleures moments comme dans les pires. De plus, je lui suis infiniment reconnaissant pour toute son aide autant qu'elle l'a fait pour la révision de cette thèse.

À quelque part, Mai 2019 P.S.

Abstract

The built environment currently represents the largest sector in terms of final energy consumption, both in Switzerland and the European Union. Most of the associated energy services, such as space heating and potable hot water preparation, are mainly satisfied by the combustion of fossil fuels, typically oil and natural gas. Hence, within the current context of national energy transition towards a sustainable and environment-friendly service provision, the building sector is facing a major challenge to integrate both efficient conversion technologies and additional renewable energy sources. Nevertheless, an increasing penetration of the latter is not a straightforward task; solar power, a typical resource available in urban areas, is indeed intrinsically volatile which renders a full exploitation of the generated electricity highly compelling. The implementation of advanced mathematical modelling methods during the phases of both design and operation represent a promising cornerstone to successfully reach the objectives targeted by the transition program.

Using a model-based approach, the following thesis therefore attempts in contributing to the latter challenge through three main targets. The first aims at the development of a holistic and modular modelling framework to optimally size and operate building energy systems. In order to provide multiple good trade-off system solutions to the various stakeholders, the proposed method relies on an epsilon-constraint multi-objective optimisation techniques and ad hoc defined key performance indicators. A systematic implementation of the thus developed framework finally allows the large-scale analysis of modern and efficient building energy systems, both in view of future market opportunities and national environmental targets.

The second topic focuses on the study of multi-building energy systems and analyses the potential benefits from involving multiple end-users during the sizing process. Through an extended system scope, potential synergies of neighbouring building types arise and hence, the initial modelling framework is further developed accordingly. Additional shared unit technologies, such as inter-day storage and heating networks become interesting elements for buildings interaction and therefore are also integrated in the modelling framework. Finally, the third target addresses the quantification of potential ancillary services performed by different energy system configurations to power network operators. Using a representative set of flexibility request profiles, the modelling framework is systematically solved to assess the associated temporal load shifting potential in comparison to standard electrical battery energy storage systems.

Acknowledgements

Résumé

L'environnement bâti représente actuellement le plus grand secteur en termes de consommation finale d'énergie, à la fois en Suisse et au sein de l'Union européenne. La majorité des services énergétiques domestiques fournis, tels que le chauffage de locaux et la production d'eau chaude sanitaire, sont en effet majoritairement satisfaits par la combustion de carburant fossile, principalement au travers de l'utilisation de chaudières à mazout et/ou au gaz naturel. Ainsi, en vue de l'actuelle transition énergétique qui vise un approvisionnement durable et écologique, le parc bâti doit faire face à des défis majeurs afin d'intégrer à la fois de nouvelles technologies de conversion efficace ainsi que davantage de ressources renouvelables. Néanmoins, augmenter la pénétration de ces dernières n'est pas n'est pas chose aisée. En effet, l'énergie solaire qui est une ressource renouvelable typiquement disponible en milieu urbain, est par nature intermittente, rendant ainsi l'utilisation complète de la production décentralisée difficile. L'application de méthodes de modélisation mathématiques avancées durant les phases de dimensionnement et d'opération représente toutefois un élément prometteur en vue des objectifs fixés par le programme de transition mise en place par la Confédération.

En utilisant une approche basée sur modèle, cette thèse espère contribuer à cette problématique par le biais de trois axes principaux. Le premier se concentre sur le développement d'un cadre de modélisation holistique et modulaire pour dimensionner et opérer de manière optimale des systèmes énergétiques de bâtiment. Afin de générer plusieurs bonnes solutions, la méthode proposée repose sur des techniques d'optimisation multi-objectives tout en intégrant des contraintes opérationnelles supplémentaires liées au réseau électrique. Une mise en œuvre systématique de ce cadre de modélisation permet enfin une analyse approfondie à grande échelle de l'impact des systèmes énergétiques modernes et efficaces, à la fois en vue des nouvelles opportunités de marché et des objectifs environnementaux nationaux.

Le deuxième axe porte sur l'étude de systèmes énergétiques multi-bâtiments en y intégrant les avantages engendrés par l'implication de multiples utilisateurs finaux au cours des phases de dimensionnement et d'opération. Au travers de cette extension des frontières du système énergétique, des synergies potentielles dues aux différents profils de demandes émergent. Ainsi, le cadre de modélisation initial est étendu en conséquence, tout en intégrant des systèmes centralisés de stockage saisonnier et des réseaux de distribution de chaleur locaux.

Enfin, le troisième sujet traite de la quantification du potentiel de services système fournis par différentes configurations de systèmes énergétiques. En vue des demandes de flexibilité typiquement requises de la part d'opérateurs de réseaux de distribution, le cadre de modélisation est implémenté de manière systématique afin d'évaluer le potentiel de déplacement de charge

associé, puis ce dernier est comparé à des technologies de stockages électriques standards.

Mots-clefs : Programmation linéaire en nombres entiers, Structure de modélisation, Système énergétique du bâtiment, Énergie renouvelable, Production décentralisée, Optimisation multi-objective

Contents

Contents

List of Figures

List of Figures

List of Tables

Nomenclature

Acronyms

BES	Building energy system
BESS	Battery energy storage system
DSM	Demand side management
ERA	Energy reference area
KPI	Key perfromance indicator
LMT	Logarithmic mean temperature
MF	Modelling framework
MILP	Mixed integer linear programming
MPC	Model predictive control
NEB	Net energy balance
P2G	Power-to-gas
RPC	Rule-based control
TFC	Total final consumption
TPES	Total primary energy supply
ZEB	Zero energy building

► Acronyms (unit technologies)

AHP	Air-souce heat pump
BAT	Stationary battery
BOI	Boiler
CHP	Combined heat and power
ELH	Electrical heater
HHS	Hydronic heating system
HST	Heat storage tank
HWT	Hot water tank
LPEM	Low temperature proton exchange membrane fuel cell
PVA	Photovoltaic array
REN	Buildung renovation
SOFC	Solid oxide fuel cell
STC	Solar thermal collector
VAC	Ventilation and air-conditioning

▶ Acronyms (energy services)

EL   Electricity
HW   Hot water
SC   Space cooling
SH   Space heating

▶ Acronyms (data clustering)

CDD   Cooling degree days
DRY   Design reference year
GHI   Global horizontal irradiance
HDD   Heating degree days
LDC   Load duration curve

▶ Acronyms (key performance indicators)

BSE   Building storage equivalence
GES   Grid energy storage
GF   Generation fraction
GM   Grid multiple
OPP   One percent peak
SC   Self-consumption
SS   Self-sufficiency

Greek Symbols (MILP parameters)

ϵ	Conversion unit first-law efficiency	[-]
η	Conversion unit second-law efficiency	[-]
λ	Conversion unit part-load limits	[-]
σ	Storage unit self-discharge rate	[-]
γ	Storage unit charging/discharge efficiency	[-]
κ	Storage unit minimum loss factor	[-]
ϕ	Building uncontrollable heat gains	[-]
Δ	Energy tariff variations	[-]

Greek Symbols (MILP variables)

δ	Conversion unit start-up (binary)	[-]
Δ	Storage unit inter-day charging/discharge	[kW]

Roman Symbols (MILP parameters)

$\dot{e}$	Reference chemical power flow	[kW]
$\dot{h}$	Reference electric power flow	[kW]
$\dot{m}$	Reference mass flow	[kg/s]
$\dot{q}$	Reference thermal power flow	[kW]
c_p	Specific heat capacity	[kJ/°C kg]
A	Area	[m^2]
C	Building thermal capacity	[kWh/°C]

D	Diameter	[m]
d	State occurence	[-]
F_{BM}	Bare module factor	[-]
i	Interest rate	[-]
inv_1	Fixed investment cost	[CHF]
inv_2	Variable investment cost	[CHF/*]
L	Unit lifetime	[yr]
N	Project lifetime	[yr]
n^{min}	Minimum unit operating time	[-]
n^{start}	Maximum unit daily start-up number	[-]
op	Energy tariff	[kWh/CHF]
SOC	State-of-charge	[kWh]
T	Temperature	[°C]
U	Thermal transfer coefficient	[kW/°C]
V	Volume	[m^3]

Roman symbols (MILP variables)

$\dot{E}_{grid}$	Chemical power flow from/to network	[kW]
$\dot{H}_{grid}$	Electtic power flow from/to network	[kW]
$\dot{m}$	Mass flow	[kg/s]
$\dot{Q}$	Thermal power flow	[kW]
$\dot{R}$	Cascaded heat	[kW]
C	Costs	[*]
F	Unit size	[*]
f	Conversion unit load or storage unit state-of-charge	[*]
f^s	Storage unit inter-day state-of-charge	[kWh]
T	Temperature	[°C]
Y	Unit activation (binary)	[-]
y	Conversion unit on-off state (binary)	[-]

Superscripts (modelling framework)

+/-	Incoming/outgoing flow	
el/ng	Electricity/natural gas	(costs)
ext	external	(ambient)
h/c	Heating/cooling	(building)
in/out	inlet/outlet thermal stream s conditions	
max/min	maximum/minimum	
op/cp/en	Operating/capital/environmental	(costs)
s/r	Supply/return flow conditions	(building)

Subscripts (modelling framework)

0	Nominal conditions (hydronic heating system)	
b	Building	(introduced in Chapter 3)

List of Tables

Introduction

Chapter overview

- An overview of the national energy supply and use in the building sector
- Major challenges of integrating renewable-based energy systems
- Thesis novelties and structure

In 2017, the total primary energy supply of Switzerland was evaluated at 1080 PJ [1]. Hence, each inhabitant consumed on average 97 kWh of energy per day, which approximately corresponds to the amount contained in 10 litres of diesel fuel[1]. The latter are used to satisfy our well-established comfort standards through different **energy services** such as lighting our homes, commuting to our workplace or heating our potable water. While around 24.5% of this total primary energy supply (TPES) is satisfied by renewable energy resources, mainly through hydro-power and waste incineration[2], the largest share is met by the conversion of nuclear (19.7%) and fossil-based fuels, primarily natural gas (11.6%) and oil derivatives (41.2%). Due to the lack of any indigenous production, these energy vectors are entirely imported, hence rendering the associated expenses as well as the security of supply highly dependent on the geopolitical situation in exporting regions. In addition, the conversion of fossil energy sources to their final use generates potent greenhouse gases, generally released to the environment and thus, is extensively contributing to human caused climate change [3].

In order to understand the application of these non-sustainable energy sources and to identify potential alternatives to the current state, a further break-down of the total final consumption (TFC), i.e. the TPES after deducting conversion losses, is illustrated in Figure 1. It highlights the largest consumption shares of the three major energy service demands in the country. The **building infrastructure** represents the highest energy consumption sector, closely followed by mobility and industrial processes; its share of the inland TFC amounts to 40% among which 87% are solely dedicated towards space heating and domestic hot water preparation [4]. The latter thermal energy services are indeed predominately satisfied through the use of heating oil (43%) and natural gas (26%) as reflected by the national primary energy consumption. Similar values can be observed within the European Union where the built environment is

---

[1]Based on the density and lower heating values reported in [1]

[2]Regarding the definition of renewable energy sources considered by the Swiss federal office for energy [2]

responsible for over 40% of the member states TFC [5]. As universally recognized, in view of keeping global temperature increase below a 2°C threshold relative to pre-industrial climate conditions, drastic reductions in greenhouse gas emissions are required in the following decades [3]. Given its significant TFC share, the built environment thus represents a crucial sector within the context of sustainable development.

TPES : 1080 PJ   TFC : 850 PJ

†Waste, Biomass, solar and wind
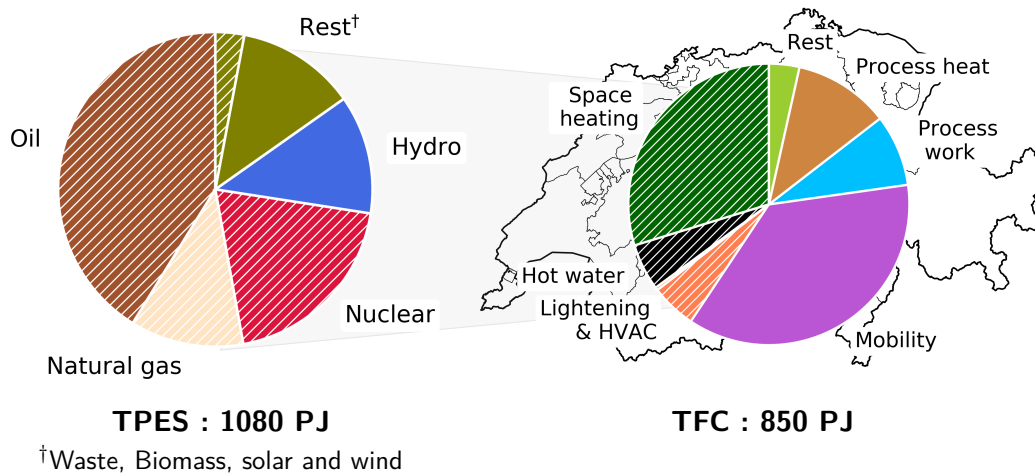
Figure 1 – National TPES (imported energy vectors are denoted through hashed surfaces) and TFC (building energy services are highlighted through hashed surfaces), data from [1, 4]

A roadmap to sustainable energy use

Although having slightly dropped over the last decade, the current national energy demand (TPES) remains far from an environmental friendly consumption level. In regard to the aforementioned challenges, the board of Swiss Federal Institutes of Technology relied on the *2000 Watt society* concept, introduced by Kesselring and Winter [6], to formulate their long-term sustainability strategy until the horizon of the following century [7]. Indeed, the vision of the *2000 Watt society* is defined through two main objectives; the first promotes a TPES threshold of 63 GJ per capita and year, which translates into an average primary power demand of 2 kW per capita. As second target, the concept proposes a maximum emission threshold of 1 tCO_2-eq. per capita and year which currently corresponds to the amount emitted by a long-haul return flight between Zürich and Southeast Asia [8]. Beyond addressing the environmental impact related to the current energy use, the *2000 Watt society* also thrives towards an equitable distribution of natural (energy) resources among developed and developing countries. While in Africa and Asia[3], the current TPES per capita is around 2 times lower than the proposed threshold, it still remains twice as high in Switzerland and the European Union [9], highlighting the need for additional efforts in the years to come.

---

[3]Excluding China

Although not explicitly adopting the *2000 Watt society* vision within their long-term energy strategies, both Switzerland [10] and the European Union [11] have however formulated clear energy supply targets by the dawn of 2050 while considering intermediate milestones defined by the *2000 Watt society* roadmap. Consequently, they committed themselves to reduce primary energy use by over 40% with respect to their consumption level of the early 2000[4]. In order to reach the latter threshold, national governments therefore promote the development of additional renewable generation capacities through economic incentives while imposing increasingly stricter efficiency requirements across all energy service sectors, ranging from mobility to the built infrastructure.

In regard to the building sector, several investment steps have indeed already been identified to steer towards the proposed consumption target; for once the gradual replacement of current, widespread conversion units (i.e. oil and natural gas boilers) through efficient technologies such as heat pumps and combined heat and power (CHP) devices to increase the system efficiency [12]. Moreover, a reduction in space heating and cooling demands can be achieved though stricter consumption standards and social behaviour awareness [13]. Finally an increasing penetration of renewable energy sources within the built environment further decreases the need of novel centralized power generation capacities to compensate both the gradual decommissioning of fossil-fuelled power plants and the increasing shift towards electrical energy vectors to satisfy thermal service demands.

The integration challenge

Among the major challenges encountered by the increasing integration of renewable energy sources within the built environment while simultaneously electrifying thermal energy services is the temporal mismatch between production and consumption. Indeed, the inherent volatile and uncontrollable behaviour of green energy resources such as solar and wind renders the challenge of using the locally produced electricity highly compelling. Excess generation is typically managed by the power network operators which are responsible for balancing the grid at all times throughout the year. In regard to the cyclic trends of both generation potential and service demands, the latter distortion problem can be analysed at two different temporal scales: on a daily and seasonal basis.

In the first case, renewable power is indeed predominantly produced during day time while consumption peaks typically occur in the morning and evening period. With the increasing penetration of renewable capacity, a distribution and transmission power networks start experiencing strong generation fluctuations. The phenomenon has been extensively observed in California (United States) where strong subsidies and feed-in tariffs have encouraged the installation of renewable energy resources across the state, both in the utility and private sector [14]. Figure 2 illustrates the net load curve of a typical spring day observed by the state independent transmission system operator (ISO). The represented profile has been denoted as

---

[4]Switzerland: 43% (2000), European Union: 41% (2005)

the duck-curve due to its typical shape; in the morning, with the rise in photovoltaic generation the network operator experiences a fast ramp down until peaking in the early afternoon. As the sun sets and the evening demand grows, the trend is reversed. This rapid loss in renewable generation is particularly impacting since network operators increasingly require larger and faster dispatching capacities (e.g. heavy duty gas turbines) to compensate for sudden loss (or gain) in renewable generation and maintain the grid balanced.
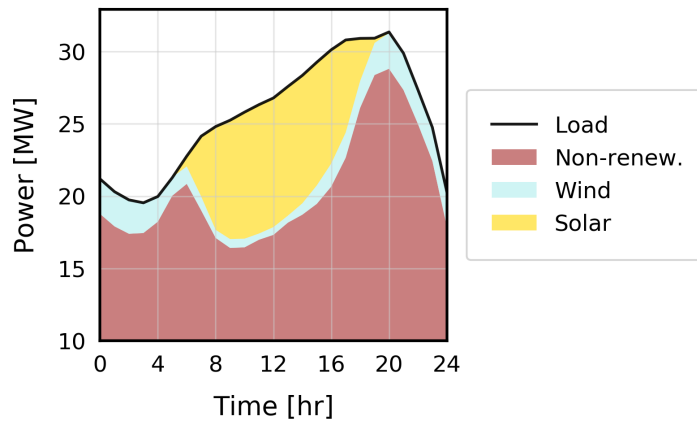
Figure 2 – Load curve and generation per source of the California ISO on May 1st 2017, data from [15]

Similar phenomena have also been observed in Europe, especially in Germany where the electricity production from wind and solar power reached peak generation levels of 40% and 42.7% respectively [16]. Hence, with the aim of maintaining the network balanced, national transimission system operators (TSO) engendered a significant generation curtailments of base load units, both from nuclear and coal power plants (Figure 3). However, since the latter technologies have solely limited part-load capabilities, typically 40-50% of their nominal output for existing plants [17], remaining excess production needed to be absorbed through different means such as international trading.

Finally, from a seasonal view point, the consecutive occurrence of daily negative electricity balances[5] however highlights the need of additional, long-term storage capacities. Although not observed yet at the national level, this behaviour is typically observed for net zero energy buildings (ZEB)[6]. In the summer, daily electricity exports exceed imports due to lower service demands while during winter, with the increase in thermal energy requirements, the phenomena is inverted. A balancing entity, currently performed by power network operators, is consequently responsible of managing long-term variations in the net electricity demand. In regard to the integrated market structure of the European continent, the need for seasonal storage remains currently marginal, excess generation being sold to neighbouring states with lower renewable production capacities [16]. Nevertheless, with the further rise in renewable

---

[5]In view of the following convention, negative values represent exiting flows from the system
[6]Buildings which fully satisfy their own energy needs on an annual basis [19]

4
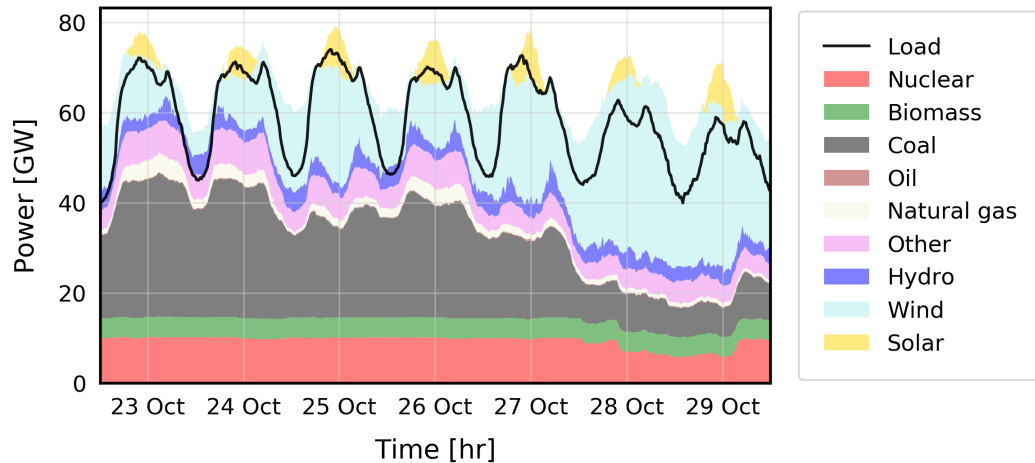
Figure 3 – Load and generation curves of Germany on an October week in 2017, data from [18]

power penetration at the continental level, additional technological solutions need to be explored in order to face the increasing instabilities [17].

Matching load and generation

Multiple technological solutions have been proposed to face the aforementioned integration challenges: the expansion of conventional storage capacities through stationary batteries [20] or pumped hydro [21], the use of multi-energy vector systems such as power-to-gas (P2G) [22] and demand side management (DSM) [23]. The latter is particularly interesting due to its relatively low investment costs - mainly composed of the local controller and instrumentation hardware - as well as easy implementation. Indeed, with DSM, electricity consumers are financially incentivized in shifting dispatchable loads to match centralized generation, the loss in operational efficiency being subsequently compensated through an economic retribution. However, in order to properly apply DSM, local controllers need to rely on advanced control techniques capable of performing the latter cost-benefit analysis and, react accordingly while still satisfying the required energy services.

Among the different options, model predictive control (MPC) represents a potential candidate; the control approach relies on mathematical programming techniques and disturbance prediction methods to define the different system control variables for a given forecasting horizon [24]. In close loop operation, this process is then repeated at each discrete time step in order to alter the input strategy according to inherent prediction and modelling errors. In addition of easily dealing with highly multi-variable systems, the use of MPC allows for an efficient incorporation of novel operative constraints *a-posteriori* by modifying the problem formulation. In view of the latter benefits and the growing complexity of modern building energy systems, predictive control applications have been heavily investigated within the field of building operation, typically for climate control [25, 26] and demand response [27].

In addition to using smart control strategies, the proper design of building energy systems remains a crucial element in the successful penetration of renewable energy sources within the built environment. Indeed, control performances are highly dependent on the associated system capacity, i.e. configuration, to react to external disturbances and consequently, should be defined simultaneously [28].

Designing smart building energy systems

Building energy systems (BES) are commonly sized on basis of national standards and norms. In addition of providing general dimensioning guidelines, the latter also serve as justification and comparison references for meeting the defined performance requirements in terms of energy consumption and environmental impact. In Switzerland, the society of engineers and architects (SIA) establishes the latter support literature; it relies on expert commissions involving different stakeholders from the construction sector and international standards (CEN, ISO) to develop and regularly update technical reports. Following the latter dimensioning guidelines, the primary heating unit size (e.g. a natural gas or wood pellet boiler) is defined according to the peak load in thermal energy service demands: space heating and domestic hot water preparation [29]. The former are, in the case of a novel or refurbished building, estimated using a component-based model of the dwelling envelope [30] or, in the case of an existing structure, on hand of the energy signature model [31]. On the other hand side, defining domestic hot water demand profiles represents a more challenging task since consumption strongly depends on the occupant behaviour; nevertheless, in case of lacking historical withdrawal measurements, standard demand profiles are implemented [32].

Thereafter, the annual environmental and economic performances of the BES are evaluated using a static, monthly [30] or temperature bins [33], modelling approach. In the case of complex building types which require additional energy services, space cooling or an active humidity control, a dynamic hourly simulation model is recommended in order to provide a reliable consumption assessment, particularly during periods reflecting both heating to cooling needs [32, 34]. Although the aforementioned sizing and operation models provided a reliable conception framework for simple BES configurations, no specific recommendations are stated regarding the sizing of bivalent systems which include a primary (e.g. an air-water heat pump) and an auxiliary conversion unit (e.g. resistive electrical heater). Similarly, no particular guidelines are mentioned in the case of BES comprising multiple primary conversion technologies (e.g. an air-water heat pump and a combined heat-and-power engine), both in view of the sizing and operation procedure.

From the renewable resource perspective, a general sizing guideline is still lacking too. Although recent norms [33] have attempted in evaluating the useful heat produced from solar thermal collectors (STC), a comprehensive and detailed **model-based** assessment method has not been proposed yet. Similarly, the economic benefits resulting from photovoltaic arrays (PVA) are still assessed through in-house support tools developed by the system manufacturer

or mandated installation company. Hence, due to the lack of a general dimensioning framework, "optimal" PVA size recommendations substantially differ between sources, ranging from an annual electricity balance [35] or a constant self-consumption[7] assumption [36] to a more detailed electricity demand profile assessment approach [37]. Nevertheless, the integration of distributed generation strongly vary with the installed capacity while impacting the respective stakeholders in a different manner.

Indeed, in order to illustrate the latter behaviour, Figure 4 depicts the different electricity *source* shares with the rise in photovoltaic array size per energy reference area[8] (ERA): 1. the distributed generation directly used on-site to satisfy different energy services (*self-sufficiency*, in green), 2. the distributed generation surplus exported to a power network operator, stored, and re-imported during generation deficit periods (*seasonal storage*, in blue) and finally, 3. the remaining net import needs from centralized (off-site) power plants (*net import*, in grey). Hence, for smaller PVA unit sizes, most on-site electricity production is self-consumed while for larger system capacities, the power network faces the increasing challenge of storing excess electricity generation throughout the year. Represented through the dotted and continuous line types, the round-trip efficiency associated to the *seasonal storage* technology considered has an additional impact on the remaining electricity requirements from external sources. Obviously, the optimal installed capacity of distributed generation is influenced by a multitude of parameters, among which the available investment capital, the different network tariffs and the energy service profiles. As mentioned previously, smart control techniques might further improve the latter integration by shifting controllable loads towards high production periods. Consequently, in light of the latter state of the art, a comprehensive sizing support tools comprising all energy services and renewable resource availabilities is still missing today and should be addressed to optimally integrate efficient BES.
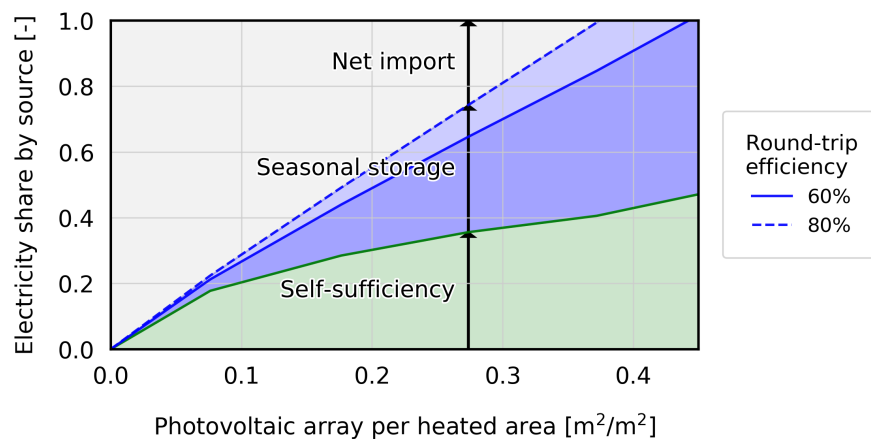
Figure 4 – Conceptual evolution of electricity provision shares in function of specific PVA size and different seasonal storage round-trip efficiencies

---

[7]Share of distributed generation consumed on-site

[8]The energy reference area (ERA) denotes the total floor area of the building associated to the different energy services

Contributions and structure

In view of the aforementioned environmental and technical issues related to national energy transitions and the key role assumed by the built environment, this thesis attempts to contribute to the cost-optimal integration of efficient and renewable-based building energy systems (BES). Four major research questions are stated and consequently addressed through the use of mathematical programming models and detailed in the following chapters:

- **Chapter 1: Optimal sizing of building energy systems**

  1st Research question: *" How does the integration of distributed energy sources vary with the system characteristics? "*

  A comprehensive building energy system modelling framework (MF) is presented including conventional and renewable-based conversion devices as well as typical storage technologies. The models are formulated using a mixed integer linear programming (MILP) technique in order to describe both their continuous and discrete behaviour. In addition, a temporal data reduction algorithm is developed in order to determine a set of representative demand and resource days, thus limiting the computational effort associated to subsequent the optimization step. Indeed, in view of the applied objective functions and system characteristics, both the optimal size and operation of each unit technology are provided to meet the user energy service requirements. Finally, a second, modified problem formulation is defined in order to describe the system behaviour when considering a non-optimal, rule-based control method. The MF is demonstrated through different case studies varying in affectation, construction periods and floor area.

- **Chapter 2: National impact of optimal building energy system designs**

  2nd Research question: *" How does the deployment of optimal building energy systems impact the national energy use? "*

  In this chapter, a novel systematic approach is presented to assess the integration of efficient and renewable-based building energy systems at national level. In regard to the latter scope, an additional spatial data clustering method is developed and applied, based on the temporal data reduction algorithm presented in Chapter 1. After defining the different BES configurations by using the aforementioned MF, the resulting BES are applied as input parameters in a second multi-objective optimization problem in view of defining optimal combinations. This systematic approach indeed provides the benefit of generating not a single but multiple good solutions for the different stakeholders involved in large scale energy system planning. The method is finally validated for the case study of Switzerland, using both the national building stock register (*RegBL* [38]) and design reference years (DRY) of indigenous weather stations as additional input parameters.

- **Chapter 3: Multi-building energy system sizing**

3rd Research question: *" Should building energy systems be sized considering their local neighbourhood and to which extent can smart grids improve the integration of distributed energy sources? "*

This chapter presents an extension to the MF detailed in Chapter 1 with the aim of analysing multi-building systems. An additional data clustering process is proposed to decrease the spatial scope of small and medium scale districts and thus, identify typical dwellings types representing the different smart grid end-users. The multi-building modelling framework is illustrated and consequently compared to the initial problem formulation through different case studies located in western Switzerland, varying both in size and density.

- **Chapter 4: Electrical flexibility of building energy system**

4th Research question: *" To which extent can building energy systems provide any ancillary services to power network stakeholders and at which additional costs? "*

A novel equivalent battery storage system approach is proposed to estimate the load shifting potential of integrated building energy systems. The definition relies on different electrical load variations between flexible and a base operating strategy, subsequently computing the associated power supply (and respectively demand) of an equivalent storage system (ESS) performing the similar deviations from the base case. Each BES load profile is defined through the initial MF (Chapter 1) and accounts for all energy service requirements. In order to generate the flexible BES load profiles, representative electricity tariffs are determined for each representative operating periods by using a *k-medoids* clustering technique. The resulting ESS performances are analysed on basis of general storage system characteristics: the average energy and power capacities. A validation is carried out by applying the proposed algorithm on previously assessed BES configurations, both at the building (Chapter 1) and micro-grid (Chapter 3) level.

1 Modelling and optimization of buildings energy systems

> **Chapter overview**
>
> - Holistic building energy system modelling framework
> - Multi-objective optimization approach
> - Grid oriented solution generation
>
> This chapter is an improved and extended version of Stadler et al. [39].

1.1 State of the Art

In view of facilitating the implementation of national performance requirements, several commercial support software have been developed (e.g. TIMES [40], DER-CAM [41], EnergyPlus [42], Polysun [43]), addressing different aspect of the building energy system (BES) design process. While detailed modelling frameworks are solely dedicated towards simulation, optimal system sizing tools tend to apply simplistic model formulations and generate unrealistic solutions as pointed out by Merkel et al. [40]. Consequently, researchers lean towards developing novel approaches [44] or improving existing solutions through additional features, typically optimization routines [40, 45] in order to tackle the considered gaps in literature.

Regarding the growing interest in providing efficient design support tools to practitioners, the issue of optimal BES sizing and operation has indeed been extensively addressed over the last years. In particular, Weber et al. [46] presented a *two-level* multi-objective optimisation approach to size a polygeneration energy system for large buildings, minimizing both the total annualized cost and environmental impact of the considered system. The framework included a solid-oxide fuel cell (SOFC) cogeneration device, heat pumps, absorption-chillers and thermal storage tanks. A case study on an office dwelling validated the developed algorithm while highlighting the role of distributed energy systems in decreasing the environmental impact of energy services. Using a similar solving strategy, the authors in [47–49] extended

the latter method by incorporating additional technologies such as natural gas boilers and ground-source heat pumps while integrating further operational constraints. Fazlollahi et al. [47] introduced the use of local biomass resources within the context of larger, urban scale energy system planning. The authors mainly focused on the comparison between different solving strategies for multi-objective optimization problems by using a simplified case study, aggregating district energy services within a single location (i.e. building). On the other hand, rather focusing on electrical network interactions, Menon et al. [48] applied minimum duration constraints on CHP devices in addition of a linearised formulation of the local power flow problem.

Fux et al. [49] further implemented solar thermal collectors and combined thermal storage tanks, hence clearly differentiating both flexible thermal energy services: space heating and domestic hot water preparation. The proposed algorithm mainly focused on remote, stand-alone (i.e. without any grid connections) dwellings. After defining the different designs, the authors finally compared their system performances when being operating using model predictive control (MPC) and rule-based control (RBC). Lately, Evins [50] presented a novel approach based on the *energy hub* concept [51], incorporating space constraints in view of the available technical room size while minimizing the system operational CO_2 equivalent emission. The authors highlighted the importance of applying a lower carbon credit for electricity exports than for imports in order to promote self-consumption and avoid oversizing distributed generation capacities.

In the case of *direct* solving strategy, MF typically implement MILP techniques in order to simultaneously solve the optimal BES configuration and schedule. The following method has indeed been proven particularly suited for the considered field [52], in addition of providing the advantage of applying powerful, deterministic solving algorithms (e.g. branch-and-bound). The use of mixed integer non-linear programming (MINLP) remains a non-trivial task as discussed by Grossmann [53]; indeed, while improving the model precision, the latter formulation reflects a poor robustness due to the initial point issue when solving each relaxed sub-problem. Within the latter context, Ashouri et al. [54] proposed a modular energy system framework to minimize the total annualized system expenses for large commercial buildings. Their investigations showed the ability of the defined problem formulation to cope with multiple system constraints while remaining tractable. The authors subsequently presented an extended, robust formulation to the initial problem in order to include uncertainties of given boundary conditions [55]. Based on a similar procedure, Steen et al. [56] introduced a multi-layer thermal storage model in order to improve the self-discharging losses estimation of thermal storage units and utility integration. Recently, Schütz et al. [44, 57] independently suggested two additional modelling formulations to analyse the impact (1) of discrete unit sizes and variable energy tariffs, while on the other hand side, (2) of setting the dwelling insulation as decision variable on the optimal BES configuration.

Regarding the provision of flexible energy services, two main approaches are identified; either by using *fixed*, pre-defined demand profiles [46, 47, 50, 56, 57] or setting thermal requirements

as decision *variables* [44, 49, 54, 58, 59]. In the latter case, the demands are defined through the implementation of additional models, namely the dwelling envelope and domestic hot water tanks. Consequently, thermal energy service time series are replaced by the required input profiles such as the ambient temperature, occupancy or solar irradiation. Furthermore, [58, 59] implemented a *discrete model* to represent the dynamic operating conditions of the hydronic heating system (i.e. supply temperature) while in [44, 49, 54] a constant supply temperature throughout the year is assumed.

Finally, in order to limit computation time, most studies commonly rely on a finite set of independent, *representative periods* with an hourly resolution and therefore reducing the problem size drastically [44, 46–48, 50, 57, 59]. Within the latter studies, several [44, 48, 57, 59] further applied data classification techniques to define the typical operating conditions arising over the system lifetime. Regarding the latter temporal decomposition, the thus generated optimal scheduling strategies can be considered as a building controller applying MPC with a daily time horizon and perfect disturbances (i.e. input time series) predictions. Table 1.1 summarizes the different highlights, identified and discussed throughout the current literature review.

Table 1.1 – Review of studies on building energy system optimization

	Time steps	Solving strategy	Multi-objective	Demand side management[a]	HHS model[d]	Conversion options[b]	Renewable options[c]
Weber et al. [46]	12 × 24	bi-level	✓	HS	-	HP, CHP	-
Fazlollahi et al. [47]	13 × 1	bi-level	✓	-	-	HP, CHP	PVA
Menon et al. [48]	8 × 24	bi-level	✓	HS	-	HP, CHP	-
Fazlollahi et al. [58]	8 × 24	simult.	×	SHS	1P	HP	STC
Marnay et al. [41]	24 × 24	simult.	×	HS, ES	-	CHP, VAC	PVA, STC
Ashouri et al. [54]	1 × 8760	simult.	×	HS, ES, SHS	FT	HP, CHP, VAC	PVA, STC
Fux et al. [49]	1 × 8760[‡]	bi-level	✓	HS, ES, SHS	FT	CHP	PVA, STC
Wakui and Yokoyama [60]	5 × 24	bi-level	×	HS, ES	-	CHP	-
Rager [59]	7 × 24	simult.	×	HS	1P	HP, CHP	STC
Schütz et al. [44]	12 × 24	simult.	✓	HS, ES, SHS	FT	HP, CHP	PVA, STC
Schütz et al. [57]	5 × 24	bi-level	×	HS, ES	-	HP, CHP	PVA, STC
Evins [50]	3 × 168	bi-level	✓	HS, ES	-	HP, CHP, VAC	PVA, STC
Steen et al. [56]	24 × 24	simult.	×	HS, ES	-	HP, CHP, VAC	PVA, STC
Kayo and Ooka [61]	3 × 24	simult.	×	-	-	HP, CHP, VAC	PVA
Lauinger et al. [62]	1 × 8760	simult.	✓	HS, ES, SHS	FT	HP, CHP	PVA, STC
Wu et al. [63]	1 × 8760	simult.	✓	HS	-	HP, CHP	PVA, STC

[a] HS: heat storage, HWS: hot water, SHS: space heating, ES: electrical storage
[b] CHP: combined heat and power, HP: Air/water source heat pump, VAC: chiller
[c] PV: photovoltaics, ST: solar thermal, WT: wind turbine
[d] FT: fixed temperature, 1P: Single set-point
[‡] The operation has been defined on basis of a receeding horizon control comprising a horizon of 3 days

1.2 Contributions

The following chapter presents an holistic approach to optimally design and operate BES within the context of integrating distributed and renewable energy sources. Although the previously presented studies have successfully targeted multiple challenges within the field of urban energy system sizing, the proposed methods are rather problem-oriented and thus solely partially succeed to answer the considered open issue. To this end, a comprehensive modelling framework is constructed, relying on MILP techniques and a direct solving strategy. The thus defined optimization problem is subsequently implemented in a *systematic* manner to generate different system designs and provide interesting trade-off solutions to the various stakeholders on the basis of specific performance indicators. Different case studies of buildings varying in size, construction period and use are finally applied to validate the proposed method and provide an preliminary answer to the tackled challenge.

Hence this chapter aims at expanding the field state-of-the-art through the following main contributions:

- the development of a systematic BES sizing method considering a comprehensive set of conversion and storage technologies. This problem formulation differs from one in the current literature by including 1) the heat cascade formulation [64] in order to efficiently manage discrete temperature levels associated to both units and energy service demands. 2) In addition, the model accounts for all flexible thermal service demands by modelling the building envelope and separating hot water requirements from space heating needs. 3) Finally, within the modelling context of 1), a discrete energy signature model is applied to describe the dwelling thermal distribution system.

- the definition of an additional problem formulation based on the initial MF to simulate and subsequently, analyse the potential benefit of optimal predictive control methods (e.g. MPC) over standard set-point control (e.g. RBC) techniques.

- the assessment of novel performance indicators to represent the advantage of optimal sizing and predictive control techniques in perspective of both the end-user and power network operator.

The following section (Section 1.3) thus presents the developed BES sizing algorithm, starting with a general overview of the three main steps composing it. Subsequently, these process stages are detailed in the associated subsections: the input data assessment in Section 1.3.1, the different unit models included and framework structure in Section 1.3.2 and the performance indicator and solving strategy in Section 1.3.2. Results generated from the implemented case studies are illustrated and discussed in Section 1.4. Finally, Section 1.5 provides concluding remarks on the presented method and potential future developments.

1.3 Sizing algorithm

This chapter presents the proposed approach to optimally size BES while integrating renewable-based and grid-aware solutions. Figure 1.1 illustrates the three major process steps included in the latter and described throughout the following sections.
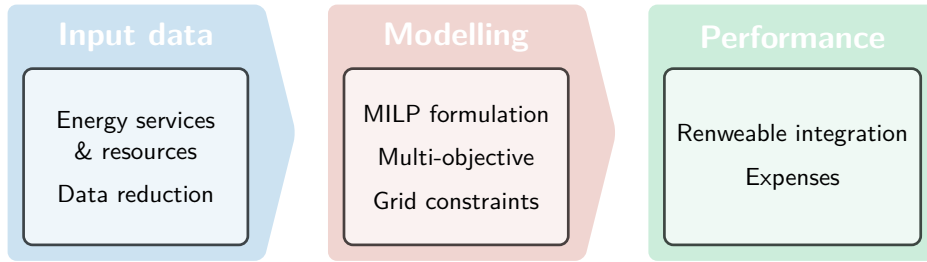
Figure 1.1 – Building energy system sizing process

1.3.1 Algorithm input data

Prior to assessing the different unit technologies, both input and output flows of the building energy system are evaluated; an illustrative overview of the latter is presented in Figure 1.2. Hence, on the output side, the different *energy service* demands of the targeted building are first evaluated. In regard to the national consumption break-down of Figure 1, the latter can be divided into three specific categories: *electricity* (EL) for domestic appliances, *hot water* preparation (HW) and *space heating* (SH) - respectively *cooling* - requirements. While the first two categories are mainly dependant on the building use[1], the latter are typically assessed in function of the dwelling envelope quality [30]. Since this study mainly focuses on the building stock of Switzerland, respective historical demand measurements and construction standards are considered henceforth.

Hence, Girardin et al. [31] implemented a cantonal GIS database of past annual fuel consumption values to identify different building SH demand categories, based on the dwelling construction period and refurbishment status. The study mainly focused on the canton of Geneva which comprises both high and low population density regions and thus, in view of the latter scope, is considered as a representative sample size of the national building stock. On the other hand side, the acquisition of historical EL and HW consumption time series remains a challenging task. With the increasing penetration of smart-meters, electricity use is monitored on a shorter time scale (ranging between 60 and 15 minutes commonly); nevertheless, due to the restrictive accessibility of such databases, the use of past measurements is insufficient to identify demand profiles for specific building categories. Hence, the following study relies on national engineering norms [65] to evaluate the energy service profiles of both EL and HW.

---

[1]E.g. residential, commercial, administrative, etc.

Finally, on the input side, the algorithm data requirements comprises the local *resource availability*. Indeed, in order to analyse the integration of renewable based technologies within the built environment, the associated generation profiles need to be evaluated throughout the unit lifetime. These time series are typically derived from climatic conditions such as the ambient temperature and the solar irradiation. Hence, considering a typical discrete time step of 1 hour and an unit lifetime of 20 years, the required profiles reach 175'200 values. In view of the latter scale, a first data processing step is performed prior introducing the following method step: temporal data reduction.
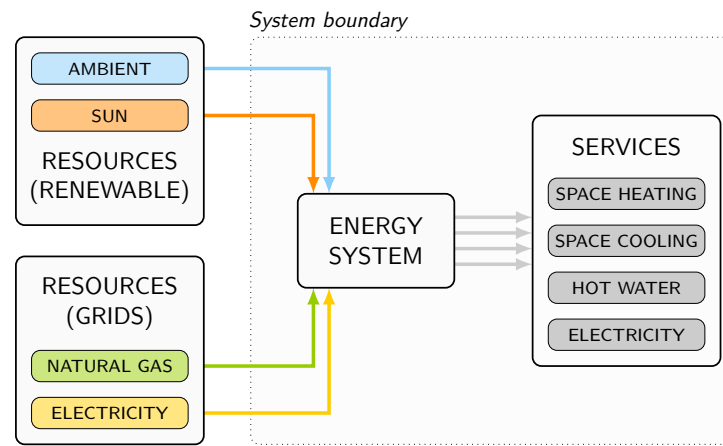
Figure 1.2 – Building energy system modelling framework: energy resources and services

Temporal data classification

In urban energy system planning, building performances are commonly assessed though the means of normalized design reference years (DRY) [66]. The latter hourly or monthly profiles are constructed from past meteorological measurements and incorporate typical climatic conditions arising at the location of interest. Regarding climatic profiles, the dominant importance of the seasonal and daily cyclicity over the variation among consecutive years has justified, until now, the assumption of a constant yearly profile over the entire equipment lifetime, hence decreasing the temporal simulation scope from about $20^{\text{year}} \times 8760^{\text{hour}}$ to $1^{\text{year}} \times 8760^{\text{hour}}$ time steps. Nevertheless, in order to manage the computational complexity of the remaining problem size, a further data clustering method has been developed and applied; a graphical overview of the latter process is presented in Figure 1.3 and detailed thereafter.

Data processing In order to avoid defining clusters predominately according to a single attribute a, the original data sets are normalized following the definition of Eq. 1.1 prior clustering. In the latter relation, x refers to an original measurement of attribute a, of day p
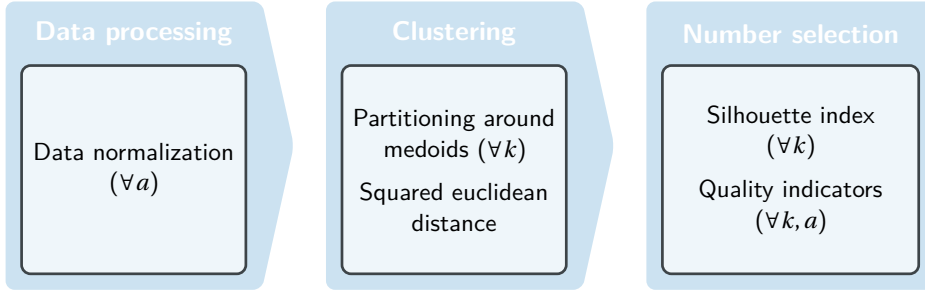
Figure 1.3 – Data classification process

and hour t while $\hat{x}$ denotes the respective standardized parameter. Following normalization, the input matrix is constructed by horizontally appending the different 365×24 data sets.

$$\hat{x}_{p,a,t} = \frac{x_{p,a,t} - \min_{p,t} x_{p,a,t}}{\max_{p,t} x_{p,a,t} - \min_{p,t} x_{p,a,t}} \qquad \forall p, a, t \quad (1.1)$$

Within the context of BES modelling, the external air temperature (T$^{\text{ext}}$) and the global solar irradiance (GHI) are commonly chosen as the only attributes during the following data clustering process [67]. Indeed, both SH/SC service requirements and the potential solar generation can be inferred from these attributes [54, 68]. The demand profiles of EL and HW are however considered constant with respect to the seasonal cyclicity and thus, invariant in between days [65]. Indeed, while changes in hydronic heating system pumping demand are included in the following modelling framework, seasonal variations in appliances use are rather low; the main disparity concerns lightning requirements which account for approximately 11% of the total EL demand and thus is neglected at this stage [69].

Partitioning around medoids The typical operating conditions are identified using a *k-medoids* classification approach; it consists in selecting specific days from the original data set based on an objective function and attributing them to the remaining observations (i.e. days). As presented by Domínguez-Muñoz et al. [70], the latter method can be formulated as an integer problem with $n \times (n+1)$ integer variables with n being the number of observations. However solving the latter for large data sets requires significant computation power and time. The greedy optimization algorithm Partitioning Around Medoids (PAM) developed by Kaufman and Rousseeuw [71] overcomes these issues; although not guaranteeing the global optimum, the proposed method nevertheless provides satisfying "good" results considering the uncertainty inherent to the original data.

In view of finding the best number of clusters, the PAM algorithm is executed in an iterative manner, increasing the cluster size at each run k. Since the algorithm results are dependent on the initial cluster selection, each run k is replicated N_r times while altering the starting point between each repetition, subsequently retaining solely the best result. The clustering performance at each repetition is assessed through a representing objective function, comput-

ing the sum of within cluster dissimilarities. In the following application, a N_r value of 50 has been implemented while the Euclidean squared is used to evaluated the dissimilarities (Eq. 1.2) as proposed by [59].

$$d_{i,j} = \sum_{a=1}^{N_a} \sum_{t=1}^{N_t} (\hat{x}_{i,a,t} - \hat{x}_{j,a,t})^2 \qquad\qquad \forall i, j \ (1.2)$$

Number selection Following the iterative computation process, the best cluster number N_k is selected on the basis of the silhouette index which reflects the cluster compactness in comparison to their separation [71]. In addition, three quality indicators are used to define a minimum threshold on N_k and thus, to ensure a good representation of the original data set: the mean squared error in load duration curve mELDC^2 (Eq. 1.5), the mean σ_{cdc} (Eq. 1.3) and σ_{profile} (Eq. 1.4) profile deviations. In the latter formulations, N_p and N_t denote the number of observation (e.g. 365 days) and measurements (e.g. 24 hours) of each attribute a respectively while LDC represents the load duration curve^2. In addition, x and μ refer to the original and associated clustered measurement value; the respective daily average values are denoted through $\bar{x}$ and $\bar{\mu}$.

$$\sigma_{\text{cdc}}^a = \left(\frac{1}{N_p} \sum_{i=1}^{N_p} \left(\bar{\hat{x}}_{p,a} - \bar{\hat{\mu}}_{p,a} \right)^2 \right)^{0.5} \qquad\qquad \forall a \ (1.3)$$

$$\sigma_{\text{profile}}^a = \left(\frac{1}{N_p \cdot N_t} \sum_{p=1}^{N_p} \sum_{t=1}^{N_t} \left((\hat{x}_{p,a,t} - \bar{\hat{x}}_{p,a}) - (\hat{\mu}_{p,a,t} - \bar{\hat{\mu}}_{p,a}) \right)^2 \right)^{0.5} \qquad\qquad \forall a \ (1.4)$$

$$\text{mELDC}^{2,a} = \frac{1}{N_p \cdot N_t} \cdot \sum_{t=1}^{N_p \cdot N_t} \left(\text{LDC}_0^a(t) - \text{LDC}^a(t) \right)^2 \qquad\qquad \forall a \ (1.5)$$

In the case of the national weather station *Geneva-Cointrin*, the highest values of the average silhouette index are observed for lower cluster numbers while the quality indicators tend to decrease with the increase in n_k (Figure 1.4). In order to define the minimum acceptable cluster number $n_k^{\min}$ the relative improvement in quality indicator is estimated [67]. Indeed, the latter approach attempts in evaluating a suitable trade-off solution between representativeness and computational effort; thus, $n_k^{\min}$ corresponds to the cluster number for which the quality gain engendered by the addition of a further medoid (i.e. cluster) is not significant enough to justify the related increase in problem complexity. In the latter case, considering a slope threshold of 15%, the minimum acceptable cluster size is $n_k^{\min}$=7 and consequently, the next peak for the silhouette index, n_k=8 has finally been chosen as the best trade-off solution. The temporal scope of the optimization problem is thus reduced from $1^{\text{years}} \times 8760^{\text{hours}}$ to $8^{\text{days}} \times 24^{\text{hours}}$ time steps.

---

^{2}The load duration curve is constructed by rearranging the annual data of each attribute in a descending order
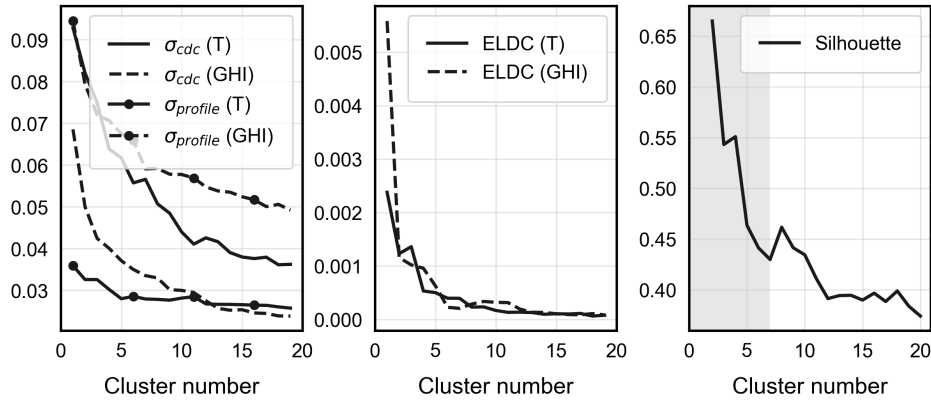
Figure 1.4 – Temporal data reduction quality indicators for GHI (diamond), T^{amb} (star) and performance indicator of Geneva-Cointrin

Figure 1.5 hence depicts the resulting load curves of the original and clustered data for the climatic of west Switzerland. As observed, the clustered and original plots correspond well with the exemption of the extreme values located at the bounds. Hence, in order to ensure the proper sizing of the energy system, these climatic conditions are added *a-posteriori* to the reduced data set.
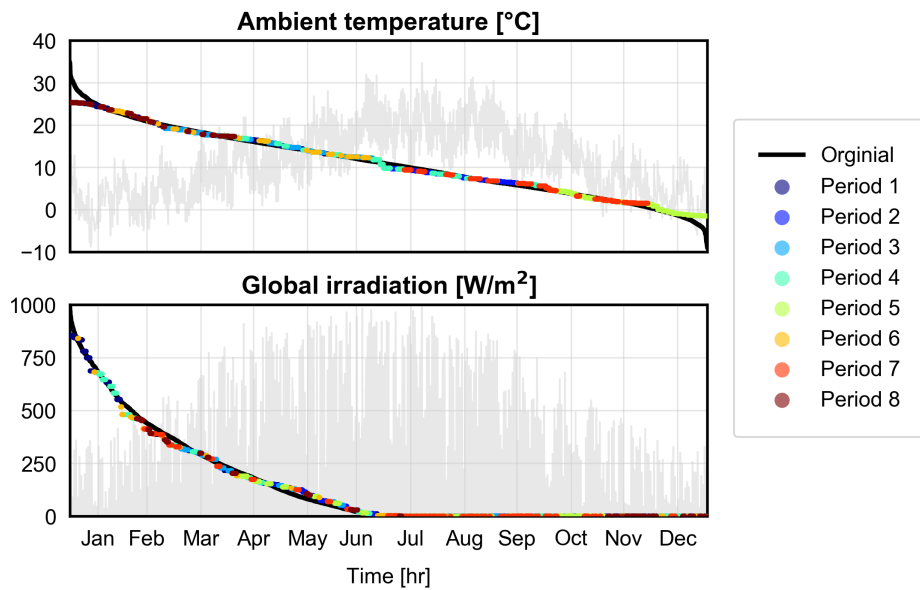
Figure 1.5 – The ambient temperature and solar irradiation DRY load duration curves (black, front) and profiles (grey, background) of Geneva-Cointrin represented by 8 typical periods (colored)

1.3.2 Modelling framework

Following the input data assessement process, this section details the proposed optimal sizing method for complex BES. The modelling framework (MF) relies on MILP techniques which have been identified as a proper approach to describe both the continuous (e.g. load modulation) and logical (e.g. start-up) behaviour of BES devices [28]. An overview of the latter is illustrated in Figure 1.6; it comprises air-water heat pumps (AHP), combined heat and power (CHP) devices and air-conditioning (VAC) systems as *primary conversion* units as well as electric heaters (ELH) and gas boilers (BOI) as *auxiliary conversion* units to satisfy the different thermal requirements. Energy is *stored* in either stationary batteries (BAT), domestic hot water (HWT) and buffer tanks (HST) or directly in the building envelope. Photovoltaic (PVA) and solar thermal collector (STC) panels act as *renewable* energy sources, the latter being only connected to the domestic hot water tanks in regard to the strong seasonal disparity between generation potential and SH service demand periods. The different units are finally interconnected through the main energy distribution networks: the natural gas and electricity grids. Although Figure 1.6 solely displays a limited amount of unit types, additional technologies and network layers can be easily incorporated into the following MF, such as the potential deployment of a low-temperature district heating network and water-water heat pumps.
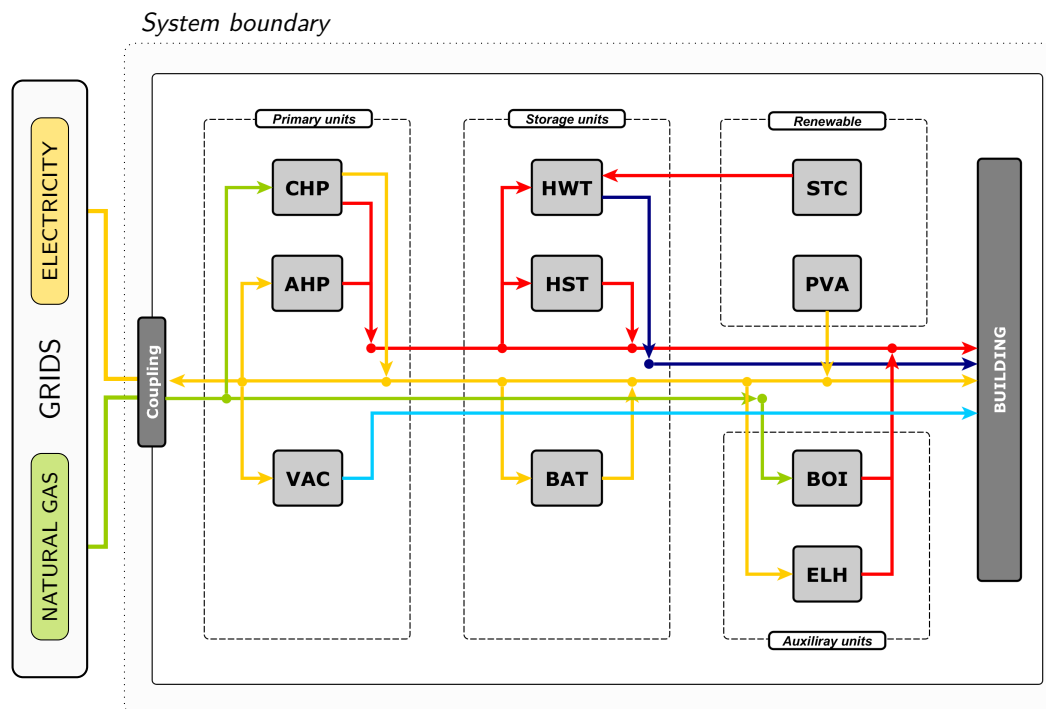
Figure 1.6 – Building energy system modelling framework: electricity flows (yellow), natural gas flows (green), hot water (dark blue), heating (red) and cooling (blue) flows

Syntax   In the following problem formulation, parameters are represented by standard roman text letters, variables by *italic* text letters and sets by ***bold italic*** text letters. The sets implemented throughout this section are defined as follows (Table 1.2); the set $\boldsymbol{U}$ comprises all units introduced in the energy system structure (Figure 1.6) while the set $\boldsymbol{S}$ includes the different thermal streams associated to each of them. From the temporal perspective, the set $\boldsymbol{P}$ denotes typical operating periods (days) whereas $\boldsymbol{T}$ refers to the hourly discrete time steps of each period: $\boldsymbol{T} \in [1, 24]$. Finally, $\boldsymbol{K}$ contains the different discrete temperature levels determined by the inlet and outlet heat streams conditions. Following the convention proposed by Borel and Favrat [72], the index + designates an incoming flow while − indicates an outgoing flow with respect to each unit or the entire system boundary in the case of the network flows.

Table 1.2 – List of defined sets with description

Set	Index	Increment	Cyclic[1]	Description
$\boldsymbol{P}$	p	d_p	×	Period (day)
$\boldsymbol{T}$	t	d_t	✓	Time (hour)
$\boldsymbol{K}$	k	-	×	Temperature level
$\boldsymbol{S}$	s	-	-	Heat stream
$\boldsymbol{U}$	u	-	-	Unit

[1] The last element is considered to precede the first one

Unit sizing   The existence Y, size F, logical state y and load f of unit u are constrained by Eqs. 1.6 to 1.8 where $\mathrm{F}^{\min}$ and $\mathrm{F}^{\max}$ denote the minimum and maximum bounds of the device size respectively.

$$\mathrm{F}_u^{\min} \cdot Y_u \le F_u \le \mathrm{F}_u^{\max} \cdot Y_u \qquad\qquad \forall\, u \in \boldsymbol{U} \quad (1.6)$$

$$f_{u,p,t} \le F_u \qquad\qquad \forall\, u \in \boldsymbol{U}, p \in \boldsymbol{P}, t \in \boldsymbol{T} \quad (1.7)$$

$$y_{u,p,t} \le Y_u \qquad\qquad \forall\, u \in \boldsymbol{U}, p \in \boldsymbol{P}, t \in \boldsymbol{T} \quad (1.8)$$

In order to avoid the generation of technically infeasible solutions and comply with regional legislative performance restrictions, additional unit activation constraints are appended to the general modelling framework. However, in view of their complementary function to the presented MF, the following constraints are detailed in Appendix A.

Energy balances   The system energy balances are expressed in Eqs. 1.9 and 1.10 where e and h represent the reference power flows of each unit u, regarding the different utility networks: in the present case, the electricity (e) and the natural gas (h) grids. Power interaction with the latter are finally represented by the variables $\dot{E}_{\mathrm{grid}}$ and $\dot{H}_{\mathrm{grid}}$ respectively. Certainly, with the addition of novel network types (e.g. district heating), the respective energy balances must be appended to the problem formulation using a similar definition to Eqs. 1.9 and 1.10 while

modifying the related expenses definitions (Eq. 1.34) accordingly.

$$\dot{E}^+_{\text{grid},p,t} + \sum_{u=1}^{|\boldsymbol{U}|} \text{e}^+_{u,p,t} \cdot f_{u,p,t} = \dot{E}^-_{\text{grid},p,t} + \sum_{u=1}^{|\boldsymbol{U}|} \text{e}^-_{u,p,t} \cdot f_{u,p,t} \qquad \forall p \in \boldsymbol{P}, t \in \boldsymbol{T} \quad (1.9)$$

$$\dot{H}^+_{\text{grid},p,t} + \sum_{u=1}^{|\boldsymbol{U}|} \text{h}^+_{u,p,t} \cdot f_{u,p,t} = \dot{H}^-_{\text{grid},p,t} + \sum_{u=1}^{|\boldsymbol{U}|} \text{h}^-_{u,p,t} \cdot f_{u,p,t} \qquad \forall p \in \boldsymbol{P}, t \in \boldsymbol{T} \quad (1.10)$$

Heat cascade The heat cascade balances the thermal loads while satisfying the second law of thermodynamics. The method consists in correcting the system heat streams s according to their respective minimum approach temperature $\Delta \text{T}^{\text{min}}$, sorting them in ascending temperature intervals k and subsequently solving the energy balance for each k [73]. Equation 1.11 hence defines the cascaded heat $\dot{R}$ from k to $k+1$ in view of the defined hot $\boldsymbol{S}_h$ and cold $\boldsymbol{S}_c$ streams. The specific heat load provided by the different streams s within each interval k are expressed in Eqs. 1.13 and 1.14 where $\text{T}^{+/-}$ denote the upper/lower interval temperatures, $\text{T}^{\text{in/out}}$ the stream inlet/outlet temperatures while $\dot{\text{q}}^{+/-}$ refer to the stream reference heat load. Equation 1.12 finally ensures that no heat is cascaded to the highest ($k=n_k$) or from the lowest ($k=1$) intervals, thus closing the thermal energy balance.

$$\dot{R}_{k,p,t} - \dot{R}_{k+1,p,t} = \sum_{i=1}^{\boldsymbol{S}_h} \dot{Q}^-_{i,k,p,t} - \sum_{j=1}^{\boldsymbol{S}_c} \dot{Q}^+_{j,k,p,t} \qquad \forall p \in \boldsymbol{P}, t \in \boldsymbol{T}, k \in \boldsymbol{K} \quad (1.11)$$

$$\dot{R}_{1,p,t} = \dot{R}_{n_k+1,p,t} = 0 \qquad \forall p \in \boldsymbol{P}, t \in \boldsymbol{T} \quad (1.12)$$

$$\dot{Q}^-_{i,k,p,t} = \frac{\left(\text{T}^+_{k,p,t} - \max\left\{\text{T}^-_{k,p,t}, \text{T}^{\text{out}}_{i,p,t} - \Delta \text{T}^{\text{min}}_{i,p,t}\right\}\right)}{\text{T}^{\text{in}}_{i,p,t} - \text{T}^{\text{out}}_{i,p,t}} \cdot$$
$$\dot{\text{q}}^-_{i,p,t} \cdot f_{u,p,t} \qquad \forall i \in \boldsymbol{S_h}, k \in \boldsymbol{K}, p \in \boldsymbol{P}, t \in \boldsymbol{T} \quad (1.13)$$

$$\dot{Q}^+_{j,k,p,t} = \frac{\left(\max\left\{\text{T}^+_{k,p,t}, \text{T}^{\text{out}}_{i,p,t} + \Delta \text{T}^{\text{min}}_{i,p,t}\right\} - \text{T}^-_{k,p,t}\right)}{\text{T}^{\text{out}}_{j,p,t} - \text{T}^{\text{in}}_{j,p,t}} \cdot$$
$$\dot{\text{q}}^+_{j,p,t} \cdot f_{u,p,t} \qquad \forall j \in \boldsymbol{S_c}, k \in \boldsymbol{K}, p \in \boldsymbol{P}, t \in \boldsymbol{T} \quad (1.14)$$

Building

The thermal behaviour of building is described using a first order dynamic 1R1C model as illustrated in Figure 1.7. In the latter case, the entire construction is lumped into a single capacity C_b while considering a single temperature node T_b as presented in [54, 74]. Eq. 1.15 expresses the related energy balance where T_b thus denotes the internal temperature, T^{ext} the external temperature, $\text{U}^{\text{ext}}_b = 1/\text{R}^{\text{ext}}_b$ the lumped thermal transfer coefficient, ϕ^{s+o}_b the

stochastic gains from solar and occupancy sources while $\dot{Q}_b^+$ refers to the heat supply by the energy system. In the case of partially and non-residential dwellings with cooling requirements, a second zone is added to the model and interconnected through the internal insulation resistance R_b^{int}. Finally, $T^{min/max}$ in Equation 1.16 define the comfort tolerance on the internal temperature.

$$C_b \cdot (T_{b,p,t+1} - T_{b,p,t}) = U_b^{ext} \cdot (T_{p,t}^{ext} - T_{b,p,t}) + \dot{\phi}_{b,p,t}^{s+o} + \dot{Q}_{b,p,t}^+ \qquad \forall p \in \boldsymbol{P}, t \in \boldsymbol{T} \quad (1.15)$$

$$T_{b,p,t}^{min} \leq T_{b,p,t} \leq T_{b,p,t}^{max} \qquad \forall p \in \boldsymbol{P}, t \in \boldsymbol{T} \quad (1.16)$$
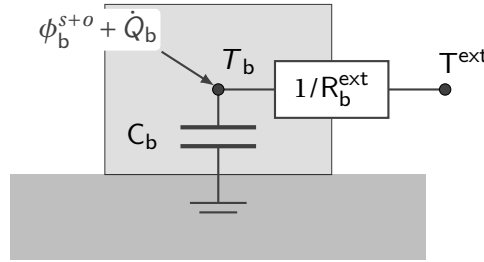
Figure 1.7 – 1R1C building model

The heat distribution system, commonly water-based in Switzerland and Northern European states, is represented by the building energy signature; during standard operation, the return water temperature $T^{h,r}$ is set in function of the daily average external temperature $\bar{T}^{ext}$. The latter model indeed considers the heat transmission through the building envelope and ventilation as being the main loss factor (aggregated in R_b^{ext}) while solar and internal gains ϕ^{s+o} are included through a fixed cut-off temperature T_{tr}^h beyond which heat provision is ceased.

In the case of the considered predictive control system, thermal inputs are set as decision variables and solely limited by the comfort tolerance (Eq. 1.16). However, in order to avoid any non-linearities in the problem formulation arising from variable return and supply temperatures, $n_s = |\boldsymbol{S}|$ operating points are discretized around the nominal set-point and added to the heat cascade (Figure 1.8). The activation of the thus defined streams is then constraint by the nominal mass flow $\dot{m}_b$ of the heating system as presented in Eq. 1.18. From a practical perspective, since the simultaneous implementation of these different operating conditions ($\dot{m}_{b,s}$) is not realistic, the computed heat loads should be subsequently reordered and applied consecutively within the associated time step [75]. In regard to non-residential buildings, an identical model formulation (Eqs. 1.17 to 1.21) is used to describe the dwelling cooling system, the design parameters being superscripted by the index (*c*) instead of (*h*). In the following definition, the subscripted index 0 refers nominal operating conditions while the

superscripted indexes s/r to the hydronic supply and return flows.

$$c_p \cdot \sum_{s=1}^{S} \dot{m}_{b,s,p,t}^{\mathrm{h}} \cdot (T_{b,s,p,t}^{\mathrm{out}} - T_{b,s,p,t}^{\mathrm{in}}) = \dot{Q}_{b,p,t}^{+} \qquad \forall p \in P, t \in T \quad (1.17)$$

$$\sum_{s=1}^{S} \dot{m}_{b,s,p,t}^{\mathrm{h}} \leq \dot{m}_{b}^{\mathrm{h}} \qquad \forall p \in P, t \in T \quad (1.18)$$

$$\dot{Q}_0 = U_b^{\mathrm{ext}} \cdot \left(T_{b,0} - T_0^{\mathrm{ext,h}} \right) \qquad (1.19)$$

$$c_p \cdot \dot{m}_b^{\mathrm{h}} = \frac{\dot{Q}_0}{\left(T_0^{\mathrm{h,s}} - T_0^{\mathrm{h,r}} \right)} \qquad (1.20)$$

$$T_{b,s,p,t}^{\mathrm{out}} = T_{b,0} - \frac{\dot{q}_{b,s,p,t}}{\dot{Q}_0} \cdot \left(T_0^{\mathrm{h,s}} - T_0^{\mathrm{h,r}} \right) \cdot \frac{\alpha}{1-\alpha} \qquad \forall s \in S, p \in P, t \in T \quad (1.21)$$

$$\alpha = \frac{T_0^{\mathrm{h,s}} - T_{b,0}}{T_0^{\mathrm{h,r}} - T_{b,0}} \qquad (1.22)$$
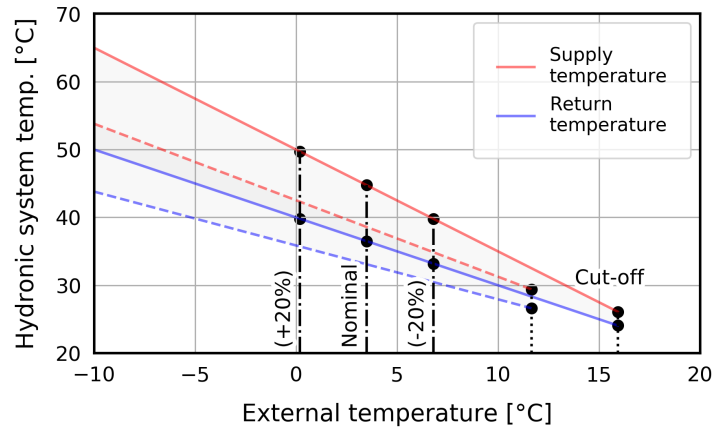
Figure 1.8 – Discrete energy signature model for an existing (plain) and refurbished (dashed) building: nominal operating point and additional ±20% load options

Conversion units

The conversion unit behaviour is described through the static model definition expressed in Eqs. 1.6 to 1.8. In addition, specific scheduling constraints are appended regarding the device type: minimum load and start-up time limitations. In order to avoid any non-linearity resulting from the multiplication of the unit size F and logical state y, the lossless reformulation of Equations 1.23 to 1.25 is implemented where λ represent the minimum (respectively maximum) part-load rates while the sub-set $U' \subseteq U$ contains devices subject to these operative

constraints.

$$\lambda_u^{\min} \cdot \mathrm{F}_u^{\min} \cdot y_{u,p,t} \leq f_{u,p,t} \leq \lambda_u^{\max} \cdot \mathrm{F}_u^{\max} \cdot y_{u,p,t} \qquad \forall\, u \in \boldsymbol{U'}, p \in \boldsymbol{P}, t \in \boldsymbol{T} \quad (1.23)$$

$$f_{u,p,t} \leq \lambda_u^{\max} \cdot F_u \qquad \forall\, u \in \boldsymbol{U'}, p \in \boldsymbol{P}, t \in \boldsymbol{T} \quad (1.24)$$

$$f_{u,p,t} \geq \lambda_u^{\min} \cdot \left(F_u - \mathrm{F}_u^{\max} \cdot \left(1 - y_{u,p,t}\right)\right) \qquad \forall\, u \in \boldsymbol{U'}, p \in \boldsymbol{P}, t \in \boldsymbol{T} \quad (1.25)$$

In the case of devices comprising multiple service temperatures (i.e. thermal streams), the load factor f is further discredited according to the number of unit streams s (Eq. 1.26).

$$\sum_{s=1}^{S} f_{u,s,p,t} = f_{u,p,t} \qquad \forall\, u \in \boldsymbol{U}, p \in \boldsymbol{P}, t \in \boldsymbol{T} \quad (1.26)$$

In addition to strict modulation ranges, complex conversion units might be subject to minimum operating hours $\mathrm{n}^{\min}$ preceding activation as well as a maximum amount of start-ups $\mathrm{n}^{\mathrm{start}}$. The latter restrictions are expressed through Eqs. 1.27 to 1.30 where δ reflects the device logical state modification (start-up or shut-down). Similarly to Eqs. 1.23 to 1.25, $\boldsymbol{U'} \subseteq \boldsymbol{U}$ only includes unit technologies affected by the following operative constraints.

$$\delta_{u,p,t} \geq y_{u,p,t} - y_{u,p,t-1} \qquad \forall\, u \in \boldsymbol{U'}, p \in \boldsymbol{P}, t \in \boldsymbol{T} \quad (1.27)$$

$$\delta_{u,p,t} \geq 0 \qquad \forall\, u \in \boldsymbol{U'}, p \in \boldsymbol{P}, t \in \boldsymbol{T} \quad (1.28)$$

$$\sum_{i=t}^{t+\mathrm{n}_u^{\min}-1} y_{u,p,i} \geq \delta_{u,p,t} \cdot \mathrm{n}_u^{\min} \qquad \forall\, u \in \boldsymbol{U'}, p \in \boldsymbol{P}, t \in \boldsymbol{T} \quad (1.29)$$

$$\sum_{t=1}^{|\boldsymbol{T}|} \delta_{u,p,t} \leq \mathrm{n}_u^{\mathrm{start}} \qquad \forall\, u \in \boldsymbol{U'}, p \in \boldsymbol{P} \quad (1.30)$$

For sake of readability, conversion unit specific modelling definitions are stated in the respective chapter appendix (Appendix A).

Storage units

The generic energy balance governing storage units is expressed in Eq. 1.31 where f refers to the device state-of-charge while $f^{+/-}$ denote the charging and respectively discharging rate. Losses are modelled through σ for self-discharging rate, γ for the charging (respectively discharging) efficiencies and a constant loss factor κ accounting for remaining unusable energy content. Similarly to conversion unit formulations, $\boldsymbol{U'} \subseteq \boldsymbol{U}$ contains devices subject to these modelling constraints.

$$f_{u,p,t+1} = (1 - \sigma_u) \cdot f_{u,p,t} + \left(\gamma_u \cdot f_{u,p,t}^+ - \gamma_u^{-1} \cdot f_{u,p,t}^-\right) \cdot \mathrm{d}_t - \kappa_u \cdot F_u \qquad \forall\, u \in \boldsymbol{U'}, p \in \boldsymbol{P}, t \in \boldsymbol{T} \quad (1.31)$$

In the case of quality discretization of the storage medium, e.g. regarding different temperature levels for heat storage, the latter single state definition is extended to multi-state formulation

as expressed in Eq. 1.32.

$$f_{u,s,p,t+1} = \left(1 - \sigma_{u,s}\right) \cdot f_{u,s,p,t} + \\ \left(\gamma_{u,s} \cdot f_{u,s,p,t}^{+} - \gamma_{u,s}^{-1} \cdot f_{u,s,p,t}^{-}\right) \cdot \mathrm{d}_t - \kappa_{u,s} \cdot F_u \qquad \forall u \in \boldsymbol{U}, s \in \boldsymbol{S}, p \in \boldsymbol{P}, t \in \boldsymbol{T} \quad (1.32)$$

$$\sum_{s=1}^{|\boldsymbol{S}|} f_{u,s,p,t} \le F_u \qquad \forall u \in \boldsymbol{U}, p \in \boldsymbol{P}, t \in \boldsymbol{T} \quad (1.33)$$

Similarly to the preceding section, storage unit specific modelling definitions are stated in the respective chapter appendix (Appendix A).

Costs and objectives

The first expenses definition is the annual operating chA_objective1 C^{op} associated to energy exchanges with the electricity and natural gas networks. Equation 1.34 defines the latter economic indicator, with op representing the different feed-in ($^-$) and purchasing ($^+$) energy tariffs related to the considered networks (Figure 1.6).

$$C^{\mathrm{op}} = \sum_{p=1}^{P} \sum_{t=1}^{T} \left(\mathrm{op}_{p,t}^{el,+} \cdot \dot{E}_{\mathrm{grid},p,t}^{+} - \mathrm{op}_{p,t}^{el,-} \cdot \dot{E}_{\mathrm{grid},p,t}^{-} + \mathrm{op}_{p,t}^{ng,+} \cdot \dot{H}_{\mathrm{grid},p,t}^{+} \right) \cdot \mathrm{d}_p \cdot \mathrm{d}_t \qquad (1.34)$$

The second group of expenses includes the present capital costs C^{ca} related to the different unit purchases over the project lifetime N. Defined in Eq. 1.35, the former includes the investment C_{inv} as well as the replacement C_{rep} costs of the energy system where $\mathrm{inv}_{1,u}$ and $\mathrm{inv}_{2,u}$ denote the linear unit investment cost function parameters and $\mathrm{F}_{\mathrm{BM},u}$ the unit bare module factor[3] [76]. In addition, L_u refers to the unit lifetime, i the project interest rate and rep_u to the number of unit replacements over the project horizon N.

$$C^{\mathrm{cp}} = \underbrace{\sum_{u=1}^{U} (\mathrm{F}_{\mathrm{BM},u} \cdot (\mathrm{inv}_{1,u} \cdot Y_u + \mathrm{inv}_{2,u} \cdot F_u))}_{C_{\mathrm{inv}}} + \underbrace{\sum_{u=1}^{U} \sum_{n=1}^{\mathrm{rep}_u} \frac{1}{(1+\mathrm{i})^{n \cdot \mathrm{L}_u}} \cdot (\mathrm{inv}_{1,u} \cdot Y_u + \mathrm{inv}_{2,u} \cdot F_u)}_{C_{\mathrm{rep}}}$$

$$(1.35)$$

Problem formulation: optimal sizing and operation

The complete problem formulation related to the optimal sizing and operation of building energy systems is stated in Eq. 1.36. It minimizes the total annualized system expenses which include both the operating (Eq. 1.34) and investment (Eq. 1.35) costs. The set of decision variables $\boldsymbol{\Sigma}$ comprises the different unit sizes F, existences Y, loads f and logical states y, the storage device charging f^- and discharging f^- rates, the dwelling indoor temperature T_b and finally the network electricity $\dot{E}$ and $\dot{H}$ power exchange. In addition, to the aforementioned

---

[3]Costing factor accounting for the installation expenses (auxiliary material and manpower)

modelling definitions (Eq. 1.6 to Eq. A.25), specific technical constraints (e.g. the building maximal solar hosting capacity) are further included in the problem formulation and detailed in Appendix A.

$$\min_{\Sigma} \ C^{\text{op}} + \frac{i \cdot (1+i)^{\text{N}}}{(1+i)^{\text{N}} - 1} \cdot C^{\text{cp}}$$

$$\Sigma = \left\{ F_u, Y_u, f_{u,p,t,(s)}, y_{u,p,t}, \delta_{u,p,t}, f^{+/-}_{u,p,t,(s)}, T_{b,p,t}, \dot{R}_{k,p,t}, \dot{Q}^{+/-}_{s,k,p,t}, \dot{E}^{+/-}_{\text{grid},p,t}, \dot{H}^{+/-}_{\text{grid},p,t} \right\}$$

(1.36)

subject to

Eq. 1.6 - Eq. 1.33 and Eq. A.1 - Eq. A.25

Problem formulation: non-optimal operation

In order to highlight the advantages of predictive control techniques (i.e. MPC) in comparison to a standard rule-based control (RBC) method, a second problem formulation is determined. It relies on the model definition described in Section 1.3.2 and therefore, the following subsection solely presents the modifications made to the original modelling framework (MF). Figure 1.9 provides an illustrative overview of the different calculation steps required to identify the associate RBC system behaviour: in a *first* step, the unit sizes are evaluated and fixed using the prior problem statement (Eq. 1.36). In a *second* step, the device sizes are fixed and a modified optimization problem, detailed thereafter, is solved to schedule the different conversion technologies. In a *third* and last step, the renewable generation profiles are integrated in the associated energy balances and specific storage behaviours are assessed.
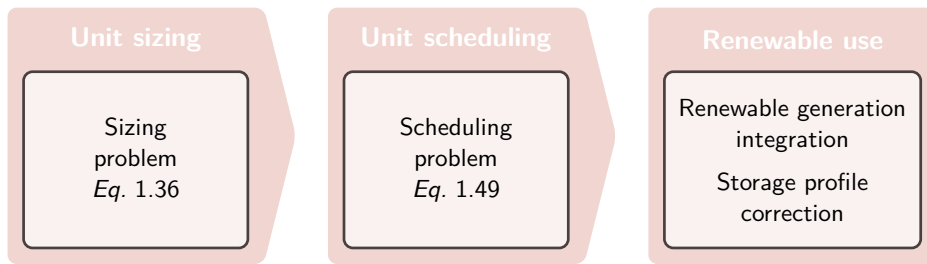
Figure 1.9 – RBC solving process

Costs   The rule-based scheduling problem objective function is the minimization of operating expenses (Eq. 1.34). Nevertheless, in order to avoid any arbitrage conditions (e.g. in the case of CHP units), the feed-in tariffs op$^-$ are set equal to the respective purchasing cost op$^+$. The annual energy bill is then corrected *a-posteriori* to be comparable to the previous optimization results.

Unit sizing Equations 1.37 and 1.38 fix the energy system sizes to a previously defined optimal solution F_u^*, except for renewable-based technologies (i.e. PVA and STC). These devices are indeed decoupled from the building and operated off-site, thus preventing the control algorithm from shifting flexible loads towards high generation periods. The electricity produced from the PVA is then subtracted *a-posteriori* from the building power demand while the operating expenses are corrected accordingly. On the other hand side, the heat generated by the STC are fed into the domestic hot water tank (HWT) while correcting the unit state-of-charge and charging profile accordingly.

$$F_u = F_u^* \qquad\qquad \forall u \in \boldsymbol{U} \setminus \{\text{PVA, STC}\} \quad (1.37)$$

$$F_u = 0 \qquad\qquad \forall u \in \boldsymbol{U} = \{\text{PVA, STC}\} \quad (1.38)$$

Building In RBC, the local regulator is following the pre-defined lower comfort temperature during the heating period, respectively the upper bound during the cooling season. According to the building model definition presented in Equations 1.15 and 1.16, no additional heat can be provided or extracted in view of the standard energy requirements: the set-point temperatures ($T_{b,s,p,t}^{\text{out}}$ and $T_{b,s,p,t}^{\text{in}}$) of the HHS are evaluated from the standard energy signature and additional operating conditions around the nominal values are fixed to null (Eqs. 1.39 and 1.40). Finally, the SH/SC profiles $\dot{Q}_{b,p,t}^*$ are assessed a-priori according to a similar method presented in [32] and fixed through Eq. 1.41. In other words, the building is solely represented by a single, fixed thermal stream $s = 1$, both for SH and SC service and hence, not exploitable for any DSM purposes.

$$\dot{m}_{b,s,p,t} = 0 \qquad\qquad \forall s \in \boldsymbol{S} \setminus \{1\}, p \in \boldsymbol{P}, t \in \boldsymbol{T} \quad (1.39)$$

$$\dot{m}_{b,s,p,t} = 0 \qquad\qquad \forall s \in \boldsymbol{S} \setminus \{1\}, p \in \boldsymbol{P}, t \in \boldsymbol{T} \quad (1.40)$$

$$\dot{Q}_{b,p,t}^{+/-} = \dot{Q}_{b,p,t}^* \qquad\qquad \forall p \in \boldsymbol{P}, t \in \boldsymbol{T} \quad (1.41)$$

Heat storage tank Since, when operating under RBC, the main role of the water tank is in providing a thermal buffer during defrosting periods and potentially limiting the number of start-up cycles, the device is solely required to follow the building HHS return temperature $T_{b,s,p,t}^{\text{in}}$, hence fixing the heat output to null (Eq. 1.42). Although this constraint deactivated the HST from a DSM perspective, the solver is still able to select the best charging period(s) to compensate for self-discharging losses in view of minimizing the considered objective function; however, due to very low heat requirement of this compensation, the latter "predictive" behaviour has been disregarded in the following RBC assessment.

$$f_{\text{HST},s,p,t}^- = 0 \qquad\qquad \forall s \in \boldsymbol{S}, p \in \boldsymbol{P}, t \in \boldsymbol{T} \quad (1.42)$$

Battery   Similarly to the photovoltaic array, the battery is decoupled from the energy system during the optimization process (Eq. 1.43) and integrated *a-posteriori* through a simple rule-based control; during excess production the battery is charged until reaching its rated storage capacity while during demand periods, the unit is discharged until reaching the lower bound in state-of-charge.

$$f_{\text{BAT},p,t}^{+/-} = 0 \qquad\qquad \forall p \in \mathbf{P}, t \in \mathbf{T} \quad (1.43)$$

Domestic hot water tank   In RBC, the domestic hot water tank is regulated through a simple two-point control method; when reaching the lower state-of-charge $\text{SOC}_{\text{HWT}}^{\min}$, the device is fully charged. Equations 1.44 to 1.48 models the latter behaviour where the binary variable y_{DWT} refers to a charging need and the parameter M to a large value. In order to offload power networks, electrically powered domestic hot water tanks are typically charged during night time and thus, at $t = 1$ the storage unit is fully charged (Eq. 1.44) and subsequently, operating according to the aforementioned regulation scheme.

$$f_{\text{HWT},n_s,p,1} = \text{F}_{\text{HWT}}^* \qquad\qquad \forall p \in \mathbf{P} \quad (1.44)$$

$$f_{\text{HWT},s,p,t}^{+} \leq \text{M} \cdot y_{\text{HWT},p,t} \qquad\qquad \forall p \in \mathbf{P}, t \in \mathbf{T}, s \in \mathbf{S} \quad (1.45)$$

$$f_{\text{HWT},n_s,p,t+1} \geq y_{\text{HWT},p,t} \cdot \text{F}_{\text{HWT}}^* \qquad\qquad \forall p \in \mathbf{P}, t \in \mathbf{T} \quad (1.46)$$

$$\begin{aligned} \text{SOC}_{\text{HWT}}^{\min} + (1 - y_{\text{HWT},p,t}) \cdot \text{M} \geq \\ (1 - \sigma_{\text{HWT},n_s}) \cdot f_{\text{HWT},n_s,p,t} - f_{\text{HWT},n_s,p,t}^{-} \cdot \text{d}_t \end{aligned} \qquad \forall p \in \mathbf{P}, t \in \mathbf{T} \quad (1.47)$$

$$\begin{aligned} (1 - y_{\text{HWT},p,t}) \cdot \text{SOC}_{\text{HWT}}^{\min} \leq \\ (1 - \sigma_{\text{HWT},n_s}) \cdot f_{\text{HWT},n_s,p,t} - f_{\text{HWT},n_s,p,t}^{-} \cdot \text{d}_t \end{aligned} \qquad \forall p \in \mathbf{P}, t \in \mathbf{T} \quad (1.48)$$

Problem formulation   Finally the modified optimization problem is stated in Eq. 1.49; the main modification with respect to Eq. 1.49 are the objective function (Eq. 1.34) and the addition of Eqs. 1.37 to 1.40, 1.42 and 1.43. Since, the following solely optimizes the system scheduling, sizing related decision variables, i.e. F and Y are removed from the respective set $\mathbf{\Sigma}$.

$$\begin{aligned} &\min_{\mathbf{\Sigma}} \; C^{\text{op}} \\ &\mathbf{\Sigma} = \big\{ f_{u,p,t,(s)}, y_{u,p,t}, \delta_{u,p,t}, f_{u,p,t,(s)}^{+/-}, T_{b,p,t}, \dot{R}_{k,p,t}, \dot{Q}_{s,k,p,t}^{+/-}, \dot{E}_{\text{grid},p,t}^{+/-}, \dot{H}_{\text{grid},p,t}^{+/-} \big\} \\ &\text{subject to} \\ &\text{Eq. 1.6 - Eq. 1.33 \; and \; Eq. A.1 - Eq. A.25 \; and \; Eq. 1.37 - Eq. 1.48} \end{aligned} \qquad (1.49)$$

1.3.3 Performance indicators

In order to analyse the BES configurations generated through the MF and problem formulations previously introduced, specific performance indicators are assessed, highlighting different aspects of the distributed generation integration. Within this context, multiple technico-economic metrics have been implemented and described as follows: the total expenses, the payback time, the self-sufficiency and consumption, the grid energy storage, the one percent peak and the building storage equivalence.

Total expenses The total expenses show the economic benefits resulting from the smart installation and operation of complex building energy systems with renewable-based conversion utilities. As stated in Eq. 1.50, the indicator is determined using the primary objective function (i) the operating expenses and the first epsilon constraint (ii) the annualized capital expenses. Furthermore, a floor area relative formulation is applied to improve the comparison between dwellings of different reference areas.

$$
C = \frac{100}{A_b} \cdot \left(C^{\mathrm{op}} + \frac{i \cdot (1+i)^{\mathrm{N}}}{(1+i)^{\mathrm{N}} - 1} \cdot C^{\mathrm{cp}} \right)
\tag{1.50}
$$

Self-consumption The self-consumption (SC) represents the ratio of on-site generated electricity consumption in regard to the total distributed production; Equation 1.51 defines the latter metric where $\boldsymbol{U'}$ solely comprises distributed generation technologies (PVA and CHP). The former measure, formalized by Luthander et al. [77], reflects the system ability in shifting controllable loads towards high production periods and thus, in decreasing grid export power flows.

$$
\mathrm{SC} = \frac{\sum_{p=1}^{\boldsymbol{P}} \sum_{t=1}^{\boldsymbol{T}} \left(\sum_{u=1}^{\boldsymbol{U'}} \dot{E}_{u,p,t}^{-} - \dot{E}_{\mathrm{grid},p,t}^{-} \right) \cdot \mathrm{d}_p \cdot \mathrm{d}_t}{\sum_{p=1}^{\boldsymbol{P}} \sum_{t=1}^{\boldsymbol{T}} \left(\sum_{u=1}^{\boldsymbol{U'}} \dot{E}_{u,p,t}^{-} \right) \cdot \mathrm{d}_p \cdot \mathrm{d}_t}
\tag{1.51}
$$

Self-sufficiency The self-sufficiency (SS) on the other hand defines the ratio of on-site generated electricity consumption in regard to the total consumption as expressed in Equation 1.52. Formalized by Luthander et al. [77], this indicator describes the degree of distributed generation integration - including renewable based conversion utilities - with respect to the total building electricity requirements.

$$
\mathrm{SS} = \frac{\sum_{p=1}^{\boldsymbol{P}} \sum_{t=1}^{\boldsymbol{T}} \left(\sum_{u=1}^{\boldsymbol{U'}} \dot{E}_{u,p,t}^{-} - \dot{E}_{\mathrm{grid},p,t}^{-} \right) \cdot \mathrm{d}_p \cdot \mathrm{d}_t}{\sum_{p=1}^{\boldsymbol{P}} \sum_{t=1}^{\boldsymbol{T}} \left(\sum_{u=1}^{\boldsymbol{U'}} \dot{E}_{u,p,t}^{-} - \dot{E}_{\mathrm{grid},p,t}^{-} + \dot{E}_{\mathrm{grid},p,t}^{+} \right) \cdot \mathrm{d}_p \cdot \mathrm{d}_t}
\tag{1.52}
$$

Generation fraction The generation fraction (GF) represents the ratio of the on-site total distributed electricity production in regard to the total consumption; Equation 1.53 defines

the latter indicator where, similarly to Eqs. 1.51 and 1.52, $\boldsymbol{U}'$ solely includes distributed generation technologies (PVA and CHP). The GF metric hence represents the system degree of net autonomy regarding its total electricity requirements. In view of Equation 1.53, the net-ZEB threshold is reached for values $\text{GF} \geq 1$.

$$\text{GF} = \frac{\sum_{p=1}^{P} \sum_{t=1}^{T} \left(\sum_{u=1}^{U'} \dot{E}_{u,p,t}^{-} \right) \cdot \mathrm{d}_p \cdot \mathrm{d}_t}{\sum_{p=1}^{P} \sum_{t=1}^{T} \left(\sum_{u=1}^{U'} \dot{E}_{u,p,t}^{-} - \dot{E}_{\text{grid},p,t}^{-} + \dot{E}_{\text{grid},p,t}^{+} \right) \cdot \mathrm{d}_p \cdot \mathrm{d}_t} \tag{1.53}$$

Grid energy storage   The grid energy storage (GES) evaluates the electrical storage system capacity required from the power network operator perspective to manage electricity exports and re-distribute the latter energy during import periods. Considering the annual sequence $\boldsymbol{I}$ of typical days p resulting from the temporal data classification process ($\boldsymbol{I} = \{p_j \mid j \in \boldsymbol{J}\}$), the storage state-of-charge SOC is defined through Eqs. 1.54 and 1.55, where the index j refers to the day of the year ($\boldsymbol{J} = \{1, ..., 365\}$). Subsequently, the GSE capacity is simply determined by the maximum SOC occurring during the clustered DRY (Eq. 1.56).

$$SOC_{j,t+1} = SOC_{j,t} + \left(\dot{E}_{\text{grid},p_j,t}^{-} - \dot{E}_{\text{grid},p_j,t}^{+} \right) \cdot \mathrm{d}_t \qquad \forall j \in \boldsymbol{J}, p_j \in \boldsymbol{I}, t \in \boldsymbol{T} \setminus \{|\boldsymbol{T}|\} \tag{1.54}$$

$$SOC_{j+1,1} = SOC_{j,t} + \left(\dot{E}_{\text{grid},p_j,t}^{-} - \dot{E}_{\text{grid},p_j,t}^{+} \right) \cdot \mathrm{d}_t \qquad \forall j \in \boldsymbol{J}, p_j \in \boldsymbol{I}, t = |\boldsymbol{T}| \tag{1.55}$$

$$C_{\text{GSE}} = \max_{j \in \boldsymbol{J},\, t \in \boldsymbol{T}} SOC_{j,t} \tag{1.56}$$

One percent peak   The one percent peak (OPP) assesses the average electric power flow within the one percentile of recorded flows throughout the year. Analysed by [78, 79], the following metric is expressed in Equation 1.57 and is implemented with the aim of assessing the grid utilization in terms of peak power requirements. In the latter definition, the operator P_i refers to the i-th percentile function while $\dot{E}_{\text{grid}}^{P_i}$ denotes the associated absolute electricity profile threshold.

$$\text{OPP} = \frac{\sum_{p=1}^{P} \sum_{t=1}^{T} \begin{cases} |\dot{E}_{p,t,\text{grid}}^{+} - \dot{E}_{p,t,\text{grid}}^{-}|, & \text{if } |\dot{E}_{p,t,\text{grid}}^{+} - \dot{E}_{p,t,\text{grid}}^{-}| \geq \dot{E}_{\text{grid}}^{P_1} \\ 0, & \text{otherwise} \end{cases}}{\sum_{p=1}^{P} \sum_{t=1}^{T} \begin{cases} \mathrm{d}_p \cdot \mathrm{d}_t, & \text{if } |\dot{E}_{p,t,\text{grid}}^{+} - \dot{E}_{p,t,\text{grid}}^{-}| \geq \dot{E}_{\text{grid}}^{P_1} \\ 0, & \text{otherwise} \end{cases}} \tag{1.57}$$

$$\dot{E}_{\text{grid}}^{P_1} = P_1 \left(|\dot{E}_{p,t,\text{grid}}^{+} - \dot{E}_{p,t,\text{grid}}^{-}| \right) \tag{1.58}$$

Building storage equivalence   The change in consumption behaviour resulting from the use of different BES control techniques can be represented, in view of the power network operator, as a virtual electrical storage capacity: the building storage equivalence (BSE). Similarly to the grid energy storage metric, the BSE is defined by interpreting differences in the

hourly net power profiles Δ for each typical period p as charging Δ^+ or discharging Δ^- rates. Equations 1.59 to 1.61 details the latter formulation where the subscripts $\prime$ refer to the initial profiles (e.g. resulting from RBC). In addition, the BSE round-trip efficiency ϵ^{BSE} resulting from the difference in BES behaviour is determined according to Equation 1.63.

$$\Delta^+_{p,t} - \Delta^-_{p,t} = \left(\dot{E}^+_{\text{grid},p,t} - \dot{E}^-_{\text{grid},p,t} \right) - \left(\dot{E}^{+,\prime}_{\text{grid},p,t} - \dot{E}^{-,\prime}_{\text{grid},p,t} \right) \qquad \forall p \in \boldsymbol{P}, t \in \boldsymbol{T} \quad (1.59)$$

$$\Delta^+_{p,t}, \Delta^-_{p,t} \geq 0 \qquad \forall p \in \boldsymbol{P}, t \in \boldsymbol{T} \quad (1.60)$$

$$SOC_{p,t+1} = SOC_{p,t} + \left(\Delta^+_{p,t} - \Delta^-_{p,t} \right) \cdot \mathrm{d}_t \qquad \forall p \in \boldsymbol{P}, t \in \boldsymbol{T} \quad (1.61)$$

$$C_{\text{BSE}} = \sum_{p=1}^{\boldsymbol{P}} \left(\max_{t \in \boldsymbol{T}} SOC_{p,t} \right) \cdot \mathrm{d}_p \qquad (1.62)$$

$$\epsilon_{\text{BSE}} = \sum_{p=1}^{\boldsymbol{P}} \left(\frac{\sum_{t=1}^{\boldsymbol{T}} \left(\Delta^-_{p,t} \cdot \mathrm{d}_t \right)}{\sum_{t=1}^{\boldsymbol{T}} \left(\Delta^+_{p,t} \cdot \mathrm{d}_t \right)} \right) \cdot \mathrm{d}_p \qquad (1.63)$$
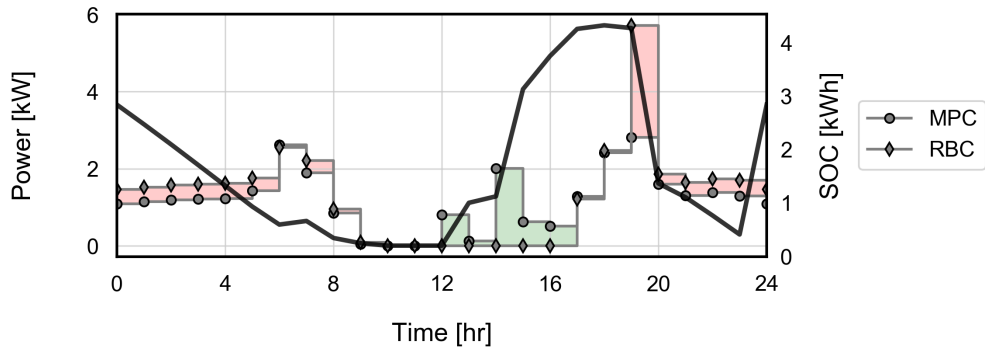
Figure 1.10 – Building net power profiles and state-of-charge of the virtual battery (BES) during typical early spring day. The coloured areas represent charging (green) and discharging (red) periods respectively

Figure 1.10 illustrates the introduced concept for typical early spring day; during day-time, the penetration of renewable energy sources engenders a negative power balance while during night-time the latter is positive. Nevertheless, when operating the building energy systems with MPC, the local controllers seek to shift controllable loads from low towards high generation periods to benefit from the on-site produced electricity which explains the difference in power profiles. The former change in consumption behaviour might be represented as a grid operated storage system charged during positive profile difference periods (green areas) and discharged during negative ones (red area). The resulting BES state-of-charge is represented by the black curve which nearly returns to its initial state at the end of the operating period

p in view of the cyclic set definition (Table 1.2). Indeed, the difference between $\text{SOC}_{1,p}$ and $\text{SOC}_{n_t+1,p}$ (Eq. 1.63) results from the change in daily electricity consumption and can be interpreted as the BES round-trip efficiency ϵ^{BES}. It is worth noting that the latter value might be both positive or negative since the use of MPC may improve the overall system efficiency.

A systematic approach: multi-objective optimization

Although representing a rapid and straightforward formulation, widely implemented in the field of BES sizing [41, 54, 56, 58, 59], single objective optimization approaches reflect substantial limitations when targeting multiple metrics simultaneously. Indeed, in order to incorporate the latter into an unique function, a weighted trade-off formulation is commonly implemented. In the case of a total expenses approach, these weights are represented by the energy tariffs, interest rate and the investment expenses associated to each unit. A small change in these parameters might however completely alter the resulting system configuration and the associated operation strategy. Moreover, since the aim of this study is in analysing the penetration of distributed and renewable generation technologies under different boundary conditions, a more effective, *systematic* optimization technique is required.

Consequently, an different problem formulation is adopted: ϵ-constraint multi-objective optimization. Indeed, the latter method has the advantage of *systematically* generating multiple interesting solutions and thus, providing different layout options to the various stakeholders. In view of properly screening the entire feasible solution space, the optimization algorithm is executed using a lexicographic approach [80] and first minimizes each objective function in an unconstrained manner prior evaluating intermediate Pareto points. In the following study, the primary objective function targets the operation expenses (Eq. 1.34) while the second is represented by the capital expenses (Eq. 1.35). Equation 1.64 states the associated problem formulation.

$$\min_{\Sigma} \ C^{\text{op}}$$

$$\Sigma = \left\{ F_u, Y_u, f_{u,p,t,(s)}, y_{u,p,t}, \delta_{u,p,t}, f_{u,p,t,(s)}^{+/-}, T_{b,p,t}, \dot{R}_{k,p,t}, \dot{Q}_{s,k,p,t}^{+/-}, \dot{E}_{\text{grid},p,t}^{+/-}, \dot{H}_{\text{grid},p,t}^{+/-} \right\}$$

subject to
$$\hspace{11cm}(1.64)$$

$$C^{\text{cp}} \le \epsilon_{\text{cp}}$$

Eq. 1.6 - Eq. 1.33 and Eq. A.1 - Eq. A.25

1.4 Application: three typical buildings

In order to validate the presented modelling and optimization framework, the latter is applied on three different building types: a single family house, an apartment block and an administrative building. The objective of these case studies is indeed to analyse the impact of dwelling characteristics on both the optimal BES configuration and the associated performance indicators. Through the application of increasingly stricter network utilization constraints, additional solutions are generated to highlight the economic and energetic impact of the related "grid-aware" system configurations. Table 1.3 presents general information for each dwelling while detailed parameters values of the different unit models are reported in Appendix A.

Table 1.3 – General building information

	Single family house	Apartment block	Office building		
Energy ref. area	189	1750	2750	$[m^2]$	
Roof area	0.30	0.06	0.07	$[m^2/m^2]$	
Heating demand	123	52	56	$[kWh/m^2]$	[81]
Cooling demand[a]	×	×	✓		
Electricity demand	18.2	18.4	43.2	$[kWh/m^2]$	[65]
Hot water demand	234	307	50	$[l/m^2]$	[65]
Internal gains	23.9	26.9	56.2	$[kWh/m^2]$	[65]
$T_0^{h,s}/T_0^{h,r}$	65/50	65/50	41.5/33.9	$[°C]$	[81]
$T_0^{c,r}/T_0^{c,r}$	-/-	-/-	12/17	$[°C]$	[81]
$T_0^{ext,h}/T_0^{ext,c}$	-4/35	-4/35	-4/35	$[°C]$	[81]
$T_{b,0}$	20	20	20	$[°C]$	[81]
U_b^{ext}	2.04	2.14	1.36	$[W/°C \cdot m^2]$	[81]

[a] No cooling measurements reported in [81] and thus no calibration on the internal gains

In regard to the weather conditions, all buildings are considered to be located in the region of Geneva, thus applying the previously defined clustered temperature (T^{ext}) and global horizontal irradiation (GHI) profiles (Section 1.3.1). Additional time series not derived from the latter (i.e. EL and HW demand profiles) are evaluated from the national engineering and architect standards (SIA 2024 [65]) without any inter-day variations. Normalized profiles of these energy service requirements are represented in Figure A.3.

Finally, in order to facilitate the result analysis, ϵ-constraint (i.e. investment expenses) thresholds are henceforth only denoted through the relative increase in between optimization processes while the unconstrained minimization of each objective function (investment and operating expenses) are represented by the labels S_0 and S_1 respectively. All following computations are performed with the commercial solver CPLEX 12.7 on a single machine including a double core 2.4 GHz CPU and 8 GB RAM. The maximum tolerated relative optimality gap

(MIP gap) is set to 0.1%.

Single family house (SFH)

Sizing and operation   In regard to the first building case study, Figure 1.11 depicts the evolution of both the different cost contributions (Fig. 1.11a) and the considered key performance indicators (Fig. 1.11b) with respect to the gradual ϵ-constraint relaxation. The minimum investment solution (S_0) solely comprises a natural gas fired boiler to satisfy all thermal energy service demands in addition of a small domestic hot water tank (Eq. A.2), thus representing the standard fossil-fuel based BES configuration. Subsequently, with the increase in available capital, following technology and performance changes are observed:

- **$S_{0.1}$** With the first increase in investment, a small PVA is installed generating nearly 86% of the annual electricity needs while solely 32% is self-consumed on-site. Due to the low carbon intensity of the national electricity mix, the observed reduction in greenhouse gas emission is rather limited (-5%).

- **$S_{0.2}$** The main conversion unit is replaced by an efficient air-water heat pump (AHP), including the required technical buffer tank (Eq. A.2) and auxiliary electrical heaters to reach higher supply temperature ($\geq$ 55°C) during strong thermal service periods. Although substantially increasing the system electricity consumption (+211%), the latter technology shift strongly reduces the associated environmental impact (-85%), mainly related to the removal of natural gas from the system primary energy supply. From a power network perspective, this electrification of thermal energy services however engendered a strong OPP rise of 144%.

- **$S_{0.3-0.4}$** The photovoltaic array (PVA) is expanded, until fully reaching the maximal roof hosting capacity (Eq. A.1). Simultaneously, electrical (BAT) and thermal storage (HST and HWT) capacities are gradually increased until reaching, in the case of HWT, the daily service demand volume[4]. These additional capacities substantially decrease operating expenses ($S_{0.4}$: -48%), mainly due to the associated drop in electricity import ($S_{0.4}$: -25%) and respectively excess exports. In regard to the distributed generation integration, the BES self-sufficiency rises from 21% to 41% while the self-consumption drops from 64% to 49% ($S_{0.4}$). Consequently, with the latter consumption reduction of on-site produced electricity, the equivalent grid storage utility (GES) increases to 1.7 MWh/100m^2, roughly representing 68 m^3/100m^2 of lithium-ion battery racks[5]. Similarly, the OPP indicator continues rising until reaching 2.6 kW/100m^2; nevertheless, in contrast to $S_{0.2}$, this further increase is mainly driven by power injection peaks from high renewable generation periods. On the other hand, the greenhouse gas emissions associated to the BES operation continue dropping, reaching solely 0.3 tCO$_2$-eq./yr for configuration $S_{0.4}$.

---

[4]Hot water (HW) energy service demands are expressed in litres
[5]Assuming a volumetric energy density of 0.04 kWh/m^3 [82]

- $S_{0.5-0.6}$ Further thermal (HST) and particularly electrical (BAT) storage capacities are implemented to improve the integration of renewable-based generation as expressed by the rise in both self-sufficiency and self-consumption. However, despite these improvements, both power network indicators solely merely change: the GES and OPP drop by $\geq 0.01\%$. Consequently, the strong increase in BAT capacity is not used to shave peaks in electricity export while solely shifting energy on a daily basis. Additionally, the operating expenses are solely slightly enhanced, decreasing by 2.4% with respect to the initial solution S_0.

- $S_{0.7-1.0}$ A combination of CHP and AHP technologies is finally activated as primary conversion system while storage capacities are drastically reduced. In view of the consequent distributed generation potential, the BES becomes electrically autonomous (SS $\geq$ SC), however still relying on the power network for balancing seasonal mismatches. With the further expansion in storage capacities, the GES finally drops to zero: the BES constantly satisfies its own electricity demand. Hence, the annual import value drops to null while the aggregated export reaches 2.1 MWh/100m^2 (S_1). On the other hand side, the OPP indicator remains around the previous value of 2.4 kW/100m^2, reflecting the lack of improvement regarding electricity export peaks. Finally, due to the anew use of natural gas, the system GHG emissions rise again to around 2.1 tCO$_2$-eq./yr (S_1), nevertheless remaining substantially lower than the impact of S_0.

Regarding the system total expenses, denoted as monthly service costs in Fig. 1.11a, the fossil-fuel based solution S_0 represents the most cost-efficient configuration under the economic parameters applied. Nevertheless, it is worth mentioning that, the latter BES solutions have been assessed with the assumption of perfectly predicting the average energy tariffs for the entire project lifetime (in this case 20 years). Therefore, in order to provide a more reliable result interpretation, Figure 1.11a further depicts the expect error ranges for each BES configuration when accounting for energy cost deviations, both for natural gas and electricity (Table 1.4). The latter parameters have indeed a strong impact on system economic performance [83]; additional inputs such as the annual electricity demand and equipment costs have however a far lower influence on the BES total expenses and thus, are not included in the following sensitivity analysis.

As observed, the increasing rise in renewable generation (PVA) and consequent degree in self-sufficiency, the economic performance uncertainty substantially decreases ($S_{0.3-0.6}$). Nevertheless, with the anew use of natural gas in cogeneration units, the error range increases again. Finally, in order to show the potential impact of an economic incentivization scheme, the same total expenses curve is represented while considering a 15% governmental investment subsidy[6] on distributed generation (CHP & PVA) and efficient conversion units (AHP). Although not altering the cost optimality of S_0, environmentally friendly and economically "robust" solutions ($S_{0.3-0.6}$) are drawn nearer to the latter threshold.

---

[6]This value approximately correspond to the national subsidy for novel PVA installations in Switzerland. Other economic retributions are however defined at state level and therefore, are subject to substantial variations.

Building energy system expenses breakdown

(a) Expense contributions per BES configuration

(b) Key performance indicator per BES configuration
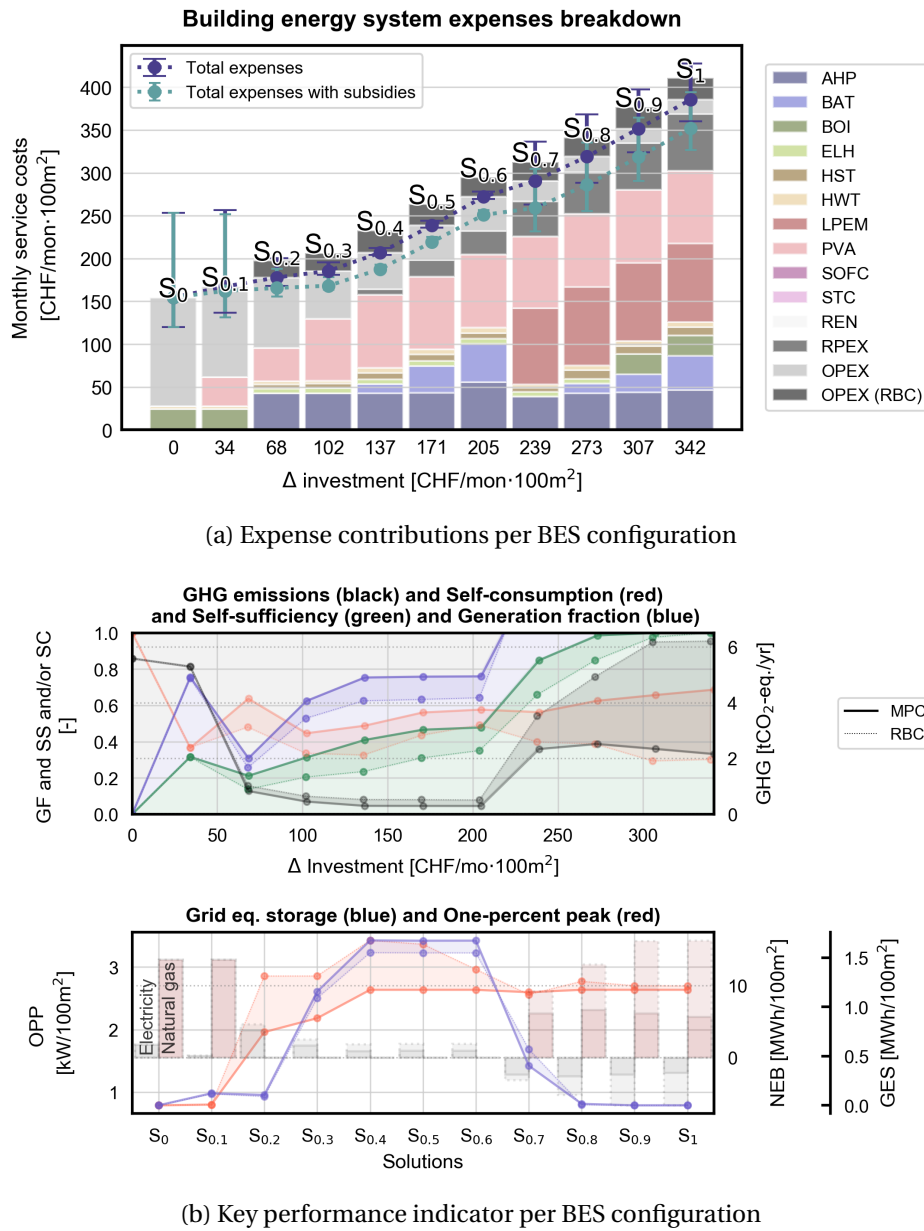
Figure 1.11 – Multi-objective optimization results for an existing single family house

Table 1.4 – Energy tariff uncertainty

	Tariff [CHF/kWh]	Range[a]
Electricity	0.24	[-13%, 30%]
Natural gas	0.08	[-33%, 97%]

[a] Estimated from historical tariff variations over 20 year periods in Switzerland [1]

Rule-based operation   In addition of analysing the system results when considering an optimal scheduling technique (MPC), Figure 1.11 highlights the impact of a non-predictive rule-based control (OPEX RBC) approach. Indeed, Figure 1.11a displays in dark grey the additional expenses due to the use of a RBC instead of an MPC, differences ranging form $\geq$ 0.01% for S_0 to 161% in the case of $S_{1.0}$. Similarly,Figure 1.11b depicts the disparities between the two control strategies in terms of distributed generation integration and power network KPI, with MPC always performing better for all BES configurations

The main differences between MPC and RBC can be explained as follows:

- In the case of S_0 and $S_{0.1}$, the minor changes in operation is explained through the HWT management since the MPC attempts in minimizing thermal storage losses in regard to the prediction of future hot water withdrawals. However, in view of the remaining service requirement, no change in strategy is noticed; SH needs are set to the lower comfort boundary when possible (i.e. minimized) while EL are fixed a-priori.

- The cost-efficient operation of a bivalent heat pump based heating system (AHP and ELH) explains the main saving in consumption appearing from $S_{0.2}$. Indeed, the MPC attempts in exploiting both the varying source temperature (T^{ext}) and the discrete supply options (T^{supply}) to improve the unit coefficient of performance (COP) and hence, to minimize electricity consumption. Hence, with the installation of an AHP-ELH bivalent heating system, the MPC applies an optimal supply temperatures in the HHS by forecasting internal and solar gains while simultaneously exploiting higher external temperatures to shift controllable thermal energy services (SH and HW). Obviously, the latter strategy engenders a rise in SH demand since the associate rise in internal temperature (T^{in}) induces additional heat losses thorough the building envelope. Nevertheless, in regard to the applied objective function, the control technique is able to drastically decrease the use of inefficient auxilary units (ELH) and consequently, to decrease the building primary energy demand. Figure 1.12a illustrates the latter phenomena.

- With the additional expansion in PVA and storage capacity, the MPC further improves the integration of distributed and renewable generation. Especially in the mid-season period, when daily demand and generation are rather similar, optimal predictive control efficiently dispatches the different conversion and storage units to fully exploit on-site electricity production (Figure 1.12b).

- Finally, with the integration of a CHP device, the operational disparity between both control strategies drastically increases. Indeed, in RBC, the CHP is *heat driven* and thus, follows thermal services requirements while the AHP, BOI or ELH act as auxiliary heating units. On the other hand side, in MPC, the CHP load is coordinated in regard to the electricity consumption of the AHP and the domestic EL energy services (*power driven*) as depicted in Figure 1.12c. The impact of this control approach is particularly reflected by strong difference in the natural gas use and thus, the associated rise in greenhouse gas emissions ($S_{1.0}$: +191%). It is worth mentioning that, in view of the current sizing

guidelines, the latter CHP capacity is typically oversized for RBC approaches when using the following optimal control based algorithm.

As introduced in Section 1.3.3, the changes in operation engendered by different control approaches can be expressed by an equivalent electrical storage capacity (BES). Table 1.5 presents the respective KPI characteristics for different BES configurations. In view of the indicator definitions in Eqs. 1.61 to 1.63, round-trip efficiency values exceeding 1.00 reflect a lower electricity consumption when applying MPC ($S_{0.2-0.6}$) as discussed previously.

Table 1.5 – General building information

			S_0	$S_{0.2}$	$S_{0.4}$	$S_{0.6}$	$S_{0.8}$
SH	*MPC*		12.06	12.48	12.36	12.32	12.3
	RBC		12.06	12.06	12.06	12.06	12.06
EL	*MPC*	[MWh/100m^2·yr]	1.82	3.78	0.91	0.98	-2.69
	RBC		1.82	4.6	1.83	1.9	-5.19
NG	*MPC*		13.62	0	0	0	6.64
	RBC		13.62	0	0	0	12.92
BES	C	[kWh/100m^2]	0	3.34	4.74	5.24	9.09
	ϵ	[-]	1	2.19	1.88	1.9	0.5

It is worth mentioning that the presented comparison solely highlights the use of two extreme control techniques (non/fully predictive) and should not be taken as a comprehensive assessment for future control strategies. The main aim of this analysis relies in highlighting the impact of using optimization-based control strategies during the sizing and operation phases to decrease the need of further downstream investments (e.g. seasonal storage). The choice of a rather simple RBC strategy as baseline performance is mainly justified by its widespread use in residential and service buildings throughout Switzerland [84]. However, different rule improvements such as a clock or voltage drop based technique are available to rise the self-consumption of renewable sources [85]. Nevertheless, the exhaustive assessment and comparison of these different operation strategies lies outside of this study's scope.
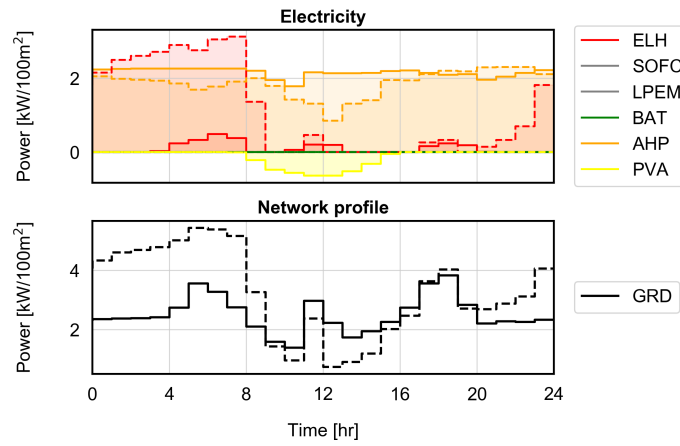
(a) BES configuration $S_{0,2}$ - unit operation for a typical winter period (day 7)
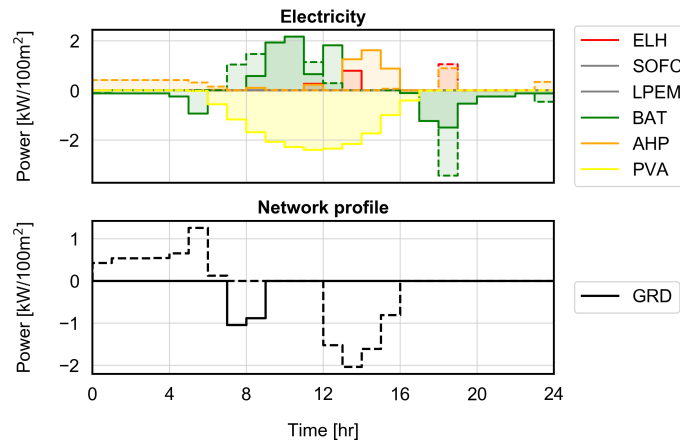
(b) BES configuration $S_{0,6}$ - unit operation for a typical early autumn period (day 264)
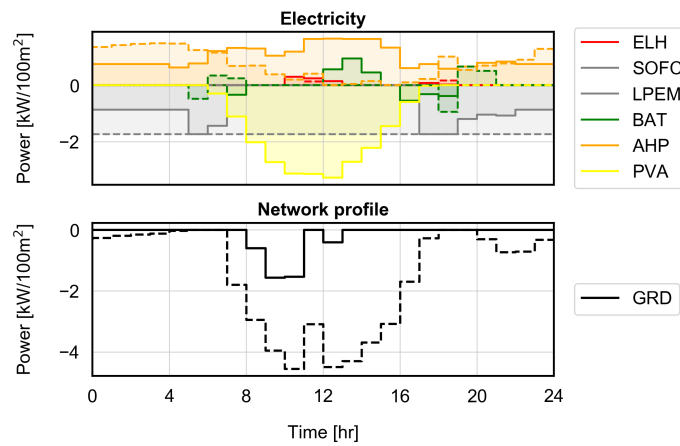
(c) BES configuration $S_{0,8}$ - unit operation for a typical early spring period (day 72)

Figure 1.12 – Typical operating period electricity consumption/generation for an existing single family house (*full line:* MPC - *dashed line*: RBC)

Grid-aware sizing   In light of the applied network performance indicators, namely the one percentile peak (OPP) and the grid equivalent storage (GES), multiple BES configurations presented in Figure 1.11 reflect a strong impact on the power grid, both in terms of seasonal storage and peak load requirements. Hence, in order to generate additional, grid-aware BES solutions, a second ϵ-constraint is implemented in the problem formulation of Eq. 1.64: the grid multiple (GM). Defined in Equation 1.65, the GM limits the maximal (and respectively minimum) electrical power exchanges between the distribution network and the building with respect to the average annual consumption.

$$\text{GM} = \frac{(\dot{E}^{+}_{\text{grid},p,t} - \dot{E}^{-}_{\text{grid},p,t})}{\frac{1}{8760} \sum\limits_{p=1}^{P} \sum\limits_{t=1}^{T} (\dot{E}^{+}_{\text{grid},p,t} - \dot{E}^{-}_{\text{grid},p,t}) \cdot \mathrm{d}_p \cdot \mathrm{d}_t} \tag{1.65}$$

Considering the same case study, Figure 1.13 depicts the associated evolution graphs when the additional constraint is enforced, with an ϵ^{GM} equal to the GM value of the standard solution S_0; the latter represents indeed the current grid utilization status of a purely fossil-based energy system satisfying all thermal services (SH and HW), the sole variations in power demand being hence related to the predefined electricity needs for appliances (EL). In light of the BES results in Figure 1.13a, major changes are related to the direct installation of a bivalent AHP-ELH heating system in $S_{0.1}$. Similarly, at higher investment thresholds, the second shift in primary conversion unit (AHP-CHP) is observed earlier ($S_{0.6}$). A small BAT remains nevertheless necessary to flatten the BES net electricity profile.

From an integration perspective, the GM ϵ-constraint and the resulting change in BES behaviour (MPC-B), strongly improve the system self-consumption; the indicator remains between 66% and 100% throughout the entire BES solution set. Consequently, due to the lack of any substantial electricity exports, GES values are strongly reduced, remaining between 0 and 0.5 MWh/100m^2 ($S_{0.4}$ -84%). A similar behaviour is observed for the OPP; despite rising with the first technology switch, from a BOI to a AHP primary conversion unit, and the associate increase in electricity consumption, the indicator continuously decreases with the increase in distributed generation capacity. Although being primarily applied to generate additional BES configurations, the GM ϵ-constraint hence provides an interesting mean to induce "grid-aware" solutions, reflected by both the GES and OPP indicators. Noticeably, in order to formerly validate the latter design and operation constraint, additional analyses should be conducted, using shorter time resolution simulations and network connection models [86]; however the latter fall beyond the main focus of this study and thus, is not carried out throughout the following sections.

Finally, in regard to the economic disparities, the difference in operating expenses between both problem formulations (with and without GM constraint) is mainly explained by the partial curtailment of the PVA generation. Figure 1.14 illustrates the latter operational disparities between both control formulations while Table 1.6 presents the difference in network oriented KPI. Interestingly, the resulting loss in electricity production is not captured by the SS

indicator, which solely accounts for the direct use of on-site electricity production and not the total amount. In order to render the latter solutions appealing also from a cost perspective (i.e. reflecting similar total annualized expenses as the associated non-constrained solutions) a subsidies scheme could be introduced by network operators to incentivize end-users in adopting grid-aware solutions and thus, mitigate future investment expenses into centralized storage systems. Table 1.6 indeed presents the associated peak (OPP) and storage (GES) equiv-
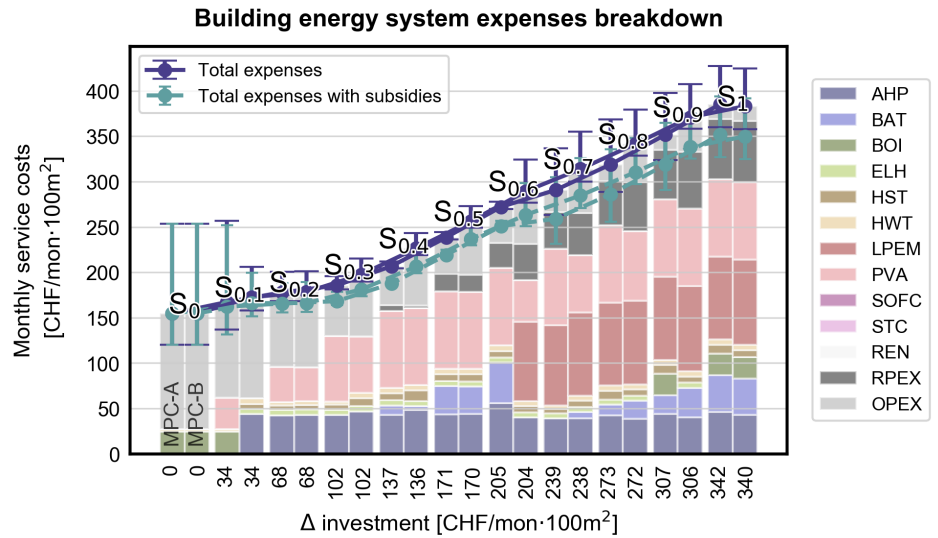
(a) Expense contributions per BES configuration
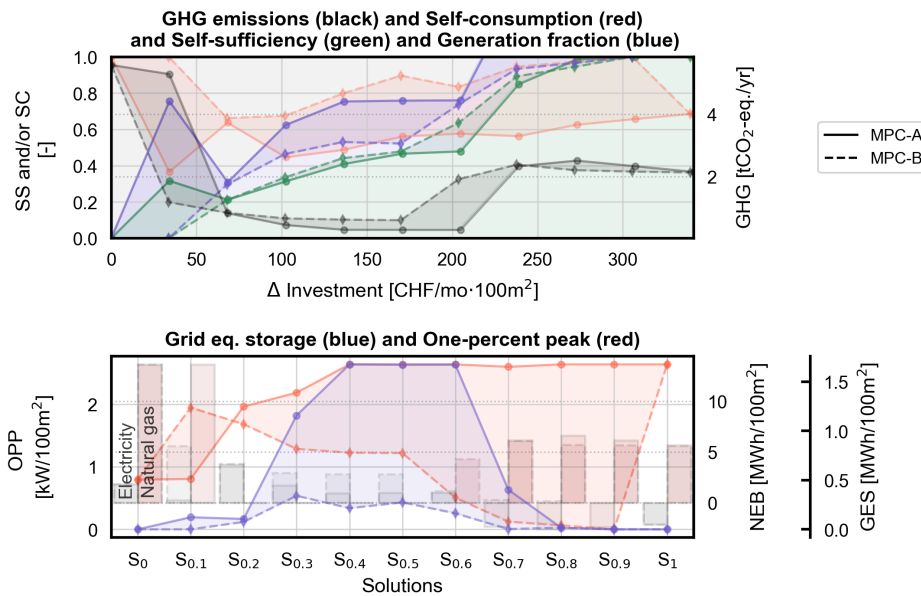
(b) Key performance indicator per BES configuration

Figure 1.13 – Multi-objective optimization results for an existing apartment block
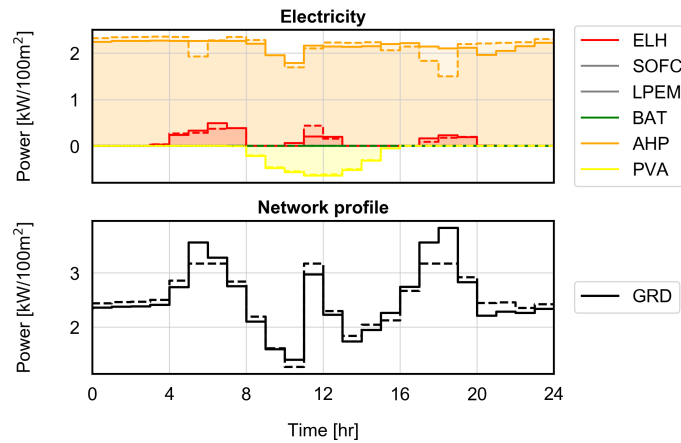
(a) BES configuration $S_{0,2}$ - unit operation for a typical winter period (day 7)
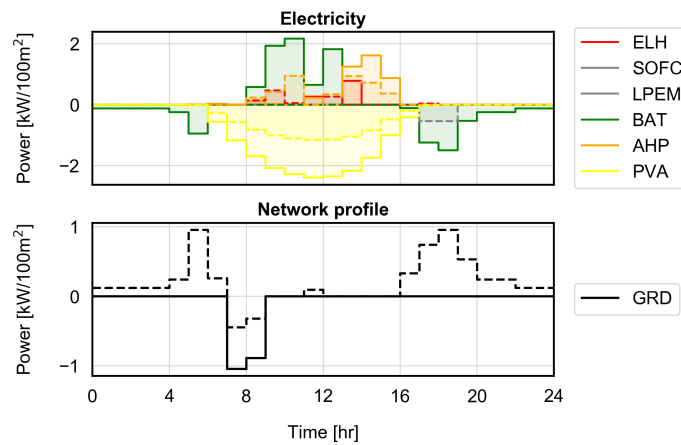
(b) BES configuration $S_{0,6}$ - unit operation for a typical early autumn period (day 264)

Figure 1.14 – Typical operating period electricity consumption/generation for an existing single family house (*full line:* MPC - *dashed line*: MPC with GM = 1)

alent investment expenses (C-eq.) required in order to render the respective GM configuration cost-optimal.

Table 1.6 – BES performances for GM constrained and unconstrained problem

		S_0	$S_{0.2}$	$S_{0.4}$	$S_{0.6}$	$S_{0.8}$
Δ C^{op}	[CHF/100m^2·mon]	0	-6.01	-243.47	-220.65	-294.31
Δ GES	[MWh/100m^2]	0	0.02	1.46	1.51	-0.02
Δ OPP	[kW/100m^2]	0	0.25	1.41	2.13	2.57
C^{GES}-eq.	[kWh/CHF]	0	0.24	0.41	0.47	0
C^{OPP}-eq.	[W/CHF]	0	2.88	0.4	0.66	0.6

[a] Considering a project interest rate of 3.125% (for the power generation and distribution system industry [87])

Large buildings

Finally, in order to compare the single family house (*a*) to additional dwelling types, Figure 1.15 presents the associated results to the case studies (*b*) and (*c*).

In the case of (***b***), a similar configuration trend is noticed with the increase in capital; nevertheless, the activation of the AHP-CHP combination occurs earlier ($S_{0.3}$), mainly due to the lower relative fixed investment inv_1 value associated to the CHP cost function. With the further relaxation of the ϵ-constraint, an increasing PVA is installed until observing a switch to the fuel cell technology ($S_{0.8}$). In order to fully render the BES self-sufficient, additional storage capacities are installed in the last configurations. In view of the total BES expenses, the standard fossil-fuel based configuration (S_0) does not represent the most economic solution. Indeed, under the considered input parameters, the cost-efficient solution is $S_{0.5}$, both with and without state subsidies. Since $S_{0.5}$ still relies on natural gas to provide the required energy services, the associated economic uncertainty remains higher than a full electrified solution ($S_{0.2}$); however, the range remains substantially lower than the error span of standard fossil-fuel based solution (S_0).

From a power network perspective, the need of seasonal storage capacity to shift distributed generation (GES) is substantially lower in comparison to (*a*): the sole noticeable increase is observed with the combination of SOFC and PVA. Indeed, due to the low operational flexibility of SOFC units, the resulting generation can not be modulated according to the current electricity demand and thus, the excess is exported to the grid. In regard to the network utilization, the installation of an AHP as primary conversion unit ($S_{0.2}$) substantially increases the OPP value (+191%). However, with the introduction of CHP units, the KPI decreases step wise, first with the installation of a SOFC and subsequently with the use of a LPEM.

In the case of (***c***), a similar configuration trend is observed; however, in view of the higher specific energy service demands (Fig. A.3) and thus, the resulting operating share within the total monthly service expenses, distributed generation from CHP is even more interesting from an economical perspective. Indeed, the latter is reflected by the stronger natural gas consumption as well as the associated greenhouse gas emissions which, for S_1, reach similar values than the initial solution S_0. Nevertheless, as reflected by the SC indicator of each BES configuration, the on-site produced electricity is directly exploited to satisfy the strong energy service demands. Similarly to (***b***), the cost-optimal configurations are represented by $S_{0.7}$, with and without state subsidies. Finally, from a power network perspective, the OPP indicator follows similar decreasing trend as (***b***) while the GES is obviously null due to the lack of electricity exports.
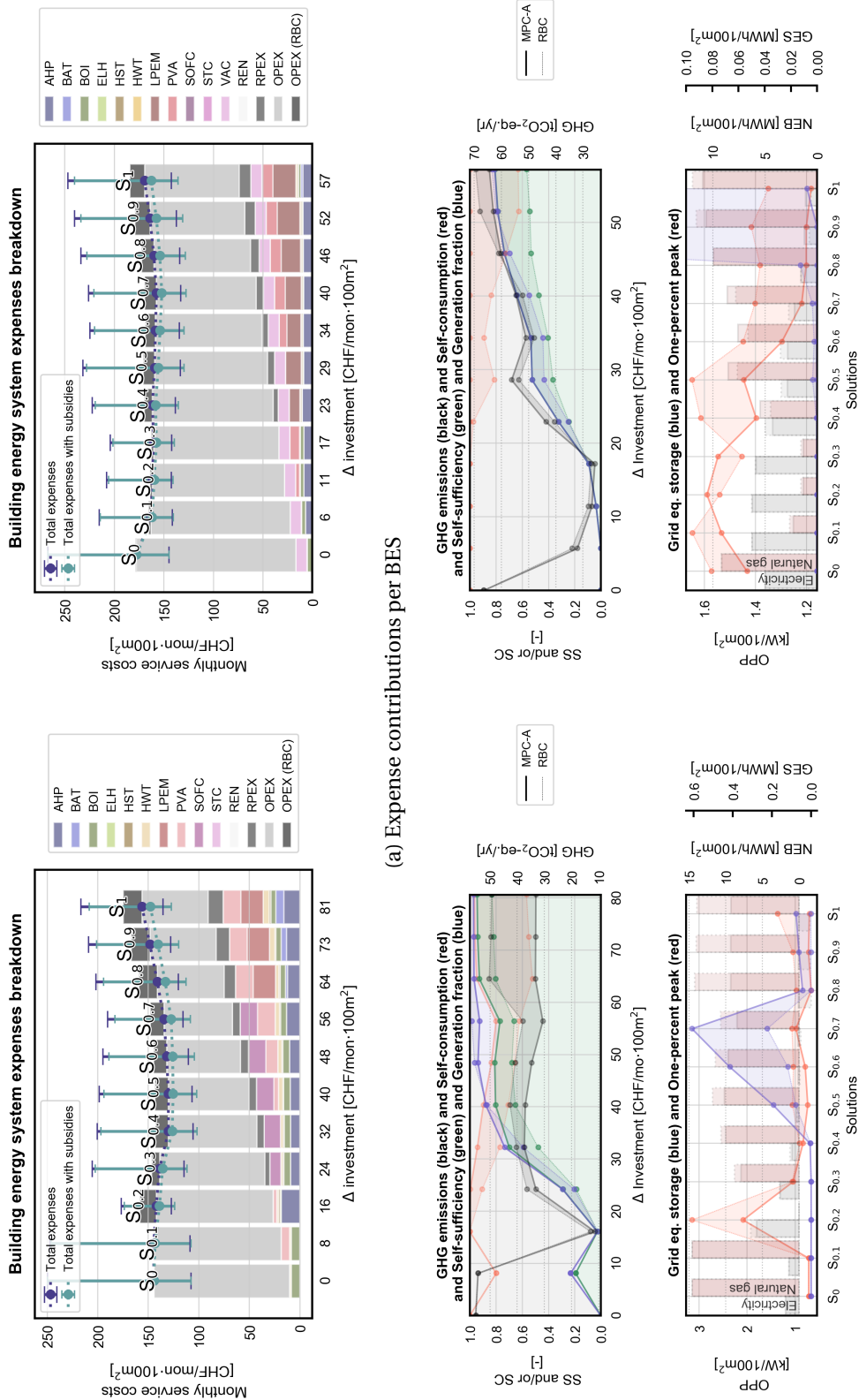
(a) Expense contributions per BES

(b) Performance indicators: self-sufficiency (red), self-consumption (green) and equivalent grid battery (blue)

Figure 1.15 – Multi-objective optimization results for *left* an apartment block (AB) and *right* an office building (OB)

1.4.1 Envelope and heating system refurbishment

In order to highlight the impact of renovation on the energy system performance indicators and configuration, the previously introduced case studies are anew implemented while considering a refurbished dwelling envelope and heat distribution system. In regard to the values assessed by [31], the first item acts on the overall heat transfer coefficient U while the second decreases both the system nominal supply $T_0^{h,s}$ and return $T_0^{h,r}$ temperatures. The corresponding investment costs are estimated using a linear function in regard to the annual space heating demand difference: 1.02 CHF/MJ·yr.[7]

Figure 1.16 hence presents the BES configuration for the renovated single family house (***a***); the refurbishment costs (REN) represent a substantial share of the total system expenses while both the unit and operating costs are decreased. These reductions are indeed explained by both the lower peak power and energy requirements in service demands (SH). However, in view of the prior results detailed in Fig. 1.11a, the dwelling renovation does not compensate the latter decreases and thus, considering the applied input parameters, is economical not viable. Similarly, Figure 1.16a highlights an expected error margin when implementing a constant uncertainty range on both energy tariffs op: electricity and natural gas. As expected, the resulting disparity decreases with the rising self-sufficiency and the shift towards an fully electrified BES ($S_{0.3-0.4}$); nevertheless, with further increase in investment expenses and the penetration of CHP units, the error margin increases again.

Additionally, Figure 1.16b directly compares the system KPI for the non- (MPC-A) and renovated (MPC-B) case study in regard to the relative increase in capital investment, the initial solution being S_0. Although observing a strong difference for the initial configuration (S_0), the economic gap rapidly decreases; indeed, starting from $S_{0.3-0.4}$, both the non- and renovated configurations show similar SS values while reaching the net-ZEB threshold (GF≥1). The latter is again explained by the lower unit size required to satisfy the novel SH demands. In regard to the power network indicators, the maximal GES observed is decreased by nearly -0.4 MWh/100m^2. On the other hand side, since for higher distributed generation penetration solutions the OPP is driven by the latter export peaks, no improvements are noticed with the building refurbishments.

In the case of a refurbished apartment block (***b***), the difference in investment expenses observed is much higher. Indeed, in regard to the linear refurbishment cost estimation applied, the REN expense share represented between 92% (S_0) and 52% (S_1) of the total investment costs. For sake of readability, distributed generation integration KPI in Figure 1.16b have been rescaled in function of S_0 investment expenses for the renovated case study. Hence, similarly to the SFH, refurbished BES configurations rapidly reach the net-ZEB threshold (GF≥1) while reflecting lower equivalent greenhouse gas emissions. From a network perspective, refurbishment allows for substantially decrease in both GES and OPP peak values observed over

---

[7]Average cost value from around 300 building refurbishment projects performed in Switzerland between 2000 and 2012 by a Swiss consulting office

(a) Expense contributions per BES

(b) Performance indicators: self-sufficiency (red), self-consumption (green) and equivalent grid battery (blue)

Figure 1.16 – Multi-objective optimization results for (refurbished) *left* an single family house (SFH) and *right* an apartment block (AB)
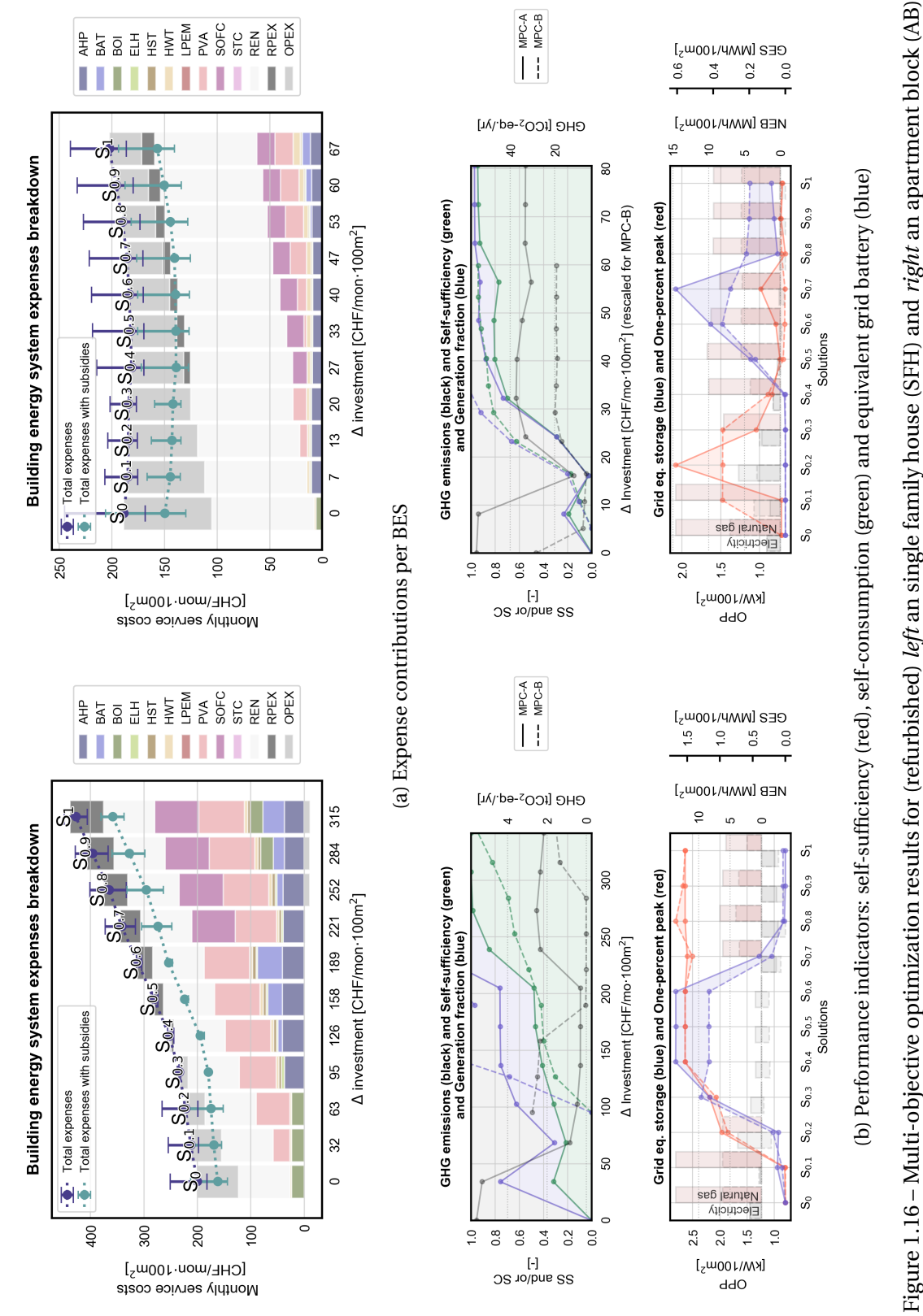
the solution set; the related disparities are noticed for $S_{0.7}$ (-0.3 MWh/100m^2) and $S_{0.2}$ (-0.6 kW/100m^2) respectively. Finally, a direct total expenses comparison between both he non- and renovated case studies is represented in Figure A.4

1.5 Conclusion

This chapter presented a comprehensive modelling framework (MF) and optimization strategy for building energy systems sizing and operation. The different units have been described using mixed integer linear programming techniques (MILP) in order to account for both the discrete and continuous dynamics of the devices while including specific scheduling and sizing constraints. In addition, the implementation of both the heat cascade and a heat distribution system model allowed filling existing gaps in the current literature, thus providing a better estimation of flexible thermal service requirements. Subsequently, the developed method has been successfully applied to analyse the integration of solar-based renewable and distributed energy sources for typical building categories. Specific performance indicators are finally assessed to reflect the latter degree of integration and compare the different system configurations generated through the proposed systematic approach.

In view of the considered economic parameters, standard fossil-based solutions (S_0) comprising a single natural gas fired boiler and a small domestic hot water tank still represent the cheapest configuration for small residential dwellings; nevertheless, in view of the inherent instability of imported energy tariffs in addition to the increasing taxation of non-renewable sources, more sustainable system designs become interesting candidates for future refurbishments:

- The combination of heat pumps (AHP) and photovoltaic arrays (PVA) recurrently appears throughout the different case studies, particularly for low service demand dwellings (i.e. single family house). In comparison to current boiler-based configurations, the latter solely reflect a slight increase in total expenses while revealing a very low environmental impact in terms of equivalent CO_2 emissions (-95%). Moreover, in view of the inherent energy tariff uncertainty and the rise in state subsidies on renewable generation units (PVA) and efficient conversion technologies (AHP), this configuration type appears the most promising cost- and environmental-efficient compromise today.

- At higher investment thresholds, the combination of CHP and AHP are regularly activated. This behaviour is especially observed in the case of stronger service demand dwellings such as apartment blocks and administrative buildings. Furthermore, for these building categories, the AHP-CHP configuration represents the cost-optimal solution. During operation, the CHP units act as base load generation while considering the electricity demand of both the auxiliary units (AHP) and the domestic requirements (EL).

- In view of achieving grid-friendly operation, generation curtailments represents the

most economic solution and thus, engendering a loss in operating revenues. However, regarding the resulting impact of the power network KPI, both the OPP and GSS (-%) are drastically reduced with disparities reaching -84%. In regard to the latter improvements, the aforementioned increase in operating expenses can be expressed as an equivalent investment cost for power networks to reduce the BES impact on the electricity grid.

- The use of predictive control techniques (MPC), in contrast to standard rule-based approaches (RBC), significantly improves the integration of distributed generation units, values reaching 17% in terms of self-sufficiency points for configurations with high PVA penetration. Similarly, from an economic perspective, the rise in autonomy significantly decreases the related operating expenses, particularly for larger, ill-sized distributed generation capacities. Finally, the use of a predictive model-based control method allows for the scheduling changes with respect to an initial demand profile, hence representing a virtual battery from the power network perspective (BES).

- Finally, the refurbishment of both the heat distribution systems and building envelope particularly decreases SH service demands and consequently, the associated conversion unit sizes. With the introduction of state subsidies, BES including the dwelling renovation reflect equal or better cost performance over non-renovated solutions, particularly for small single family houses. In addition, the deployment of renovated BES configurations substantially reduced the maximum GES and OPP values observed over the solution space.

Limitation and perspectives Although the latter chapter focuses on the development of a holistic MF for BES, additional data processing steps regarding the building classification and parameter identification is advised. Indeed, the presented algorithm makes use of a defined set of building parameters, evaluated in a previous study. Such an "up-stream" extension would provide a user-friendly preliminary screening interface for both end-users and practitioners while reliably identifying the corresponding input parameters. In addition, a user-specific approach allows for a converse "diagnostic" problem formulation by including the current system performances(e.g. the remaining component lifetime) and subsequently to generate a set of cost-efficient improvements regarding the desired eco-environmental targets.

In regard to the MF, additional features could be implemented in future versions; potential extensions comprise the option of selecting discrete unit sizes and combined investment functions (e.g. manufacturers quotes), especially in view of commercial application purposes. Indeed, with the introduction of novel technologies (e.g fuel cells), market availability remains rather low and thus, solely a limited number of sizes should be implemented. In addition, future versions could incorporate orientation specific renewable generation potential, both regarding the dwelling façade and roof surfaces. The latter qualifications might hence highlight a discontinuous cost benefit function when increasingly exploiting the solar potential while targeting generation profiles corresponding to the end-user load demand.

Finally, this chapter successfully addressed the simultaneous sizing and scheduling of BES for specific building types; however the presented approach remains focused on a local case study: a single building. In order to provide a general perspective of the presented sizing method, a consequent extension of local decision making to a larger scope is required. In view of the latter challenge, the following chapter attempts to answer the question of how the BES designs should be integrated on a larger scale, such as at the district and national level.

2 National impact of optimal building energy systems

<div style="border:1px solid #c0504d; border-radius:8px;">

Chapter overview

- Spatial climate data reduction
- ϵMOO problem formulation to attribute local system designs
- Large-scale impact assessment of modern building energy systems

This chapter is an improved and extended version of Stadler et al. [88] and [89].

</div>

2.1 State of the Art

In view of current energy transition, large-scale modelling frameworks related to the planning of future energy systems are critical to the various stakeholders involved in the decision process. Since the built environment embodies the largest end-user of the national total final consumption (TFC), the proper sizing of efficient building energy systems (BES) represents a key element in reaching environmental targets within the scheduled time horizon. The deployment of optimal energy system solutions integrating efficient and renewable-based technologies represent an interesting option to face the upcoming objective. Regarding the growing interest in assessing the large-scale impact of building related energy services (e.g. space heating and domestic hot water preparation), several studies in literature have addressed specific questions related to the former topic.

Heiple and Sailor [90] hence introduced a bottom-up based simulation method to assess detailed energy demand profiles of buildings in urban areas. The authors relied on a prior typology classification and calibrated the associated model parameters to match actual consumption values within a given tolerance. The method was finally validated through a large US city case study and the subsequent results compared to aggregated top-down demand values. Similarly, Girardin [81] developed a systematic algorithm to evaluated the thermal energy service requirements using annual total final consumption values and GIS databases. The

method has been successfully demonstrated for the canton of Geneva in Switzerland while providing first insights on the impact of district scale BES planning. Dascalaki et al. [91] studied the national heat consumption of the Hellenic residential building sector. Based on the European dwelling classification project TABULA[1], the authors estimated the aggregated energy use within the considered sector and highlighted the effect of possible efficiency measures on curbing the latter demand. Anew from a bottom-up perspective, Ren et al. [92] analysed the cost benefit of optimally designed distributed generation units for an aggregated, typical urban area in China. The authors systematically applied the presented LP model for different climatic zones arising within the country and compared the subsequent configurations. Their results showed the strong influence of the environmental taxes and ambient conditions on penetration of renewable and CHP conversion technologies.

From a top-down perspective, Lund and Münster [93] presented a national energy system model relying on the commercial software EnergyPlan[2] to study the integration of distributed and renewable-based energy systems. The authors demonstrated the latter through the case study of Denmark, considering aggregated final energy demand profiles and a pre-defined set of different rule-based regulation methods. Consequent application results showed the influence of decentralized unit operation strategies in reaching low surplus production levels. Recently, Codina Gironès et al. [94] presented an extended top-down modelling framework to define different national energy scenarios within the context of the energy transition. The thus developed tool is primarily targeting decision makers by providing a holistic and nevertheless straightforward support platform to assess the economic and environmental impact of future investment and consumption objective. The authors successfully demonstrated the proposed approach considering the case study of Switzerland and rendered the consequent modelling platform publicly available online[3]. Table 2.1 briefly summarized the main highlights associated to the aforementioned studies.

Table 2.1 – Review of studies on large-scale BES integration

	Optimization	Conversion options[a]	Storage options[b]	Scope	Demand estimation
Heiple and Sailor [90]	×	-	-	Country	SH
Dascalaki et al. [91]	×	-	-	Country	SH
Ren et al. [92]	✓	CHP, PVA	-	Country	-
Lund and Münster [93]	✓[†]	CHP, W/AHP	HST	Country	-
Codina Gironès et al. [94]	×	CHP, W/AHP	-	Country	SH, HW, EL
Girardin [81]	×	-	-	Region	SH, HW
Pensini et al. [95]	✓	ELH, BOI	HST	Region	-

[†] Only unit operation
[a] Primary (and auxiliary) conversion and renewable technologies according to Figure 1.6
[b] Storage conversion technologies according to Figure 1.6

---

[1] www.building-typology.eu, last accessed on 23.11.2018
[2] www.energyplan.eu, last accessed on 27.11.2018
[3] www.energyscope.ch, last accessed on 23.11.2018

2.2 Contributions

This chapter presents a novel method to estimate the large-scale potential of modern and efficient building energy systems (BES) within the context of sustainable service provision scenarios. First, a set of BES solutions is defined for each representative building type included in the scope of interest (e.g. Switzerland). In a second phase, an ϵ-multi objective optimization problem is implemented to allocate the resulting configurations to the respective building types, using the energy reference area (ERA) as scaling factor. Finally, specific techno-economic key performance indicators (KPI) are evaluated to compare the generated system combinations and provide multiple trade-off options for the different stakeholders involved in the energy transition.

Although the aforementioned studies (Table 2.1) have successfully targeted specific issues related to the problematic of large-scale BES performance assessment, a comprehensive approach applying a database of user-oriented optimal BES has not been proposed yet. Indeed, while [81, 90, 91] mainly focused on the thermal energy service demand estimation problem, [92, 93, 95] specifically targeted the allocation issue while solely considering a limited number of technology combinations. The following chapter therefore attempts in contributing to the current state-of-the-art through three main novel elements:

- the development of a spatial classification algorithm to identify typical climatic regions at national scale. In regard to the high problem complexity related to large assessment scales, a data reduction process is defined to decrease the number of ambient conditions arising within the considered system boundary. The empirical climatic zones provided by national guidelines [66, 92] are indeed mainly established on hand of solely ambient temperature conditions while not specifying any representative demand profiles. Hence, in order to provide a efficient and detailed spatial estimation, the proposed method relies on a feature-based *k-medoid* clustering technique and is applied in an iterative manner to identify the best trade-off number of representative climatic zones.

- the definition of an optimization problem using MILP techniques to allocate pre-defined BES configurations to a large scope of representative building classes, varying in use, construction (and renovation) period and location. In order to analyse the energy system allocation under different boundary conditions, the latter formulation is solved in a systematic manner.

- the application of an efficient visualization method to provide a compact user interface for analysing large, multi-parametric solution spaces.

Hence, this chapter is structured in the following manner: Section 2.3 presents the problem input data, the associated pre-processing techniques and the developed optimization problem formulation. Section 2.4 details the considered case study, the country of Switzerland, results and subsequently their analysis. Section 2.5 finally provides concluding remarks and com-

ments on the presented results and a critical observations on the approach while additional information on both the method and results are reported in Appendix B.

2.3   Modelling method

The presented method comprises three main consecutive steps, illustrated in Figure 2.1. Each addresses a specific aspect of the proposed algorithm, detailed in the corresponding following sub-sections:

1. The input **data assessment** step (section 2.3.1) in which the problem scope is defined and subsequently refined to improve both tractability and solvability.

2. The **optimal allocation** step (section 2.3.2) in which the BES selection problem is systematically solved for different boundary conditions.

3. The **performance analysis** step (section 2.3.3) in which the generated solutions are evaluated to provide interesting trade-off options to stakeholders.

Data assessment

National building
stock analysis

Data reduction

Optimal allocation

MILP formulation

Performance analysis

Key performance
indicator analysis

Spatial analysis

Parallel coordinates
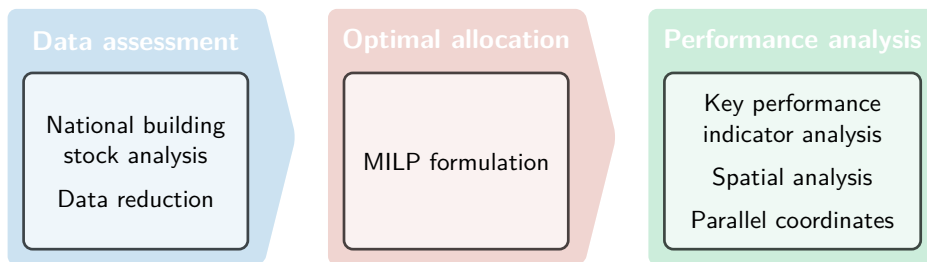
Figure 2.1 – Illustrative representation of the assessment method

2.3.1   Data assessment

The first step consists in defining the problem boundary and the associated data requirements. Since the following method relies on the presented BES sizing algorithm (Chapter 1), energy service demands (i.e. space heating, hot water and process electricity) are assessed on the basis of specific building characteristics. Hence, the applied database should include a sufficient number of features in order to derive the necessary consumption values.

Building classification

The initial input data consists of the *national building register* (RegBL [38]) which comprises generic information on around 1.6 million dwellings such as their use, construction period and footprint area. In view of the latter number, an individual assessment is completely intractable

while requiring a tremendous computational effort. Consequently, a first data reduction step is performed: building classification. Regarding the completeness rate of the national database[4] and a previous categorization result presented by Girardin [81], three specific building types have been defined and analysed throughout the following study; a *single family house,* an *apartment block* and a *mixed use building,* each of them comprising nine sub-categories regarding their construction period and refurbishment state [88].

As presented in the building BES sizing algorithm (Chapter 1), both domestic hot water (HW) and electricity (EL) demand profiles are estimated in regard to the building use while the magnitude is scaled in function of the energy reference area A_b. To this end, standards of the Swiss society of engineers and architects (SIA 2024 [65]) are applied. On the other hand, space heating (SH), respectively cooling demands are inferred from the building construction period which reflects the envelope quality. Thus, using the energy signature model of Girardin [81], specific heat loss rates U_b are computed for each dwelling category. Table 2.2 summarizes the respective input values while further details on each building class energy service demands are reported in Table B.1.

Table 2.2 – Building class specific input parameters

Parameter	Single family house	Apartment block	Mixed-use building		Ref.
HW[a]	12.2	16.0	10.7	[kWh/m^2·yr]	[65]
EL	18.2	18.4	34.0	[kWh/m^2·yr]	[65]
IG[b]	23.9	26.9	38.6	[kWh/m^2·yr]	[65]
U_b[c]	0.63-2.09		0.60-2.15	[W/K·m^2]	[31]
C_b	120	120.6	125.8/105.8[d]	[Wh/K·m^2]	[65]

[a] Assuming a temperature rise from 15 to 55°C
[b] IG: internal heat gains
[c] Includes thermal losses through transmission and ventilation
[d] Building described by a two-zone model due to cooling requirements

Although the presented data reduction has strongly decreased the problem size from nearly 1.6 millions to $3^{\text{use}} \times 9^{\text{age}}$ representative building classes, further time series used as data input to the BES sizing algorithm have not been addressed. Indeed, regarding its location within the national territory, each building type is subject to different climatic conditions (defined by the external temperature and global horizontal irradiance) which, in regard to the applied modelling framework (MF), directly impact both energy service demands (SH) and unit performances (e.g. AHP). Therefore, a supplementary data reduction is required to group similar climate regions and subsequently, increase the number of building classes by an additional dimension.

---

[4]Currently, several important building parameters (e.g. footprint area or floor number) are not required to be provided by law and thus, are solely partly available in function of the good will of communes

Spatial clustering

Spatial data reduction aims at identifying typical geographical regions with similar climatic conditions. The applied method relies on a modified algorithm initially proposed by Domínguez-Muñoz et al. [70] and uses a specific implementation of the *k-medoids* clustering technique: mixed-integer linear programming (MILP). Indeed, *k-medoids* appears to provide more robust results in terms of outliers than the commonly applied k-means technique [59, 71, 96]. An additional benefit of *k-medoid* regards the cluster structure which uses actual observations as centres (i.e. medoid) while the k-means generates a novel average element (i.e. centroid). This feature is particularly interesting when limiting the potential cluster centres to a pre-defined set of medoids. Consequently, the *k-medoid* has been used in the following data reduction algorithm. The considered input data can be described as follows:

- The initial observations i consist of the 2294 different communes territories[5] of Switzerland. Indeed, buildings located within a same commune have been considered exposed to identical climatic conditions and hence, clustered *a-priori* within those territories. The national building stock can thus be directly clustered at the commune scale.

- The commune attributes a include the number of heating (HDD) and cooling (CDD) degree-days as well as the annual global horizontal irradiance (GHI) related to the i-th hour of the design reference year (DRY) profile. The definitions of these parameters are hence expressed in Eqs. 2.1 to 2.3 where the index d represents a day and $\bar{T}^{\text{ext}}$ the mean daily ambient temperature [97].

$$\text{HDD}_i = \sum_{d=1}^{365} (18 - \bar{T}_{i,d}^{\text{ext}}) \quad \forall \bar{T}_{i,d}^{\text{ext}} \leq 15 \tag{2.1}$$

$$\text{CDD}_i = \sum_{d=1}^{365} (\bar{T}_{i,d}^{\text{ext}} - 18) \quad \forall \bar{T}_{i,d}^{\text{ext}} \geq 18.3 \tag{2.2}$$

$$\text{GHI}_i = \sum_{d=1}^{365} \text{GHI}_{i,d} \tag{2.3}$$

In order to assess the different attributes a of each observation i, the available data of 40 national weather stations have been extended by using the inverse distance squared interpolation method introduced by Shepard [98] and further developed by Lefèvre et al. [99]. However, in order to properly assess the annual load profiles of the different cluster centres subsequently the classification process, the medoids locations are constraint in the MILP problem formulation to the latter weather stations. Following computation, the optimal cluster size is finally selected with respect to the silhouette index [71].

Nevertheless, in order to guarantee a reliable representation of the original data by the reduced

---

[5]Smallest political entity in Switzerland and Europe

data set, a minimum acceptable number of clusters is defined prior evaluating the Silhouette index, on the basis of a quality indicator presented in [67]:

- The mean profile deviation σ^a_{cdc} (Eq. 1.3) which evaluates the difference between the observations (commune) and their representative cluster medoid. In view of the applied single-measurement attributes a, the latter metric is equivalent to mean square error (MSE).

- The maximum load difference Δ^a corresponds to the relative number of observations (i.e. communes) for which the error engendered by the cluster attribution is higher (or respectively lower) by a margin γ. Equation 2.4 expresses the latter definition where N_p denotes the number of observations, N_t the number of measurements, $\hat{x}$ the normalized original data and $\hat{\mu}$ the associated cluster value.

$$\Delta^a = \frac{1}{N_p} \cdot \sum_{p=1}^{N_p} \begin{cases} 1, & \text{if } \sum_{t=1}^{N_t} |\hat{x}_{p,a,t} - \hat{\mu}_{p,a,t}| \geq \gamma^a \\ 0, & \text{otherwise} \end{cases} \qquad \forall a \quad (2.4)$$

Figure 2.2 presents the evolution of the different indicators with respect to the cluster number n_k. The highest values of the average silhouette index are observed for small n_k values while the mean profile deviations continuously decrease with the rise in n_k. The minimum acceptable cluster number $n_k^{\min}$ is assessed on hand of the relative improvement in quality indicators through the gradual increase in n_k [67]. In other words, $n_k^{\min}$ corresponds to the n_k for which the decrease in quality indicators is not significant enough to implement an additional cluster and subsequently, rise the computational effort related to a larger problem size. In the latter case, considering a slope threshold of 10%, the minimum acceptable number is $n_k^{\min} = 5$. Consequently, in view of this value, the next local performance indicator maximum is $n_k = 7$ and finally, the latter number of climatic region has been selected.
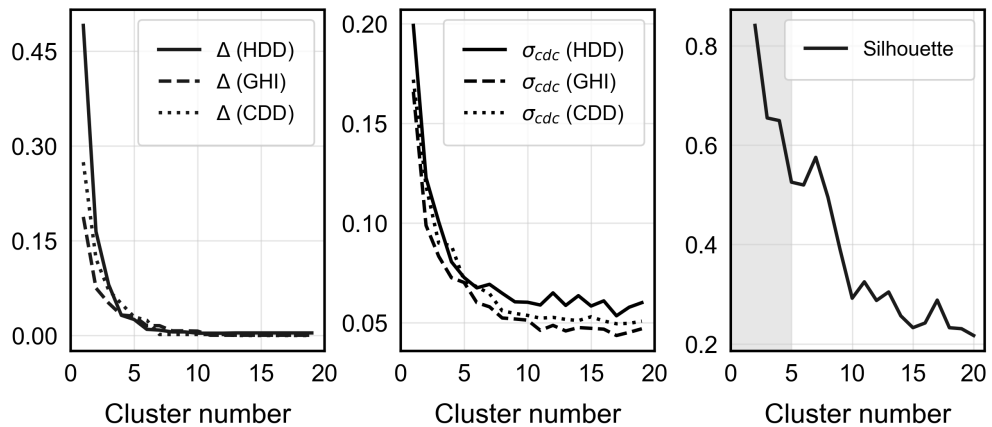
Figure 2.2 – Spatial data reduction quality indicators σ_{cdc} for each attribute (left) and performance indicator (right)

The spatial cluster layout resulting from the aforementioned algorithm is illustrated in Figure 2.3. As expected, the different geographical topologies of the communes are well reflected within the assessed partition: i. The *Alps* (south and east), ii. The *Plateau* (west and the north-east) and iii. The *Jura* (north-west). Consequently, in addition to the previously discussed statistical quality indicators, the figure provides a good graphical validation of the selected cluster size. Finally, Table 2.3 provides an overview of the average climatic conditions and aggregated annual energy service requirements of each representative zones. Detailed demand values at the state level (i.e. canton) are reported in the Appendix B.

Table 2.3 – Annual demand and climatic conditions

Climatic zone	$\bar{T}^{amb}$ [°C]	GHI [kWh/m^2]	ERA[1] [mio m^2]	EL [TWh]	HW [TWh]	SH[2] [TWh]
Bern-Liebefeld	9.48	136.25	158.91	3.22	2.06	18.07
Davos	4.38	163.16	46.69	0.97	0.60	9.88
Disentis	7.04	153.01	32.54	0.67	0.42	4.99
Geneve-Cointrin	11.03	142.05	58.98	1.22	0.77	5.47
Lugano	12.76	144.03	11.01	0.22	0.14	0.74
Piotta	8.11	139.37	49.16	0.99	0.63	6.91
Zuerich-SMA	9.87	127.85	312.25	6.42	4.05	32.42
National			669.54	13.71	8.68	78.48

[1] Energetic reference area
[2] Estimated from [31] and corrected with the respective HDD of each climatic zones

Temporal classification

The preceding data reduction steps have drastically decreased the problem size from around 1.6 million to $3^{use} \times 9^{age} \times 7^{zone}$ representative buildings. Hence, for each class, the BES sizing algorithm is applied to generate a set of different energy system configurations (Chapter 1). Nevertheless, in regard to the latter method pathway, a final data reduction is required prior solving the optimization problem: temporal classification. Subsequently, for each representative climatic zone a set of representative operating periods is identified, reducing the final problem size to $(3^{use} \times 9^{age} \times 7^{zone}) \times 10^{period}$. The associated results are reported as appendix in Appendix B.

Approach validation

The national building energy service demands summarized in Table 2.3 are assessed using a bottom-up approach: building specific values are scaled up regarding the respective aggregated energy reference areas within the region of interest. However, in order to provide a critical review of the latter assessment result with respect to existing evaluations, Table 2.4 presents the analysis of a second bottom-up assessment approach performed each year for

the federal office of energy (BFE) [100].

Table 2.4 – Assessment approach comparison

	ERA	EL	HW	SH
	[mio m^2]	[TWh]	[TWh]	[TWh]
Present study	669.54	13.71	8.68	78.48
[100][a]	692	12.44	8.70	56.41
Δ Deviation	-3%	9%	-0.2%	28%

[a] Residential and service sectors

Except for space heating (SH), the differences between both approaches remain within a ±10% tolerance bandwidth. The latter seems a reasonable deviation threshold, particularly when considering the underlying uncertainty related to the different demand assumptions. In the case of SH, the strong disparity can indeed be explained by the difference in specific heating demand allocated to the building stock. The statistical consumption values derived from [81] suggest, after including a correction factor in view of the difference in HDD among climatic zones, an average demand of 117 kWh/m^2. On the other hand side, the BFE study assumed an average value of 87 kWh/m^2. Subsequently, when including the latter difference in the demand estimation, the deviation drops to solely 3% and hence, validating the presented data assessment step in view of existing approaches.
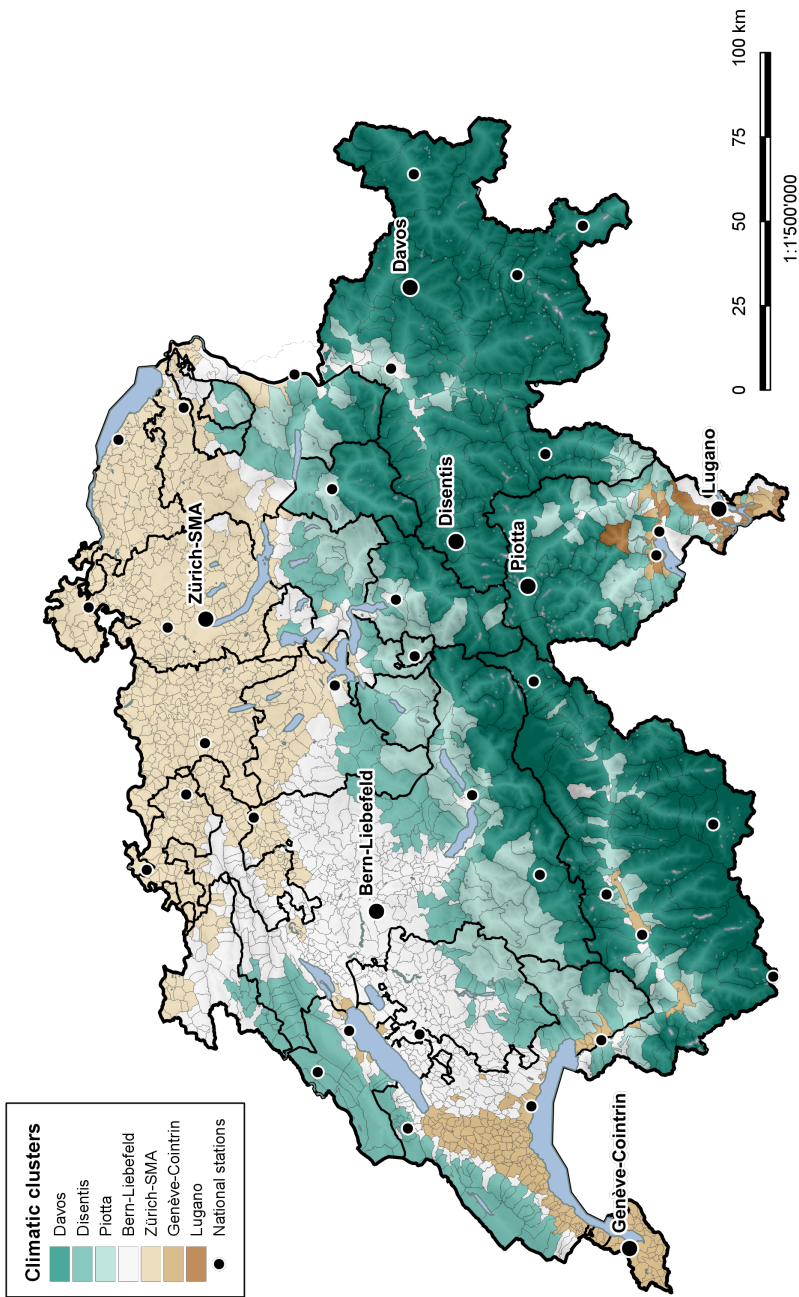
Figure 2.3 – Typical climatic zones in Switzerland

2.3.2 Optimal system allocation

Following the input data assessment step, different building energy system (BES) configurations c are evaluated for each representative building class b and climatic zone z using the sizing algorithm presented in Chapter 1. Henceforth, a resulting BES configuration is referenced by the associated representative class index combination: (b, z, c).

In order to properly allocate the thus generated BES to the national building stock, a second optimization problem is defined; the latter aims at optimally attributing a share F of each BES configuration c to the respective building types b and climatic zones z while using the energy reference area (ERA) as scaling factor. Indeed, using the aggregated ERA of each representative building b and zone z, the associated BES consumption (e.g. natural gas imports) and costing (e.g. the capital expenses) results are up-scaled and applied as input parameters to the following problem formulation (Eq. 2.5)

$$\min_{F_{b,z,c}} C^{en}$$

subject to

$$\text{Eq. 2.7 - Eq. 2.10}$$

(2.5)

where C^{en} denotes the global system environmental impact and F the allocation ratio of each BES configuration (b, z, c). Further details on the problem objective function, constraints and variables are presented below.

Objective   The objective function minimizes the environmental impact of the global building energy system and is expressed in Eq. 2.6 where $ip^{+/-}$ denote the equivalent CO_2 emissions associated to the considered energy vectors. The parameters $E_{grid}^{+/-}$ and H_{grid}^{+} represent the total annual electric and chemical (natural gas) energy demand (receptively supply) of each BES configuration (b, z, c).

$$C^{en} = \sum_{b=1}^{B} \sum_{z=1}^{Z} \sum_{c=1}^{C} \left(ip^{el,+} \cdot E_{grid,b,z,c}^{+} - ip^{el,-} \cdot E_{grid,b,z,c}^{-} + ip^{ng,+} \cdot H_{grid,b,z,c}^{+} \right) \cdot F_{b,z,c} \qquad (2.6)$$

Allocation constraints   The only mandatory problem constraints are related to the energy system design allocation (Eqs. 2.7 and 2.8). The latter indeed ensure that at least a single BES configuration c is attribute to each building type b and climatic zone z. In order to avoid very small affectation percentages, F is modelled through a binary variable, hence limiting the allocation share to a single BES configuration per b and z.

Finally, to provide the option of reducing future service demands, it is worth noting that S includes configurations for both the standard and renovated building categories b. Subsequently, the respective investment costs C_{b}^{inv} are corrected in the latter case to account for the

dwelling envelope and heating system refurbishment.

$$\sum_{s=1}^{C} F_{b,z,c} = 1 \qquad\qquad \forall\, b \in \boldsymbol{B}, z \in \boldsymbol{Z} \quad (2.7)$$

$$F_{b,z,c} \geq 0 \qquad\qquad \forall\, b \in \boldsymbol{B}, z \in \boldsymbol{Z} \quad (2.8)$$

National resource constraints   In order to avoid completely phasing out any complex and efficient solution applying natual-gas (e.g. the combination of CHP and HP), a supplementary constraints is added to the problem formulation: the bio-gas potential. Indeed, although Switzerland is lacking any indigenous production of the latter energy vector, it possesses a substantial potential of bio-gas generation from organic waste and wood [101]. Hence, in order to integrate the remaining untapped potential in future energy scenarios, Eqs. 2.9 and 2.10 define the annual natural-gas consumption surplus demand H^+ with respect to the available bio-gas H_{bio}. Subsequently, solely the following amount is penalized by the environmental impact costs $ip^{ng,+}$, the bio-gas being considered carbon neutral.

$$H^+ \geq \sum_{b=1}^{B} \sum_{z=1}^{Z} \sum_{c=1}^{C} \left(H_{\mathrm{grid},b,z,c}^+ \right) \cdot F_{b,z,c} - H_{\mathrm{bio}} \qquad\qquad (2.9)$$

$$H^+ \geq 0 \qquad\qquad (2.10)$$

2.3.3 Performance indicators

In order to represent the system characteristics targeted through this analysis, namely the integration of renewable generation and the subsequent impact on the national power network of the built environment, specific metrics are evaluated for each solutions determined. Among others, the following KPI are implemented henceforth:

- The specific operating (OPEX) and capital (CAPEX) expenses of the global system configuration to highlight the economic impact associated to future BES scenarios (Equations 1.34 and 1.35)

- The self-sufficiency (SS) and self-consumption (SC) to represent the local use of distributed energy systems within the building stock (Equations 1.51 and 1.52)

- The equivalent grid battery (GES - Equation 1.56) and net peak electricity (PEL) to reflect the additional stress on the power network, both in view of long-term electrical energy storage capacities and grid utilization. Indeed, the hourly mean peak load arising during the reconstructed clustered DRY represent an interesting metric to the national transmission system operator and thus is assessed using the definition in Eq. 2.11.

$$\mathrm{PEL} = \max_{i \in \boldsymbol{I}} |\dot{E}_{\mathrm{grid},i,t}^+ - \dot{E}_{\mathrm{grid},i,t}^-| \qquad\qquad (2.11)$$

Since the proposed algorithm aims at studying the penetration of renewable generation within the national building stock under different system conditions (e.g. by varying the available capital), a systematic approach is adopted by targeting multiple objectives simultaneously. To this end, the initial problem formulation (Eq. 2.5) is enhanced to an ϵ-constraint multi-objective optimization formulation [80]. Detailed in Equation 2.12, the latter thus includes a second objective function: the system investment expenses C^{inv}.

$$\min_{F_{b,z,c}} C^{\text{en}}$$

subject to

$$C^{\text{inv}} \leq \epsilon_{\text{inv}}$$

Eq. 2.7 - Eq. 2.10

$$(2.12)$$

Regarding the BES share F of each configuration c, building type b and climatic zone z, Eq. 2.13 finally defines the total investment costs where $C^{\text{inv}}_{b,z,c}$ represents the individual system capital expenses related to the BES configuration (b, z, c).

$$C^{\text{inv}} = \sum_{b=1}^{B} \sum_{z=1}^{Z} \sum_{c=1}^{C} C^{\text{inv}}_{b,z,c} \cdot F_{b,z,c} \qquad (2.13)$$

2.4   Applications - national scale

Figure 2.4 depicts two Pareto fronts considering different input parameter values: a national electricity mix (EL mix) with (*1*) 0.113 and (*2*) 0.376 kgCO$_2$-eq./kWh (Table 2.5). The former reflects the actual situation which mainly relies on hydro and nuclear energy sources as reflected in Figure 1. However, since hydro-power availability is rather low during strong demand periods (i.e. winter) while the national government is targeting a nuclear phase-out by 2050, a comparative mix value is applied additionally, assuming a homogeneous conversion from natural-gas fired combined-cycle plants.

Configurations on the left extreme of both Pareto fronts are thus representing the cost effective solutions, comprising solely natural-gas boilers and, in the case of mixed-use buildings, ventilation units. With the increase in investment expenses, the environmental impact of the global building energy system is strongly reduced (zone A) until reaching around 60 CHF/month·100m^2 after which, the slope significantly decreases (zone B) while the system self-sufficiency increases from 1 to 55%. Finally, in regard to the last solutions (zone C), no significant improvement in both the equivalent emissions and self-sufficiency is noticed with the further rise in capital costs. A similar trend is observed in the case of a carbon intensive electricity mix (2), the inflexion in zone B being however less pronounced.
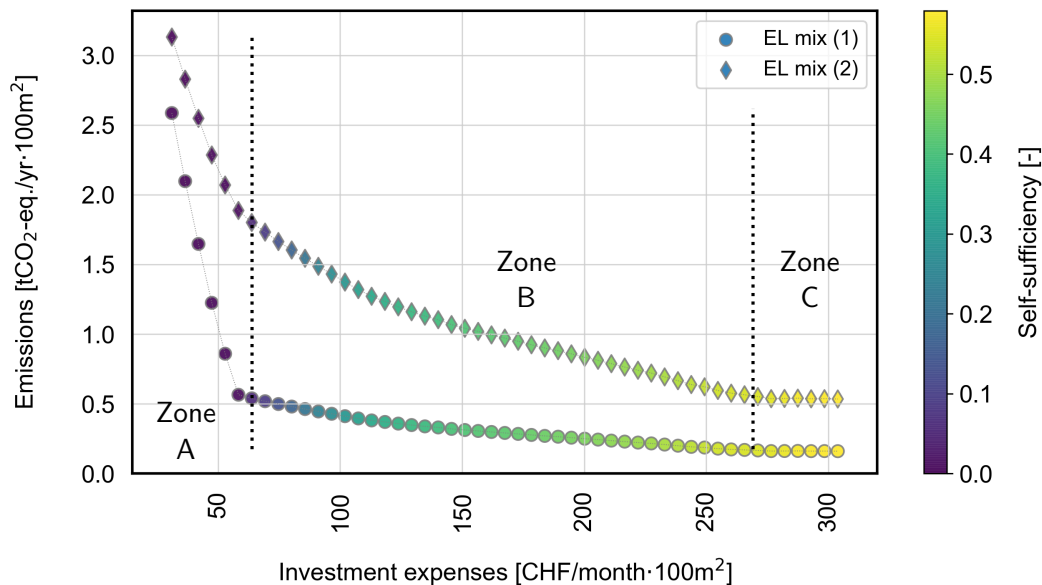
Figure 2.4 – Pareto fronts for Switzerland

In order to explain the latter behaviours, the following graphs in Figure 2.5 illustrate the evolutions of specific conversion units and performance indicators. Indeed, in the first phase (zone A), the purely fossil-based solutions (S$_0$) are rapidly replaced by air-source heat pump (AHP) based energy systems until reaching the carbon neutral bio-gas production threshold.

This shift of energy-carrier obviously engenders a strong impact on the electricity network which has to cope with the related demand increase in both power (+250%) and energy (+240%). In a second phase (zone B), both photovoltaic arrays (PVA) and CHP units (SOFC) are gradually installed to reduce electricity imports and thus, the greenhouse gas emissions associated to the electricity mix. In parallel, the aggregated capacity of gas-fired boilers (BOI) further decreases in order to remain below the national bio-gas threshold. Starting around the complete BOI phase out, the building stock is gradually renovated, hence decreasing the required heat pump capacity as well as the electrical peak power related to it (-52%). As the services demand decrease with the refurbishment rate, the aggregated system self-consumption drops and hence, the grid equivalent storage (GES) need rises from 0 to nearly 10 kWh/100·m^2. Finally, following the complete refurbishment of the building stock (zone C), no significant change in primary conversion units is noticed, the objective improvement being also hardly noticeable. Nevertheless, a sharp rise in stationary battery (BAT) capacity is observed, slightly improving the system self-sufficiency/consumption and thus, decreasing electricity imports.
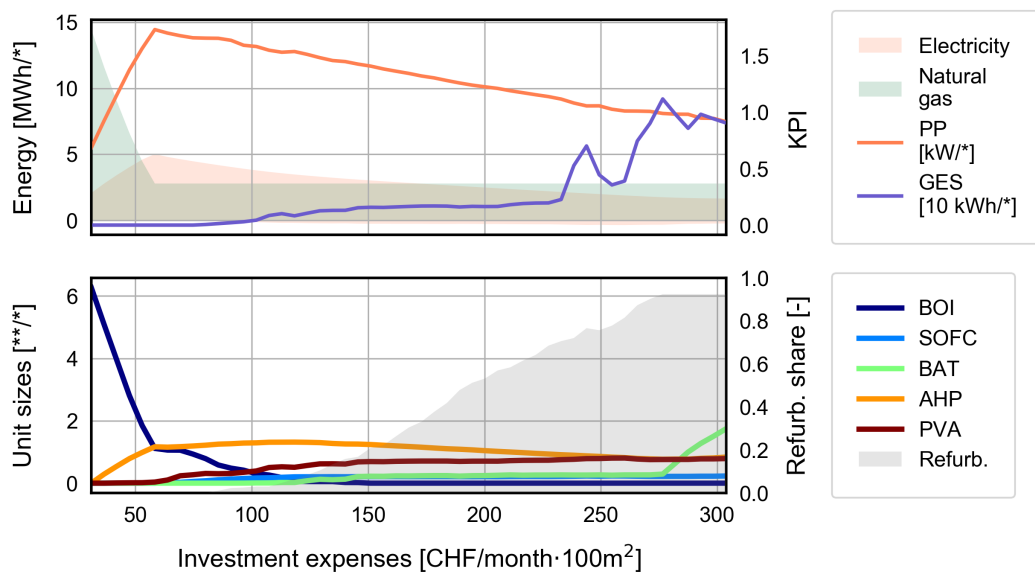
Figure 2.5 – Optimal solution evolution with the rise in investment cost and a standard electricity mix (1). The superscripts * represent [100/m^2] while ** reflect the specific unit sizing dimensions.

A similar behaviour is noticed in the case of a higher carbon intensive electricity mix (2), as shown in Figure 2.6. Consequently, this parameter has no particularly effect on the aggregated building energy system design, the strong difference between both fronts in Fig. 2.4 being thus solely related to the environmental impacts of centralized electricity generation. It is worth noting that the presented graphs (Figs. 2.5 and 2.6) only represented independent system solutions and not a global pathway towards a future emission target. Indeed, as illustrated,

conversion units such as heat pumps are first rising before decreasing due to the increasing renovation share and hence drop in space heating demand.
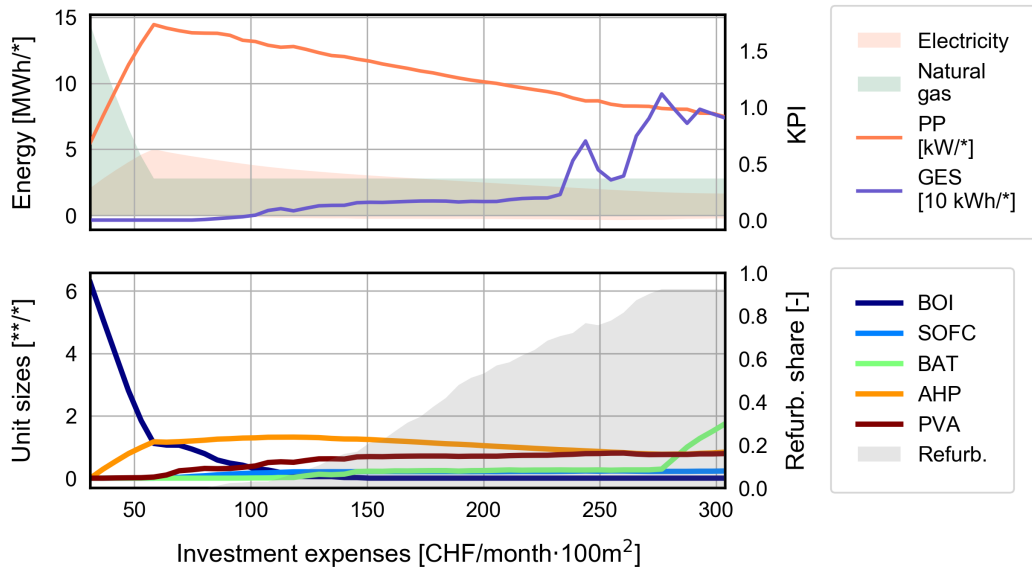
Figure 2.6 – Optimal solution evolution with the rise in investment cost and a carbon intensive electricity mix (2). The superscripts * represent $[100/m^2]$ while ** reflect the specific unit sizing dimensions.

Finally, in order to analyse the impact of optimally designed building energy systems from the spatial perspective, Figures 2.7 to 2.9 display geopolitical maps of Switzerland while highlighting the specific natural/bio-has and electricity use. As observed in Figure 2.7, the indigenous bio-gas production is generally allocated towards (i) cold and rural climate zones, located in the *Alps* (South) and the *Jura* (North-west), with higher space heating demands in addition to (ii) urban areas with higher electrical base load requirements. The total annual electricity exports illustrated in Figure 2.8 supports the latter statement; generation excess from CHP units is injected into the network within (i) while (ii) reflect low export values. The figure presents additional strong exporting regions in the *Tessin* (South) and *Plateau romand* (West) which possess stronger solar irradiation and hence, higher generation potential from photovoltaic arrays. In regard to the specific annual electricity import metric, colder communes with low bio-gas use such as the region of the *Alpes romandes* (South-west), the *Alpes tessinoises* (South) and the *Préalpes* (Centre) in addition to (ii) are particularly predominant. Although solely presenting annual and aggregated values, the latter figures provided interesting insights on the allocation of indigenous energy resources as well as future power exhange trends, from the southern and western regions towards urban centre and pre-alpine regions.
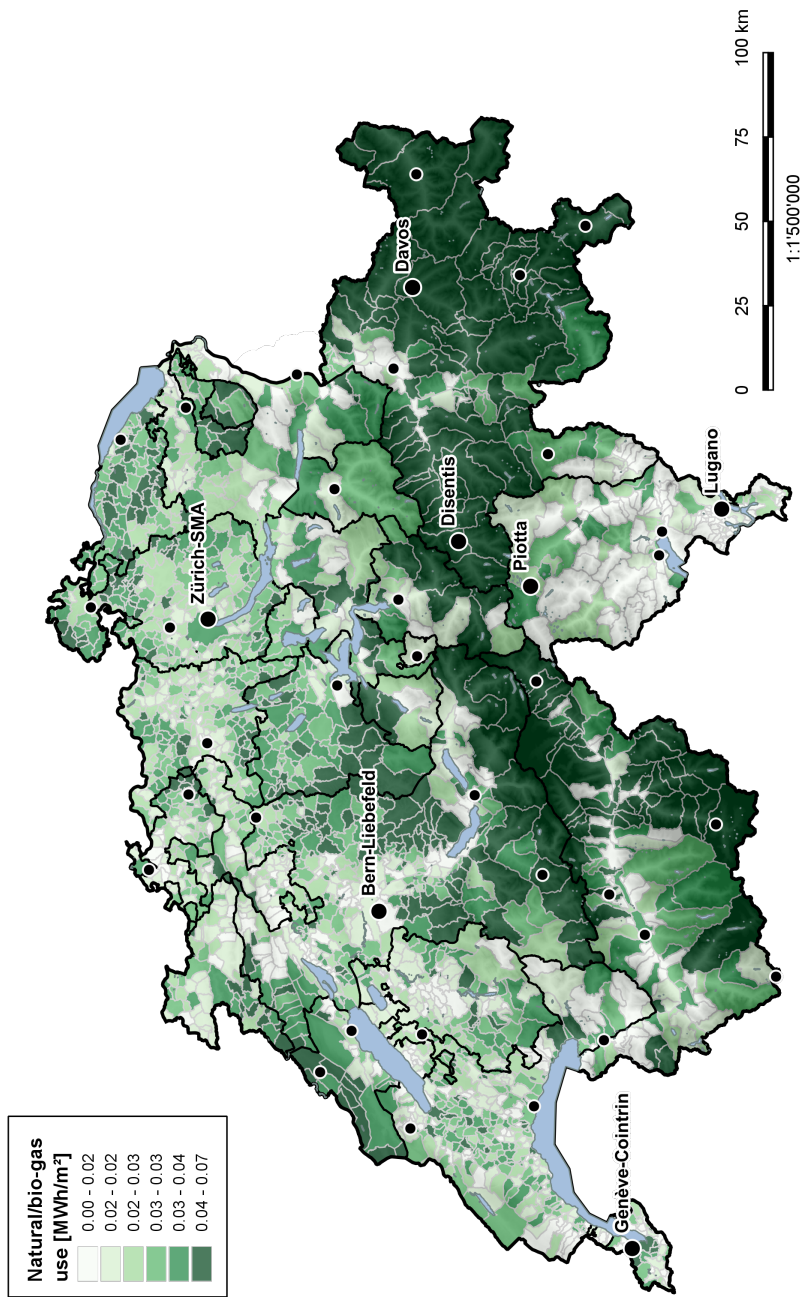
Figure 2.7 – Specific annual natural/bio-gas use per commune for an investment threshold of 300 CHF/month·100m²

69
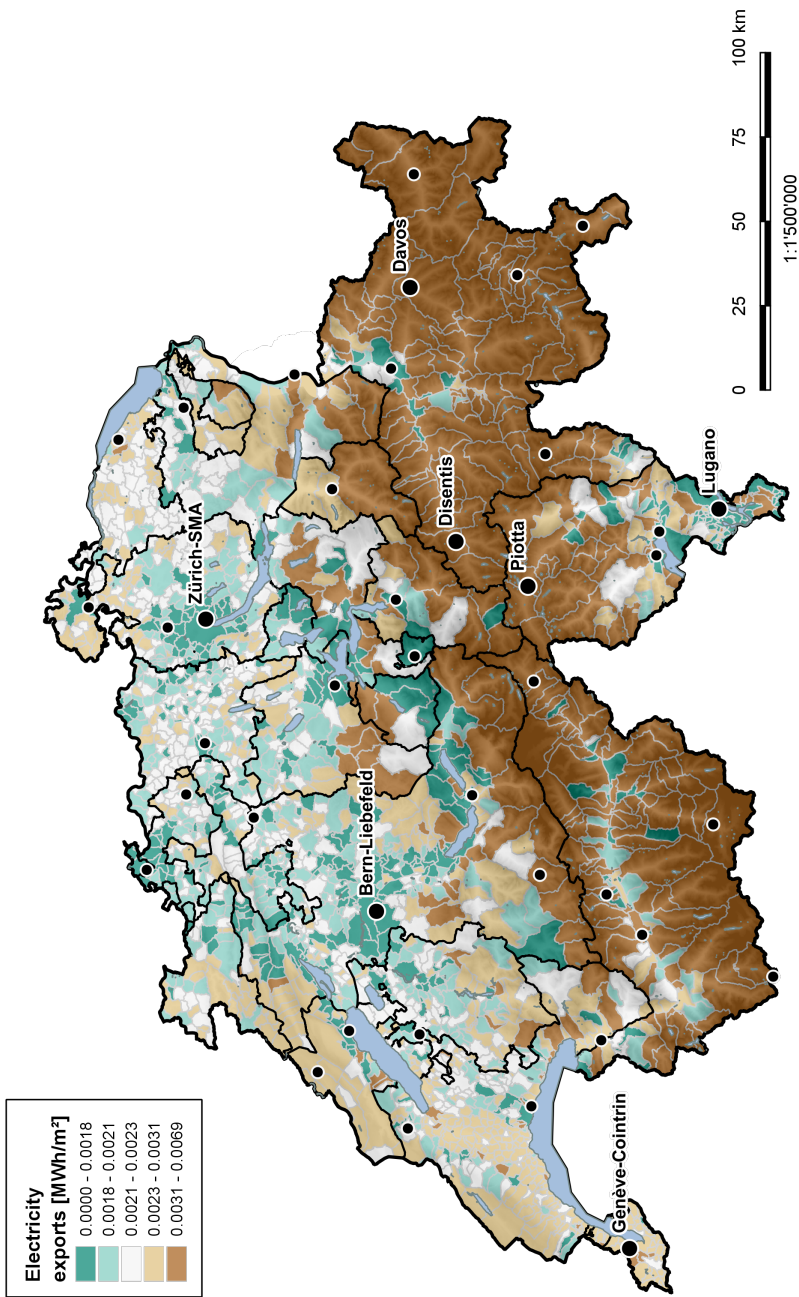
Figure 2.8 – Specific annual electricity export per commune for an investment threshold of 300 CHF/month·100m^2
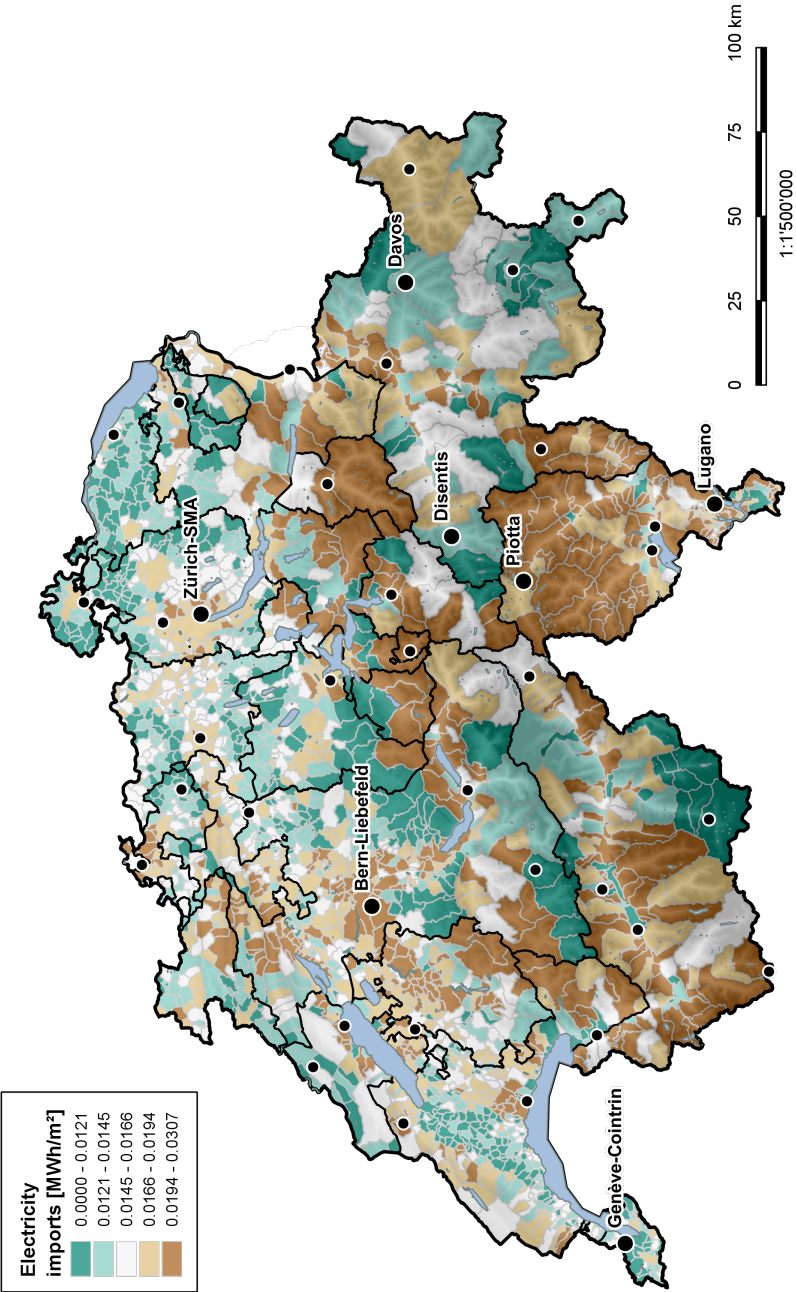
Figure 2.9 – Specific annual electricity imports per commune for an investment threshold of 300 CHF/month·100m^2

71

2.4.1   Multi-parameter result representation

In view of large solution space generated through the systematic approach, the following section analyses the use of an efficient representation method to analysis the interdependencies between different key performance indicators (KPI). To this end, a parallel coordinate graph is implemented; the latter solely exposes pre-defined evaluation criteria through vertical axis while solutions are represented by lines crossing each bar at the corresponding values. The interactive implementation subsequently allows for specific range selection for each KPI in order to highlight solutions respecting desired performance characteristics of the various stakeholders.

Consequently, Figure 2.10 presents the solutions spectrum through parallel coordinates for the national building energy system design. The first three columns represents input parameters altered in between each optimization process, through the means of additional ϵ-constraints: the electricity mix (ELX), the equivalent solar area of the built environment (ESA) and the bio-gas affectation (BGU). The corresponding ϵ values and associated indexes i are reported in Table 2.5. While the ELX impact is discussed in the previous section, the second parameter (ESA) relies both on the average potential value defined on hands of the detailed assessment study performed by the state of Geneva [102] (i=1) and the recently published national GIS database [103] (i=2). Finally, the third parameter (BGU) is discretized into five usage thresholds, including both the maximal sustainable production potential (i=5) and the additional amount available after disregarding the current use (i=3), in form of bio-gas while considering an average conversion efficiency of 69%.
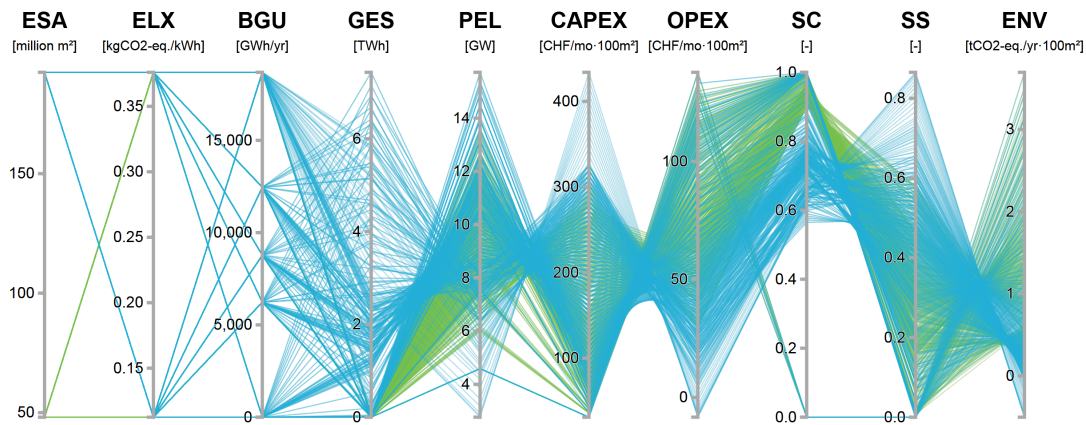
Figure 2.10 – Parallel coordinates graph of the national BES allocation: ESA values are represented through green (i=1) and blue (i=2) lines

Table 2.5 – Discrete input parameters

Parameter		ϵ-values				
		i=1	i=2	i=3	i=4	i=5
ELX	[kgCO$_2$-eq./kWh]	0.113	0.376			
ESA	[mio m^2]	48.1	192.4			
BGU	[TWh]	0.0	6.2	8.8	12.5	18.7

In regard to large possible decision space, solely two specific solution characteristics are further discussed while demonstrating the effectiveness of the applied representation method: environmental neutral and grid-friendly.

- The **net zero-emission** threshold regarding the national provision of domestic energy services is theoretically achievable, although under specific conditions (Figure 2.11). Indeed, after setting the upper bound of the environmental indicator to zero (ENV ≤ 0 tCO$_2$-eq./yr·100m^2), solely solutions assuming a strong solar potential (i=2) remain active while requiring both significant investment expenses (CAPEX ≥ 250 CHF/mo·100m^2) and centralized electrical storage capacities (GES ≥ 6 TWh). In addition, a high biomass resource availability (i=2) is necessary to reaching the considered target; nevertheless, near net-zero configurations which correspond to the *2000 watt society* sustainability objective by 2050 (ENV ≤ 0.5 tCO$_2$-eq./yr·100m^2)[6] are feasible with lower biogas consumption values, a current electricity mix and lower photovoltaic penetration.
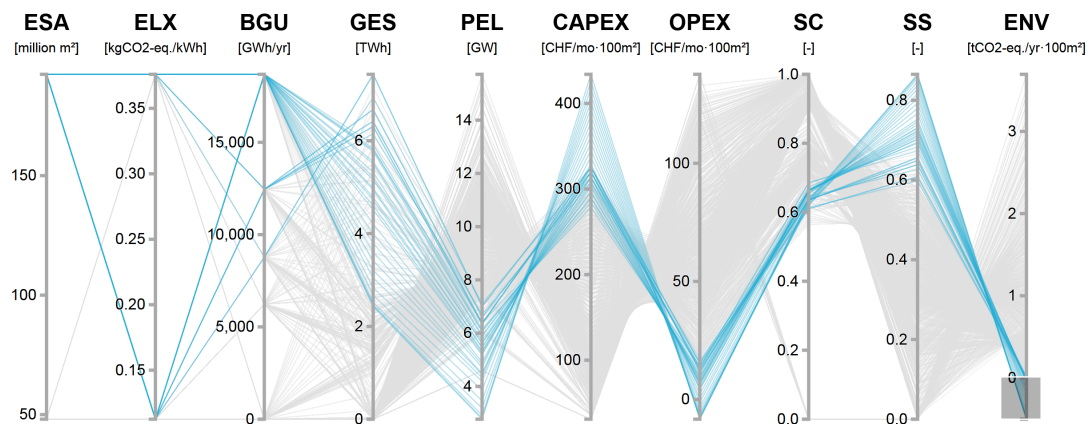
Figure 2.11 – Parallel coordinates graph for different input parameters - *Focus*: net zero-emission solutions

---

[6]In regard to the sustainability roadmap established by [104] building energy services are assumed to represent 50% of the total greenhouse gas emission budget

- In order to highlight **grid-friendly** solutions, the peak power metric is limited to current values, represented in the latter case study by the base scenario S_0 (PEL ≤ 4.5 kW/100m^2). As observed in Figure 2.12, the remaining active solutions all reflect both high bio-gas and seasonal storage capacity requirements (≥ 9.5 MWh/100m^2). With an increasing relaxation of the PEL performance indicator (PEL ≤ 7.0 kW/100m^2), further configurations involving lower centralized storage finally enter the feasible solution space. The latter include both low and high solar potential designs while satisfying the aforementioned near net-zero emission target. Nevertheless, this objective comes along with substantial investment expenses from the end-user perspective, values ranging from 230 to 425 CHF/mo·100m^2.
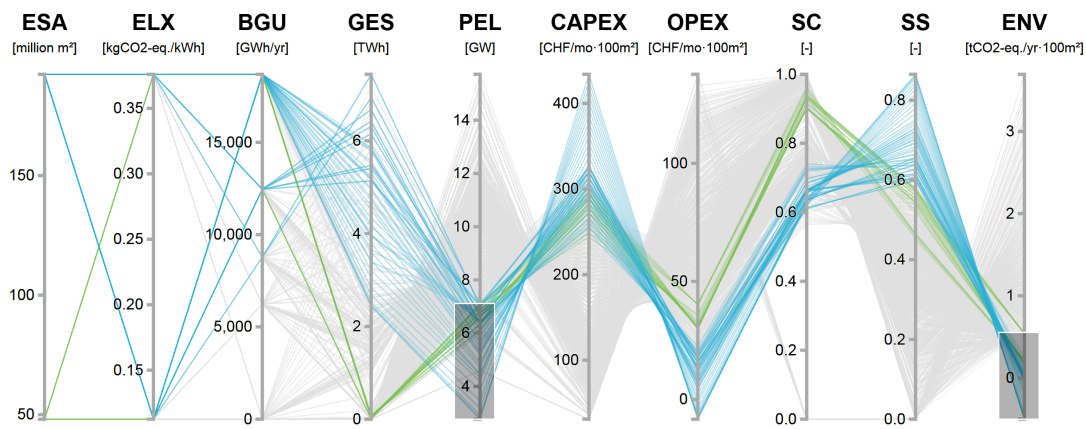
Figure 2.12 – Parallel coordinates graph for different input parameters - *Focus*: net zero-emission & grid-friendly solutions

Future power network   Regarding the implemented problem formulation of Section 2.3.2, no specific constraints have applied on transmission capacity currently available between the different typical climatic regions in Switzerland. However, in order to account for the potentially rising stress on the national electricity grid, two specific performance indicators where included during the results analysis: the GES and the PEL. An alternative to the implemented screening process (Figure 2.12) could be the addition of a linear transmission network model [105] into the applied problem formulation and consequently, to include the possibility of upgrading existing line capacities between critical locations. However, in order to properly allocate the capacity needs specific to the building sector and the associated potential investment requirements, such an approach should account for all sectors demands across the country and hence, outreaches the scope of the tackled issue.

2.5 Conclusion

The latter chapter presented a novel approach to assess the large-scale impact of complex energy systems evaluated for individual buildings. A multi-objective optimization problem formulation is therefore defined in order to assign a specific system configuration to each dwelling considering the climatic environment, affectation and heat demand. Nevertheless, in regard to the problem size, a spatial and additional temporal classification processes are implemented to improve both tractability and solvability. Consequently, in view of research question stated in introduction and the aforementioned simulation results, following conclusions can be drawn:

- The large-scale deployment of optimal design and scheduled building energy systems allows for a strong drop in equivalent CO_2 emissions, in the best scenarios even achieve a CO_2 neutral state. The replacement of fossil-fuel based conversion units represented the strongest contributor with a relative improvement of 78%, assuming a current electricity mix, while solely requiring a specific investment costs of 60 CHF/month·100m2. Further reduction measures require the gradual installation of additional generation capacities and the refurbishment of older dwellings. The deployment of extensive storage units solely merely improves the system environmental impact although further decreasing the considered grid metrics.

- The spatial affectation of indigenous bio-gas production predominantly targets colder rural regions and densely populated urban centre. While the former consequently reflect higher electricity export value, the latter remain substantial importers. Furthermore, the analysis facilitates the identification of future power flow trends, from rural communes towards agglomerations.

- A larger share of distributed power generation, renewable-based, strongly impacts the subsequent energy system design. Indeed, although reaching net-zero consumption levels, both the electrical network peak power and seasonal storage requirements highly increase, thus reflecting the need of substantial infrastructure investments. The further screening however reveals interesting trade-off solutions, balancing the economical impact on both the system user (buildings) and the network operators.

Limitation and perspectives   A first limitation of the presented work relies within the prior building classification processes implemented in previous studies and applied as input data in the considered case study. Indeed, the different building classes have been assessed using pre-defined feature categories (e.g. construction period) disregarding any clustering techniques to determine both their optimal number and ranges. A novel re-assessment using *k-medoids* or *k-means* based algorithm might thus highly improve the quality of the predicted service demands while potentially decreasing the required amount of building types.

In view of the problem scale addressed within the presented case study, additional energy

service requirements occurring in the sector of *services, industry* and *mobility* should be considered for future developments. Indeed, a fully integrated approach might exploit synergies between the different temporal and spatial demand profiles while overcoming the need of sector-specific resource affectation constraints (e.g. the biomass use). Hence, a future combination between the modelling framework previously presented by Codina Gironès et al. [94] and the method proposed in the latter chapter provide an interesting interface to assess future national energy systems, accounting for both all energy services and optimal unit scheduling. Moreover, such a fully integrated approach might evaluate the future need of network upgrades as well as the associate investment expenses. Nevertheless, this perspective outreaches the scope of this thesis and hence, is not addressed thereafter.

Finally, the last comment addresses the optimization processes. Indeed, the developed approach relied on two independent problem formulations; the system design performed in Chapter 1 and the following extension to the national scale presented in Chapter 2. However, the lack of any direct interdependencies between both optimization processes does not allow for any sizing or scheduling changes to benefit from potential synergies between neighbouring systems. Hence, the following remark leads to the subsidiary questions related to the potential benefit resulting from multi-building problem formulations on both the energy system design and performances. In view of the latter shortcoming, the following chapter (Chapter 3) attempts in providing additional answers on this latter topic.

3 Multi-building energy systems

> **Chapter overview**
>
> - Multi-building energy system MILP modelling framework
> - Building typology classification process
> - Multi-building technologies: seasonal electrical storage and heating network

3.1   State of the Art

Within the context of the energy transition, future energy systems should incorporate efficient energy conversion and storage devices to satisfy comfort demands while maximizing the penetration of sustainable resources. Nevertheless, in such future scenarios, both the electricity and natural gas networks are facing an important issue of managing the remaining daily and monthly fluctuations resulting from uncontrollable loads and seasonal service demands. Smart-grids might represent a promising approach to face the latter challenge; indeed these networks exploit the growing deployment of telecommunication systems within the power distribution infrastructure to regulate the grid status [106]. Buildings and network operators are therefore able to interact and identify potential opportunities from multiple generation and consumption points connected to a given feeder. Indeed, synergies between residential, commercial or industrial *energy service* requirements (e.g. space heating, domestic hot water preparation and electricity) might arise and hence, improve the penetration of renewable energy sources at the neighbourhood level. In addition, the thus created smart grid might act as a virtual power plant, providing ancillary services to the distribution networks given the economic boundary conditions.

In light of the growing interest in curbing the environmental impact of building service provision, the problem of optimal design and control of energy systems in smart grids is gathering an increasing attention in literature.

Hence, within the former context, Mehleri et al. [107] studied the optimal integration of distributed generation systems including combined heat and power (CHP) technologies and photovoltaic panels at the neighbourhood level. Their applied MILP framework incorporated a district heating network model in order to identify economic opportunities arising from centralized micro-CHP plants over conventional heating system designs. Omu et al. [108] extended thereafter the latter approach by adding different conversion units and increasing the number of operating periods from 3×6 to 4×24. The generated results highlighted the importance of the costing - including potential state subsidies - parameters to activate renewable based solutions. Yang et al. [109] further enhanced the MILP modelling framework by incorporating additional technologies such as wind turbines, cooling units and a respective district network.

With the introduction of the energy hub concept [51], multiple studies have implemented this modelling structure to analyze the sizing of distributed energy systems; thus, Orehounig et al. [110] presented a framework to assess the environmental impact and self-sufficiency degree of different energy supply scenarios for a rural neighbourhood. Similarly to the strategic planning tool developed by [94], the latter relies on a top-down approach, using aggregated demand and potential renewable generation profiles. The authors compared four different energy system layouts in regard to the renewable decentralized generation potential and subsequently showed drastic decrease in CO_2 emissions as well as a strong rise in self-sufficiency. Nevertheless, the use of the power network remained necessary to balance seasonal production-consumption mismatches. Still within the context of system control, Ondeck et al. [111] studied the optimal scheduling of an integrated large-scale tri-generation plant, featuring both renewable and conventional energy sources. The associated model incorporated detailed component descriptions in order to tune all operative decision variables, however resulting in a challenging problem size. A case study on a residential district located in a southern US city finally validated the optimization framework while showing the benefit of applying the considered technology over a standard centralized coal-fired power plant.

On the other hand, anew within the context of the energy hub approach, Morvaj et al. [112] proposed a bottom-up implementation of the aforementioned modelling framework to design domestic heating units connected to a low-voltage feeder while considering potential power network upgrades. The authors compared three different MILP problem formulations: a direct, hybrid and a bi-level approach. Although all methods reflect extensive computational effort, the results suggest the use of the power flow model in the problem formulation in order to assess the feasibility from the power network perspective, especially at very high thresholds of distributed energy sources. In order to overcome the computational time issue inherent to large MILP formulations, Schütz et al. [113] recently presented a problem decomposition approach based on the work of [114]. The study showed the promising potential of the Dantzig-Wolfe method, significantly decreasing the required calculation time while remaining within a reasonable tolerance margin from the global optimal. However, the proposed approach reflected worst computing performances at smaller problem scales, typically for single digit building numbers. Finally, Gabrielli et al. [115] presented a novel seasonal storage problem

formulation within the context of clustered time series based MILP optimization frameworks. The authors compared the latter definition with a daily and full-year formulation through the implementation of a urban case study, a district of Zürich, Switzerland. Their results highlighted the benefit of long-term storage units, especially when considering high penetration levels of distributed energy systems.

In view of the power network operator, Nick et al. [116] developed a MIQP problem formulation to define the optimal size and location of battery energy storage systems (BESS) in a low voltage feeder. Their results suggests that the deployment of a large storage unit strongly improves the integration of distributed generation while avoiding massive grid reinforcement costs. From the generation perspective, Kefayat et al. [117] proposed a multi-objective optimization framework to sit distributed energy resources (DER) in low voltage feeders while including uncertainty on load and wind forecasts. The authors selected an black-box solving approach, using and ant-colony algorithm and successfully validate their method on two IEEE benchmark distribution grids. At a higher network scale, Sossan et al. [118] proposed a GIS-based optimization framework to assess the maximum penetration potential of photovoltaic arrays in a sub-urban medium voltage grid. Finally, Halu et al. [119] assessed the optimal configuration of microgrids in an urban area under different levels of photovoltaic deployment. In order to decrease the computationally complexity inherent to the non-linear power network modelling, the authors described the distribution grid behaviour through a DC formulation.

In a nutshell, Table 3.1 provides a summary of the aforementioned literature review, including specific highlights addressed by each presented study. Additionally, the table comprises further similar studies within the field of multi-building energy system design.

3.2 Contributions

This chapter aims at identifying the potential gain resulting from multi-building energy system (MBES) sizing in comparison to a single dwelling approach. The method builds up on the modelling framework (MF) introduced in Chapter 1 and details the necessary modifications to implement multi-building problems. In addition, both heating network and long-term (i.e. seasonal) storage models are included in the MF to further improve integration of distributed generation. Benefits of the novel BES sizing method are finally illustrated though several case studies, varying in neighbourhood type and dwelling number.

Indeed, in view of the presented literature review associated to multi-location formulations, different problem aspects have already been successfully tackled: the application of heating networks to dispatch large generation units [107–109, 120–122], the implementation of thermal and electrical demand side options [109, 110, 112–115, 120, 122] and finally the use of inter-day (i.e. seasonal) storage units [115]. Nevertheless, a holistic MF simultaneously incorporating all the latter features is still lacking. Although being assessed in detail for single building the case studies (e.g. [54, 123]), multi-building formulations limit load shifting capacities to the

Table 3.1 – Review of studies on building energy system optimization

	Time steps	Solving method	Sizing	Demand side management[a]	Conversion options[b]	Renewable options[c]	HN option	Multi-location[d]
Harb et al. [114]	24 × 15	decomp.	×	HS	HP, CHP	PV, ST, WT	×	MB
Mehleri et al. [107]	3 × 6	simult.	✓	-	CHP	PV	✓	MB
Omu et al. [108]	4 × 24	simult.	✓	-	HP, CHP	PV, ST, WT	✓	MB
Orehounig et al. [110]	8760	simult.	×	ES	HP, CHP	PV, ST	×	MB
Morvaj et al. [112]	12 × 24	simult.	✓	HS	HP, CHP	PV	×	MB
Schütz et al. [113]	12 × 24	decomp.	✓	HS	HP, CHP	PV, ST	×	MB
Ondeck et al. [111]	7 × 24	simult.	×	-	CHP, VAC	PV	×	AD
Gabrielli et al. [115]	48[‡] × 24	simult.	✓	ES, HS	HP, CHP	PV, ST	×	AD
Yang et al. [109]	3 × 24	simult.	✓	HS	HP, CHP, VAC	PV, WT	✓	MB
Harb et al. [120]	12 × 24	simult.	✓	HS	HP, CHP	PV	✓	MB
Weber and Shah [121]	3 × 6	simult.	✓	-	HP, CHP[†]	PV, ST	✓	MS
Schiefelbein et al. [122]	8[‡] × 24	simult.	×	HS	CHP	-	✓	MB
Voll et al. [124]	3 × 6	simult.	✓	-	HP, CHP	PV, ST, WT	✓	AD
Ondeck et al. [125]	8 × 24	decomp.	✓	-	CHP, VAC	PV	×	AD

[a] HS: heat storage, HWS: hot water, SHS: space heating, ES: electrical storage
[b] CHP: combined heat and power, HP: Air/water source heat pump, VAC: chiller - † centralized
[c] PV: photovoltaics, ST: solar thermal, WT: wind turbine
[d] MB: multi-building, MS: multi-subdistrict, AD: aggregated district
[‡] Varying according to study

use of storage units (BAT & HST) and hence, typically disregarding the potential of domestic hot water and dwelling envelope energy storage. Moreover, the potential benefit arising from different (1) BES sizing approaches for multi-building case studies and (2) system boundary constraints has not been addressed yet to the best knowledge of the author. Consequently, the following chapter attempts in contributing to the existing state-of-the-art thorough three main elements:

- the implementation of comprehensive modelling framework (MF) including intra- (i.e daily)and inter-day (i.e. seasonal) storage unit, efficient conversion unit, a heating network and a dynamic building model. The latter definition thus allows for a further demand side management option by storing thermal energy in the dwelling envelope (SHS).

- a systematic approach to identify multiple BES configurations and analyse the penetration of distributed generation capacity with respect to different system constraints, e.g. the available investment capital. To this end, an ϵ-constraint multi-objective optimization technique is applied. Stakeholder specific key performance indicators (KPI) are thus used to compare the generated solutions and provide preliminary design considerations.

- the use of a spatial data reduction method to decrease the required computational effort during the optimization process. Similarly to the temporal and climatic classification approaches presented in Chapter 1 and Chapter 2 respectively, a *k-medoid* type clustering technique is implemented to identify different building classes within the neighbour in regard to their use and service requirements.

This chapter is structured in the following manner; Section 3.3 details the developed method to systematically evaluate optimal MBES for smart grids while Section 3.4 discusses the main findings of the implemented case studies. Section 3.5 finally provides concluding notes on the presented work and possible outlooks for future developments.

3.3 Multi-building sizing algorithm

The multi-location energy system sizing method presented below relies on the single building approach defined in Chapter 1. Consequently, the following section solely details amendments made to the initial algorithm. In order to facilitate the understanding of each modification, the latter follows a similar presentation structure: *input data* (Section 3.3.1), *modelling framework* (Section 3.3.2) and *performance analysis* (Section 3.3.3).

3.3.1 Input data assessment

In regard to the input requirements defined in Section 1.3.1, space heating/cooling service (SH/SC) demands are estimated through both ambient conditions (T^{ext} & GHI) and the dwelling construction age while electricity (EL) and hot water (HW) service demands are derived from both the dwelling use and size. Since the main focus of the following chapter relies on the comparison between different sizing approaches, solely a single climatic region is considered thereafter: *Geneva-Cointrin*. Indeed, the different geographical information system (GIS) databases provided by the associated canton (Geneva) reflect a much higher data completeness than the national building register (RegBL) applied in Chapter 2 and thus, allow for a better demand estimation. Hence, in regard to additional information availability, further building classes have been identified and appended to the existing classification structure: *educational* and *administrative* building types. Table 3.2 presents an brief overview of the associated energy service demands and dwelling model parameters, estimated from annual consumption measurements [81] or, if lacking, national norms [65].

Table 3.2 – Building category parameters (II)

Parameter[a]	Administrative building	Educational building	Ref.	
HW[b]	8.4	77.3	[kWh/m^2·yr]	[65]
EL	43.2	23.8	[kWh/m^2·yr]	[65]
IG	56.2	54.0	[kWh/m^2·yr]	[65]
U_b[c]	0.00-0.00	0.00-0.00	[W/K·m^2]	[81]
C_b[d]	15.1/93.1	88.8/23.8	[Wh/K·m^2]	[65]

[a] HW: hot water, EL: electricity, IG: internal heat gains
[b] Assuming a temperature rise from 15 to 55°C
[c] Includes thermal losses through transmission and ventilation
[d] All building classes are described by a two-zone model due to cooling requirements

Building clustering

From the spatial consumption perspective, a further clustering process step has been performed at the building level. Indeed, similarly to the typical operating conditions approach, a district might be expressed as a collection of *typical energy service* demand profiles with a given probability of occurrence. Therefore, the aforementioned temporal data reduction method

(Section 1.3.1) is applied by considering 8 representative attributes a for each dwelling: the annual (i) electricity, (ii) domestic hot water and (iii) internal heat loads, (iv) the available solar potential, (v-vi) the space heating (and respectively cooling if required) energy signature(s) as well as the (vii-viii) diurnal and nocturnal utilization hours. Due to the lack of multiple measurements g (i.e. time series) for each a, solely the mean profile deviations σ^a_{cdc} - which in this case is similar to the normalized mean-square deviation (nMSE) - (Eq. 1.3) and the maximum load difference Δ^a (Eq. 2.4) are used as quality indicators. Indeed, while σ^a_{cdc} evaluates the disparities of aggregated attribute values, Δ^a accounts for the sum of individual differences in a between the building and associated cluster centre. From the performance indicator perspective, the average silhouette index [71] is implemented. Thus, in order to illustrate the latter method, Figure 3.1 displays the iteration results for a sub-rural neighbourhood located in west Switzerland and including 13 buildings.
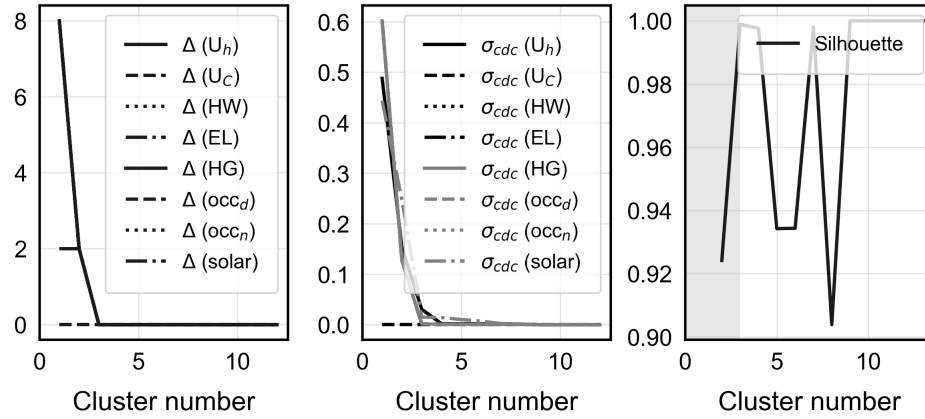
Figure 3.1 – Quality indicators for a rural district data reduction

As observed, local silhouette index maxima are located at $n_k = 3$, 7 and 9. Similarly to Chapters 1 and 2, the lower bound on the optimal cluster number n_k^{opt} is defined on basis of the relative improvement of each quality indicator (i.e from which point onward, the increase in n_k remains below a given rate). Considering a threshold value of 10%, the acceptable minimum cluster number is located at $n_k = 3$ and consequently, given the silhouette values, $n_k^{\mathrm{opt}} = \mathbf{3}$. Table 3.3 provides further information on the aggregated (district) and disaggregated (building) level. As observed, the former is well represented, absolute errors ranging from 0 to nearly 1% which remains within an acceptable range of tolerance.

Temporal clustering

In order to limit the computational effort related to presented problem formulation, time dependent input profiles are clustered into several independent, typical operating periods using the clustering method introduced in Section 1.3.1. Regarding the geographical location of the neighbours analysed in the following section, the climatic zone of *Geneva-Cointrin* is used and thus, the associated **8** operating periods are implemented.

Table 3.3 – Aggregated demand and potential comparison for a rural district data reduction

Attribute	original demand	clustered demand	dif. [%]	
U_h	12.6	12.5	0.77	[MW/K]
U_c	0.0	0.0	0.00	[MW/K]
EL	204.8	205.0	-0.11	[MWh/yr]
HW	178.0	178.2	-0.11	[MWh/yr]
HG	298.8	299.2	-0.11	[MWh/yr]
Solar	3864.3	3870.7	-0.17	[m^2]

3.3.2 Multi-building modelling framework

In the multi-location MF, the different BES are interconnected through the main distribution networks: the natural gas and electricity grid (Figure 3.2). Since the novel problem formulation builds on the preceding one, solely the required amendments and modifications are detailed while referencing initial definition in the latter case.
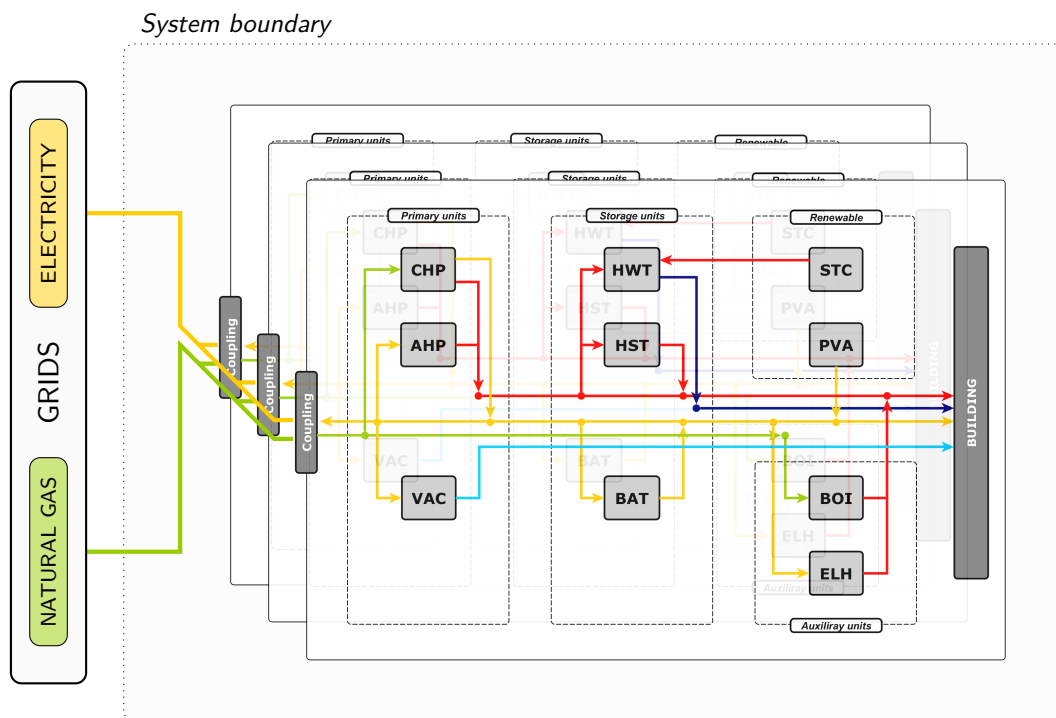
Figure 3.2 – Multi-building energy system modelling framework

Problem formulation

Syntax   In regard to the presented syntax, a novel index b is introduced to denote the different buildings (i.e. locations) which are represented by the set $\boldsymbol{B}$. Additionally, unit ($\boldsymbol{U}_b$) and temperature interval ($\boldsymbol{K}_b$) sub-sets are defined in order to refer building b specific devices in local balancing constraints.

Heat cascade   Since no heat exchanges are directly occurring between the different BES, the heat cascade constraints are reformulated for each b. Equations 3.1 and 3.2 hence substitute Eqs. 1.11 and 1.12 where $\boldsymbol{S}_b^h$ and $\boldsymbol{S}_b^c$ include the hot and respectively cold thermal streams s associated to the dwelling units $\boldsymbol{U}_b$. Nevertheless, in order to bridge the latter limitation, a local heating network (HN) definition is included into the multi-location MF and described thereafter.

$$\dot{R}_{b,k,p,t} - \dot{R}_{b,k+1,p,t} = \sum_{i=1}^{\boldsymbol{S}_b^h} \dot{Q}_{i,k,p,t}^- - \sum_{j=1}^{\boldsymbol{S}_b^c} \dot{Q}_{j,k,p,t}^+ \qquad\qquad \forall p \in \boldsymbol{P}, t \in \boldsymbol{T}, k \in \boldsymbol{K}_b \quad (3.1)$$

$$\dot{R}_{b,1,p,t} = \dot{R}_{b,n_k+1,p,t} = 0 \qquad\qquad \forall p \in \boldsymbol{P}, t \in \boldsymbol{T} \quad (3.2)$$

Costing   No major modifications are added to the operation and investment expenses definition stated in Equations 1.34 and 1.35. However, in view of the novel system boundary, no costs are associated to internal energy exchanges (i.e. from one building to the other) while $\dot{E}_{\mathrm{grid}}^{+/-}$ and $\dot{H}_{\mathrm{grid}}^{+/-}$ refer to hourly average power interactions with the respective networks at the point of common coupling bewteen the community and the local distribution networks.

Long-term storage units   In addition to the local (b) and global (grid) balancing constraint modifications, a long-term storage formulation is implemented in the multi-location approach. Indeed, regarding the increase in distributed generation potential and specific purchasing power arising through the aggregation of multiple BES owners, inter-day battery energy storage systems (BAT GRD) shared among different owners might become an interesting alternative to multiple smaller distributed devices (BAT).

Therefore, based on the model formulation of Gabrielli et al. [115], Eqs. 3.3 to 3.7 present the novel unit energy balances and sizing constraints; at the end of each typical operating period p, energy excess/deficit is compensated through the variable Δ, hence closing the daily cycle. Subsequently, Eq. 3.5 defines a second first-order storage formulation where the index j refers to the different days of the year, f^s to the state-of-charge and n_t to the representative period duration (i.e 24 hours). Similarly to the GES performance metric introduced in Section 1.3.3, the operating periods p and the 365 days j are linked through the indexing set $\boldsymbol{I}$ resulting from the temporal data reduction algorithm which contains the associated clusters centre p for each j ($\boldsymbol{I} = \{p_j \,|\, j \in \boldsymbol{J}\}$). Finally, the sum of both state-of-charge variables is constraint

by the unit size (Eqs. 3.6 and 3.7). Additionally, minimum and maximum state-of-charge constraints(Eqs. A.17 and A.18) can be reformulated using the sum of f and f^s. In regard to the BAT parameter values implemented in Chapter 1, Table 3.4 solely presents the values varying between both unit types: the linear cost function parameters inv_{1-2} and the unit lifetime N.

$$f_{u,p,t+1} = (1 - \sigma_u) \cdot f_{u,p,t} +$$
$$\left(\gamma_u \cdot f_{u,p,t}^+ - \gamma_u^{-1} \cdot f_{u,p,t}^- \right) \cdot d_t - \kappa_u \cdot F_u \qquad \forall u \in \boldsymbol{U}, p \in \boldsymbol{P}, t \in \boldsymbol{T} \setminus \{|\boldsymbol{T}|\} \quad (3.3)$$

$$f_{u,p,t+1} = (1 - \sigma_u) \cdot f_{u,p,t} +$$
$$\left(\gamma_u \cdot f_{u,p,t}^+ - \gamma_u^{-1} \cdot f_{u,p,t}^- \right) \cdot d_t - \kappa_u \cdot F_u - \Delta_{u,p} \qquad \forall u \in \boldsymbol{U}, p \in \boldsymbol{P}, t \in \{|\boldsymbol{T}|\} \quad (3.4)$$

$$f_{u,j+1}^s = \left(1 - \sigma_u^{n_t} \right) \cdot f_{u,j}^s + \Delta_{u,p_j} \qquad \forall u \in \boldsymbol{U}, j \in \boldsymbol{J}, p_j \in \boldsymbol{I} \quad (3.5)$$

$$f_{u,j}^s + f_{u,p_j,t} \le F_u \qquad \forall u \in \boldsymbol{U}, j \in \boldsymbol{J}, p_j \in \boldsymbol{I}, t \in \boldsymbol{T} \quad (3.6)$$

$$f_{u,j}^s + f_{u,p_j,t} \ge 0 \qquad \forall u \in \boldsymbol{U}, j \in \boldsymbol{J}, p_j \in \boldsymbol{I}, t \in \boldsymbol{T} \quad (3.7)$$

Table 3.4 – BAT (GRD) unit model parameters

Parameter	Value	Ref.	
inv_1	20'000	[CHF/u]	[126]
inv_2	240	[CHF/kWh]	[126]
N	20	[yr]	[126]

Heating network   Until now, no thermal energy exchange has been implemented between different BES; each system has been considered thermally independent and the associated heat cascades (Eqs. 3.1 and 3.2) have been closed at the respective building level. The integration of a district heating network (HN) overcomes the latter limitation. Following the formulation of Harb et al. [120], Eqs. 3.8 to 3.10 define the HN deployment constraints where the binary variable X represents the existence of a connection between building b_i and b_j. In particular, Eq. 3.8 enforces a tree network structure by limiting a single "father" connection per building b_i while Eq. 3.9 defines an univocal characteristic to further simplify the HN layout [120, 127].

$$\sum_{b_i=1}^{\boldsymbol{B}} X_{u,b_i,b_j} \le 1 \qquad \forall u \in \boldsymbol{U}, b_j \in \boldsymbol{B} \quad (3.8)$$

$$X_{u,b_i,b_j} \le 1 - X_{u,b_j,b_i} \qquad \forall u \in \boldsymbol{U}, b_i \in \boldsymbol{B}, b_j \in \boldsymbol{B} \quad (3.9)$$

The working fluid mass flow $\dot{m}$ transiting between location b_i and b_j is finally limited by the specific unit characteristics and defined in Eq. 3.10, where the parameter D denotes the pipe

diameter, ρ the working fluid (i.e. water) density, v the fluid speed. Both the HN capital and operating expenses are expressed by Eq. 3.11 and Eq. 3.12 where L refers to the connection length, p to the specific pressure losses and η^p the pumping efficiency. Indeed, in the former equation, investments are mainly represented by digging, piping and engineering works which can be expressed in function of the total network distance. On the other hand side, the latter costs account for the pumping power required to match pressure drops along the network. It is worth noting that, in the case of this unit technology (HN) implementation, the sizing constraint (Eq. 1.7) is dropped.

$$\dot{m}_{u,b_i,b_j,p,t} \le \pi \cdot \frac{D_u^2}{4} \cdot v \cdot \rho \cdot X_{u,b_i,b_j} \qquad \forall u \in \boldsymbol{U}, b_i \in \boldsymbol{B}, b_j \in \boldsymbol{B}, p \in \boldsymbol{P}, t \in \boldsymbol{T} \quad (3.10)$$

$$F_u = \sum_{b_i=1}^{\boldsymbol{B}} \sum_{b_j=1}^{\boldsymbol{B}} \left(L_{b_i,b_j} \cdot X_{u,b_i,b_j} \right) \qquad \forall u \in \boldsymbol{U} \quad (3.11)$$

$$\dot{E}_{u,p,t}^+ = \frac{1}{\eta^p} \cdot \sum_{b_i=1}^{\boldsymbol{B}} \sum_{b_j=1}^{\boldsymbol{B}} \left(p_{b_i,b_j} \cdot L_{b_i,b_j} \cdot X_{u,b_i,b_j} \cdot \frac{\dot{m}_{u,b_i,b_j,p,t}}{\rho} \right) \qquad \forall u \in \boldsymbol{U}, p \in \boldsymbol{P}, t \in \boldsymbol{T} \quad (3.12)$$

In addition, Eq. 3.13 expresses the local mass balance for each node b (i.e building); $\dot{m}_s^{+/-}$ refers to the reference value in working fluid mass flow demand (respectively supply) of the associated BES stream s at location b. Finally, Eqs. 3.14 and 3.15 define the specific heat load associated to the unit thermal streams; the latter are integrated into each heat cascade of node b. Parameter values considered in the following applications are reported in Table 3.5.

$$\sum_{b_j=1}^{\boldsymbol{B}} \dot{m}_{u,b_j,b_i,p,t} + \dot{m}_{s,p,t}^+ \cdot f_{u,s,p,t} =$$
$$\sum_{b_j=1}^{\boldsymbol{B}} \dot{m}_{u,b_i,b_j,p,t} + \dot{m}_{s,p,t}^- \cdot f_{u,s,p,t} \qquad \forall u \in \boldsymbol{U}, b \in \boldsymbol{B}, s \in \boldsymbol{S}_u \cap \boldsymbol{S}_{b_i}, p \in \boldsymbol{P}, t \in \boldsymbol{T} \quad (3.13)$$

$$\dot{m}_{s,p,t}^{+/-} = 1 \qquad \forall u \in \boldsymbol{U}, b \in \boldsymbol{B}, s \in \boldsymbol{S}_u \cap \boldsymbol{S}_b, p \in \boldsymbol{P}, t \in \boldsymbol{T} \quad (3.14)$$

$$q_{s,p,t}^{+/-} = c_p \cdot \left(T_{s,p,t} - T_{s,p,t} \right) \cdot \dot{m}_{s,p,t}^{+/-} \qquad \forall u \in \boldsymbol{U}, b \in \boldsymbol{B}, s \in \boldsymbol{S}_u \cap \boldsymbol{S}_b, p \in \boldsymbol{P}, t \in \boldsymbol{T} \quad (3.15)$$

Table 3.5 – HN unit model parameters

Parameter	Value	Ref.		Parameter	Value	Ref.	
inv_1	0	[CHF/u]	[81]	D	0.25	[m]	[120]
inv_2	900	[CHF/m]	[81]	v	1.00	[m/s]	[120]
N	40	[yr]	[128]	η^p	0.85	[-]	[120]
p	244	[Pa/m]	[120]				

3.3.3 Multi-building performance indicators

Similarly to the single location BES sizing algorithm presented in Chapter 1, the multi-location approach implements specific key performance indicators (KPI) to analyse and compare the different system configurations generated. These metrics comprise among others:

- The community self-sufficiency (SS) and generation fraction (GF) in order to evaluate the integration of distributed generation capacities. The latter includes round-trip loss due to intra- and inter-day energy storage when exported to the local distribution network.

- The one percent peak (OPP) and grid equivalent storage (GES) metrics in order to reflect the community energy system impact on the electricity network, both in view of power and energy requirements.

- The equivalent greenhouse gas emissions in order to assess the environmental impact arising from the BES operation.

- The annual and monthly energy service expenses (C^{op} and C^{cp}) in order to measure the economic viability of each BES configuration. In addition, error ranges are estimated regarding the inherent uncertainty related to energy tariff predictions.

3.4 Applications

The following section presents the different case study results performed to illustrated the impact of district level energy systems design. For this purpose, two particular neighbourhoods are selected and analysed in regard to their specific typology and demands. In order to assess the benefit of the proposed multi-building problem formulation, the results are subsequently compared to the aggregated solutions generated from a building level problem formulation. The following computations have been performed with the commercial solver CPLEX 12.7 on a single machine which comprises a quadruple core 2.4 GHz CPU and 16 GB RAM. In addition, the maximum tolerated relative optimality gap (MIP gap) is fixed to 0.5%.

3.4.1 A two building example

In order to demonstrate the potential advantages from considering multi-building energy system sizing, a simple example of two neighbouring dwellings is implemented and subsequently analysed: (i) an old and (ii) new residential block. Both are assumed to be connected through a common node to the distribution network. The first apartment block (i), with an energy reference area of 500 m^2, reflects a strong specific space heating demand in addition to a high hosting capacity of photovoltaic panels. On the other hand side, the novel building (ii) which possesses an energy reference area of 750 m^2, is characterized through low density service requirements and a poor solar potential.

Figure 3.3 presents the installed capacities when applying a multi-location (*right*) and the subsequent differences when using a single building approach (*left*). In addition, Table 3.6 exposes both economic and renewable integration performance indicators (Section 3.3.3). As noticed, considering an equivalent investment threshold of C^{cp}=115 CHF/mon·100m^2, the district level solution reflects a 0.48 points higher self-sufficiency over the building level one while the operating expenses are decreased by 21.6%. This reduction can be explained through the larger feasible solution space of the former problem formulation. Indeed, at the multi-building level, the solver solely invests in a single photovoltaic array in addition of installing a small CHP unit in order to reduce the related specific investment cost and hence, increases the annual electricity generation. The distributed capacity is totally shifted towards the high consumption building (i) due to the higher supply temperature requirements reachable with CHP devices as well as the stronger solar potential. Consequently, the former solution highlights a potential benefit resulting from district level energy system optimization in comparison to building level solutions. However, while the presented scenario solely included two dwellings, the study of actual urban and sub-urban neighbourhoods which incorporated a higher number of energy service end-users, considerably complicates the problem resolution and hence, requires a second data reduction step: spatial classification.
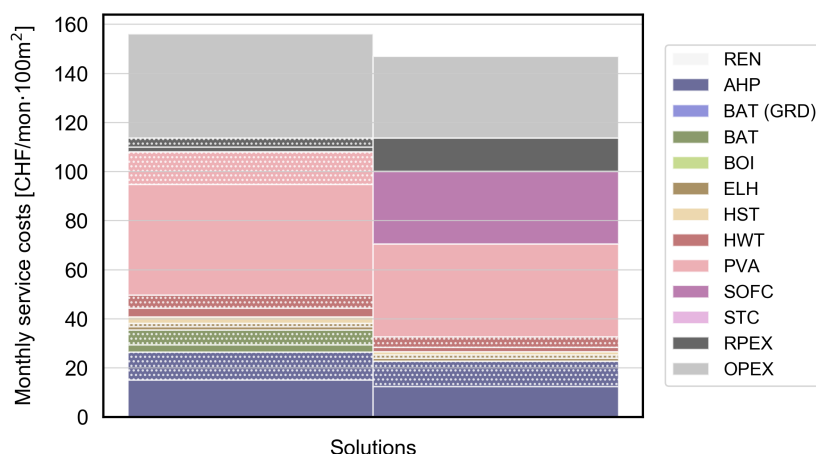
Figure 3.3 – Total expense shares for a two-building community - *left*: Single building (BES), *right*: Multi-location (MBES) problem formulation

Table 3.6 – Two-building community KPI

Indicator	Single building (BES)	Multi-location (MBES)	
C^{op}	42.5	33.3	[CHF/mo·100m^2]
E_{gen}	24.0 (i) / 6.4 (ii)	50.4 (i) / 0 (ii)	[MWh]
SC	0.61	0.74	[-]
SS	0.36	0.84	[-]

3.4.2   Real neighbourhoods study: a rural and urban case

In this investigation, a **rural** and **urban** community are analysed in regard to their specific generation potential and energy service densities. Illustrated in Figure 3.4, both areas solely comprises neighbouring dwellings and are characterized as follows:

- The **rural** neighbourhood (Figure 3.4a) consists of 13 residential buildings located in the commune of Satigny (Geneva). The dwellings are sparsely spread across a region of approximatively 1.4 ha and are solely affected to residential purposes. Following the data reduction approach proposed in Section 3.3.1, the latter have been clustered into 3 representative buildings; the related service demand profiles (EL & HW) are presented in Appendix C while additional information on the specific clusters are reported in Table C.2. Today, thermal service requirements (i.e. space heating and domestic hot water preparation) are mainly satisfied through the use of direct electrical heating (3/5) and natural gas (1/5) typical for the concerned dwelling construction period (1980-2012). Table 3.7 finally provides additional information on aggregated energy demands.

- The **urban** neighbourhood (Figure 3.4b) includes 5 registered buildings, comprising both mix-use and administrative affectations, located in the city centre of Geneva. The

dwellings are spread across a region of approximatively 0.3 ha. The neighbourhood is clustered into 3 representative buildings as illustrated in Figure 3.4b while further information on the data reduction process is provided in Appendix C. Primary energy vectors currently used to satisfy thermal energy service demands are the following: natural gas (2/5), electricity[1] (2/5) and heating oil (1/5). Finally, similarly to (i), Table 3.7 provides additional information on the neighbourhood generation potential and annual services demands.

Table 3.7 – Rural and urban district characteristics

| Prameter | Community | | |
	Rural	Urban	
Energy reference area (ERA)	11'126	8'317	[m^2]
Space heating (SH)	12.5	16.6	[kW/°C]
Space cooling (SC)	-	16.6	[kW/°C]
Hot water (HW)	178	70	[MWh/yr]
Electricity (EL)	205	271	[MWh/yr]
Solar potential[1]	3'870	1580	[m^2]

[1] Potential surfaces extracted from [36]

(a) Rural community

(b) Urban community

Figure 3.4 – Micro-grid case studies with *right* 13 buildings clustered into three classes (A–C) and *left* 5 buildings clustered into three classes (A–C).

Figures 3.5 and 3.6 show the aggregated BES configurations and distributed generation integration KPI of both communities respectively; MPC-A denotes the results associated to the multi-location problem formulation while MPC-B and DMPC refer to the building-level problem formulation, considering a distributed and centralized control approach respectively. The latter is indeed achieved by implementing the BES configurations defined in MPC-B and subsequently solving the multi-location scheduling problem. In order to differentiate

---

[1]Resistive electrical heaters (ELH)

the investment expense shared allocates to each representative building, the associated bar surfaces are hashed (Figs. 3.5a and 3.6a) in the following manner: none for cluster A, dots for cluster B and diagonal lines for cluster C. Additionally, since the MBES configurations are identical for MPC-B and MPC-C, the latter results are not represented in the respective bar charts (Figs. 3.5a and 3.6a). Following computation, multiple case specific observations are stated and analysed in the paragraphs below.

In case of the **rural** community, the implementation of a multi-location problem formulation (MPC-A) substantially rises the integration of distributed generation capacities for smaller investment thresholds ($S_{0.1}$-$S_{0.4}$); the district self-sufficiency is increased by 19.4-29.0 points, the generation fraction (80% round-trip) by 17.6-31.9 points while the annual equivalent greenhouse gas emissions are deteriorated within a range of 40-228%. On the other hand side, the operating expenses are decreased by 6 to 8% within the same solution range. Indeed, when solving the BES sizing problem at the community level, a cogeneration device (SOFC) is rapidly activated due to the higher investment threshold available to the optimizer ($S_{0.1}$). Hence, in comparison to MPC-B where photovoltaic arrays (PVA) are developed simultaneously on each roof, the SOFC represents a more economic solution to decrease the community energy bill despite worsen its environmental impact. Following the installation of a large SOFC unit, the multi-location configurations further reduce capital expenses associated to distributed generation units (PVA) by first fully exploiting a single roof area prior targeting an additional building hosting capacity ($S_{0.2}$-$S_{0.4}$).

At higher investment thresholds ($S_{0.5}$), the disparity in generation fraction between both problem formulation results decreases (41 points) while the difference operating expenses remains substantial (-11%). This behaviour can be explained through lower solar potential dwellings (cluster A) in MPC-B which reached their full solar hosting capacity and start investing in storage units (BAT) while high potential buildings (cluster B & C) are still not exploiting their full roof area. From a practical point of view, the former and latter solutions of the community level problem formulation (MPC-A) might be interpreted as roof (or photovoltaic system) shares of large buildings purchased or rented by low renewable integration potential BES located within the same community. Moreover, in MPC-A, the locally placed storage units are replaced by a centralized battery system. Similarly to the previously discussed PVA deployment, the large-scale battery system (BAT GRD) indeed reflects a lower specific investment cost (Table 3.4) compared to the distributed solutions and hence, is selected by the solver at higher investment threshold values ($S_{0.6}$-$S_{0.8}$). With the stronger use of natural gas engendered by the deployment of SOFC device in MPC-A configurations ($S_{0.1}$-$S_{0.9}$), the expect total expenses ranges reflect a higher degree in uncertainty than the solutions of MPC-B.

Due to the integration of a base-load CHP unit since $S_{0.1}$, the OPP metric of MPC-A reflects lower values for $S_{0.1}$-$S_{0.4}$ as shown in Figure 3.5b. Nevertheless, with the further increase in distributed generation capacity (PVA & CHP) and the associated power exports peaks, the OPP rises to comparable values as MPC-B. On the other hand side, the GES indicator remains close to null for $S_{0.1}$-$S_{0.3}$ prior rapidly rising until $S_{0.6}$. Finally, when operating the building-level

BES configurations in a centralized manner (DMPC), the solver is able to slightly improve the community self-sufficiency and generation fraction in the presence of CHP devices with differences ranging between 2.3 ($S_{0.6}$) - 3.2 ($S_{0.8}$) and 2.1 ($S_{0.6}$) - 0.9 ($S_{0.8}$) points respectively.

(a) Expense contributions per BES configuration

(b) Key performance indicator per BES configuration
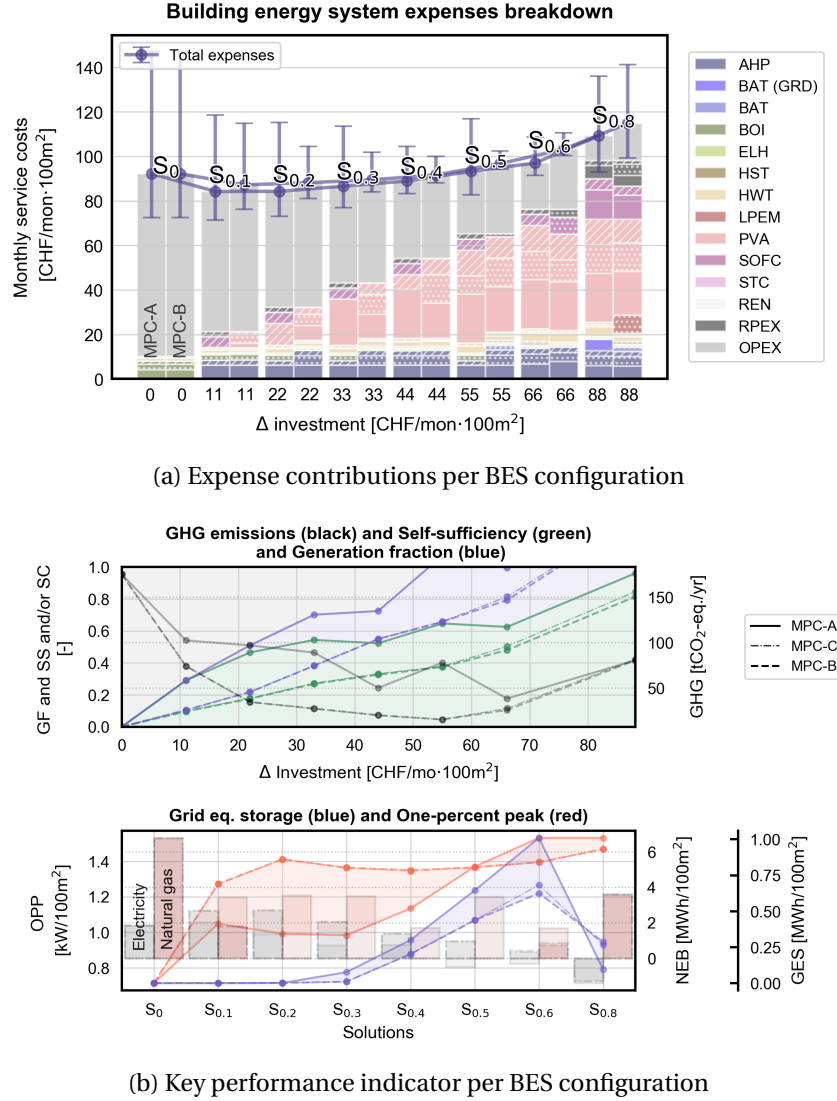
Figure 3.5 – Multi-objective optimization results for an existing rural community in Western Switzerland

In the case of the **urban** community, the impact of a multi-location sizing approach (MPC-A) is more pronounced (Figure 3.6a); indeed, a strong difference in self-sufficiency between both formulations is noticed, starting from $S_{0.2}$ until reaching 35.7 points ($S_{0.3}$) before finally steadily decreasing again until 4.1 points ($S_{0.8}$). In regard to the strong energy service demands and low solar generation potential of the studied community (Table 3.7), a substantial use of flexible (LPEM) and unflexible (SOFC) CHP devices is observed for both scenarios (MPC-A & MPC-B), thus shifting electricity requirements towards the natural gas energy carrier.

Indeed, throughout the entire solutions set, distributed electricity generation from PVA units solely accounts for 6-31% of the total production. However, in view of the lower variance and higher daytime amplitudes of the EL demand profile illustrated in Figure C.4, the electricity production from PVA and CHP units is entirely self-consumed for each BES configurations as reflected by both GES and the SS indicators (SS=GF). With the introduction of flexible CHP units in the case MPC-A, the OPP metric reflects lower values in comparison to MPC-B; with the rise in investment expenses and the increasing similarity in BES configurations between MPC-A and MPC-B, the latter disparity finally decreases.

From an economic perspective, the use of a multi-location sizing method (MPC-A) slightly decreases the BES operating expenses, differences ranging between 0.5 and 7.7%. Similarly to the rural community scenario, the solver first attempts in implementing large "centralized" generation units (LPEM) in order to reduce the associated specific capital costs. Similarly to the office building case study in Chapter 1, the cost-optimal BES solutions is located at higher investment thresholds ($S_{0.6}$), for both problem formulations. Obviously, as observed in the rural case study, with the stronger consumption of natural gas driven by the higher penetration of CHP units and finally highlighted by the net energy balances (NEB), the associated uncertainty in tariffs decreases the error margin in expected service costs. Simultaneously, the consequent drop in primary energy supply reduces the BES environmental impact, the equivalent greenhouse gas emissions improving by 34% between S_0 and $S_{0.8}$.
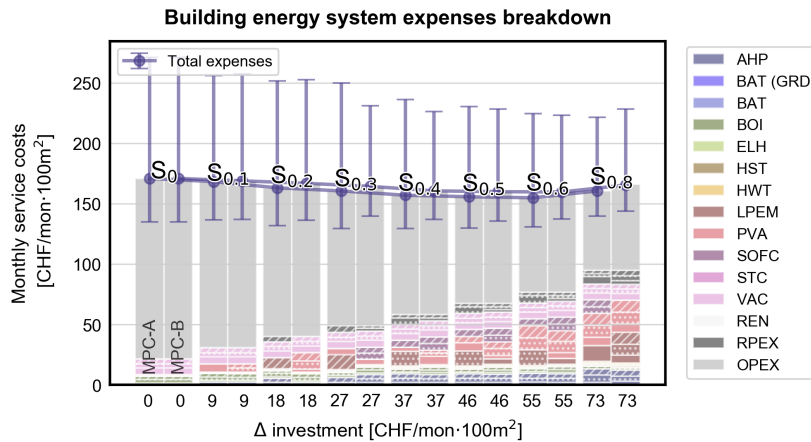
(a) Expense contributions per BES configuration
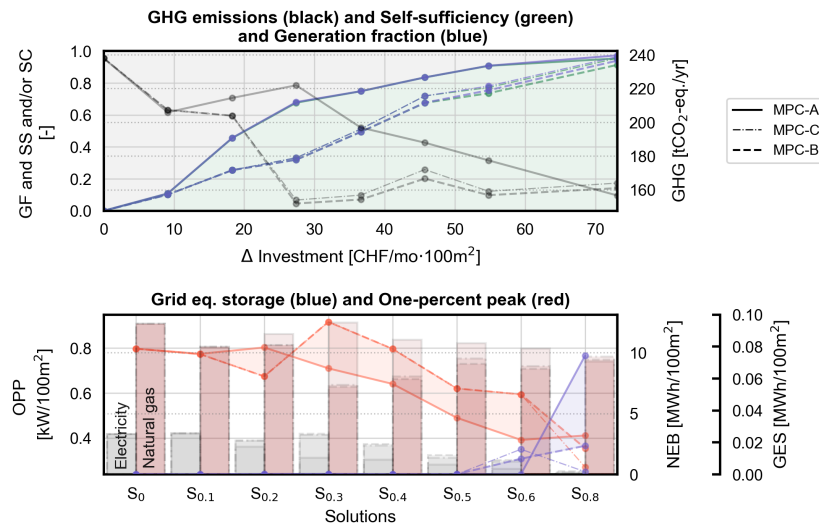
(b) Key performance indicator per BES configuration

Figure 3.6 – Multi-objective optimization results for an existing urban community in Western Switzerland

Community configuration

Although presenting perceptible economical benefits from considering a multi-location problem formulation, the presence of a single building category (residential) in the **rural** case study is not demonstrating the full potential of service demand synergies. Indeed, in view of the data input assessment approach applied in this study, no energy service demand shifts associated to different occupant behaviours are considered. In light of the latter lack of heterogeneity, the rural community is reconfigured, replacing two apartment blocks by a large primary school located in proximity. The resulting difference in energy service demands are represented in Table 3.8 on an annual basis while the daily profiles are illustrated in Figure C.4. Furthermore, Figure 3.7 depicts the novel layout while highlighting the different clusters resulting from the data reduction process.

Table 3.8 – Reconfigured rural community characteristics

Prameter	Community		
	Rural	Reconfigured	
Energy reference area (ERA)	11'126	11'903	[m^2]
Space heating (SH)	12.5	20.9	[kW/°C]
Space cooling (SC)	-	11.4	[kW/°C]
Hot water (HW)	178	145	[MWh/yr]
Electricity (EL)	205	240	[MWh/yr]
Solar potential[1]	3'870	4'333	[m^2]

[1] Potential surfaces extracted from [36]
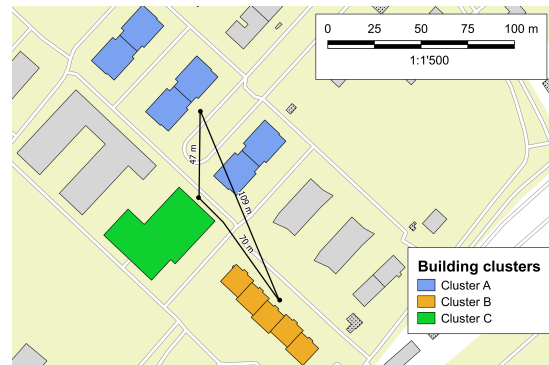
Figure 3.7 – Rural (reconfigured) community 12 buildings clustered into three classes (A–C)

The associated system results are presented in Figure 3.8; the upper graph illustrating the different expenses shares while the lower graph depicts the respective KPI for the original (MPC-A) and reconfigured (MPC-B) rural communities. Since both case studies (MPC-A and MPC-B) have been sized independently, a slight difference in specific investment costs can be noticed. As observed, no economic benefits are reported; indeed, due to the stronger energy service demands of the reconfigured community (EL and SC), the associated monthly annualized expenses reflect higher values. The latter is confirmed by the cost disparity observed for the initial configuration (S_0) which, in this case, amounts to 9%. Nevertheless, with the further rise in investment expenses and the consequent penetration of distributed generation (PVA and CHP), the economic difference between both communities drops until reaching a gap of 4% ($S_{0.8-0.6}$).

On the other hand side, in view of the disparities in Figure 3.8b, the use of more homogeneous[2] service demand profile improves the integration of distributed generation: considering rather similar investment thresholds, the BES self-sufficiency is increased by up to 18 points while the generation fraction remains solely 7 points lower ($S_{0.4}$). Furthermore, the latter phenomena is reflected by the GES indicator which highlights drops in equivalent storage needs between 0.08 and 0.45 MWh/100·m^2. Always from a power network point of view, the reconfigured community improves the OPP metric too. While for the initial configuration (S_0) the slight decrease in OPP is related to the change in uncontrollable energy service profiles (Figure C.4), the integration of a flexible CHP device (LPEM) for the subsequent configurations further reduces the network KPI, values ranging between 0.10 ($S_{0.1}$) and 0.34 ($S_{0.4}$) kW/100·m^2

Nevertheless, this strong level of electrical autonomy for low investment BES configurations ($S_{0.1-0.3}$) is mainly achieved through the operation of this large and flexible CHP unit (LPEM) and thus, substantially worsen the system environmental impact in comparison to the initial community layout. Finally, it is worth noting that, starting from $S_{0.4}$, distributed generation from renewable sources (PVA) is higher in the reconfigured case, the latter increase ranging

---

[2]In regard to the temporal variations

between 3.5 ($S_{0.4}$) to 12% ($S_{0.8}$).
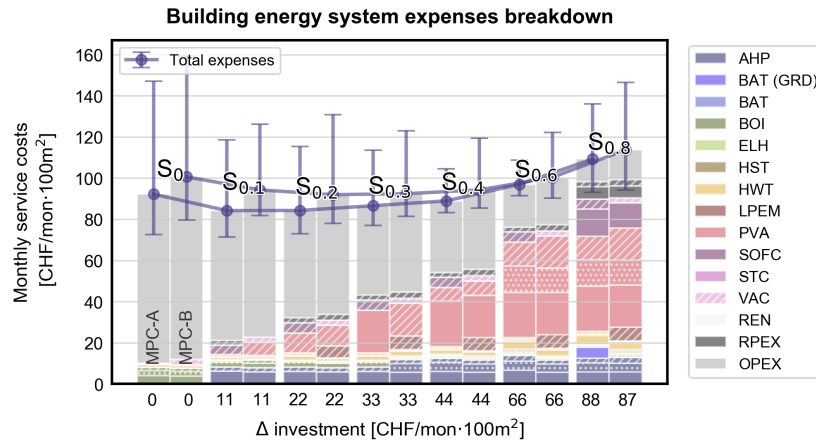
(a) Expense contributions and per BES configuration
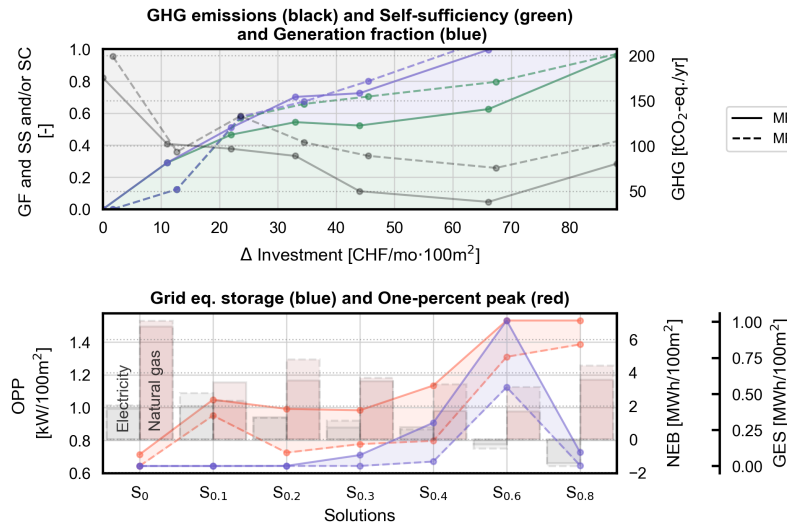
(b) Key performance indicator per BES configuration

Figure 3.8 – Multi-objective optimization results for an existing rural community in Western Switzerland

Building refurbishment and heating networks

This last scenario analyses the impact of both the dwelling refurbishment (envelope & hydronic heating system) and the integration of a heating network (HN) unit on the BES configurations and their respective performances. Figure 3.9 thus illustrates the consequent system results for both the rural (reconfigured) and urban community.

Interestingly, in the **rural** community case study, BES configurations comprising the refurbished buildings and the option of a local heating network (MPC-B) reflect substantial re-

ductions in total annualized expenses; although comprising strong investment costs, mainly related to the partial neighbourhood refurbishment (REN), the respective decrease in operating costs compensates the latter for each BES configuration, except the initial scenario (S_0). Indeed, already for low investment threshold, the deployment of a local HN allows for the installation of an efficient and unflexible CHP device (SOFC), excess heat generation being transferred to the surrounding dwellings. Indeed, as discussed in the previous chapter (Chapter 1), the SOFC capacity is limited by minimum thermal energy service requirements of each representative period (Eq. A.4), the lower bound being typically represented by the summer period where the sole heating service include hot water preparation. Although rapidly reaching a strong degree in self-sufficiency for low investment thresholds ($S_{0.2}$: 78%), over 90% of the local electricity production arises from the CHP unit in the case of MPC-A and thus, solely merely improves the BES environmental impact in comparison to the respective initial configuration (S_0). Nevertheless, considering both the lower service demands and the integration of an efficient SOFC unit in the case of MPC-A, the equivalent green house gas emissions reflect similar values for both scenarios starting from solutions $S_{0.3}$.

From power network point of view, the BES configurations of MPC-B reflect lower OPP and GES values. However, with the further penetration in distributed generation, in particular PVA units, the OPP metric rises towards similar values than the MPC-A case since no limitations are applied on electricity injection peaks.

On the other hand side, in the **urban** case, the economic implementation of community including refurbished buildings and a HN unit is not advantageous. Indeed, since the community solely includes poorly insulated dwellings (Table C.3), renovation expenses (REN) represent the highest share among the different cost contributions. Solely when considering a 40% state subsidy on renovation expenses, MPC-B configurations start becoming cost-optimal with respect to MPC-A solutions for $S_{0.6}$-$S_{0.8}$. As noticed in Figure 3.9b, the HN unit is not implemented throughout the entire solution set. Similarly to MPC-A, the solver first seeks in implementing CHP units to decrease operational expenses while deploying AHP as additional primary conversion units. Subsequently, renewable-based distributed generation capacities (PVA) are expanded before finally integrating a more flexible LPEM.

Indeed, due to the lack of flexible CHP units (LPEM) for low investment thresholds in the case of MPC-B, the related OPP exceed respective values of the MPC-A scenario, with exception of $S_{0.2}$ in which only a single representative building type applies an AHP. However, with integration of a LPEM device for high investment thresholds ($S_{0.6}$-$S_{0.8}$), the disparity drastically drops. Finally, similarly to MPC-B, the GES remains close to null; on-site electricity production from PVA and CHP is indeed self-consumed (SS=GF) in view of both the strong energy service (EL & SC) demands and low solar generation potential.

(a) Expense contributions and per BES configuration

(b) Key performance indicator per BES configuration

(c) Expense contributions and payback time per BES configuration

(d) Key performance indicator per BES configuration
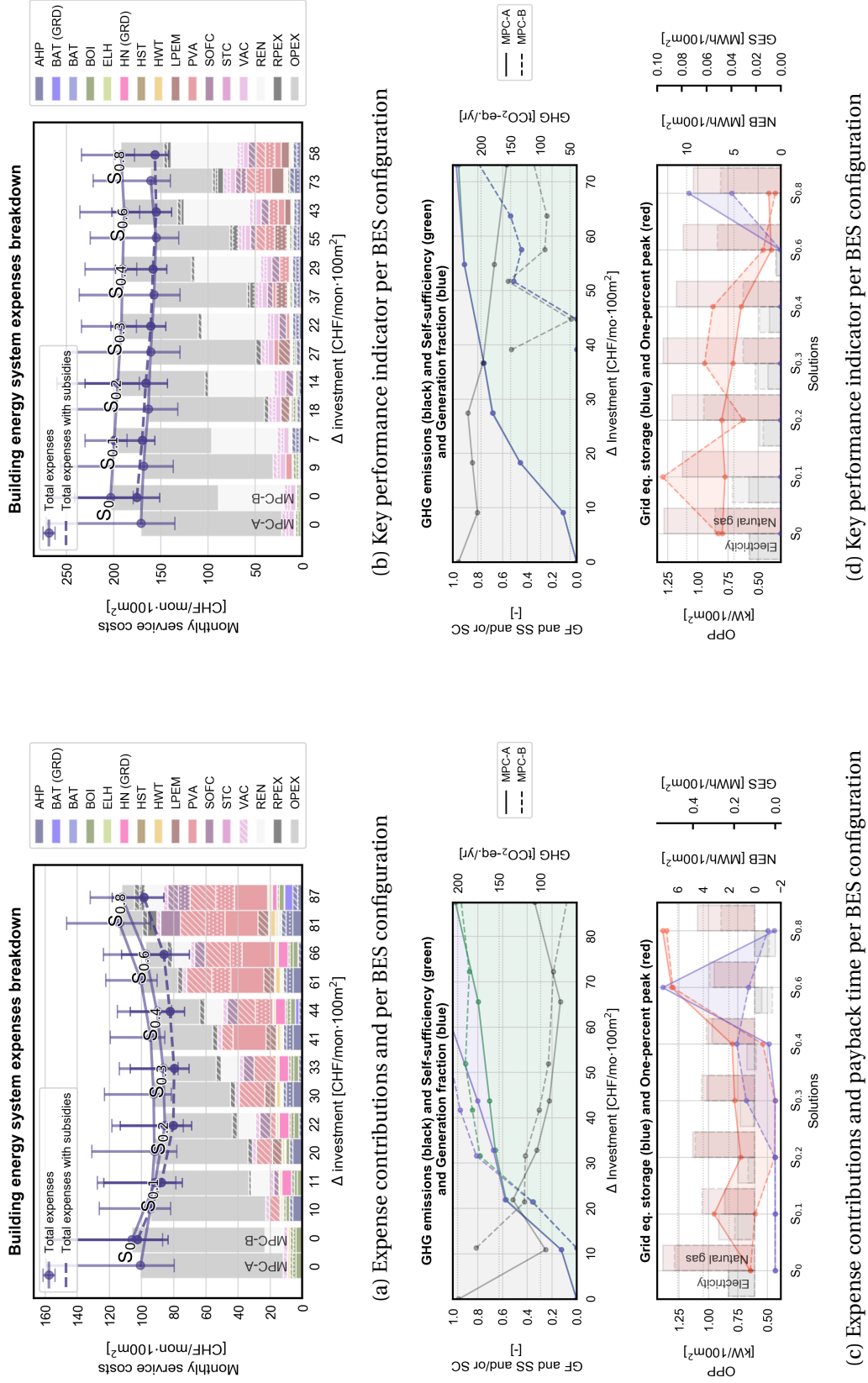
Figure 3.9 – Multi-objective optimization results for the refurnished urban (right) and reconfigured rural (left) communities with HN options

Computational effort

Although not residing within the main research focus of the latter chapter, the following section briefly discusses the computational efficiency of the proposed method. Indeed, regarding the targeted audience for future wide-scale applications, the latter should require a reasonable computing capacity. Hence, Table 3.9 provides the average MILP problem sizes in addition to the mean solving times of the presented case studies. In regard to the standard hardware applied (single machine with a quadruple core 2.4 GHz CPU and 16 GB RAM), the following values seem acceptable for wide spread applications, especially since practitioners rarely have access to tremendous calculation power. Nevertheless, with the rise in representative building number, a direct solving strategy, as implemented in this study, does not represent the best choice; MILP decomposition methods (e.g. Dantzig-Wolfe) might indeed reflect better performances [113].

Table 3.9 – Mean and (standard deviation) problem sizes & computation times

	HN	Building level	Community level	
Variables[1]	×	22'452 (6'652)	120'367 (9'550)	[-]
	✓		127'325 (12'027)	[-]
Constraints[1]	×	24'063 (6'869)	159'262 (6'992)	[-]
	✓		163'908 (9'718)	[-]
CPU time	×	55 (92)	3'347 (3'139)	[sec]
	✓		2'779 (2'122)	[sec]

[1] Prior presolve

3.5 Conclusion

This chapter presented a MILP formulation to optimally size building energy systems for multi-location problems (neighbourhoods). In order to limit the required computational effort while simultaneously rendering the problem more tractable, both a temporal and spatial clustering process have been performed prior solving the optimization problem. Following the implementation and validation of the proposed method through different case studies, several interesting aspects have been brought into light:

- The use of a multi-location approach substantially improves the integration of distributed energy technologies, particularly for lower investment thresholds. Both the rural and urban case studies highlighted a strong increase in generation fraction (18-35 points) while additionally, for the rural community, a rise in self-sufficiency (19-29 points). Simultaneously the implementation engendered a decrease in operating expenses by 6-8% in comparison to a single location method. Nevertheless, the latter performance disparities drop for higher investment thresholds since the generated BES configurations increasingly grow similar. In addition, the use of multi-location approach showed potential benefits from the power network operator by both decreasing the OPP and GES metrics, mainly due to the increased integration of flexible CHP devices.

- Nevertheless, with the additional implementation of community units such as a local heating network (HN) and large battery energy storage systems (BAT GRD), the use of a multi-location approach regains in interest, even for higher investment expenses. Results of rural case study showed a particular benefit from implementing both technologies while for the considered urban community, the latter units presented less interest.

- The use of a centralized predictive control technique (DMPC) to operate BES assessed independently, solely merely improves the community performances. Indeed, the sole changes in behaviour are noticed with a partial penetration of CHP devices; in the case of a centralized control approach, the solver maximizes its utilization by exporting excess electricity production to neighbouring BES deprived of the latter technology.

In a nutshell, the implementation of multi-location problem formulations allows for a more cost-efficient use of available energy resources by first targeting large unit capacities and thus, decreasing the respective investment expenses. Furthermore, in the latter case studies, the consequent rise in required computational effort lies within the characteristics of standard office hardware while solving times remain reasonable.

Limitation and perspectives While the latter chapter mainly focused on demonstrating the benefit of multi-building energy system design in regard to single dwelling approaches, the micro-grid selection process has not been addressed. Indeed, the latter chapter solely included

a continuity condition while defining the different case studies. Nevertheless, when addressing a large district, a formal clustering method should be applied to identify smaller entities in view of energy service demand synergies and potential distributed generation capacity. In addition of considering the latter demand and resource information, local network characteristics might be incorporated in order to account for eventual redrawing (upgrading or deploying power cables) expenses and thus, balancing the environmental and economic benefits of expanding the distribution network.

From a modelling perspective, further development could be performed regarding district heating networks. Indeed, the model appended to the MF solely considers a single distribution temperature option and thus, targets only space heating and hot water preparation energy services. Nevertheless, when analysing communities comprising complex buildings categories (e.g. administrative or commercial) requiring space cooling services, the use of a low temperature network might represent an interesting alternative to further exploit the synergies between different dwelling types (anergy networks). In addition, through the latter decrease in operating temperature, further ambient heat sources such as lakes, rivers and soil could be exploited. On the other hand, regarding the problem formulation strategy, additional performance constraints might be added to steer towards good trade-off solutions for all stakeholders. Indeed, as observed throughout the different case studies in this and the previous chapters, the use of an ϵ-constraints multi-objective approach might provide multiple interesting system configuration, although reflecting limitations when targeting specific performance requirements. Hence, a multi-parametric optimization formulation (mp-MILP), which relies on the alteration of parametric constraints to generate novel solutions and thus, resembles the applied ϵ-constraint approach, might provide an interesting extension within the context of future developments.

The presented method relied on the assumption of a combined investment and consequently, of a combined operational benefit. Nevertheless, from a practical point of view, the latter implementation might engender a critical follow-up question: which costing share is allocated to each end-users? Particularly in the case of strong investment disparities among the different BES as observed in the case of a partial stock refurbishment, this questions is not straightforward to answer. Hence, future investigations should address the topic by defining fair and attractive business models in regard to each stakeholder involved in the planning process: end-users, system owners and distribution network operators.

Finally, a remaining aspect concerns the assessment of operational flexibility. Indeed, the repetitive comparison of different scheduling strategies for similar system configurations raises the question of a formal flexibility definition. Although briefly addressed in Chapter 1 with the introduction of a equivalent building storage (BES) performance indicator, the latter method solely considered two specific operating strategies (rule-based and predictive control), regardless any ancillary service demands from the power network side. Hence, the following chapter will address the latter challenge by introducing a generic flexibility assessment approach to evaluate the cost-benefit of installing efficient and smart BES for power network

operators.

4 Flexibility of building energy systems

<div style="border:1px solid #c0504d; border-radius:8px;">

Chapter overview

- Equivalent battery definition for building energy systems
- Systematic cost incentive approach
- Large-scale assessment

</div>

4.1 State of the Art

In view of the increasing generation volatility resulting from a deeper penetration of renewable energy sources, power network operators face a rising need of load flexibility. While the large scale deployment of battery energy storage systems (BESS) might help in balancing distortions between production and consumption on a both daily and seasonal basis, this measure comes with a strong economic cost and technological constraints. The implementation of demand side management (DSM) provides however an interesting solution in decreasing the future need of BESS: the associated expenses solely comprises the development and deployment of an advanced control framework while the building energy system (BES) has already been purchased with the aim to satisfy domestic *energy service* requirements. Recent investigations within the field of smart BES management have highlighted the use of optimal and predictive control methods, i.e. model predictive control (MPC), as a good candidate to perform ancillary services such as load shifting and peak shaving [129, 130].

Indeed, regarding the increasing interest in providing load flexibility, the subject of quantifying the potential of DSM through BES has been recently emerged in literature, particularly in view of the different stakeholders interests. From a power network operator perspective, Ulbig and Andersson [131] introduced a generic framework to quantitatively assess and visualize the operational flexibility of electric power systems. The proposed definition builds on the power node model [132, 133] and allows for a straightforward aggregation of multiple technologies using the minkowski summation technique. Mainly developed for power network operators,

the authors principally targeted medium and large-scale generation capacities. Locally, at the unit level, Namor et al. [134] proposed and subsequently validated experimentally, a novel control algorithm for large-scale battery energy storage systems to simultaneously provide multiple ancillary services to the respective stakeholders. Their approach included (1) the operational dispatching of a medium voltage feeder holding different heterogeneous loads and generation capacities in combination to (2) primary frequency control. Two daily experiments have demonstrated the deployability of the presented control algorithm, although contingency protocols still need to be defined. Considering a larger problem boundary, the *FlexiTool* modelling framework (MF) optimally assesses electric power system portfolios at regional and national levels while targeting a specific penetration of intermittent renewable sources, i.e. wind and solar [17, 135]. The MF included technological constraints regarding unit ramping rates, part-load limits and reserve capacity requirements. Subsequently, the authors successfully validated the proposed tool through two case studies, considering a single and 15 nodes network configuration respectively.

On the other hand side, from an end-user (i.e. building) perspective, Oldewurtel et al. [130] presented a standardized framework to define the load shifting potential of buildings through the flexible provision of space heating (SH) and cooling (SC) services. The proposed algorithm relied on an iterative process during which the system disturbances (e.g. external temperature) and the upward (respectively downward) power requests for each discrete time step are altered. In order to successfully implement the related operative constraints, the authors applied a non-linear model predictive control formulation previously developed by [136]. Their simulation demonstrated a strong impact of both the climatic conditions and the hour of day on the shifting potential. A similar approach has been proposed by De Coninck and Helsen [137] who validated their control algorithm on an office building in Continental Europe. Blum et al. [138] proposed a multi-step control algorithm to define the ancillary services opportunity costs for large HVAC systems. The authors focused the load shifting potential arising from displacing SC requirements and thus, exploiting the thermal inertia of the considered dwelling type. In regard to the presented case study, their simulation results reflected similar ancillary costs as [137]. Still within an operational context, Good et al. [139] developed an air-source heat pump control approach from the power network operator perspective to exploit the thermal storage capacity of multiple buildings to decrease imbalance costs. The method comprises a financial compensation to occupants when deviating from the desired comfort temperature dead band. In a more recent study, Sossan [140] defined an iterative approach based on Monte-Carlo simulations to assess the flexibility provided by thermostatically controlled loads (SH & HW[1]). The proposed algorithm computed the equivalent, mean BESS performances in terms of power and energy capacities and compared the latter performance with a state-of-the-art electrical energy storage systems. The simulation results have been performed considering a 30 days timespan during the autumn/winter seasons and showed a substantial financial benefit. Finally, from a rather planning perspective, Stinner et al. [141] presented a simulation-based method to estimate the operational flexibility of a BES comprising either air-source heat

---

[1]Hot water preparation

pumps or combined heat and power (CHP) units in combination to thermal storage tanks. In their case studies, the authors showed the impact of both the relative unit sizes as well as the aggregation of multiple buildings on the achievable flexibility performances.

4.2 Contributions

The following chapter presents a novel approach to quantify the potential flexibility provided by optimally sized BES configurations. The method builds upon a MILP modelling framework (MF) defined in Chapter 1 and uses an equivalent battery energy storage system (BESS) model to characterize the load shifting capabilities of each BES. In regard to the recent literature, this chapter attempts in contributing to the state-of-the art through the following three main elements:

- The implementation of a holistic energy systems modelling framework (MF), considering renewable energy sources as well as both thermal (space heating/cooling and domestic hot water preparation) and electrical energy service demands. Although, previous studies have successfully addressed the challenge of modelling and analysing complex building energy systems, most of the analyses solely focused on a limited set of empirically defined [141] or fixed [130, 140] system configurations and therefore, lack of an integrated approach.

- A generic flexibility assessment of BES prior operation, using representative request profiles as typical imbalance indicators. Indeed, most studies solely focused on the development of detailed control algorithms to perform load shifting [130, 137, 138] while only a few actually targeted the quantification of the provided ancillary service provision in an early design phase.

- Based on the formulation of [140], an equivalent BESS definition considering different round-trip efficiency thresholds is defined. The use of a discrete performance approach indeed allows for the straightforward comparison of the associated BES configurations to currently available, large-scale storage technologies such as pumped hydro, power-to-gas or electro-chemical (i.e. batteries) systems.

Hence, in order to tackle the aforementioned challenges, the following chapter is structured in four main parts. Section 4.3 details the different elements comprised within the developed algorithm, among which: the definition of representative flexibility profiles, the problem formulation and equivalent BESS key characteristics. Section 4.4 validates the approach through the means of several case studies at both building and community scale. Finally, Section 4.5 provides concluding remarks on the presented results as well as limitations and future perspectives regarding the presented method.

4.3   Material and methods

The following section presents a model-based algorithm to define the load shifting potential of BES while satisfying the required energy service demands. Figure 4.1 illustrates the method pathway which comprises three main process steps summarized as follows:

- The flexibility **demand profiles** definition (Section 4.3.1)

- The **optimal control** strategy (Section 4.3.2)

- The BESS **performance** assessment (Section 4.3.3)
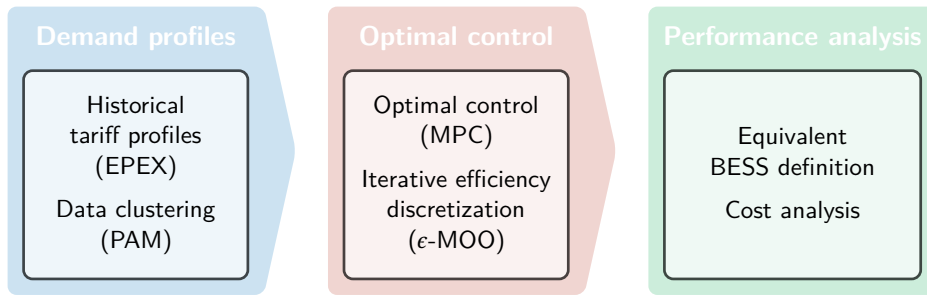
Figure 4.1 – Illustrative representation of the assessment method

The main idea of the following algorithm consists in comparing a *base* electricity profile resulting from a standard operation strategy with multiple *flexible* electricity profiles achieved with a cost-based demand response scheme. Hence, using different load variation request profiles s associated to a given probability of occurrence d_s, the algorithm systematically solves the MILP control problem formulation for each specific request profiles s prior summarizing the system performances through an equivalent BESS definition. In regard to the considered focus on BES, the following chapter solely targets slower ancillary services, mainly *load shifting* and optionally *peak shaving,* since thermal conversion and storage units of BES commonly reflect slower response times.

4.3.1   Demand profiles

Prior estimating the system capabilities in shifting dispatchable loads, direct or indirect *flexibility* request profiles from network operators are required; the latter should inform the BES users of desired upward or downward power changes in exchange of an economic compensation. To that end, a dynamic tariff scheme is applied, as proposed and discussed by Lutz et al. [142]. Indeed, the authors reported a noticeable correlation between the European day-ahead (EPEX) electricity price variations and imbalances within local distribution networks throughout Germany and thus, identified the latter market disparities as an acceptable reference signal for the provision of ancillary services.

Consequently, in view of determining *representative* flexibility request profiles *s*, a clustering algorithm is defined and subsequently applied on historical data of the hourly electricity tariffs of the European day-ahead market (2007-2016)[2]. Similarly to the approach developed to the define representative operating periods *p* of specific climate zones (Section 1.3.1), the tariffs representative profiles are identified using a k-medoid clustering technique: partitioning around medoids (PAM).

Data processing   Prior clustering, the EPEX day-ahead tariff variations $\Delta_{k,t}$ are determined from the reported price values $x_{k,t}$ using Equation 4.1. In the latter definition, the subscript k refers to a day within the $10^{\text{year}} \times 365^{\text{day}}$ data sets, t to the hourly time step and $\bar{x}_k$ to the daily average tariff values. The thus defined variations profiles are subsequently clustered *a-priori* according to the annual index of the different representative operating periods *p* previously identified for each climatic zone (Section 1.3.1). Hence, $|\boldsymbol{P}|$ sets of dynamic tariff profiles $\boldsymbol{X}_p$ are generated for each climatic zone by applying the same annual index function ϕ for each of the 10^{year}. Consequently, each $\boldsymbol{X}_p$ has a size of 10 times the occurrence of period p within the annual index function. Equation 4.2 finally details the following process.

$$\Delta_{k,t} = \frac{x_{k,t}}{\bar{x}_k} - 1 \qquad\qquad\qquad \forall k \in \boldsymbol{K} \quad (4.1)$$

$$\boldsymbol{X}_p = \left\{ \Delta_{k,t} : \phi(k) = p \right\} \qquad\qquad\qquad \forall p \in \boldsymbol{P} \quad (4.2)$$

Partitioning around medoids   The aim of the following clustering process is to define *s* representative profiles for each of the representative period *p* among the pre-defined subsets $\boldsymbol{X}_p$. Therefore, a k-medoid clustering algorithm (PAM) is implemented on the corresponding tariff variation subset $\boldsymbol{X}_p$ in an iterative manner while the best cluster number is selected on basis of the silhouette index [71]. During the clustering process, the squared Euclidean distance function is applied in order to further penalize outliers. Since solely a single attribute *a* is considered in the following clustering problem (i.e. the EPEX tariff), no normalization is required prior computation. Consequently, $|\boldsymbol{F}_p| = \text{n}_f$ representative variation profiles $\Delta_{f,p,t}$ are defined for each representative operating period *p* with a given probability of occurrence d_s. An illustrative example of the generate results is provided in Figure 4.2 when considering the climatic zone of Geneva-Cointrin (Section 1.3.1).

4.3.2   Optimal control

Following the assessment of representative flexibility request profiles, the respective building responses are determined. While the reference *base* electricity profile $\dot{\text{E}}_{\text{grid}}$ is defined using a constant energy tariff op^{el}, both for purchasing ($^+$) and feed-in ($^-$), the flexible response profiles $\dot{E}_{\text{grid}}$ are defined using the electricity cost definition of Eq. 4.3. Hence, the optimal

---

[2]Data publicly available at https://www.epexspot.com/en/market-data, last accessed 17 October 2018
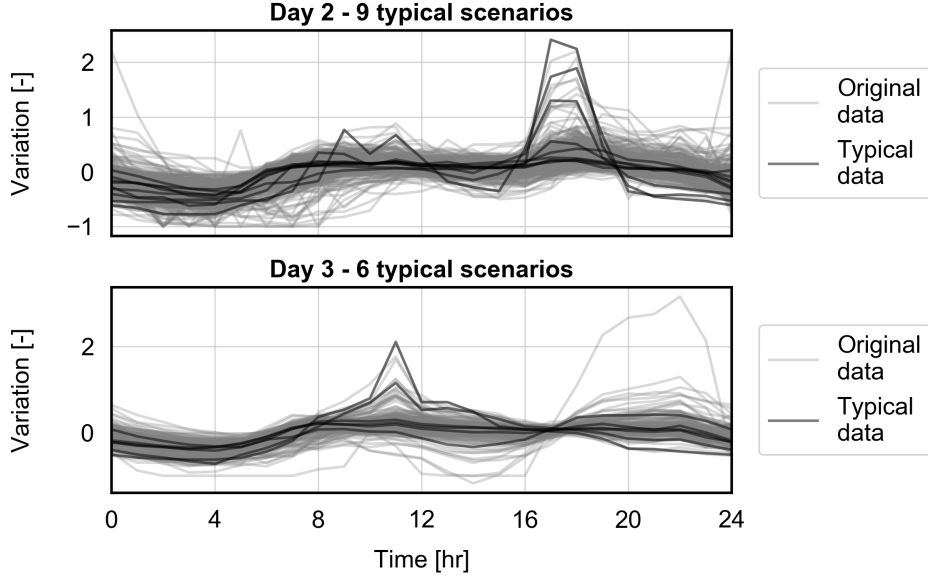
Figure 4.2 – Original and representative profile variations for two of the representative operating periods in Geneva-Cointrin

control problem is solved iteratively, for each request scenario f of each period p while the resulting performance indicators are subsequently computed by considering the associated frequency of occurrence, d_f and d_p respectively.

$$\mathrm{op}^{\mathrm{el},+/-}_{f,p,t} = \left(1 + \Delta_{f,p,t}\right) \cdot \mathrm{op}^{\mathrm{el},+/-} \qquad \forall p \in \boldsymbol{P}, t \in \boldsymbol{T}, f \in \boldsymbol{F}_p \quad (4.3)$$

Moreover, in order to analyse different equivalent BESS round-trip efficiencies, a parametric optimization (p-MILP) technique is implemented [143]. Indeed, since the applied demand method solely relies on electricity cost incentives, no specific constraint is limiting a probable energy consumption increase with respect to the reference *base* case. In the p-MILP formulation, the latter is limited through an additional constraint while the associated right hand side (the considered efficiency bound ϵ_{eff}) is varied in between each optimization run. Similarly to the previous chapters, the BES behaviour is described using the modelling framework (MF) previously defined in Section 1.3.2, upon which this flexibility assessment algorithm constructs on. Equation 4.4 finally states the associated problem formulation

$$\min_{\boldsymbol{\Sigma}} C^{\mathrm{op}}_{f,p}$$

$$\boldsymbol{\Sigma} = \left\{ f_{u,p,t,(s)}, y_{u,p,t}, \delta_{u,p,t}, f^{+/-}_{u,p,t,(s)}, T_{b,p,t}, \dot{R}_{k,p,t}, \dot{Q}^{+/-}_{s,k,p,t}, \dot{E}^{+/-}_{\mathrm{grid},p,t}, \dot{H}^{+/-}_{\mathrm{grid},p,t} \right\}$$

subject to $\qquad\qquad\qquad\qquad\qquad\qquad\qquad\qquad\qquad\qquad\qquad\qquad\qquad$ (4.4)

$$C^{\mathrm{eff}}_{f,p} \le \epsilon_{\mathrm{eff}}$$

Eq. 1.6 - Eq. 1.33 and Eq. A.1 - Eq. A.25

where C^{op} denotes the BES operating expenses, C^{eff} the equivalent BESS round-trip efficiency while Σ refers to the set of decision variables: the conversion unit load (respectively storage unit state-of-charge) f, the storage unit charging/discharging rate $f^{+/-}$, the conversion unit logical state y and the building indoor temperature T. Both the objective function (C^{op}) and the parametric constraint (C^{eff}) are further detailed in the following paragraphs.

Objectives   Since the flexibility request profiles are translated through cost incentives, the objective function of the optimization problem is the minimization of the annual operating expenses associated to energy exchanges with the networks (Eq. 4.5). Regarding the formulations used in the previous chapters (Eq. 1.34), the unit sizes are not included in the decision variable set since the BES is fixed a-priori.

$$C^{\text{op}}_{f,p} = \sum_{t=1}^{T} \left(\text{op}^{\text{el},+}_{f,p,t} \cdot \dot{E}^{+}_{\text{grid},f,p,t} - \text{op}^{\text{el},-}_{f,p,t} \cdot \dot{E}^{-}_{\text{grid},f,p,t} + \text{op}^{\text{ng},+}_{p,t} \cdot \dot{H}^{+}_{\text{grid},f,p,t} \right) \cdot \mathrm{d}_t \quad \forall p \in \boldsymbol{P}, f \in \boldsymbol{F}_p \quad (4.5)$$

Parametric constraint   The parametric constraint limits the additional amount of electrical energy consumed with respect to initial reference *base* solution. Hence, similarly to the BES sizing algorithm, the following p-MILP problem formulation allows for a systematic generation of different operation strategies (i.e. demand responses) for each flexibility request profile f. Equation 4.6 expresses the resulting round-trip efficiency definition for each representative period p

$$C^{\text{eff}}_{f,p} = \frac{\sum_{t=1}^{T} \left(\Delta^{-}_{f,p,t} \right) \cdot \mathrm{d}_t}{\sum_{t=1}^{T} \left(\Delta^{+}_{f,p,t} \right) \cdot \mathrm{d}_t} \qquad \forall p \in \boldsymbol{P}, f \in \boldsymbol{F}_p \quad (4.6)$$

where $\Delta^{+/-}$ denotes the charging/discharging rate of the equivalent BESS, as defined in Equations 4.7 to 4.10. Additionally, the binary variable y prevents the BESS from charging and discharging energy within a same time step t while M refers to a large number (e.g. 10^6).

$$\Delta^{+}_{f,p,t} - \Delta^{-}_{f,p,t} = \left(\dot{E}^{+}_{\text{grid},f,p,t} - \dot{E}^{-}_{\text{grid},f,p,t} \right) - \left(\dot{\mathrm{E}}^{+}_{\text{grid},p,t} - \dot{\mathrm{E}}^{-}_{\text{grid},p,t} \right) \qquad \forall p \in \boldsymbol{P}, t \in \boldsymbol{T}, f \in \boldsymbol{F}_p \quad (4.7)$$

$$\Delta^{+}_{f,p,t} \leq y_{f,p,t} \cdot \mathrm{M} \qquad \forall p \in \boldsymbol{P}, t \in \boldsymbol{T}, f \in \boldsymbol{F}_p \quad (4.8)$$

$$\Delta^{-}_{f,p,t} \leq (1 - y_{f,p,t}) \cdot \mathrm{M} \qquad \forall p \in \boldsymbol{P}, t \in \boldsymbol{T}, f \in \boldsymbol{F}_p \quad (4.9)$$

$$\Delta^{+}_{f,p,t}, \Delta^{-}_{f,p,t} \geq 0 \qquad \forall p \in \boldsymbol{P}, t \in \boldsymbol{T}, f \in \boldsymbol{F}_p \quad (4.10)$$

4.3.3 Performance analysis

After assessing the different *flexible* load profiles $\dot{E}_{\text{grid}}$ perceived by the local distribution network operator, the related equivalent BESS characteristics are determined. Figure 4.3 illustrates the latter concept; in regard to the costs profile applied, the optimal predictive controller shifts dispatchable loads towards low tariff periods (night-time) and consequently decreases electricity consumption during high tariff periods respectively (day-time). The equivalent BESS operation is represented through the thick black line in the lower graph, highlighting the associated charging (green) and discharging (red) periods. The following paragraphs hence describe the required characteristics definitions in view of evaluating the equivalent BESS. Regarding the data reduction applied (PAM), each representative flexibility request f and related operating periods p is associated to a given probability of occurrence d_f. Hence, the following BESS characteristic definitions x^{BESS} can be expressed both at a daily and an annual basis using Equation 4.11 and Equation 4.12 respectively, where d_s and d_p refer to the probability of occurrence of both the flexibility request and the operating period respectively.

$$x_p^{\text{BESS}} = \sum_{f=1}^{|\boldsymbol{F}_p|} x_{s,p}^{\text{BESS}} \cdot \text{d}_f \tag{4.11}$$

$$x^{\text{BESS}} = \sum_{f=1}^{|\boldsymbol{F}_p|} \sum_{p=1}^{|\boldsymbol{P}|} x_{f,p}^{\text{BESS}} \cdot \text{d}_f \cdot \text{d}_p \tag{4.12}$$
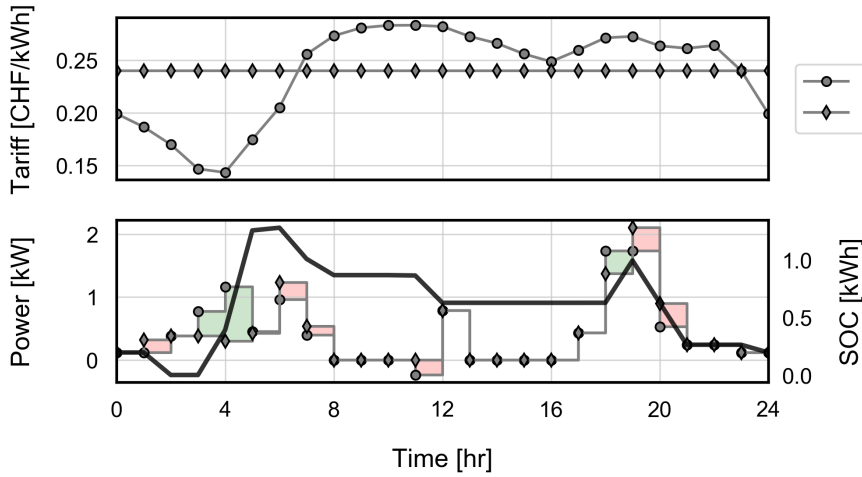
Figure 4.3 – Tariff (top) and resulting load (bottom) profiles for the reference and a flexible operating strategies

Virtual battery   The equivalent BESS behaviour (i.e state-of-charge *SOC*) related to each specific variable electricity cost profile f is assessed *a-posteriori* through the means of Equa-

tions 4.13, 4.15 and 4.16. First, the positive and respectively negative differences between the reference *base* $\dot{\mathrm{E}}_{\mathrm{grid}}$ and *flexible* $\dot{E}_{\mathrm{grid}}$ net electricity profiles are computed (Eq. 4.13). Subsequently, considering an initial energy content of zero at the beginning of each operating period (Eq. 4.14), the BESS state of charge is computed for each following time step (Eq. 4.15). Finally, in view of initial state of charge condition (Eq. 4.14), the resulting *SOC* profile is corrected by subtracting the minimum value reached over the operating period (Eq. 4.16).

$$\Delta \dot{E}_{f,p,t} = \left(\dot{E}^+_{\mathrm{grid},f,p,t} - \dot{E}^-_{\mathrm{grid},f,p,t} \right) - \left(\dot{\mathrm{E}}^+_{\mathrm{grid},p,t} - \dot{\mathrm{E}}^-_{\mathrm{grid},p,t} \right) \qquad \forall\, p \in \boldsymbol{P}, t \in \boldsymbol{T}, f \in \boldsymbol{F}_p \quad (4.13)$$

$$SOC_{f,p,1} = 0 \qquad \forall\, p \in \boldsymbol{P}, f \in \boldsymbol{F}_p \quad (4.14)$$

$$SOC_{f,p,t+1} = SOC_{f,p,t} + (\Delta \dot{E}_{f,p,t}) \cdot \mathrm{d}_t \qquad \forall\, p \in \boldsymbol{P}, t \in \boldsymbol{T}, f \in \boldsymbol{F}_p \quad (4.15)$$

$$SOC_{f,p,t} = SOC_{f,p,t} - \min_{t \in \boldsymbol{T}} \left(SOC_{f,p,t} \right) \qquad \forall\, p \in \boldsymbol{P}, t \in \boldsymbol{T}, f \in \boldsymbol{F}_p \quad (4.16)$$

In order to assess the main characteristics of the equivalent BESS, two specific performance metrics are defined. To this end, both the equivalent power $\dot{E}$ and energy E capacities are implemented [140]. The latter BESS parameters are defined in Equations 4.17 and 4.18 respectively where $\mathrm{n}_t = |\boldsymbol{T}|$ denotes the number of time steps within each representative operating period p (i.e. 24 hours).

$$\dot{E}_{f,p} = \frac{1}{\mathrm{n}_t} \cdot \sum_{t=1}^{|\boldsymbol{T}|} \left| \Delta \dot{E}_{f,p,t} \right| \qquad \forall\, p \in \boldsymbol{P}, f \in \boldsymbol{F}_p \quad (4.17)$$

$$E_{f,p} = \max_{t \in \boldsymbol{T}} \left(SOC_{f,p,t} \right) \qquad \forall\, p \in \boldsymbol{P}, f \in \boldsymbol{F}_p \quad (4.18)$$

4.4 Applications

The following section presents results generated from the implementation of optimal BES assessed and discussed in Chapters 1 and 3. First, the analysis focuses on single building problem formulations (Section 4.4.1) prior investigating the impact of multi-location energy systems (Section 4.4.2).

4.4.1 Single buildings

In order to demonstrate the developed method, the latter is implemented on three different building types introduced in Section 1.3.2: a single family house (SFH), an apartment block (AB) and a large office building (OF). Each dwelling is located within the climatic zone of *Geneva-Cointrin.* The following case studies aim at analysing the temporal disparity in ancillary services potential for different BES configurations prior focusing on the associated cost. Nevertheless, in regard to the challenging task of presenting the subsequent multi-dimensional results in a concise and clear manner, Figure 4.4 first provides an illustrative example of the employed performance representation. In the latter graph, the daily median values of a BESS characteristic (e.g. the storage capacity) are depicted through a thick and continuous line. The respective daily distributions are described by the 0th, 25th, 75th and 100th percentiles which are illustrated through coloured areas of different transparency degrees, according to their spread from the distribution median (i.e. 50th percentile).
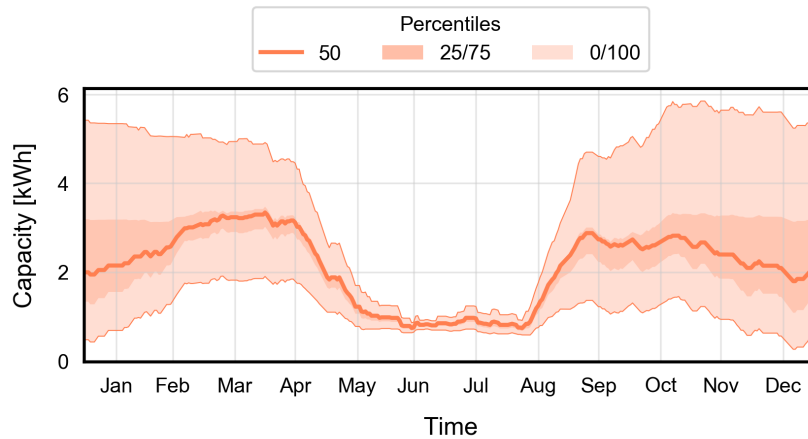
Figure 4.4 – Example of a temporal equivalent BESS performance indicator distribution

Single family house (SFH)   Consequently, Figure 4.5 displays the daily BESS performances in view of the previously introduced system characteristics: the equivalent energy E (upper sub-graph) and power $\dot{E}$ (lower sub-graph) capacities as defined in Section 4.3.3. Furthermore, each BES specific figure includes three distinct results regarding the considered equivalent round-trip efficiency thresholds ϵ; 90, 80 and 60%. Finally, the associated BES configurations

are recapitulated in Table 4.1.
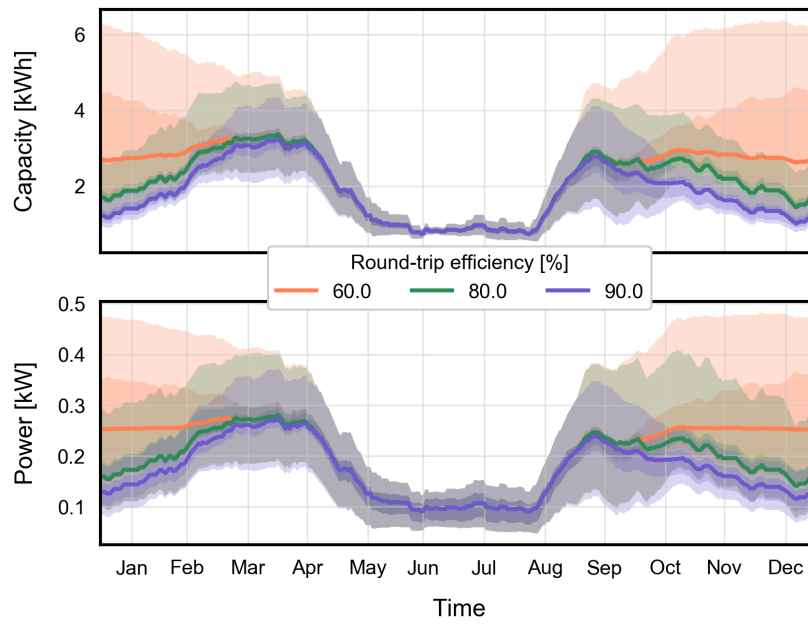
(a) System configuration *a*
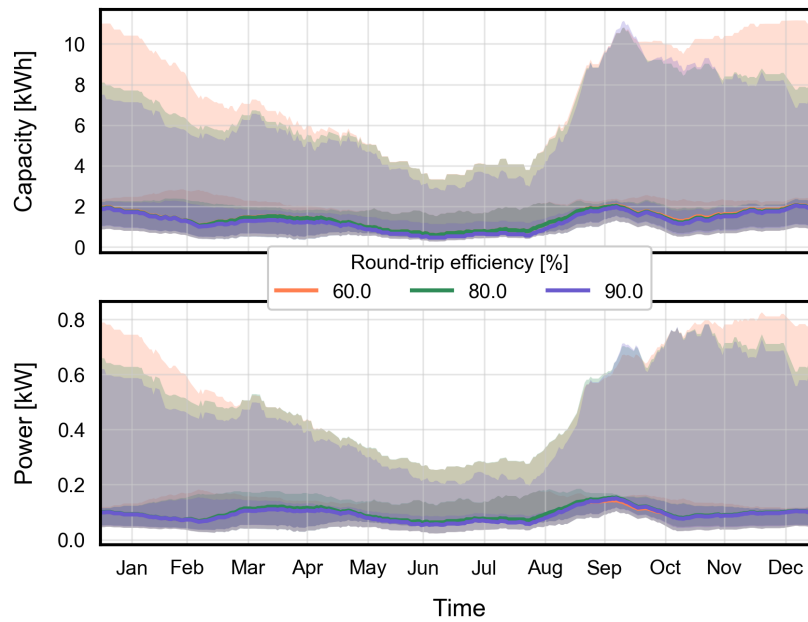
(b) System configuration *b*

Figure 4.5 – Temporal equivalent BESS performance indicator distribution for a single family house located in the climatic zone of Geneva

Hence, in the case of configuration (*a*) presented in Figure 4.5a, a strong seasonal variation

is observed; indeed, in summer time, due to the lack of any cooling demand, the sole load shifting potential relies within the domestic hot water preparation. Interestingly, no difference is noticed regarding the round-trip efficiency threshold while the probability distribution remains very tight. With the increase of space heating requirements during the mid-season[3] periods, the load shifting potential starts rising. Simultaneously, the indicator distributions spread out while a clear difference in system efficiency is noticed, particularly between $\epsilon^{\text{eff}} = 0.9$ and $\epsilon^{\text{eff}} = 0.8$. However, with the further increase in thermal service demands during winter time, the median indicator values fall again while the probability distributions reaching their highest dispersion. Especially for $\epsilon^{\text{eff}} = 0.9$, the median BESS characteristics drop to nearly 0.5 kWh. Indeed, in comparison to the values observed in summer time, efficient unit capacities (i.e. AHP) are already reaching their nominal load and hence, the shifting of space heating or domestic hot water preparation requires the activation of inefficient auxiliary capacities (i.e ELH).

In the case of configuration (*b*), although among seasons a certain distribution difference remains, the annual variation is much less pronounced with respect to the previous case. Indeed, median performance values are rather constant throughout the year with slight increases noticed around the mid-seasons. This behaviour can be explained by the efficient use of the AHP-CHP combination; similarly to (*a*), the BES flexibility is limited during the winter period since it is running at nearly full load. Nevertheless, in this case, the controller is able to slightly alter the dispatched generation among the CHP unit and the AHP, consequently either increasing electricity generation or consumption. Regarding the effect of the efficiency threshold a much lower impact on the BESS characteristic with respect to the previous case can be noticed. Indeed, the similar results obtained can be explained by the limited use of electric auxiliary heaters (ELH) to shift thermal services demands.

Apartment block (AB)   In view of the BES configuration similarities between (SFH) and (AB), the following case study results are reported in Appendix D. Hence, considering the similarities between the respective BES, Figure D.1a displays similar BESS behaviours to the ones depicted in Figure 4.5a, the main difference relying within the performance magnitude due to the larger service requirements and consequently, BES size.

On other hand side, in the case of Figure D.1b, different characteristics results are observed. Similarly to the system potential displayed in Figure 4.5b, the analysed BES comprises a combination of AHP-CHP as primary conversion units. However, both the equivalent power and energy metric distributions are tighter while rising not only during the mid-season but also in winter period. Moreover, no significant difference is noted between the different round-trip efficiency thresholds. A reason for the latter behaviour is related to the presence and subsequently further use of the auxiliary gas-based heating unit (BOI). Indeed, in regard to the purely electricity based definition considered in Equation 4.6, natural gas consumption is not included within the efficiency statement.

---

[3]Spring and autumn

Office building (OB)   With the introduction of an additional shiftable energy service requirement, space cooling (SC), the systems flexibility provision is further improved. Hence, Figure 4.6a highlights a rather constant characteristics distribution band throughout the year, although showing higher seasonal variation of the median values. This increase is indeed related to the associated growing demand of SC; since the unique cooling unit (VAC) is sized according to the peak requirements, the service provision is efficiently shifted during the considered period. In addition, similarly to the BES configuration of Figure D.1b, the presence of a BOI as auxiliary conversion unit allows for a higher lower bound on the characteristic distribution during the winter and mid-season period.

In the case of configuration (*b*), the flexibility potential drastically rises during the summer period although a similar VAC capacity to (*a*) is installed. The latter behaviour is explained by the presence of a large CHP in the BES: indeed, in order to further increase the distributed electricity production during the cooling period, the CHP utilization is expanded while the resulting excess heat generation is dumped. Obviously, from a BES sizing perspective, this response behaviour does not align with the aim of a rational and sustainable use of available energy resources; nevertheless, since the goal of this chapter is in assessing the probability of providing critical ancillary services to power network operators, the latter system conditions can be considered as sporadic and thus, as non-representative of a usual operation strategy. On the other hand side, during the winter period, the BESS metric performances drop. Indeed, due to the lack of any non-electrical auxiliary heating unit (BOI), the BES is limited in efficiently shifting heating demands especially since the AHP-CHP combination is not sized with respect to the thermal peak requirements.

Table 4.1 – Building energy system configurations

Unit		System configurations							
		SFH (*a*)	SFH (*b*)	AB (*a*)	AB (*b*)	OF (*a*)	OF (*b*)	RUR	URB
ELH	kW	9.4	8.5	98.7	0	0	52.6	403	197.7
BOI	kW	0	0	0	76.9	69.3	0	0	0
SOFC	kW	0	0	0	8	0	0	0	19.8
LPEM	kW	0	1.3	0	0	0	12.6	33	20.1
BAT	kWh	0	0	0	0	0	0	0	0
AHP	kW	2.4	1.8	23.2	10.9	16	17.8	66.8	41.7
PVA	kW	3.1	7.8	2.5	10.6	14.1	10.7	301.4	73.6
STC	m^2	0	0	0	0	0	0	0	0
HWT	m^3	0.1	0.1	0.6	1.3	0.2	0.2	7.8	1.9
HST	m^3	0.2	0.2	2.2	1	0	3	3.5	4.2
VAC	kW	-	-	-	-	21.9	21.9	21	64.2
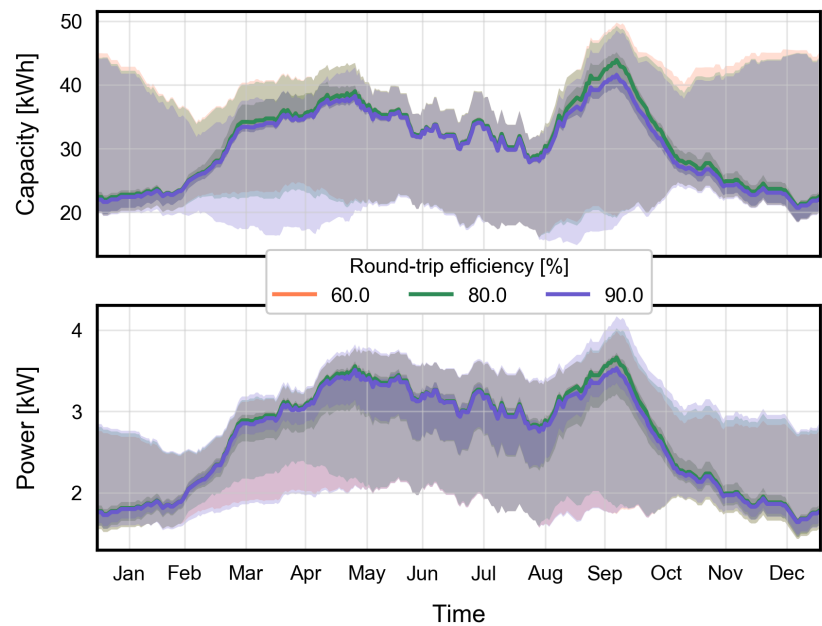
(a) System configuration *a*
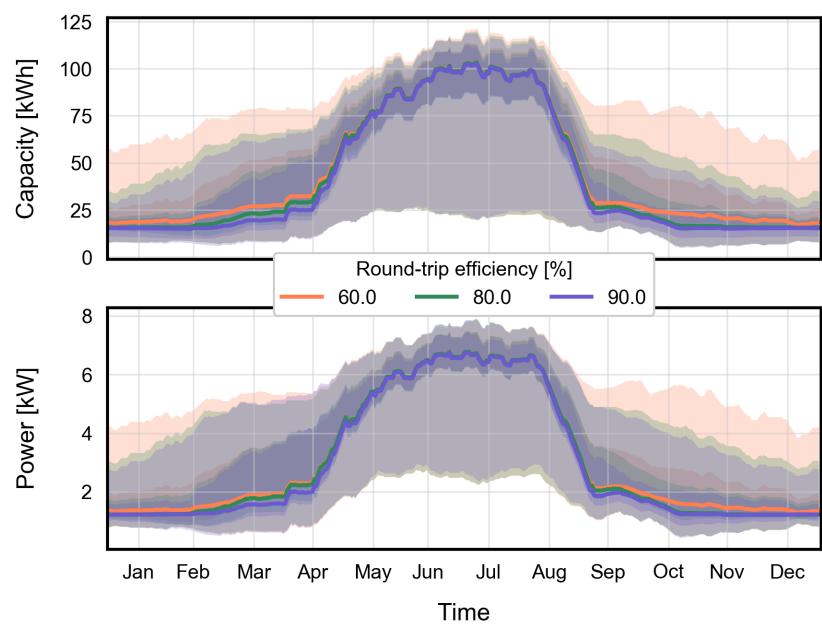
(b) System configuration *b*

Figure 4.6 – Temporal equivalent BESS performance indicator distribution for an office building located in the climatic zone of Geneva

Single buildings: cost-benefit comparison

In order to directly compare the BESS performances of each optimal BES generated, Figure 4.7 depicts the annual mean characteristics (Equation 4.12) of each BES configuration presented in Section 1.4. Hence, each point represents a specific system size while the associated parameters regarding building type b, ancillary service efficiency ϵ^{eff} and technology use are highlighted by the marker shape, colour and edge style respectively. In order to avoid a strong disparity between the different results while providing a energy service relative analysis, the mean characteristics are reported in function of the building energy reference area (ERA). A linear trend is observed between both BESS characteristics. AB and OF solutions are mainly located within the range of 0.05-0.20 kWh/100m^2 and 2-15 W/100m^2 while SFH solutions span until 1.0 kWh/100m^2 and 0.08 kW/100m^2. In general, BES solely comprising an AHP primary conversion unit (without any red edge) reflect slightly higher mean power capacities for a given mean energy capacity. Similarly, configurations at both high energy and power capacities mainly include BES configurations solely featuring an AHP. It is worth mentioning that the latter results are highly dependent on the ambient conditions as presented in the preceding figures (Figures 4.5 and 4.6) and thus, should be treated with caution. However, the aim of this analysis is to provide a first indication of achievable potential load shifting while comparing different BES configurations among each other.
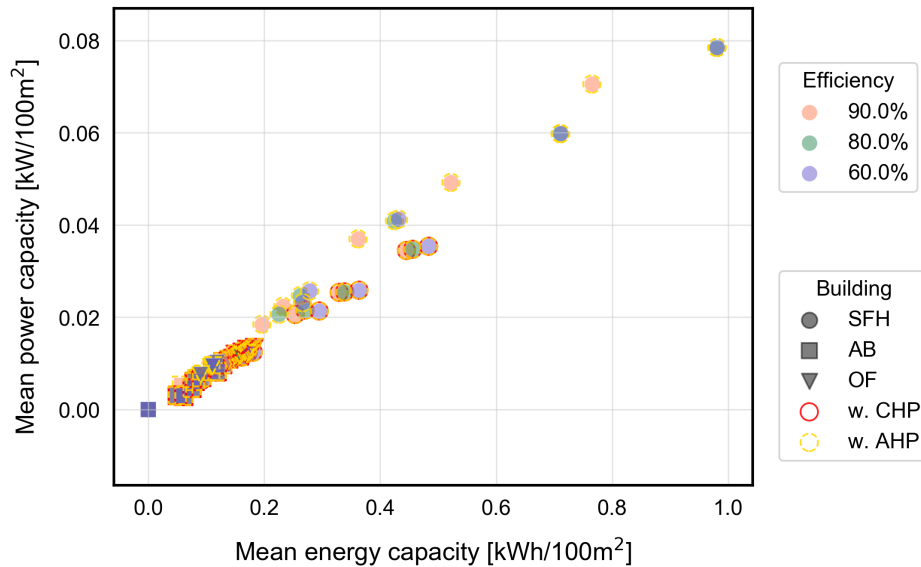
Figure 4.7 – Power and energy storage capacity per ERA for different BES configurations located in Geneva-Cointrin

Moreover, a cost-benefit comparison of the BESS performances presented in Figure 4.7 is finally depicted in Figure 4.8. Indeed, the equivalent expenses related to each BESS are evaluated through the difference in annualized total expenses C between the associated BES i and the most cost-efficient system configuration observed among the entire solution set $\boldsymbol{I}$. Equation 4.19 expresses the latter definition where Δ denotes the cost difference associated to

each BESS, index b the representative building category studied and i the BES configuration. Additionally, in order to relate the identified equivalent BESS costs to existing electrical energy storage technologies, Figure 4.8 includes small and large scale state-of-the-art BESS commercially available. Their characteristic specific costs parameters are reported in Table D.1.

$$\Delta_{b,i} = C_{b,i} - \min_{i \in \boldsymbol{I}} C_{b,i} \qquad\qquad \forall i \in \boldsymbol{I}, b \in \boldsymbol{B} \quad (4.19)$$
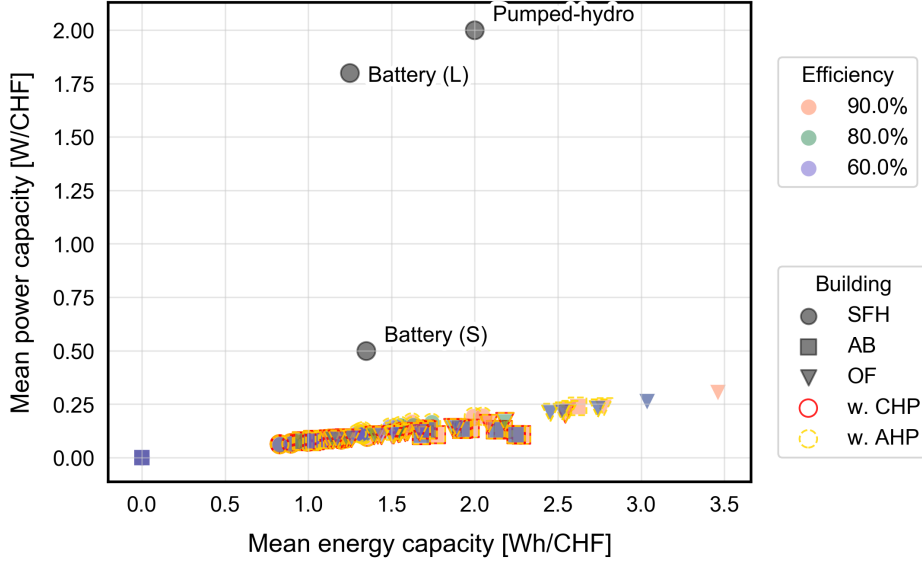
Figure 4.8 – Power and energy storage capacity per cost for different BES configurations located in Geneva-Cointrin

Similarly to the results of Figure 4.7, a linear trend is noticed for all BESS characteristics. The majority of BES configurations are located within the range of 0.8-2.2 Wh/CHF and 0.06-0.20 W/CHF; BES outliers typically comprises OF buildings. In comparison to the standard BESS options displayed, the implementation of DSM represents an interesting alternative regarding the presented mean energy capacity dimension. On the other hand side, from a mean power perspective, the use of DSM does not reflect any cost-efficient solution. Indeed, considering both the dynamics of thermal energy services in addition to the sizes of efficient conversion units, average power changes remain indeed relatively low. Finally, it is worth noting that the latter comparison solely proposes a potential cost-benefit assessment and should not be translated to a complete disregard of standard BESS in future. Indeed, as discussed in [140], additional factors such as power injection and long-term (inter-day) storage capacities should be estimated prior incorporating DSM options into grid planning.

4.4.2 Smart communities

In a second phase, the flexibility potential of smart communities is analysed. The following results are illustrated in Appendix D while Table 4.1 provides the associated multi-building energy system (MBES) sizes. Hence, Figure D.2 depicts the equivalent BESS performance distributions for a rural community (Section 3.4.2) BES. Similarly to the SFH case study, the strongest disparities are observed during the heating period (winter) while during the cooling period (summer), the latter decrease. However, in this case, the median performance values are rather constant. Indeed, given the service demand heterogeneity of the considered rural community (apartment blocks & educational buildings) , both space cooling and heating needs contribute to the flexibility availability. On the other hand side, in the urban case study, the flexibility distribution trend is inverted; the strongest disparities are observed during the cooling period (summer) while in the heating period (winter) the latter drop. Indeed, regarding the community configuration (refurbished mixed-use & office buildings), space cooling needs reflect the highest share among the total energy service requirements.

Smart communities: cost-benefit comparison

Similarly to single building case studies, the equivalent BESS performances resulting from the deploymnent of smart MBES is hereby discussed. Hence, Figure 4.9 displays the corresponding cost-specific comparison graph including the two smart-grid configurations aforementioned: an urban and rural community of 5 and 12 buildings respectively. The associated MBES are defined in the preceding chapter (Chapter 3) and thus are not further detailed here; interested readers are referred to the related result discussion in Section 3.4.2.
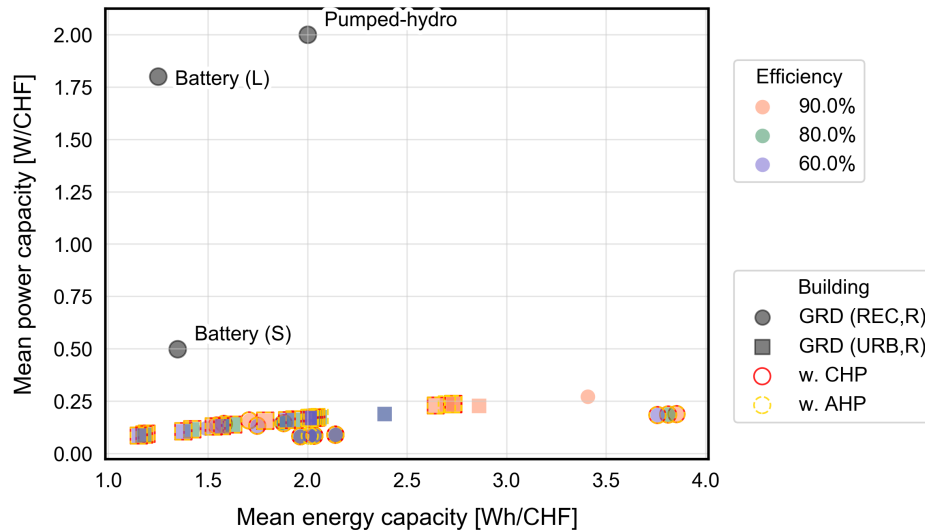
Figure 4.9 – Power and energy storage capacity per cost for a rural (REC) and urban (RUR) community located in Geneva-Cointrin

In comparison to the single building results (Fig. 4.8), the equivalent BESS of smart communi-

ties reflect slightly better performances, values ranging within 0.08-0.27 W/CHF and 1.15-3.85 Wh/CHF. From a rather intra-community perspective, the rural case study appears reflecting more cost-efficient solutions. Similarly to the single building case studies, the equivalent BESS cost-efficiency regarding mean energy capacity mainly compares and/or outperforms standard BESS solutions. However, from a mean power capacity perspective, the equivalent BESS still remains far from reaching the performance associated to standard BESS.

4.5 Conclusion

This chapter presented a novel method to quantify the ancillary service potential of building energy systems in the early design stage. The model-based approach relies on the MILP modelling framework (MF) previously defined in this same work and applies a multi-objective optimization technique to systematically generate different response strategies. Similarly to classical demand response schemes, the system objective function targets the minimization in operating expenses while power profile modification requests are translated through energy tariff variations over the considered control horizon of 24 hours. Finally, the developed algorithm is validated on hand of multiple case studies, ranging from an existing residential building to an small urban community (smart-grid). Noticeable results can be summarized as follows:

- The temporal availability of the ancillary services is strongly dependent on the considered BES configurations; the use of multi-energy systems unit further extends the potential flexibility distribution. Particularly the application of non-electrical auxiliary heating (BOI) units allows for more certain flexibility provision during the heating period.

- The cost-benefit comparison of the equivalent BESS and standard BESS, showed a moderate potential for the use of DSM in BES. Particularly from a mean energy capacity perspective, different BES configurations reflect better performances while from a mean power capacity perspective none of the considered solution is competitive. Additionally, the intra-BES comparison showed substantial disparity among the equivalent BESS cost performance ranging from 0.8-2.2 Wh/CHF and 0.06-0.20 W/CHF respectively.

- The use of smart communities (MBES) reflects slightly better equivalent BESS performances in comparison to single buildings (BES); nevertheless, from a mean power capacity perspective, the MBES still remain far from standard BESS options.

Limitation and perspectives In regard to the recent interest on flexibility quantification for BES within literature, the following paragraphs attempts in providing final critical remarks on the presented assessment method. Hence, a first limitation targets the estimation of flexibility demands profiles. Indeed, within the current study, the latter have been estimated from past hourly day-ahead market (EPEX) prices; however, the applied tariffs solely reflect the flexibility demand on a global scale and thus, might not reflect regional network requirements and bottlenecks. Hence, further demand assessment should be performed in coordination with regional power network operators data and future reserve capacity requirements due to the increasing penetration of volatile and intermittent resources.

A second aspect worth mentioning targets the demand profile distribution within smart communities (micro-grids). Indeed, in the case of multi-building energy systems, each end-user currently perceives a similar tariff profile and thus activates controllable load simultaneously

to benefit from the economic incentive. Future investigations could hence analyse the implementation of additional, building-specific and potentially asynchronous electricity cost profiles to improve the system ancillary service potential. A latter approach might indeed produce smoother temporal distribution while decreasing the generation of virtual demand peaks ("rebound peak"). Similarly, this strategy might be applied for large communities.

Finally, in regard to possible modelling developments, an interesting MF extension involves the simultaneous sizing and scheduling of building energy system while providing ancillary services. Indeed, the latter problem formulation could alter the reference system configuration in order to further improve load shifting capacity while considering an annualized total expenses as objective function. Nevertheless, the additional dimension related to the multiple flexibility demand scenarios would highly increase the problem size, especially in the case of multi-building systems. Future developments might therefore attempt in overcoming the latter challenge by assessing additional solving strategies (i.e. Benders decomposition).

Conclusions

Chapter overview

- General summary
- Recommendations on building energy system design practices
- Future perspectives

In light of the current state-of-the-art, this thesis has addressed four main research questions within the field of building energy system optimization:

1. "How does the integration of distributed energy sources vary with the system characteristics?"

2. "How does the deployment of optimal building energy systems impact the national energy use?"

3. "Should building energy systems be sized considering their local neighbourhood and to which extent can smart grids improve the integration of distributed energy sources?"

4. "To which extent can building energy systems provide any ancillary services to power network stakeholders and at which additional costs?"

Different methods have thus been developed and detailed throughout the preceding chapters in order to attempt tackling the latter challenges; the first defined a comprehensive and generic mixed integer linear programming (MILP) modelling framework (MF) to optimally assess building energy system (BES) designs and operation. In the second chapter, the MF has been systematically implemented for different building types in Switzerland, identified according to their construction period, use and geographical location. The thus generated results have progressively been expanded to the national scale through a second optimization process, attributing a specific BES design among the previously generated solution set to each associated building type. Chapter 3 lastly extended the initial MF in order to consider multi-location problem formulations and hence, analyse the implementation of small smart-grids. Finally the last chapter proposed a novel application of MF to estimate the ancillary service potential of different energy system designs with a particular focus on load shifting.

It follows a detailed summary of the methods developed in each chapter and the main conclusions drawn from the associated results. For a more extensive explanation the reader is

readdressed to the concluding sections of each chapter.

Key messages

The aforementioned open questions were addressed in this work through a modelling approach to simulate the performance of BES for different problem statements. Hence, in the first chapter, a holistic and modular MF is defined identify potential BES configurations. The framework relies on MILP techniques to describe both the continuous and discrete behaviour inherent to specific machines. It includes efficient state-of-the-art conversion technologies, auxiliary heating units, renewable energy sources and storage devices. In order to analyse the integration of distributed generation in BES, a multi-objective optimization is carried on. The epsilon-constraint formulation is adopted to deal with conflicting objectives, thus generating multiple pareto optimal solutions. The developed method has been illustrated on basis of different case studies, varying in size and type. In a nutshell results have shown that the BES choice is highly affected by the building type. Indeed, for low service demand dwellings (i.e. single family houses), the combination of AHP and PVA appears today as the most promising cost- and environmental- efficient compromise. On the contrary, in stronger service demand dwellings, such as apartment blocks and administrative buildings, the combination of CHP and AHP represent the cost-optimal solution. Moreover, in the case of single family houses a potential reduction of 95% in equivalent greenhouse gas emissions can be achieved. However, such advanced system configurations do not represent the most cost-effective solution under the current market conditions. Nevertheless, uncertainty on energy prices has revealed to highly affect the monthly expenses, shifting the interest towards grid independent solutions characterized by deeper renewable penetration.

In a second step, the benefit of predictive operation in contrast to standard rule-based control (RBC) is estimated. Therefore, in order to prevent the solver from shifting energy demand in time (i.e. avoid a predictive behaviour), the MF is altered by appending operative restrictions on storage units while renewable generation is entirely decoupled from the BES. Energy production from the latter units is subtracted a-posteriori from the respective energy balances. Results have shown that with the combination of AHP and PVA, the use of predictive control techniques allows to gain up to 17% in self-sufficiency.

Following the definition and subsequently validation of a generic MF for BES, Chapter 2 targets the large scale performance assessment of efficient BES. In regard to the latter scope, the presented method relied on a pre-defined set of representative building types while disparities in both thermal service demands and resource availability have been grouped through a novel spatial clustering algorithm. On hand of theses different boundary conditions, multiple BES configurations have been systematically evaluated for each of the resulting cluster dimension: building use, construction period, refurbishment status and location.

Through the means of a second problem formulation, the thus generated BES configurations are subsequently optimally affected to the respective building cluster. The applied multi-

objective optimization problem targeted both the environmental impact and the investment expense of the global BES. Results from the latter preliminary assessment approach highlighted promising alternatives to the status quo; in view of the considered boundary conditions, the 2000 watt society environmental impact thresholds (0.5 tCO2-eq/yr/100m^2) can be reached with an equivalent cost of 250 CHF/mo·100m^2. On the other hand, a drastic reduction in equivalent greenhouse gas emissions up to 78% is already achievable at a lower monthly cost of 60 CHF/mo·100m^2.

Chapter 3 focused on the sizing and comparison of multi-building energy systems (MBES) with respect to BES configurations. In view of potential heat and electricity generation disparities, both inter-day energy storage and heating network models have been appended to the multi-location MF. In order to validate the resulting problem formulation, several case studies have been finally carried out. Based on the latter results, multi-location sizing approaches indeed provide cost-benefits over multiple, independent executions; considering a similar investment threshold, changes in operating expenses range within 6-8%. However, with rising capital available, both the BES and MBES sizes increasingly grow similar while the consequent economic benefit drops. Nevertheless, the implementation of shared units (i.e. heating network & inter-day storage) further improves the penetration of distributed generation capacities, particularly in the case of rural communities which reflect stronger resource availabilities (solar) and lower service demands. Moreover, the use of multi-location approaches at the BES sizing stage appears beneficial also for power network operators. Indeed more "grid-aware" solutions are generated, confirmed by the improvement of the related key performance indicators.

Finally, in Chapter 4, both BES and MBES configurations are analysed in view of their potential ancillary service provision. In order to represent the latter flexibility performances to the associated stakeholders, an equivalent battery electricity storage system (BESS) model is developed. In a first step, the (M)BES response to different typical flexibility request profiles is assessed. In comparison to the baseline eclectic consumption profile, differences are subsequently translated into charging/discharging rates of an equivalent BESS. In order to allow an easier comparison to standard BESS, a parametric threshold is added to the equivalent BESS round-trip efficiency definition. Preliminary results suggest that multiple BES might be a competitive solutions to decreasing future BESS needs with values ranging between 0.8-2.2 Wh/CHF. Particularly multi-energy systems comprising non-electric auxiliary conversion devices presented an interesting potential, even during strong service demand periods. However, from a power perspective, BES remain far from meeting the capacities of traditional systems.

Future perspectives

Although problem specific limitations and perspectives have already been discussed in the associated concluding sections of each chapter, the following paragraphs summarizes main

considerations and ideas for future developments.

Demand estimation Throughout the presented work, building energy service requirements were based on average consumption estimations or, in case of lacking information, on reference values of national construction standards (SIA). Although aggregated consumption values might correspond to national demand estimations, building specific consumption profiles can drastically vary even among buildings with similar pre-defined construction periods and use. In order to provide a better demand assessment, a comprehensive clustering method should be developed, including different key building characteristics such as the associated heat distribution system and envelope performances. Certainly, the efficiency of this approach heavily relies on data availability which, especially at national scale, is not an easy matter. Alternatively, regions facing partial information loss might be modelled on a hand of better documented areas.

Multi-parametric sizing In view of further exploring the potential solution space, a multi-parametric optimization approach should be investigated within the context of future MF developments. The presented sizing algorithm mainly relied on a cost-based method, generating optimal trade-off configurations between investment and operating expenses: low investment systems typically rely on non-efficient conversion units while more expensive configurations aim at integrating distributed generation in regard to the given energy tariffs. Nevertheless, regarding the considered system boundary conditions, the latter approach might occasionally sideline additional key performance indicators such as the equivalent greenhouse gas emissions or the integration within national energy scenarios. The use of a multi-parametric sizing approach (mp-MILP) might provide an interesting option to broaden the applied ϵ-constraint technique.

Smart community definitions While the latter study revealed potential cost-benefits from considering a multi-location over an independent sizing approach, a formal identification method of "good" building communities has not been addressed yet. Indeed, although relying on existing built environments, the presented case studies were selected with the sole constraint of the surface continuity, i.e. each building land area is appending another one. A potential approach could be the use of k-means or k-medoids clustering techniques including spatial continuity constraints in order to account for the latter requirement. Furthermore, on basis of national GIS building register (e.g. RegBL), representative neighbourhood structures in function of the considered density types (e.g. rural, sub-rural and urban) might be defined. Nevertheless, in order to properly perform the latter assessment and avoid substantial redrawing expenses, additional information on existing local and regional energy network configurations should be incorporated if available.

A | Chapter 1: model descriptions and data

Additional modelling constraints

System constraints

The following section presents additional BES constraints related to both technical and legislative requirements. The latter include:

1. The maximal hosting capacity of solar-based technologies (i.e. PVA and STC) where A_b^{roof} denotes the building net roof area.

$$\sum_{u=1}^{\boldsymbol{U}_{\text{PVA}}} F_u + \sum_{u=1}^{\boldsymbol{U}_{\text{STC}}} F_u \leq A_b^{\text{roof}} \tag{A.1}$$

2. The minimum buffer tank (HST) size when considering hydronic heating systems with low inertia, V^{min} representing the specific volume requirement (37 l/kW for CHP and 15 l/kW for AHP [144]).

$$\sum_{u=1}^{\boldsymbol{U}_{\text{HST}}} F_u \geq \sum_{u=1}^{\boldsymbol{U}_{\text{AHP}}} V_u^{\text{min}} \cdot F_u + \sum_{u=1}^{\boldsymbol{U}_{\text{CHP}}} V_u^{\text{min}} \cdot F_u \tag{A.2}$$

3. The minimum hot water tank (HWT) size related to the maximal peak demand coverage [145], $\dot{m}$ referring to the aggregated hot water withdrawal profile.

$$\sum_{u=1}^{\boldsymbol{U}_{\text{HWT}}} F_u \geq \max_{p \in \boldsymbol{P}, t \in \boldsymbol{T}} \dot{m}_{p,t}^{\text{HW}} \cdot d_t \tag{A.3}$$

4. The size of slow CHP units with extremely low start-up numbers (i.e. SOFC, comprised in $\boldsymbol{U}_{\text{CHP}}'$) is limited by the daily service demand of HW, where T_u denotes the minimum

(respectively maximum) water service temperatures.

$$\sum_{u=1}^{U'_{\text{CHP}}} \lambda^{\min} \cdot F_u \le \max_{p \in P} \left(c_p \cdot \sum_{t=1}^{T} \dot{m}_{p,t}^{\text{hw}} \cdot (\text{T}_{\text{HWT}}^{\max} - \text{T}_{\text{HWT}}^{\min}) \cdot d_t \right) \tag{A.4}$$

5. The activation of auxiliary electrical heaters (ELH) is allowed solely in combination with air-water heat pumps (AHP).

$$\sum_{u=1}^{U_{\text{ELH}}} Y_u \le 2 \cdot \sum_{u=1}^{U_{\text{AHP}}} Y_u \tag{A.5}$$

Conversion units

Based on the generic formulation of Equations 1.6 to 1.8, this section details the specific model definition of conversion units included in the MF: natural gas fired boilers, electrical heaters, a combined heat and power devices, air-source heat pumps, photovoltaic arrays and solar thermal collectors.

Boiler (BOI)   The natural gas boiler is described using a static system model formulation (Eqs. 1.6 to 1.8) and is implemented as an auxiliary heating utility, the sizing dimension being the thermal power output. Minimum load (Eqs. 1.23 to 1.25) and duration (Eqs. 1.27, 1.29 and 1.30) constraints have not been considered for the following technology. Applied parameters values are reported in Table A.1.

$$\dot{h}_{\text{BOI},p,t}^{+} = \epsilon_{\text{BOI}}^{-1} \qquad\qquad \forall p \in P, t \in T \tag{A.6}$$

Table A.1 – Parameter data (BOI)

Parameter	Value	Unit	Ref.
λ^{min}	-	[-]	
λ^{max}	-	[-]	
ϵ	0.98	[-]	[59]
$n^{\min}$	-	[-]	
n^{start}	-	[-]	
L	20	[yr]	[57, 59]
inv_1	3800	[CHF]	est. from Fig. A.1
inv_2	105	[CHF/kW]	est. from Fig. A.1
F_{BM}	1.8	[-]	est. from [146]

Electrical heater (ELH)   The electrical heater is described using a static system model formulation (Eqs. 1.6 to 1.8) and is implemented as an auxiliary heating utility, the sizing dimension

being the thermal power output. Minimum load (Eqs. 1.23 to 1.25) and duration (Eqs. 1.27, 1.29 and 1.30) constraints have not been considered for the following technology. Applied parameters values are reported in Table A.2.

$$\dot{e}^{+}_{\text{ELH},p,t} = \epsilon^{-1}_{\text{ELH}} \qquad\qquad \forall p \in \boldsymbol{P}, t \in \boldsymbol{T} \quad (\text{A.7})$$

Table A.2 – Parameter data (ELH)

Parameter	Value	Unit	Ref.
λ^{min}	-	[-]	
λ^{max}	-	[-]	
ϵ	0.99	[-]	est.
n^{min}	-	[-]	
n^{start}	-	[-]	
L	20	[yr]	[57]
inv_1	968	[CHF]	est. from Fig. A.1
inv_2	13	[CHF/kW]	est. from Fig. A.1
F_{BM}	1	[-]	est.

Air-source heat pump (AHP) The air-source heat pump unit is described using a static system model formulation (Eqs. 1.6 to 1.8) and is implemented as a primary heating utility, the sizing dimension being the electrical power input. As illustrated in Figure 1.6, the device is connected to both the electricity (*input*) and heat (*output*) layers. Minimum load (Eqs. 1.23 to 1.25) and duration (Eqs. 1.27, 1.29 and 1.30) constraints have not been considered for the following technology. Indeed, since modern units are commonly equipped with inverters, an almost continuous output control is achievable, a typical on-off operation method being applied below the device minimum load threshold. In view of the considered time step length d_t (1 hour), lower rates can be translated through a shorter operation within d_t.

Hence, the conversion efficiency in Eqs. A.8 and A.9 is determined using the ideal coefficient of performance (COP) and the second law efficiency η to account for irreversibilities in the different cycle components (e.g. compressor). In order to avoid any non-linearities arising from the a variable supply temperature and the latter definition, the generated heat load is discretized into $n_s = |\boldsymbol{S}_{\text{AHP}}|$ streams s, according to both thermal energy services: the building envelope (BUI) and the domestic hot water tank (DHW). It is worth noting that, when considering different heat sources (e.g. water-source heat pumps) in the problem formulation, a similar model definition might be applied, the solely modification being the *a-priori* determined source temperature (e.g. $T^{\text{water}}_{p,t}$) and the respective second-law efficiency η. Applied parameters values are reported in Tables A.3, A.11 and A.12.

$$\text{COP}_{\text{AHP},s,p,t} = \frac{T^{\text{LMT}}_{\text{AHP},s}}{T^{\text{LMT}}_{\text{AHP},s} - T^{\text{ext}}_{p,t}} \qquad\qquad \forall s \in \boldsymbol{S}_{\text{AHP}}, p \in \boldsymbol{P}, t \in \boldsymbol{T} \quad (\text{A.8})$$

$$\dot{q}^-_{\text{AHP},s,p,t} = \eta_{\text{AHP},s,p,t} \cdot \text{COP}_{\text{AHP},s,p,t} \qquad\qquad \forall s \in \boldsymbol{S}_{\text{AHP}}, p \in \boldsymbol{P}, t \in \boldsymbol{T} \quad \text{(A.9)}$$

Table A.3 – Parameter data (AHP/VAC)

Parameter	Value	Unit	Ref.
λ^{min}	-	[-]	
λ^{max}	-	[-]	
n^{min}	-	[-]	
n^{start}	-	[-]	
L	20	[yr]	[146]
inv_1	5680	[CHF]	[128]
inv_2	1240	[CHF/kW]	[128]
F_{BM}	1.8	[-]	est. from [146]

Combined heat and power (CHP) The cogeneration unit is described using a static system model formulation (Eqs. 1.6 to 1.8) and is implemented as a primary heating utility, the sizing dimension being the electrical power output. As illustrated in Figure 1.6, the device is connected to the natural gas (*input*), the heat and electricity layers (*output*). The latter technology is subject to both minimum load (Eqs. 1.23 to 1.25) and duration (Eqs. 1.27, 1.29 and 1.30) constraints. Applied parameters values are reported in Table A.4.

$$\dot{h}^+_{\text{CHP},p,t} = \frac{1}{\epsilon^{\text{el}}_{\text{CHP}}} \qquad\qquad \forall p \in \boldsymbol{P}, t \in \boldsymbol{T} \quad \text{(A.10)}$$

$$\dot{q}^-_{\text{CHP},s,p,t} = \epsilon^{\text{el},-1}_{\text{CHP}} \cdot \epsilon^{\text{th}}_{\text{CHP}} \qquad\qquad \forall s \in \boldsymbol{S}_{\text{CHP}}, p \in \boldsymbol{P}, t \in \boldsymbol{T} \quad \text{(A.11)}$$

Table A.4 – Parameter data (CHP)

Parameter	Value		Unit	Ref.
	SOFC	LPEM		
λ^{min}	0.5	0.5	[-]	est.
λ^{max}	1	1	[-]	est.
ϵ	0.50/0.40[†]	0.37/0.53[†]	[-]	est.
n^{min}	24	3	[-]	est.
n^{start}	-	1	[-]	est.
L	10	10	[yr]	est.
inv_1	15542	15542	[CHF]	est. from Fig. A.1
inv_2	2100	2100	[CHF/kW]	est. from Fig. A.1
F_{BM}	1.8	1.8	[-]	est. from [146]

[†]Electric/thermal

Photovoltaic array (PVA) The photovoltaic array is described using a system static model formulation (Eqs. 1.6 to 1.8)), the sizing dimension being the panel electrical power output[1]. As shown in Figure 1.6, the unit is only connected to the electricity layer (*output*). The conversion efficiency ϵ accounts for the cell temperature T_{PVA} as proposed by Duffie and Beckman [68]; the latter is thus defined by Eqs. A.12 to A.14 where U_{PVA} denotes the module heat transfer coefficient, f_{PVA} the absorption coefficient, π_{PVA} the temperature efficiency coefficient while (*ref*) superscripted parameters represent reference values evaluated under standard test conditions. Finally, potential inverter losses are accounted through ϵ_{PVA}^{inv}. Applied parameters values are reported in Table A.5.

$$T_{PVA,p,t} = \frac{U_{PVA} \cdot T_{p,t}^{ext}}{U_{PVA} - \pi_{PVA} \cdot GHI_{p,t}} +$$
$$\frac{GHI_{p,t} \cdot (f_{PVA} - \epsilon_{PVA}^{ref} - \pi_{PVA} \cdot T_{PVA}^{ref})}{U_{PVA} - \pi_{PVA} \cdot GHI_{p,t}} \qquad \forall p \in \boldsymbol{P}, t \in \boldsymbol{T} \quad (A.12)$$

$$\epsilon_{PVA} = \epsilon_{PVA}^{ref} - \pi_{PV} \cdot \left(T_{PVA,p,t} - T_{PVA}^{ref}\right) \qquad \forall p \in \boldsymbol{P}, t \in \boldsymbol{T} \quad (A.13)$$

$$\dot{e}_{PVA,p,t}^{-} = \epsilon_{PVA}^{inv} \cdot \epsilon_{PVA} \cdot GHI_{p,t} \qquad \forall p \in \boldsymbol{P}, t \in \boldsymbol{T} \quad (A.14)$$

Table A.5 – Parameter data (PVA)

Parameter	Value	Unit	Ref.
ϵ^{ref}	0.14	[-]	[28]
ϵ^{var}	0.0012	[°C^{-1}]	[28]
U	29.1	[W/m^2·K]	[28]
f	0.9	[-]	[28]
L	20	[yr]	[57]
inv$_1$	2495	[CHF]	est. from Fig. A.1
inv$_2$	2656	[CHF/kW]	est. from Fig. A.1
F$_{BM}$	1.33	[-]	est. from [147]

Solar thermal collector (STC) The solar thermal collector technology is described using a system static model formulation (Eqs. 1.6 to 1.8), the sizing dimension being the panel area. As illustrated in Figure 1.6, the unit is solely connected to the heat layer (*output*). The conversion efficiency ϵ is defined in function of the working fluid temperatures [148] as detailed in Eq. A.15, where η_{STC}, a_{STC} and b_{STC} denote fitted model parameters. Similarly to the previously introduced thermal unit models, the generated heat load is discretized into $n_s = |\boldsymbol{S}_{STC}|$ heat streams, according to the thermal demand streams of the domestic hot water

---

[1]At standard test conditions and typically expressed as [kW] peak.

tank. Applied parameters values are reported in Table A.6.

$$\epsilon_{\text{STC},s} = \eta_{\text{STC}} - a_{\text{STC}} \cdot \frac{\left(T_{\text{STC},s}^{\text{LMT}} - T_{p,t}^{\text{ext}}\right)}{\text{GHI}_{p,t}} - b_{\text{STC}} \cdot \frac{\left(T_{\text{STC},k}^{\text{LMT}} - T_{p,t}^{\text{ext}}\right)^2}{\text{GHI}_{p,t}} \qquad \forall s \in \mathbf{S}_{\text{STC}}, p \in \mathbf{P}, t \in \mathbf{T} \quad \text{(A.15)}$$

$$\dot{q}_{\text{STP},s,p,t}^{-} = \epsilon_{\text{STP},s} \cdot \text{GHI}_{p,t} \qquad \forall s \in \mathbf{S}_{\text{STC}}, p \in \mathbf{P}, t \in \mathbf{T} \quad \text{(A.16)}$$

Table A.6 – Parameter data (STC)

Parameter	Value	Unit	Ref.
η	0.836	[-]	[149]
a	4.16	[W/(m$^2\cdot$K)]	[149]
b	0.073	[W/(m$^2\cdot$K^2)]	[149]
L	20	[yr]	[57, 59]
inv$_1$	347	[CHF]	est. from Fig. A.1
inv$_2$	126	[CHF/m^2]	est. from Fig. A.1
F$_{\text{BM}}$	1.33	[-]	est. from [147]

Storage units

Based on the generic formulation of Equations 1.31 to 1.33, this section details the specific model definition of storage units included in the MF: stationary battery stacks, heat storage tanks and domestic hot water tanks.

Battery stack (BAT)   Stationary batteries are described using a single state dynamic model formulation (Eq. 1.31), the sizing dimension being the electrical energy stored. The former accounts for the system self-discharging σ rate as well as dis- and charging losses γ which, in addition, include the inverter efficiency. In order to limit any premature degradation of the stack, both the minimum and maximum battery states of charge SOC are constrained (Eqs. A.17 and A.18). Applied parameters values are reported in Table A.7.

$$f_{\text{BAT},p,t} \geq \text{SOC}_{\text{BAT}}^{min} \cdot F_{\text{BAT}} \qquad\qquad \forall p \in \boldsymbol{P}, t \in \boldsymbol{T} \quad (A.17)$$

$$f_{\text{BAT},p,t} \leq \text{SOC}_{\text{BAT}}^{max} \cdot F_{\text{BAT}} \qquad\qquad \forall p \in \boldsymbol{P}, t \in \boldsymbol{T} \quad (A.18)$$

Table A.7 – Parameter data (BAT)

Parameter	Value	Unit	Ref.
γ^{ch}	0.9	[-]	[27]
γ^{di}	0.9	[-]	[27]
σ	0	[-]	[27]
κ	-	[-]	
L	10	[yr]	est.
inv_1	620	[CHF]	est. from Fig. A.1
inv_2	970	[CHF/kWh]	est. from Fig. A.1
F_{BM}	1.33	[-]	est.
SOC^{max}	0.8	[-]	[20]
SOC^{min}	0.2	[-]	[20]

Heat storage tank (HST)   Thermal energy storages are described through a single state, first order dynamic model formulation as shown in Eq. 1.31, the sizing dimension being the unit volume. The minimum state-of-charge SOC^{min} is set to the current building return temperature $T_{b,p,t}^{\text{h,r}}$ during space heating periods while the maximum operating temperature T_u^{max} is the defined as the lowest value between the heat pump operating limit and the nominal supply temperature of the hydronic heating system ($T_b^{\text{h,s}}$). The required parameters include the tank diameter D, the specific heat loss rate U as well as the charging and discharging efficiencies γ. The unit is consequently added into the heat cascade formulation (Eqs. 1.11 to 1.14) through the single charging (cold) and discharging (hot) streams as defined in Eq.

Eq. A.19 and Eq. A.22. Applied parameters values are reported in Table A.8.

$$\sigma_{\mathrm{HST}} = \frac{4 \cdot U_{\mathrm{HST}}}{D_{\mathrm{HST}}} \cdot \left(T_{\mathrm{HST}}^{\max} - T_{b,p,t}^{\mathrm{h,r}} \right) \qquad \forall p \in \boldsymbol{P}, t \in \boldsymbol{T} \quad (\mathrm{A.19})$$

$$\kappa_{\mathrm{HST}} = \frac{4 \cdot U_{\mathrm{HST}}}{D_{\mathrm{HST}}} \cdot \left(T_{b,p,t}^{\mathrm{h,r}} - T^{\mathrm{amb}} \right) \qquad \forall p \in \boldsymbol{P}, t \in \boldsymbol{T} \quad (\mathrm{A.20})$$

$$\dot{q}_{\mathrm{HST},s,p,t}^{+} = c_p \cdot \rho \cdot \left(T_{\mathrm{HST}}^{\max} - T_{b,p,t}^{\mathrm{h,r}} \right) \qquad \forall p \in \boldsymbol{P}, t \in \boldsymbol{T} \quad (\mathrm{A.21})$$

$$\dot{q}_{\mathrm{HST},s,p,t}^{-} = c_p \cdot \rho \cdot \left(T_{\mathrm{HST}}^{\max} - T_{b,p,t}^{\mathrm{h,r}} \right) \qquad \forall p \in \boldsymbol{P}, t \in \boldsymbol{T} \quad (\mathrm{A.22})$$

Table A.8 – Parameter data (HST)

Parameter	Value	Unit	Ref.
γ^{ch}	0.99	[-]	est.
γ^{di}	0.99	[-]	est.
L	20	[yr]	[57, 59, 146]
inv_1	760	[CHF]	est. from Fig. A.1
inv_2	1040	[CHF/m^3]	est. from Fig. A.1
F_{BM}	1.87	[-]	est. from [147]
D	0.98	[m]	est.
U	0.0013	[kW/m^2]	[59]

Storage - Domestic hot water tank (HWT)   Domestic hot water tanks are described through a similar multi-state dynamic model formulation as shown in Eq. 1.32, the sizing dimension being the unit volume. The hot water demand profile $\dot{m}_{b,p,t}$ is thus translated into an *a-priori* determined discharging load $f_{u,s,p,t}$ at the last model layer, the remaining variables being fixed to null as detailed in Eq. A.25. The minimum state-of-charge is fixed to the fresh water temperature $T_u^{\min}$ while the maximum operating temperature $T_u^{\max}$ is set to the required service temperature (55°C). Similarly to the heat storage, the required parameters include the tank diameter D, the specific heat loss rate U as well as the charging efficiency γ. Finally, the unit is incorporate into the heat cascade (Eqs. 1.11 to 1.14) through the charging streams in Eq. A.24. Applied parameters values are reported in Table A.9.

$$\sigma_{\mathrm{HWT},s} = \frac{4 \cdot U_{\mathrm{HWT}}}{D_{\mathrm{HWT}}} \cdot \left(T_{\mathrm{HWT},s}^{\mathrm{out}} - T^{\mathrm{amb}} \right) \qquad \forall s \in \boldsymbol{S} \quad (\mathrm{A.23})$$

$$\dot{q}_{\mathrm{HWT},s}^{+} = c_p \cdot \rho \cdot \left(T_{\mathrm{HWT},s}^{\mathrm{out}} - T_{\mathrm{HWT},s}^{\mathrm{in}} \right) \qquad \forall s \in \boldsymbol{S} \quad (\mathrm{A.24})$$

$$f_{\mathrm{HWT},s=n_s,p,t}^{-} = \dot{m}_{b,p,t}^{\mathrm{HW}} \qquad \forall p \in \boldsymbol{P}, t \in \boldsymbol{T} \quad (\mathrm{A.25})$$

Table A.9 – Parameter data (HWT)

Parameter	Value	Unit	Ref.
γ^{ch}	0.95	[-]	est.
γ^{di}	1	[-]	est.
L	20	[yr]	[57, 59, 146]
inv_1	295	[CHF]	est. from Fig. A.1
inv_2	6100	[CHF/m^3]	est. from Fig. A.1
F_{BM}	1.68	[-]	est. from [147]
D	0.7	[m]	est.
U	0.0013	[kW/m^2]	[59]

Additional parameter values

The following section provides additional information of the heat integration parameters required. First, Table A.10 lists the different thermal streams associated to each unit and subsequently incorporated in the heat cascade. High temperature conversion utilities (e.g. BOI, ELH & SOFC) are represented by a single discrete thermal stream s set to the maximal operating limit. Furthermore, Figures A.1 and A.2 illustrate the linear investment cost regressions on basis of current market technologies available in Switzerland and Europe. Finally, Figure A.3 depicts the building input profiles (electricity demand, hot water withdrawals and internal gains) for the presented case studies: a single family house (SFH), an apartment block (AB) and an office building (OB).

Table A.10 – Default parameters values for the unit thermal streams s. The last column specifies incoming (+) or outgoing (-) flows

Unit	s	T^{in} [°C]	T^{out} [°C]	ΔT^{min} [°C]	$\dot{q}$ [kW]
AHP	1-3	var.[1,2]	var.[1,2]	0	
	4	55	50	0	Eq. A.9 ($^-$)
	5	55	10	14	
BOI	1	80	70	0	1 ($^-$)
SOFC	1	80	70	0	Eq. A.11 ($^-$)
LPEM	1	60	50	0	Eq. A.11 ($^-$)
HWT	1	55	10	14	Eq. A.24 ($^+$)
ELH	1	80	70	0	1 ($^-$)
HHS	1-3	var.[1]	var.[1]	0	1 ($^+$)
	1-3	var.[1]	var.[1]	0	1 ($^-$)
HST	1	var.[1,2]	var.[1,2]	0	Eq. A.22 ($^-$)
	1	var.[1,2]	var.[1,2]	0	Eq. A.21 ($^+$)
STC	1	69	54	14	
	2	54	39	14	Eq. A.16 ($^-$)
	3	39	24	14	

[1] Ambient condition dependent
[2] According to the temperature discretization of HHS

The second-law efficiency η and maximum electrical load for each thermal stream s are evaluated using a bi-dimensional interpolation method from specific operating points. The latter are reported in Tables A.11 and A.12. For the AHP and VAC, the source and sink temperatures corresponds to the ambient T^{ext} and the stream logarithmic mean temperatures respectively.

Table A.11 – Default parameters values for the AHP second-law efficiency and part-load limit, evaluated from [144]

	Par.	T^{sink}	T^{source} [°C]									
		[°C]	-20	-15	-10	-7	-2	2	7	10	15	20
AHP	η	35	0	0.464	0.458	0.458	0.469	0.462	0.435	0.416	0.37	0.307
		45	0	0.445	0.463	0.464	0.46	0.446	0.439	0.436	0.43	0.396
		55	0	0	0	0.421	0.423	0.416	0.439	0.436	0.412	0.395
	$\dot{e}^{+,max}$	35	0	0.62	0.65	0.65	0.65	0.65	0.68	0.68	0.68	0.68
		45	0	0.74	0.74	0.74	0.76	0.79	0.82	0.82	0.79	0.79
		55	0	0	0	0.91	0.94	0.97	0.97	0.97	1	1

Table A.12 – Default parameters values for the VAC second-law efficiency and part-load limit, evaluated from [144]

	Par.	T^{sink}	T^{source} [°C]					
			20	25	30	35	40	45
VAC	η	13	0.103	0.159	0.198	0.219	0.249	0.224
		15	0.076	0.14	0.181	0.243	0.243	0.224
		18	0.033	0.101	0.146	0.209	0.209	0.218
		22	0	0.005	0.106	0.184	0.184	0.215
	$\dot{e}^{+,max}$	13	0.71	0.78	0.86	0.95	0.91	1
		15	0.73	0.78	0.87	0.95	0.91	0.96
		18	0.73	0.8	0.89	0.96	0.93	0.89
		22	0.75	0.82	0.91	1	0.95	0.8
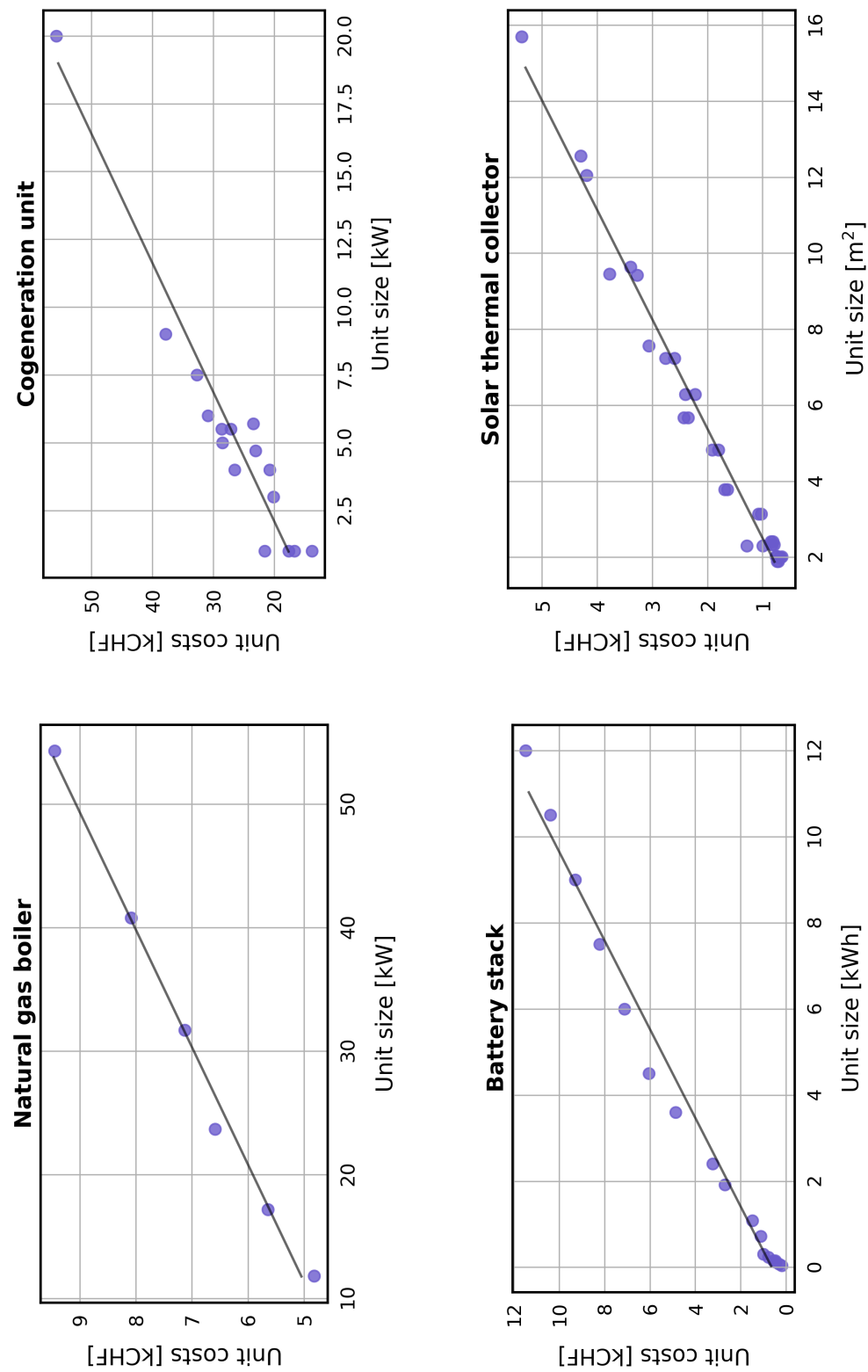
Figure A.1 – Unit Investment cost function - linear regressions (Part I)
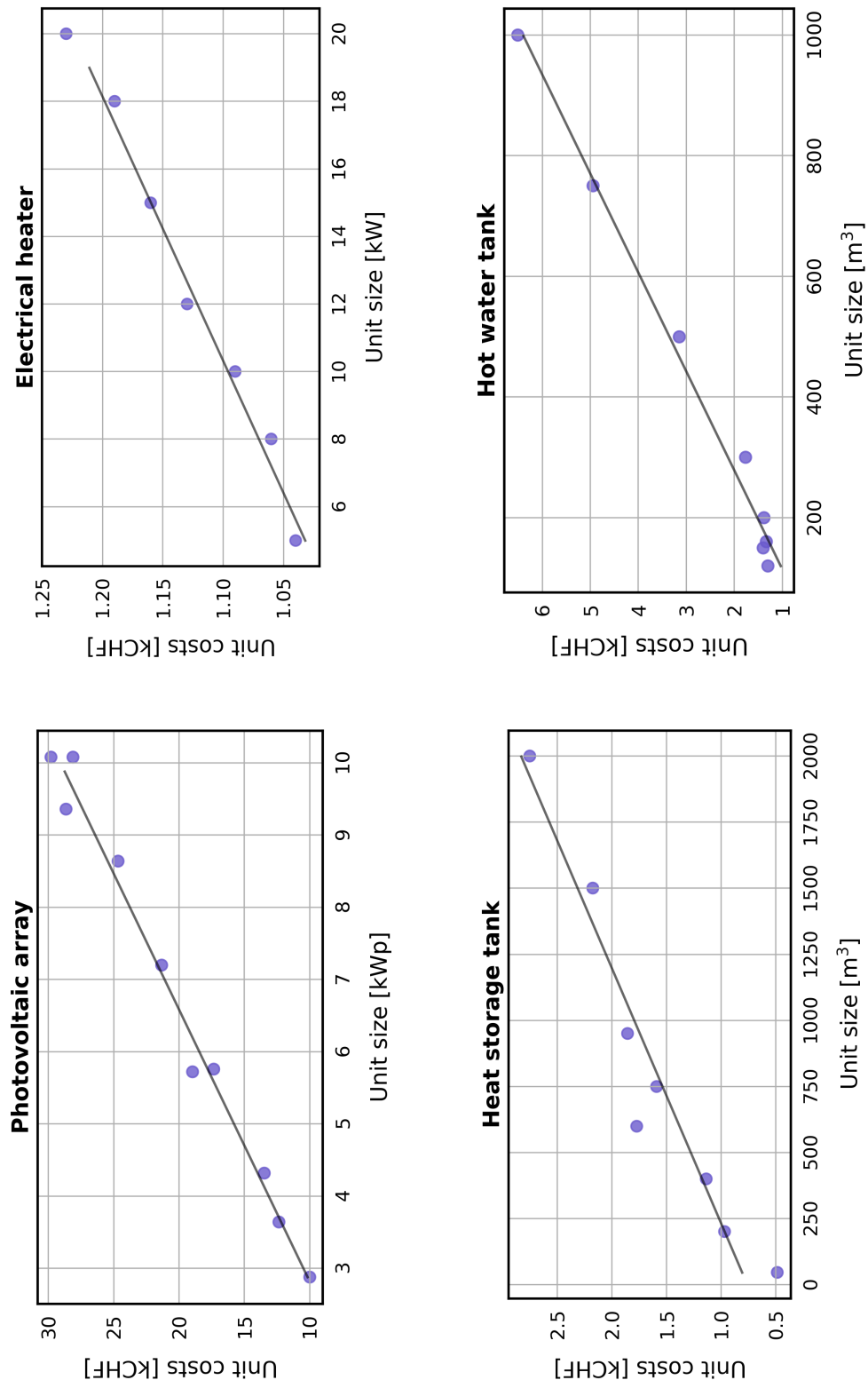
Figure A.2 – Unit Investment cost function - linear regressions (Part II)
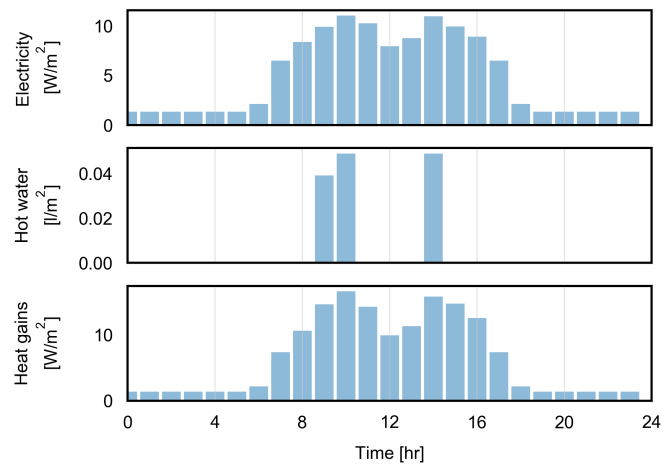
(a) Office building
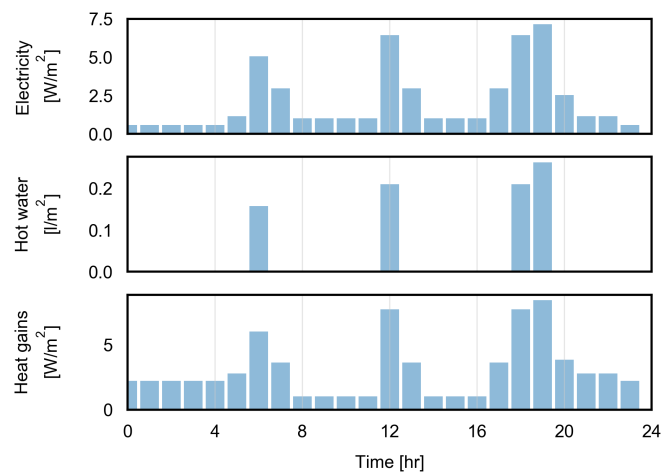
(b) Apartment block
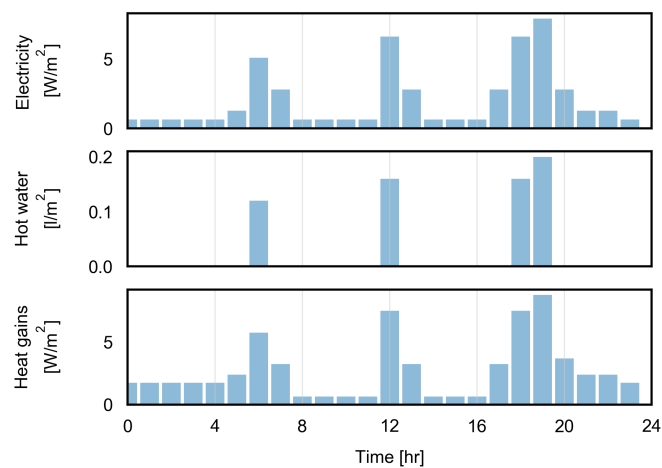
(c) Single family house

Figure A.3 – Energy services demand profiles of three representative building types

Additional results: renovation cost comparison

Figure A.4 compares the different expense contributions of both the non- and renovated BES for a single family house (SFH) and an apartment block (AB). In the case of SFH, renovated BES configurations (including state subsidies) start being cost-efficient from $S_{0.3}$ onward while in the case of AB, the latter refurbished solutions are nearly equal for multiple BES configurations: $S_{0-0.2}$ and $S_{0.7-1}$

(a) Single family house (SFH)

(b) Apartment block (AP)
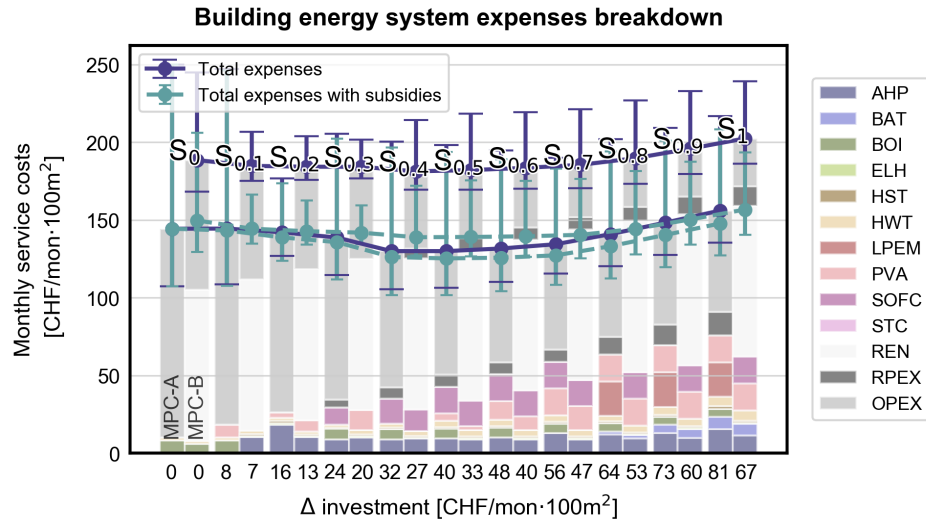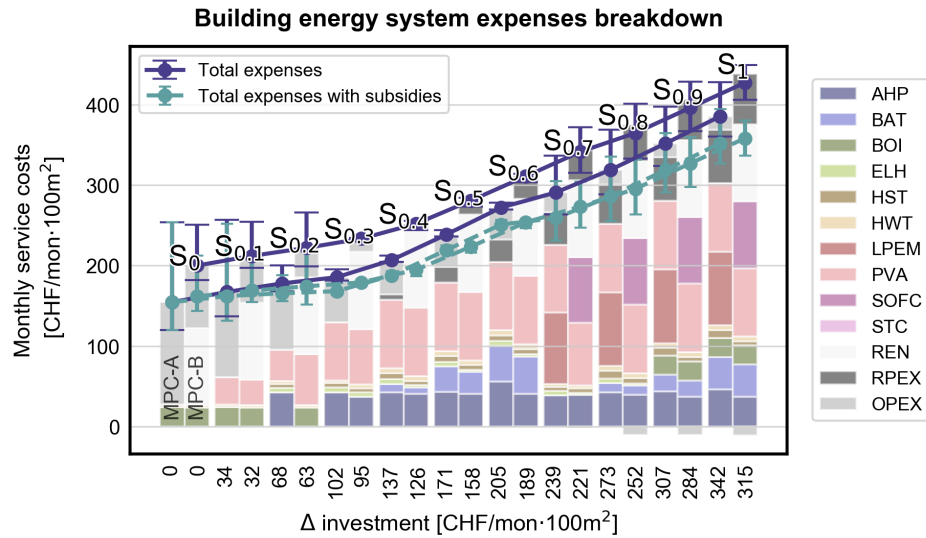
Figure A.4 – Expense contributions per BES for two building types (*left*: non-, *right*: refurbished solution)

B Chapter 2: National energy services

Building classification

Table B.1 reveals further details on model parameters estimated for each representative building type and used to infer space heating (and cooling) service demands.

Table B.1 – National representative building classes

Age	Ref.	Use	U [kW/°C·m²]	T^s [°C]	T^r [°C]	Use	U [kW/°C·m²]	T^s [°C]	T^r °C]
>1920	×		1.93	65	50		1.91	65	50
1920-1970	×		2.14	65	50		2.03	65	50
1970-1980	×		2.04	65	50		2.00	65	50
1980-2005	×		1.62	65	50		1.66	65	50
2005-2020	×	SFH/MFH	1.00	41.5	33.9	MIX	1.07	41.5	33.9
>1920	✓		0.94	54.4	44.1		1.02	54.4	44.1
1920-1970	✓		1.17	54.4	44.1		1.23	54.4	44.1
1970-1980	✓		1.11	53.8	43.8		1.18	53.8	43.8
1980-2005	✓		1.21	56.3	45.3		1.27	56.3	45.3

Spatial classification

The following table (Table B.2) presents additional information on the aggregated building energy service demands for each states (i.e. Canton) resulting from the spatial classification process.

Table B.2 – Estimated annual energy service demands for each canton

Canton name	ERA[1] [mio m^2]	EL [GWh]	HW [GWh]	SH[2] [GWh]
Zürich	102.46	2105.20	1317.54	10570.03
Bern	99.56	1985.05	1288.94	12325.59
Luzern	30.61	649.54	392.70	3348.87
Uri	3.27	68.38	42.26	508.43
Schwyz	12.46	275.82	158.89	1481.59
Obwalden	4.07	86.17	51.92	601.50
Nidwalden	3.81	82.99	48.53	469.41
Glarus	4.38	85.51	56.66	760.36
Zug	8.00	178.59	100.51	861.84
Fribourg	25.86	536.49	337.53	3070.77
Solothurn	23.64	473.55	310.51	2430.43
Basel-Stadt	11.97	231.12	157.61	1223.10
Basel-Landschaft	20.53	415.36	271.55	2113.86
Schaffhausen	6.65	132.78	86.27	702.93
Appenzell Ausserrhoden	6.46	126.44	82.00	812.11
Appenzell Innerrhoden	2.03	40.84	26.32	277.68
St. Gallen	38.37	792.73	501.46	4356.06
Graubünden	26.99	568.54	343.23	5234.02
Aargau	53.03	1098.10	693.52	5466.55
Thurgau	23.37	479.28	302.83	2547.46
Ticino	29.45	587.77	384.02	2883.32
Vaud	51.13	1043.24	661.94	5711.41
Valais	35.57	743.39	465.16	5723.61
Neuchâtel	13.83	272.04	177.05	1803.52
Genève	24.12	496.77	317.69	2275.65
Jura	7.93	155.55	104.16	922.70
National	669.54	13.71	8.68	78.48

[1] Energetic reference area

[2] Estimated from [31] and corrected with the respective HDD of each climatic zones

Temporal classification

This section presents the temporal classification results for the different spatial clusters defined in Section 2.3.1. In order to reconstruct the clustered load curves from the original design reference years (DRY), Table B.3 provides the selected days (cluster centres) and annual frequency of occurrence.

Table B.3 – Temporal cluster centres and frequencies for each representative climatic zone

Zone		Indexes								
Bern-Liebefeld	*days*	336	309	138	142	74	236	209	184	
	freq.	46	58	45	45	57	48	48	18	
Davos	*days*	20	274	43	198	103	225			
	freq.	75	65	40	46	62	77			
Disentis	*days*	221	263	140	349	17	83			
	freq.	71	59	53	68	59	55			
Genève-Cointrin	*days*	206	59	264	254	7	222	72	169	
	freq.	52	46	54	49	68	17	49	30	
Lugano	*days*	74	137	364	95	325	209	227	224	
	freq.	54	48	64	42	57	36	48	16	
Piotta	*days*	233	8	78	213	178	61	264	266	33
	freq.	43	49	42	18	37	31	36	44	65
Zürich-SMA	*days*	343	147	74	182	309	122	219		
	freq.	59	35	37	47	77	52	58		

Bern-Liebefeld

In regard to the performance indicators behaviours illustrated in Figure B.1, the climatic region of Bern-Liebefeld is represented through n_k = **8 typical operating periods** (i.e. days), the minimum acceptable cluster size being $n_k^{\min}$ = 8. Figure B.2 presents the original data of the Bern-Liebefeld DRY with the respective 8 typical days and thus provides a graphical validation of the load curve durations. Finally, Table B.4 provides a comparison between the applied method and an empirical representative day selection approach based on monthly average values.

Figure B.1 – Quality and performance indicators for Bern-Liebefeld

Table B.4 – Quality comparison between *k-medoids* and empirical period selection for Bern-Liebefeld

No. periods	Typical 8		Empirical 12		Deviation	
Attribute	T	GHI	T	GHI	T	GHI
mELDC^2	0.0004	0.0004	0.0010	0.0021	-0.61	-0.81
σ_{cdc}	0.0523	0.0358	0.0822	0.0567	-0.36	-0.37
σ_{profile}	0.0287	0.0638	0.0334	0.0797	-0.14	-0.20
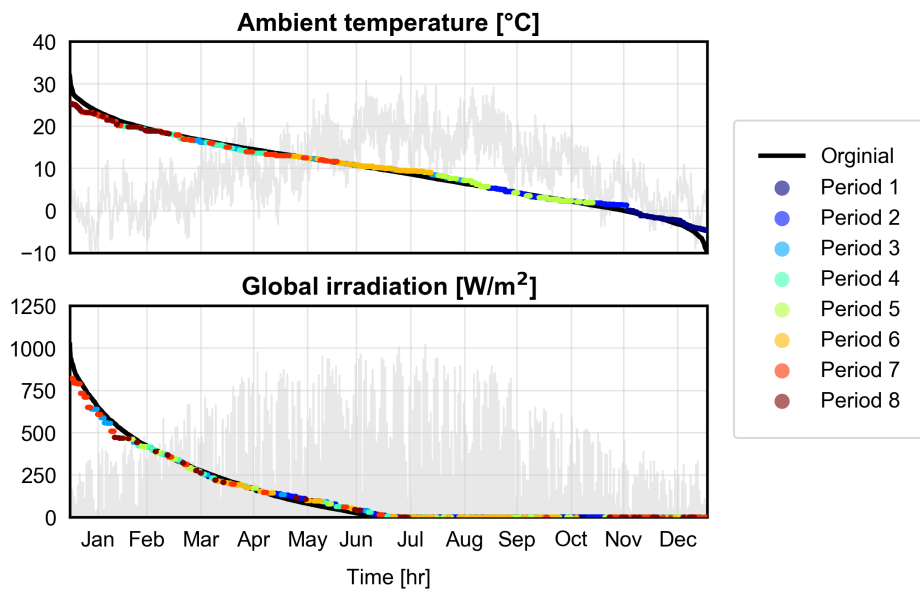
Figure B.2 – Load duration curve of the ambient temperature and global horizontal irradiation for Bern-Liebefeld of original data and 8 typical periods extreme days. In background annual distribution of the original data.

Zürich-SMA

In regard to the performance indicators behaviours illustrated in Figure B.3, the climatic region of Zürich is represented through n_k = **7 typical operating periods** (i.e. days), the minimum acceptable cluster size being $n_k^{\min}$ = 6. Figure B.4 presents the original data of the Zürich-SMA DRY with the respective 7 typical days and thus provides a graphical validation of the load curve durations. Finally, Table B.5 provides a comparison between the applied method and an empirical representative day selection approach based on monthly average values.

Figure B.3 – Quality and performance indicators for Zürich

Table B.5 – Quality comparison between *k-medoids* and empirical period selection for Zürich-SMA

No. periods	Typical 7		Empirical 12		Deviation	
Attribute	T	GHI	T	GHI	T	GHI
mELDC^2	0.0004	0.0005	0.0013	0.0021	-0.70	-0.76
σ_{cdc}	0.0558	0.0339	0.0868	0.0556	-0.36	-0.39
σ_{profile}	0.0295	0.0642	0.0317	0.0783	-0.07	-0.18
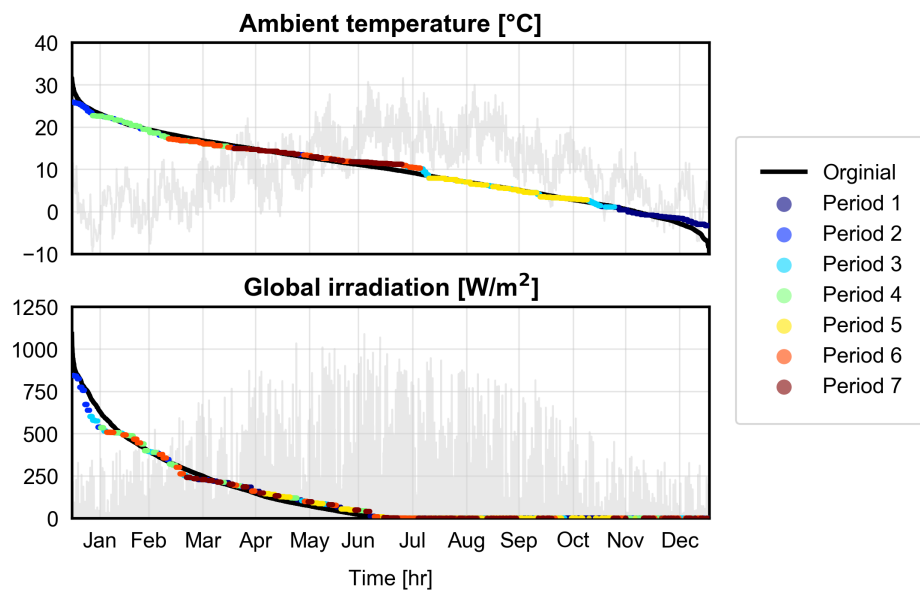
Figure B.4 – Load duration curve of the ambient temperature and global horizontal irradiation for Zürich of original data and 7 typical periods extreme days. In background annual distribution of the original data.

Davos

In regard to the performance indicators behaviours illustrated in Figure B.5, the climatic region of Davos is represented through n_k = **6 typical operating periods** (i.e. days), the minimum acceptable cluster size being $n_k^{\min}$ = 6. Figure B.6 presents the original data of the Davos DRY with the respective 6 typical days and thus provides a graphical validation of the load curve durations. Finally, Table B.6 provides a comparison between the applied method and an empirical representative day selection approach based on monthly average values.

Figure B.5 – Quality and performance indicators for Davos

Table B.6 – Quality comparison between *k-medoids* and empirical period selection for Davos

No. periods	Typical 6		Empirical 12		Deviation	
Attribute	T	GHI	T	GHI	T	GHI
mELDC^2	0.0005	0.0004	0.0010	0.0016	-0.54	-0.76
σ_{cdc}	0.0570	0.0379	0.0843	0.0502	-0.32	-0.25
σ_{profile}	0.0341	0.0660	0.0343	0.0730	-0.01	-0.10
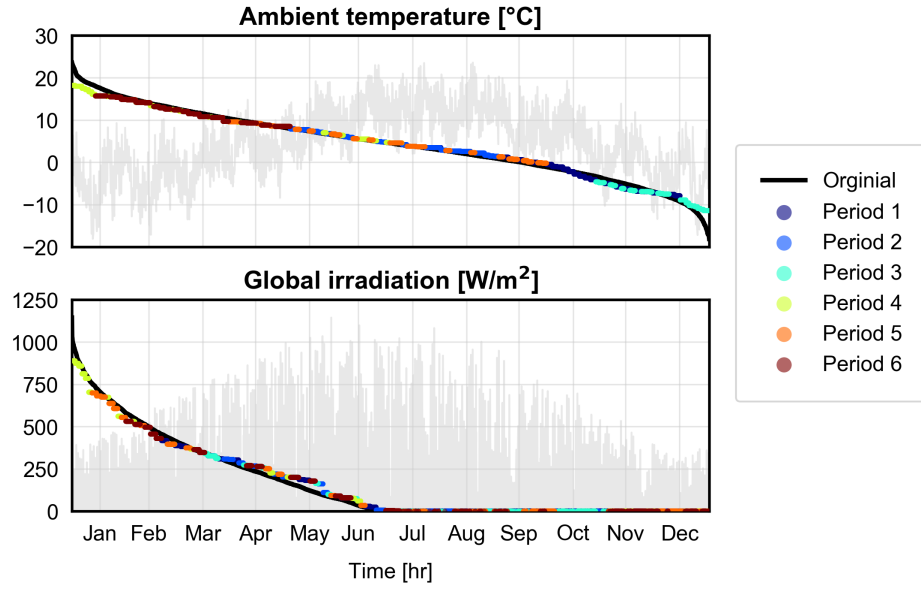
Figure B.6 – Load duration curve of the ambient temperature and global horizontal irradiation for Davos of original data and 6 typical periods extreme days. In background annual distribution of the original data.

Lugano

In regard to the performance indicators behaviours illustrated in Figure B.7, the climatic region of Lugano is represented through n_k = **8 typical operating periods** (i.e. days), the minimum acceptable cluster size being n_k^{min} = 7. Figure B.8 presents the original data of the Lugano DRY with the respective 8 typical days and thus provides a graphical validation of the load curve durations. Finally, Table B.7 provides a comparison between the applied method and an empirical representative day selection approach based on monthly average values.
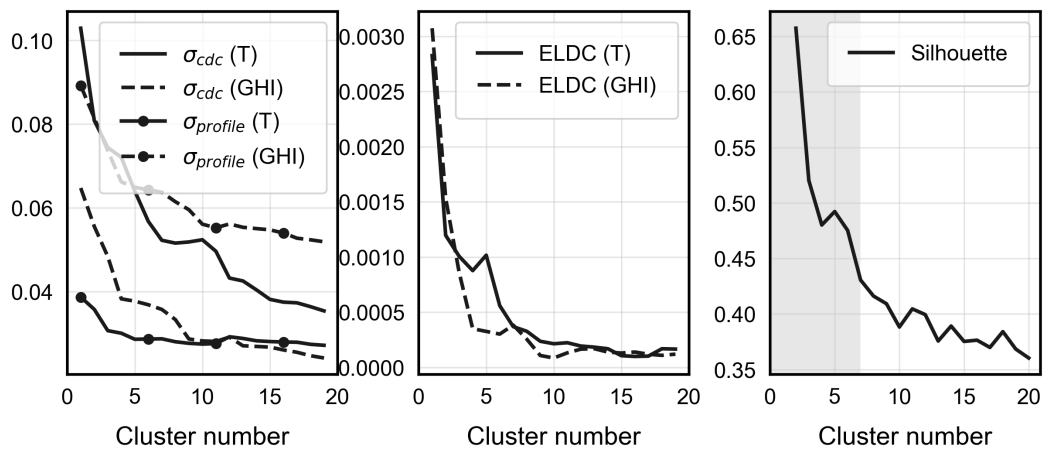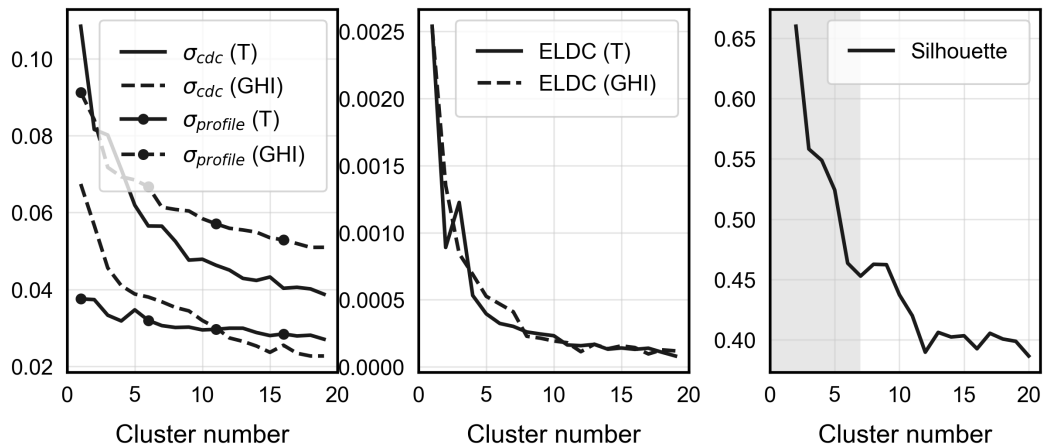

Figure B.7 – Quality and performance indicators for Lugano

Table B.7 – Quality comparison between *k-medoids* and empirical period selection for Lugano

No. periods	Typical 8		Empirical 12		Deviation	
Attribute	T	GHI	T	GHI	T	GHI
mELDC^2	0.0003	0.0004	0.0003	0.0020	-0.10	-0.80
σ_{cdc}	0.0565	0.0368	0.0682	0.0581	-0.17	-0.37
σ_{profile}	0.0306	0.0614	0.0361	0.0822	-0.15	-0.25
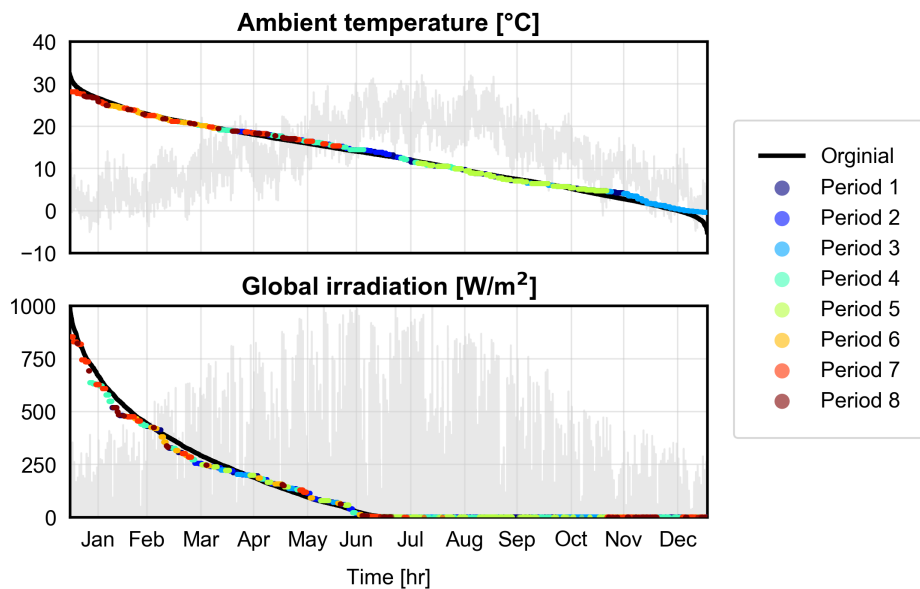
Figure B.8 – Load duration curve of the ambient temperature and global horizontal irradiation for Lugano of original data and 8 typical periods extreme days. In background annual distribution of the original data.

Disentis

In regard to the performance indicators behaviours illustrated in Figure B.9, the climatic region of Disentis is represented through n_k = **6 typical operating periods** (i.e. days), the minimum acceptable cluster size being $n_k^{\min}$ = 6. Figure B.10 presents the original data of the Disentis DRY with the respective 6 typical days and thus provides a graphical validation of the load curve durations. Finally, Table B.8 provides a comparison between the applied method and an empirical representative day selection approach based on monthly average values.
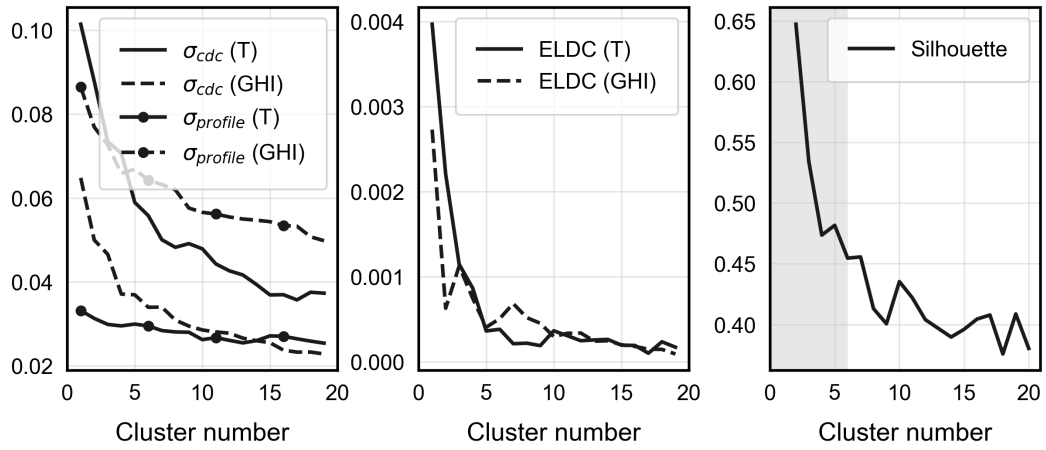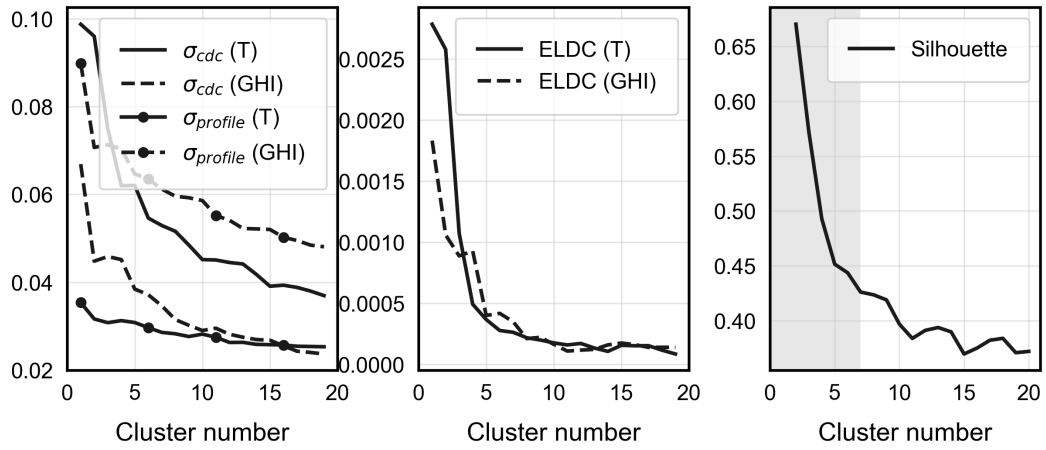
Figure B.9 – Quality and performance indicators for Disentis

Table B.8 – Quality comparison between *k-medoids* and empirical period selection for Disentis

| No. periods	Typical 6		Empirical 12		Deviation	
Attribute	T	GHI	T	GHI	T	GHI
mELDC^2	0.0004	0.0004	0.0009	0.0021	-0.61	-0.81
σ_{cdc}	0.0620	0.0384	0.0835	0.0548	-0.26	-0.30
$\sigma_{profile}$	0.0308	0.0647	0.0322	0.0760	-0.04	-0.15
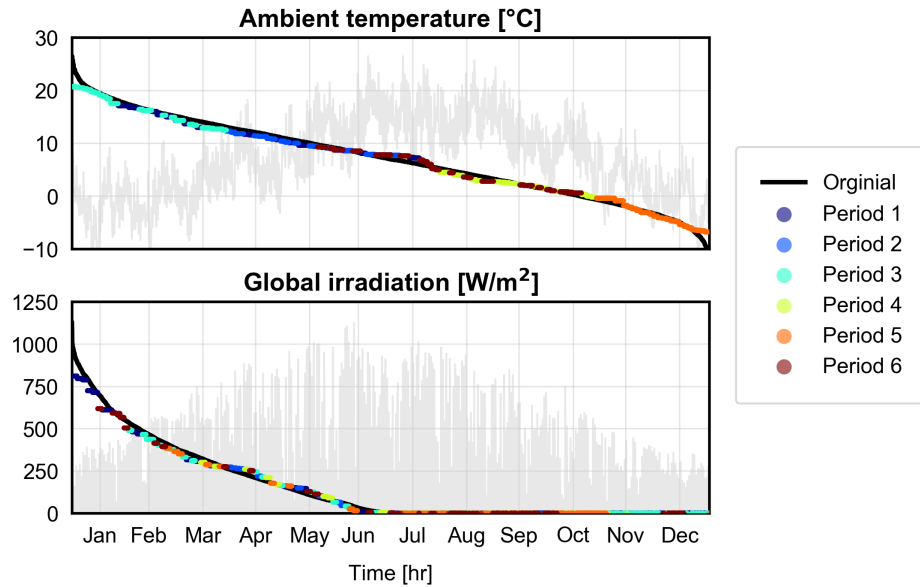
Figure B.10 – Load duration curve of the ambient temperature and global horizontal irradiation for Disentis of original data and 6 typical periods extreme days. In background annual distribution of the original data.

Piotta

In regard to the performance indicators behaviours illustrated in Figure B.11, the climatic region of Disentis is represented through n_k = **9 typical operating periods** (i.e. days), the minimum acceptable cluster size being $n_k^{\min}$ = 8. Figure B.12 presents the original data of the Piotta DRY with the respective 9 typical days and thus provides a graphical validation of the load curve durations. Finally, Table B.9 provides a comparison between the applied method and an empirical representative day selection approach based on monthly average values.
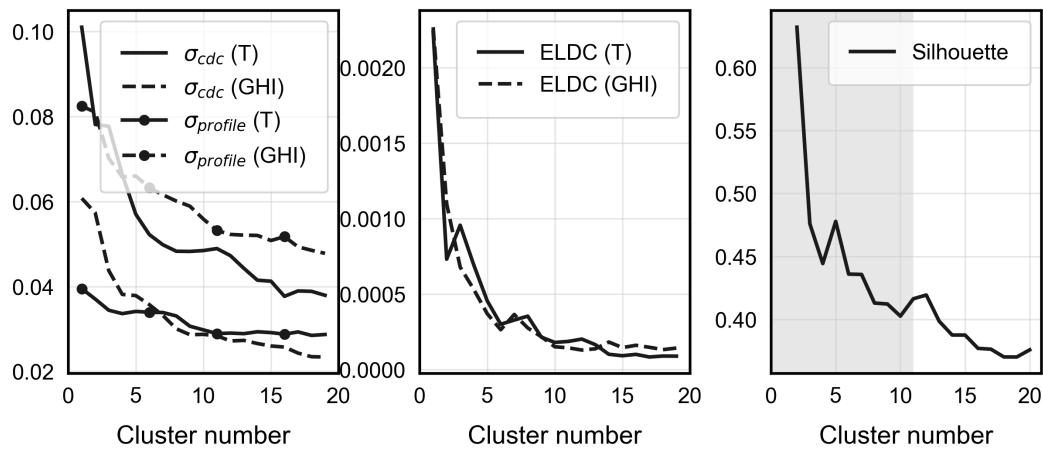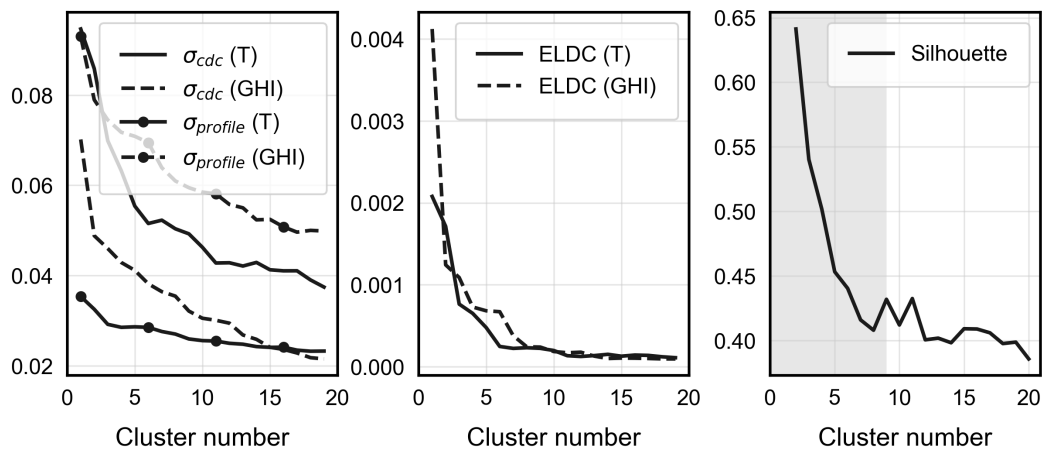

Figure B.11 – Quality and performance indicators for Piotta

Table B.9 – Quality comparison between *k-medoids* and empirical period selection for Piotta

| No. periods	Typical 9		Empirical 12		Deviation	
Attribute	T	GHI	T	GHI	T	GHI
mELDC^2	0.0002	0.0002	0.0006	0.0026	-0.62	-0.91
σ_{cdc}	0.0503	0.0354	0.0718	0.0561	-0.30	-0.37
$\sigma_{\mathrm{profile}}$	0.0270	0.0610	0.0319	0.0820	-0.15	-0.26
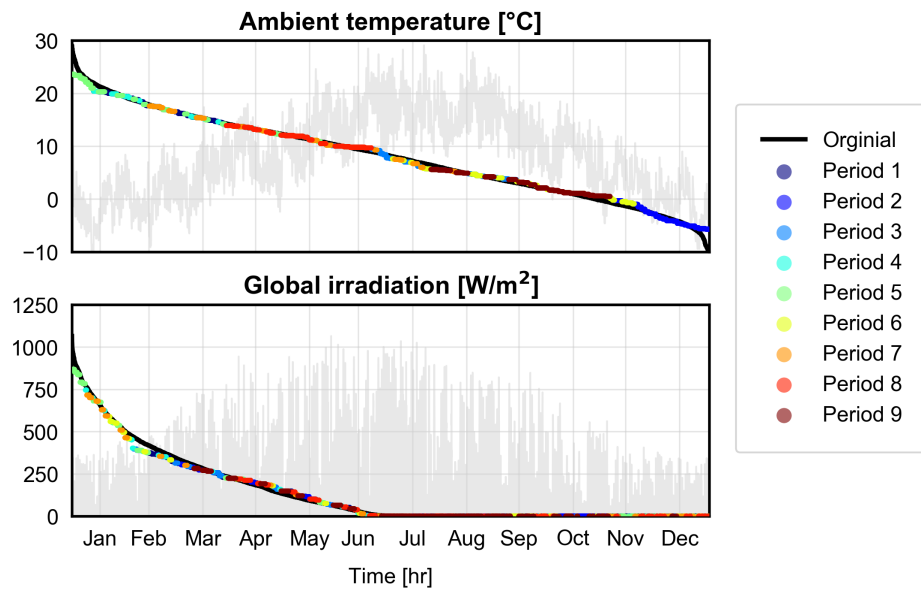
Figure B.12 – Load duration curve of the ambient temperature and global horizontal irradiation for Piotta of original data and 9 typical periods extreme days. In background annual distribution of the original data.

Chapter 3: community descriptions and data

Building demands

Table C.1 reveals further details on model parameters estimated for each building type occurring in the different case studies. In addition, Figure C.1 illustrates the normalized daily energy service profiles (EL and HW) assessed from the national architecture and engineering standards in Switzerland (SIA 2024 [65]).

Table C.1 – Building classes in the Geneva area [81]

Construction per.	Ref.[‡]	Use	U [kW/°C·m^2]	T^s [°C]	T^r [°C]	Use	U [kW/°C·m^2]	T^s [°C]	T^r °C]
>1920	×		1.93	65	50		1.91	65	50
1920-1970	×		2.14	65	50		2.03	65	50
1970-1980	×		2.04	65	50		2	65	50
1980-2005	×	SFH/MFH	1.62	65	50	MIX	1.66	65	50
2005-2020	×		1	41.5	33.9		1.07	41.5	33.9
>1920	✓		0.94	54.4	44.1		1.02	54.4	44.1
1920-1970	✓		1.17	54.4	44.1		1.23	54.4	44.1
1970-1980	✓		1.11	53.8	43.8		1.18	53.8	43.8
1980-2005	✓		1.21	56.3	45.3		1.27	56.3	45.3
>1920	×		2.08	65	50		1.90	65	50
1920-1970	×		2.08	65	50		2.99	65	50
1970-1980	×		2.13	65	50		3.02	65	50
1980-2005	×	EDU	1.92	65	50	ADM	3.02	65	50
2005-2020	×		1.36	41.5	33.9		2.12	41.5	33.9
>1920	✓		1.31	54.4	44.1		2.03	54.4	44.1
1920-1970	✓		1.52	54.4	44.1		2.35	54.4	44.1

Table C.1 – continued from previous page

Construction per.	Ref.	Use	U [kW/°C·m^2]	T^s [°C]	T^r [°C]	Use	U [kW/°C·m^2]	T^s [°C]	T^r °C]
1970-1980	✓		1.46	53.8	43.8		2.28	53.8	43.8
1980-2005	✓		1.57	56.3	45.3		2.41	56.3	45.3

‡ Refurbished

(a) Administrative (ADM)

(b) Residential (SFH)

(c) Residential (MFH)

(d) Educational (EDU)
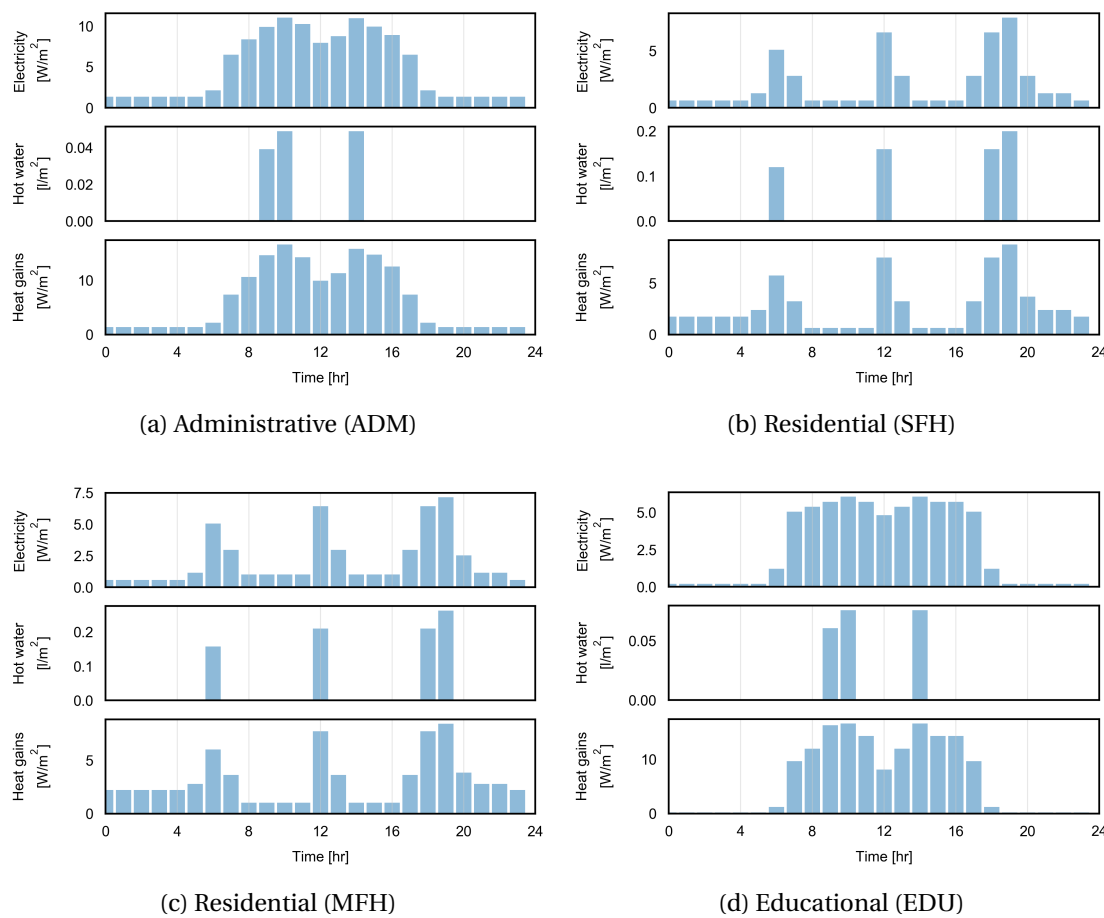
Figure C.1 – Daily specific energy service profiles for different dwelling affectation

Building clustering results

The following tables (Tables C.2 to C.6) present additional information on the different building clustering processes applied for each case study analysed. Similarly, Figures C.2 and C.3 illustrate the quality and performance indicators evolution with the rise in cluster number associated to the urban and reconfigured rural communities.

Rural community

Following the building clustering process presented in Section 3.3.1, Table C.2 shows the main characteristics of the generated clusters while additional information can be inferred from the associated building use and construction period (Table C.1).

Table C.2 – Cluster characteristics for the rural scenario

Parameter	Cluster			
	A	B	C	
Energy ref. area	1508.4	284.4	1112.4	[m^2]
Roof area	0.33	0.73	0.27	[m^2/m^2]
Construction per.	2005-2020	1980-2005	2005-2020	[-]
Use	MFH	MFH	MFH	[-]
Refurbished	-	×	-	[-]

Urban community

Regarding the clustering method defined in Section 3.3.1, the urban community is clustered into **three** representative building categories. The consequent cluster characteristics are reported in Table C.3 while additional information can be inferred from the associated building use and construction period (Table C.1). Finally, Figure C.2 and Table C.4 highlight further the clustering results regarding both the quality-performance indicators evolution and the final disparities between the original and clustered data respectively.

Table C.3 – Cluster characteristics for the urban scenario

Parameter	Cluster			
	A	B	C	
Energy ref. area	2349.9	1372.5	1619.1	[m^2]
Roof area	0.18	0.23	0.17	[m^2/m^2]
Construction per.	1980-2005	1970-1980	1920-1970	[-]
Use	ADM	MIX	MIX	[-]
Refurbished	×	×	×	[-]
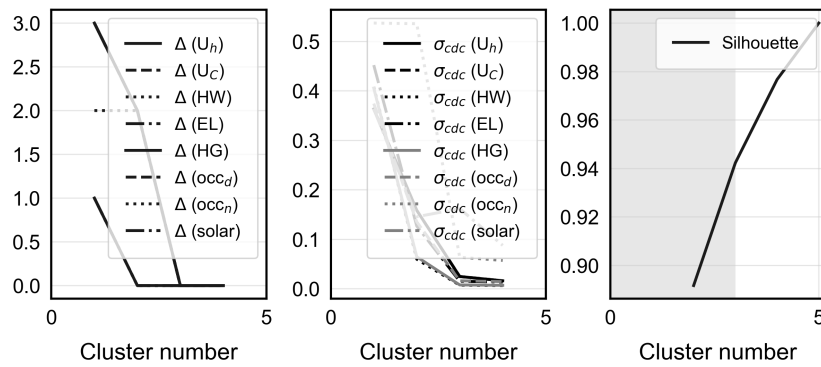
Figure C.2 – Quality indicators for a urban district data reduction

Table C.4 – Attribute error for an urban community data reduction

Attribute	Original value	Clustered value	dif. [%]	
U_h	16.6	16.6	0.06	[MW/K]
U_c	16.6	16.6	0.06	[MW/K]
EL	270.4	270.8	-0.17	[MWh/yr]
HW	69.6	69.7	-0.25	[MWh/yr]
HG	361.7	362.3	-0.17	[MWh/yr]
Solar	1561.9	1579.5	-1.11	[m^2]

Rural (reconfigured) community

Regarding the clustering method defined in Section 3.3.1, the reconfigured rural community is clustered into **three** representative building categories. The consequent cluster characteristics are reported in Table C.5 while additional information can be inferred from the associated building use and construction period (Table C.1). Finally, Figure C.3 and Table C.6 highlight further the clustering results regarding both the quality-performance indicators evolution and the final disparities between the original and clustered data respectively.

Table C.5 – Cluster characteristics for the rural (reconfigured) scenario

Parameter	Cluster			
	A	B	C	
Energy ref. area	3793.5	286.2	1112.4	[m^2]
Roof area	0.38	0.73	0.27	[m^2/m^2]
Construction per.	2005-2020	1980-2005	2005-2020	[-]
Use	EDU	MFH	MFH	[-]
Refurbished	-	×	-	[-]
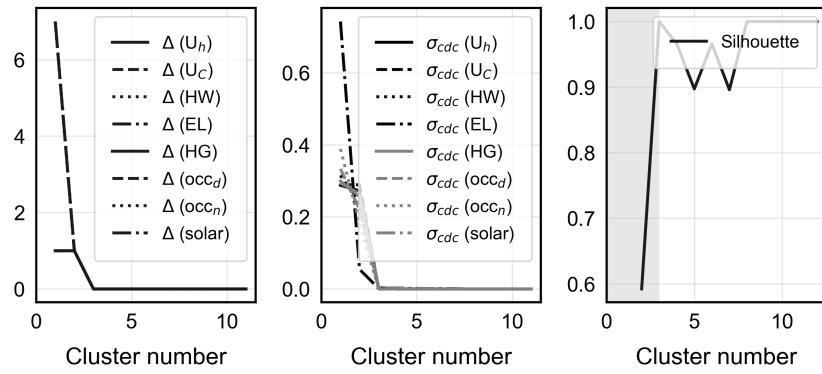
Figure C.3 – Quality indicators for a rural (reconfigured) community data reduction

Table C.6 – Attribute error for a rural (reconfigured) community data reduction

Attribute	Original value	Clustered value	dif. [%]	
U_h	12.6	12.5	0.77	[MW/K]
U_c	0.0	0.0	0.00	[MW/K]
EL	204.8	205.0	-0.11	[MWh/yr]
HW	178.0	178.2	-0.11	[MWh/yr]
HG	298.8	299.2	-0.11	[MWh/yr]
Solar	3864.3	3870.7	-0.17	[m^2]

Community demands

Figure C.4 represents the aggregated daily energy service profiles (EL and HW) of the rural and urban building communities studied in the respective chapter (Chapter 3). Following the service assessment approach implemented throughout this study, the chart values are based on the national architecture and engineering standards of Switzerland (SIA 2024 [65]).
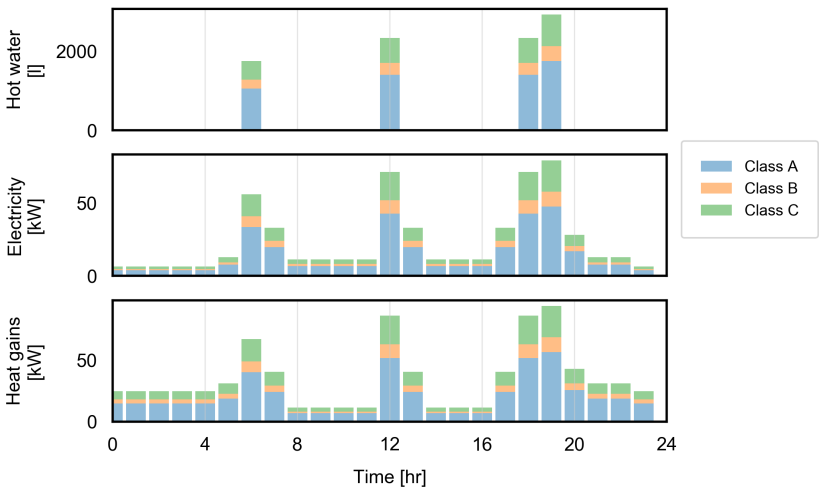
(a) Rural community
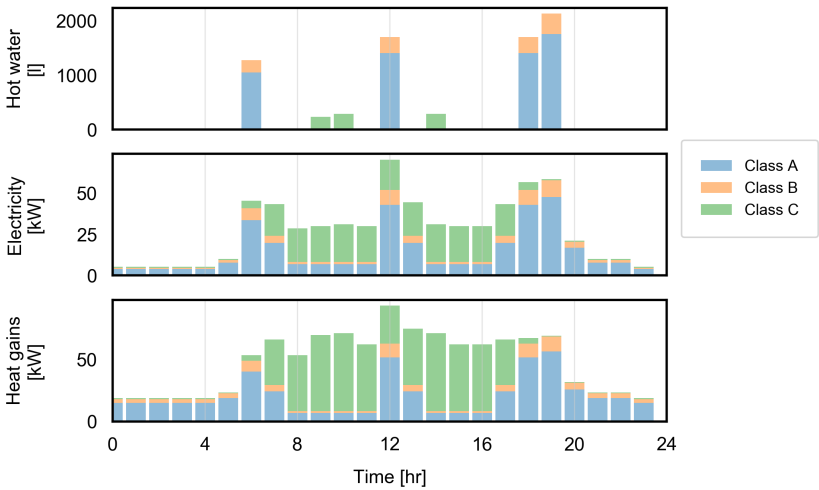
(b) Rural community (reconfigured)
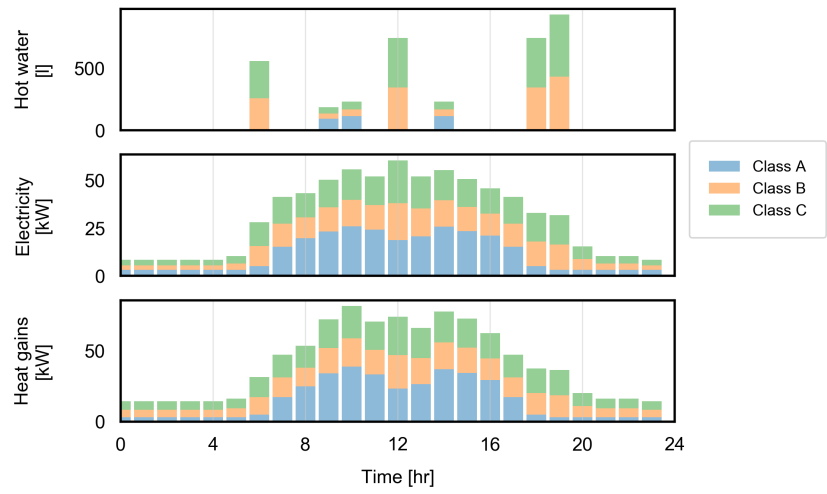
(c) Urban community

Figure C.4 – Aggregated daily energy service profiles for different building communities

Chapter 4: Request profiles and further results

Demand classification

Table D.2 details the representative tariff variation profiles $\Delta_{s,p}$ for each representative operating day p resulting from the data clustering process.

Additional parameters

Table D.1 reports specific investment costs values per BESS characteristic for different state-of-the-art storage technology types.

Table D.1 – State-of-the-art commercial BESS

Name	Power costs [kW/CHF]	Energy costs [kWh/CHF]	Ref.
Pumped-hydro[c]	500	500	[150]
Battery (S)[a]	2003	742	[151]
Battery (L)[b]	556	800	[140]

[a] Domestic battery stack (5 kVA/13.5 kWh)
[b] Industrial lithium-ion battery system (720 kVA/500 kWh)
[c] Lower bound on existing projects extension costs

Additional results

Figure D.1 displays the daily equivalent BESS characteristics for two BES configurations of an apartment block (AB) located in the climatic region of Geneva-Cointrin.
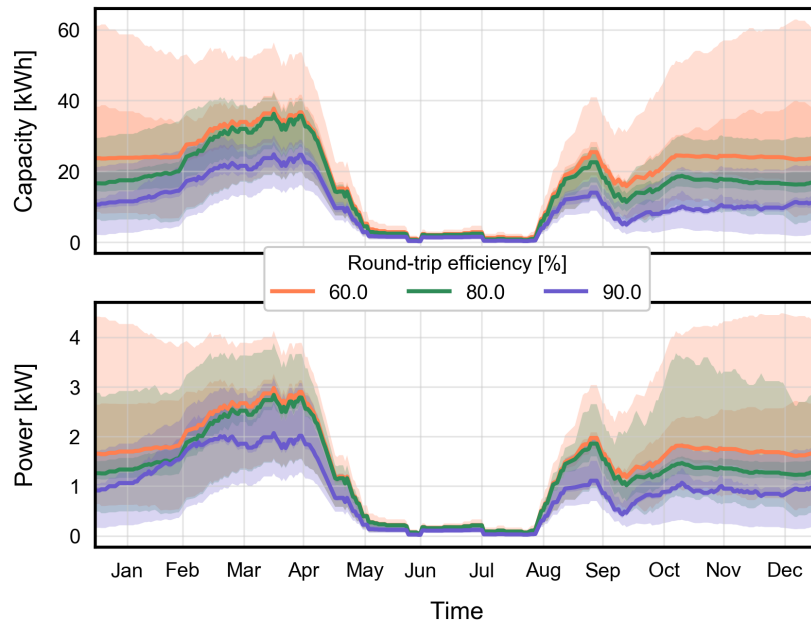
(a) System configuration *a*
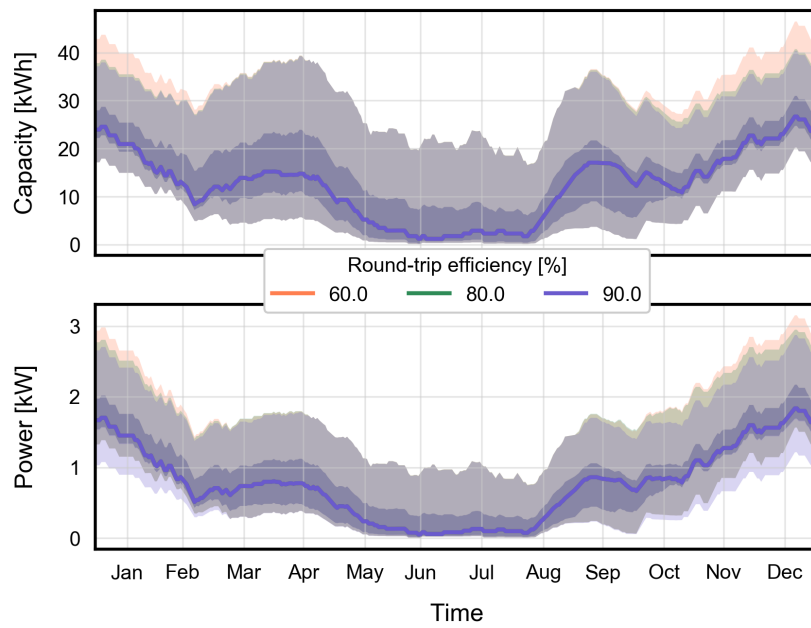
(b) System configuration *b*

Figure D.1 – Temporal equivalent BESS performance indicator distribution for an apartment block located in the climatic zone of Geneva

Table D.2 – Typical flexibility electricity tariff variation profiles

		1	2	3	4	5	6	7	8	9	10	11	12	13	14	15	16	17	18	19	20	21	22	23	24
														Hour											
Day 1	1	-0.17	-0.22	-0.29	-0.39	-0.40	-0.27	-0.15	0.07	0.14	0.17	0.18	0.18	0.18	0.14	0.11	0.07	0.04	0.08	0.13	0.14	0.10	0.09	0.10	0.00
	2	-0.23	-0.30	-0.41	-0.44	-0.45	-0.38	-0.06	0.16	0.21	0.23	0.22	0.23	0.15	0.15	0.14	0.09	0.06	0.09	0.15	0.28	0.15	0.02	0.03	-0.09
	3	-0.29	-0.42	-0.57	-0.57	-0.55	-0.51	-0.30	-0.15	0.12	0.67	0.55	0.68	0.41	0.32	0.51	0.28	0.23	0.13	0.05	-0.04	-0.10	-0.12	-0.09	-0.25
	4	-0.23	-0.29	-0.38	-0.44	-0.43	-0.26	-0.02	0.10	0.24	0.20	0.22	0.22	0.20	0.14	0.09	0.06	0.04	0.09	0.12	0.20	0.20	0.06	-0.01	-0.11
	5	-0.30	-0.36	-0.48	-0.50	-0.49	-0.32	-0.12	0.21	0.24	0.26	0.27	0.33	0.22	0.22	0.21	0.15	0.17	0.12	0.08	0.21	0.19	-0.01	-0.08	-0.23
	6	0.11	-0.03	-0.06	-0.10	-0.16	-0.17	-0.21	-0.20	-0.09	-0.11	-0.12	-0.06	-0.04	-0.11	-0.19	-0.22	-0.18	-0.01	0.18	0.31	0.36	0.45	0.43	0.25
	7	-0.21	-0.28	-0.37	-0.38	-0.39	-0.32	-0.07	0.20	0.26	0.24	0.23	0.18	0.15	0.11	0.10	0.06	0.04	0.09	0.11	0.18	0.09	0.05	0.08	-0.10
	8	-0.08	-0.17	-0.25	-0.23	-0.27	-0.26	-0.17	0.08	0.09	0.09	0.16	0.16	0.05	0.06	0.05	0.08	0.08	0.09	0.09	0.16	0.12	0.06	0.04	-0.02
	9	-0.45	-0.56	-0.60	-0.60	-0.67	-0.50	-0.37	-0.20	0.27	0.43	0.95	1.65	0.80	0.65	0.38	0.20	-0.05	-0.05	-0.05	-0.13	-0.18	-0.17	-0.30	-0.39
	10	0.05	-0.07	-0.15	-0.20	-0.25	-0.20	-0.08	-0.02	0.05	0.06	0.06	0.04	0.01	-0.04	-0.07	-0.06	-0.05	0.04	0.16	0.22	0.21	0.14	0.11	0.03
Day 2	1	-0.16	-0.21	-0.27	-0.31	-0.32	-0.26	0.04	0.10	0.11	0.10	0.08	0.07	0.04	0.05	0.05	0.08	0.09	0.22	0.19	0.14	0.08	0.05	0.03	0.00
	2	-0.53	-0.55	-0.55	-0.56	-0.58	-0.53	-0.53	-0.25	-0.17	0.77	0.33	0.67	0.25	-0.18	-0.28	-0.36	0.41	1.74	1.89	0.66	-0.36	-0.44	-0.42	-0.44
	3	0.03	-0.08	-0.20	-0.31	-0.36	-0.38	-0.21	-0.19	-0.03	0.03	0.04	0.06	0.05	-0.06	-0.15	-0.04	0.18	0.35	0.42	0.39	0.22	0.18	0.09	-0.03
	4	-0.31	-0.34	-0.40	-0.41	-0.42	-0.36	-0.08	0.09	0.17	0.18	0.16	0.15	0.11	0.11	0.15	0.17	0.20	0.26	0.25	0.18	0.15	0.08	-0.01	-0.09
	5	-0.10	-0.22	-0.28	-0.44	-0.48	-0.38	-0.05	0.08	0.12	0.15	0.15	0.17	0.15	0.10	0.08	0.07	0.12	0.17	0.23	0.16	0.06	0.05	0.05	0.02
	6	-0.41	-0.48	-0.51	-0.51	-0.51	-0.49	-0.34	0.12	0.19	0.16	0.15	0.16	0.08	0.06	-0.02	0.16	0.33	1.30	1.29	0.26	-0.09	-0.25	-0.30	-0.35
	7	-0.28	-0.46	-0.47	-0.62	-0.60	-0.28	-0.01	0.14	0.14	0.14	0.14	0.19	0.10	0.12	0.09	0.08	0.14	0.56	0.51	0.25	0.14	0.02	0.03	-0.05
	8	-0.20	-0.20	-0.33	-0.38	-0.44	-0.24	0.01	0.08	0.12	0.17	0.15	0.19	0.11	0.09	0.08	0.07	0.08	0.20	0.20	0.08	0.06	0.06	0.06	-0.02
	9	-0.61	-0.66	-0.77	-0.78	-0.78	-0.62	-0.49	-0.36	0.35	0.32	0.12	0.22	0.14	0.18	0.10	0.13	0.12	2.41	2.24	0.47	-0.26	-0.46	-0.50	-0.54
Day 3	1	-0.21	-0.29	-0.33	-0.39	-0.42	-0.33	-0.17	0.09	0.26	0.28	0.26	0.30	0.20	0.16	0.13	0.09	0.07	0.09	0.10	0.11	0.04	0.02	0.06	-0.11
	2	-0.18	-0.24	-0.31	-0.34	-0.34	-0.27	-0.09	0.12	0.21	0.19	0.15	0.19	0.09	0.05	0.01	0.01	-0.01	0.04	0.15	0.21	0.13	0.06	0.16	0.01
	3	0.08	-0.09	-0.19	-0.28	-0.32	-0.34	-0.16	-0.10	0.08	0.08	0.03	0.02	-0.13	-0.27	-0.33	-0.26	-0.16	0.09	0.35	0.40	0.40	0.42	0.41	0.27
	4	-0.51	-0.58	-0.61	-0.62	-0.62	-0.59	-0.44	-0.19	0.37	0.54	0.80	2.11	0.71	0.71	0.49	0.15	0.09	0.03	-0.01	-0.14	-0.37	-0.38	-0.44	-0.48
	5	-0.40	-0.51	-0.58	-0.66	-0.72	-0.52	-0.35	-0.14	0.14	0.44	0.70	1.16	0.53	0.57	0.47	0.31	0.15	0.11	0.06	-0.01	-0.14	-0.17	-0.16	-0.28
	6	-0.22	-0.30	-0.33	-0.38	-0.34	-0.24	-0.10	0.09	0.22	0.19	0.19	0.23	0.15	0.12	0.12	0.12	0.08	0.06	0.08	0.08	0.09	0.08	0.07	-0.05
Day 4	1	-0.02	-0.07	-0.15	-0.16	-0.17	-0.17	-0.10	-0.05	0.04	0.07	0.03	0.03	0.00	-0.03	0.01	0.03	0.07	0.12	0.12	0.11	0.09	0.09	0.09	0.01
	2	-0.23	-0.38	-0.48	-0.50	-0.50	-0.38	-0.07	0.12	0.25	0.25	0.18	0.21	0.05	0.05	0.11	0.14	0.18	0.20	0.27	0.26	0.23	0.08	0.08	-0.11
	3	-0.24	-0.28	-0.28	-0.08	-0.32	-0.21	0.05	0.07	0.10	0.11	0.12	0.14	0.10	0.07	0.07	0.06	0.06	0.05	0.22	0.23	0.05	0.05	0.05	0.01
	4	0.21	0.08	-0.04	-0.08	-0.16	-0.22	-0.30	-0.52	-0.21	-0.05	-0.04	0.05	0.03	-0.06	-0.30	-0.48	-0.49	0.05	0.34	0.42	0.44	0.43	0.46	0.44
	5	-0.14	-0.31	-0.46	-0.49	-0.48	-0.27	-0.03	0.13	0.15	0.20	0.20	0.20	0.11	0.12	0.12	0.15	0.14	0.14	0.19	0.19	0.20	0.11	-0.03	-0.15
	6	-0.31	-0.44	-0.52	-0.54	-0.53	-0.46	-0.20	0.15	0.21	0.21	0.21	0.27	0.19	0.21	0.20	0.17	0.21	0.41	0.38	0.35	0.08	0.03	-0.11	-0.08
	7	0.03	-0.09	-0.21	-0.25	-0.33	-0.27	-0.14	0.00	0.07	0.11	0.11	0.11	0.10	-0.02	0.03	0.03	0.03	0.05	0.16	0.21	0.18	0.12	0.03	-0.31
	8	-0.44	-0.56	-0.57	-0.56	-0.57	-0.44	-0.30	-0.20	0.00	0.10	0.15	0.19	0.06	0.01	-0.02	-0.02	0.89	1.34	1.26	0.54	-0.08	-0.19	-0.27	-0.31
Day 5	1	-0.29	-0.36	-0.45	-0.51	-0.54	-0.43	-0.26	-0.05	0.05	0.28	0.67	0.94	0.42	0.48	0.53	0.32	0.07	0.00	-0.05	-0.11	-0.10	-0.15	-0.15	-0.28
	2	-0.23	-0.32	-0.48	-0.54	-0.53	-0.42	-0.19	0.07	0.17	0.23	0.30	0.52	0.36	0.27	0.29	0.24	0.15	0.10	0.09	0.05	0.02	0.00	0.00	-0.12
	3	-0.08	-0.17	-0.29	-0.34	-0.35	-0.26	-0.11	0.03	0.13	0.07	0.07	0.11	0.04	0.05	0.00	-0.02	-0.02	0.05	0.14	0.22	0.20	0.20	0.22	0.10
	4	-0.13	-0.18	-0.24	-0.28	-0.30	-0.21	-0.11	0.07	0.14	0.15	0.18	0.21	0.17	0.15	0.11	0.07	0.07	0.07	0.00	0.07	0.03	0.00	-0.02	-0.12
	5	-0.40	-0.50	-0.56	-0.57	-0.67	-0.45	-0.35	-0.09	0.40	0.50	0.62	1.29	0.57	0.51	0.42	0.33	0.23	0.08	0.11	0.05	0.05	0.05	-0.03	-0.37
	6	-0.20	-0.34	-0.47	-0.59	-0.65	-0.44	-0.21	0.02	0.13	0.23	0.37	0.54	0.36	0.27	0.25	0.17	0.09	0.08	0.11	0.05	0.05	0.05	0.12	-0.01
	7	0.25	-0.02	-0.16	-0.21	-0.23	-0.31	-0.29	-0.28	-0.17	-0.01	-0.02	-0.02	-0.12	-0.24	-0.35	-0.38	-0.42	-0.02	0.37	0.44	0.54	0.52	0.69	0.44
	8	-0.21	-0.25	-0.32	-0.39	-0.43	-0.30	-0.13	0.09	0.18	0.18	0.18	0.23	0.14	0.15	0.13	0.10	0.07	0.10	0.12	0.12	0.12	0.07	0.07	-0.05
	9	-0.15	-0.22	-0.24	-0.25	-0.25	-0.22	-0.09	0.15	0.18	0.17	0.15	0.17	0.16	0.08	0.01	0.00	0.00	0.06	0.10	0.11	0.05	0.02	0.09	-0.07

Continued on next page

Appendix D. Chapter 4: Request profiles and further results

Table D.2 – continued from previous page

		Hour																							
		1	2	3	4	5	6	7	8	9	10	11	12	13	14	15	16	17	18	19	20	21	22	23	24
Day 6	1	-0.23	-0.37	-0.41	-0.43	-0.43	-0.33	-0.11	0.11	0.19	0.19	0.19	0.18	0.12	0.12	0.12	0.13	0.15	0.19	0.26	0.25	0.16	0.08	-0.03	-0.10
	2	-0.23	-0.32	-0.29	-0.35	-0.43	-0.35	-0.26	0.12	0.23	0.22	0.23	0.21	0.14	0.14	0.08	0.14	0.21	0.36	0.43	0.31	-0.03	-0.13	-0.19	-0.23
	3	-0.18	-0.32	-0.41	-0.45	-0.43	-0.24	-0.02	0.14	0.17	0.16	0.16	0.17	0.10	0.10	0.10	0.12	0.13	0.17	0.19	0.16	0.10	0.09	0.04	-0.03
	4	-0.17	-0.25	-0.36	-0.41	-0.48	-0.26	-0.06	0.06	0.13	0.18	0.16	0.17	0.05	0.03	0.05	0.11	0.19	0.28	0.36	0.19	0.08	0.04	0.01	-0.11
	5	0.00	-0.17	-0.21	-0.24	-0.25	-0.23	-0.09	-0.01	0.00	0.05	0.09	0.07	0.05	0.01	0.01	0.00	0.04	0.17	0.24	0.24	0.19	0.06	0.04	-0.04
	6	-0.12	-0.20	-0.24	-0.32	-0.35	-0.31	-0.32	-0.16	-0.10	0.03	0.11	0.17	0.16	0.05	-0.07	-0.07	0.08	0.35	0.39	0.33	0.19	0.10	0.14	0.14
	7	-0.47	-0.50	-0.52	-0.52	-0.52	-0.49	-0.43	-0.02	1.14	1.14	1.13	0.37	0.08	-0.28	-0.22	-0.07	0.28	0.47	0.73	0.29	-0.35	-0.42	-0.36	-0.44
	8	0.19	0.03	-0.16	-0.37	-0.55	-0.55	-0.40	-0.27	-0.27	-0.03	0.04	0.13	0.21	0.15	-0.11	-0.22	-0.18	0.37	0.46	0.55	0.43	0.20	0.20	0.15
	9	-0.70	-0.74	-0.76	-0.72	-0.71	-0.48	-0.38	-0.16	0.20	0.38	0.50	0.68	0.33	0.09	0.06	0.06	0.29	1.21	1.52	0.56	-0.20	-0.33	-0.35	-0.38
	10	-0.14	-0.14	-0.22	-0.26	-0.29	-0.18	-0.08	0.07	0.10	0.10	0.09	0.10	0.04	0.03	0.03	0.03	0.05	0.21	0.22	0.12	0.08	0.00	0.01	0.01
	11	-0.50	-0.50	-0.50	-0.50	-0.50	-0.50	-0.39	0.35	0.38	0.38	0.37	0.35	0.22	-0.11	0.21	0.36	0.42	0.48	0.42	0.74	0.03	-0.32	-0.40	-0.49
	12	0.00	-0.18	-0.36	-0.38	-0.43	-0.45	-0.42	-0.51	-0.33	-0.01	0.11	0.13	0.15	0.10	0.03	0.08	0.16	0.36	0.38	0.37	0.39	0.30	0.30	0.22
Day 7	1	-0.18	-0.22	-0.24	-0.29	-0.29	-0.22	-0.09	0.10	0.19	0.20	0.16	0.15	0.07	0.02	0.01	0.01	-0.05	0.00	0.08	0.18	0.22	0.14	0.09	-0.05
	2	0.06	0.01	-0.17	-0.27	-0.31	-0.25	-0.27	-0.06	0.02	0.17	0.16	0.14	0.14	-0.02	-0.18	-0.24	-0.27	-0.11	0.10	0.26	0.38	0.26	0.32	0.13
	3	-0.22	-0.29	-0.33	-0.36	-0.32	-0.22	-0.03	0.10	0.18	0.18	0.18	0.17	0.09	0.10	0.13	0.10	0.10	0.03	0.07	0.16	0.14	0.12	0.00	-0.06
	4	-0.24	-0.30	-0.37	-0.45	-0.45	-0.31	-0.03	0.19	0.30	0.29	0.29	0.25	0.13	0.09	0.10	0.04	0.02	0.01	0.06	0.13	0.19	0.05	0.03	0.00
	5	-0.27	-0.36	-0.51	-0.57	-0.53	-0.27	-0.08	0.12	0.20	0.22	0.22	0.22	0.16	0.16	0.16	0.15	0.17	0.12	0.13	0.20	0.22	0.19	0.05	-0.08
	6	-0.35	-0.43	-0.47	-0.49	-0.47	-0.37	-0.19	0.01	0.28	0.38	0.41	0.48	0.28	0.29	0.29	0.20	0.12	0.12	0.11	0.15	0.09	-0.05	-0.17	-0.23
	7	0.02	-0.06	-0.03	-0.03	-0.12	-0.12	-0.12	-0.13	-0.07	0.00	-0.02	-0.02	-0.08	-0.30	-0.43	-0.45	-0.35	-0.04	0.19	0.40	0.49	0.52	0.43	0.33
	8	-0.25	-0.30	-0.36	-0.39	-0.36	-0.25	-0.04	0.11	0.17	0.17	0.17	0.19	0.16	0.14	0.11	0.09	0.09	0.10	0.12	0.17	0.19	0.09	-0.01	-0.12
	9	0.02	-0.05	-0.12	-0.16	-0.20	-0.19	-0.11	-0.09	-0.03	0.09	0.09	0.09	0.11	0.04	-0.05	-0.06	-0.10	-0.01	0.08	0.13	0.27	0.13	0.13	0.01
	10	-0.19	-0.28	-0.31	-0.40	-0.39	-0.30	-0.02	0.14	0.26	0.24	0.22	0.16	0.10	0.10	0.08	0.03	0.02	0.05	0.09	0.21	0.15	0.03	0.03	-0.01
Day 8	1	0.04	-0.02	-0.07	-0.17	-0.22	-0.27	-0.25	-0.15	-0.10	-0.06	-0.07	-0.04	-0.01	0.00	-0.05	-0.07	-0.08	0.00	0.14	0.28	0.32	0.29	0.34	0.21
	2	-0.24	-0.36	-0.48	-0.59	-0.59	-0.47	-0.26	0.08	0.15	0.28	0.35	0.66	0.36	0.33	0.34	0.23	0.15	0.13	0.11	0.02	0.03	-0.03	0.00	-0.19
	3	-0.16	-0.26	-0.32	-0.35	-0.38	-0.28	-0.08	0.14	0.26	0.23	0.22	0.25	0.16	0.08	0.01	-0.04	0.00	0.04	0.10	0.16	0.08	0.04	0.10	0.00
	4	-0.17	-0.21	-0.26	-0.30	-0.32	-0.22	-0.16	0.03	0.12	0.15	0.16	0.18	0.16	0.14	0.13	0.11	0.08	0.08	0.12	0.11	0.05	0.03	0.04	-0.06
	5	-0.20	-0.28	-0.37	-0.43	-0.43	-0.28	-0.08	0.09	0.15	0.20	0.20	0.22	0.19	0.16	0.13	0.09	0.09	0.10	0.11	0.10	0.08	0.06	0.09	0.01
	6	-0.50	-0.59	-0.62	-0.67	-0.65	-0.51	-0.44	-0.09	0.29	0.41	0.74	1.52	0.76	0.76	0.45	0.31	0.11	0.07	-0.01	-0.10	-0.27	-0.27	-0.27	-0.42
	7	-0.31	-0.40	-0.48	-0.53	-0.54	-0.46	-0.31	-0.08	0.09	0.34	0.57	0.83	0.51	0.38	0.49	0.36	0.24	0.12	0.00	-0.07	-0.14	-0.21	-0.14	-0.26

In addition, Figures D.2 and D.3 show the daily equivalent BESS characteristics for a BES configuration of a rural (RUR) and urban (URB) community respectively located in the climatic region of Geneva-Cointrin.
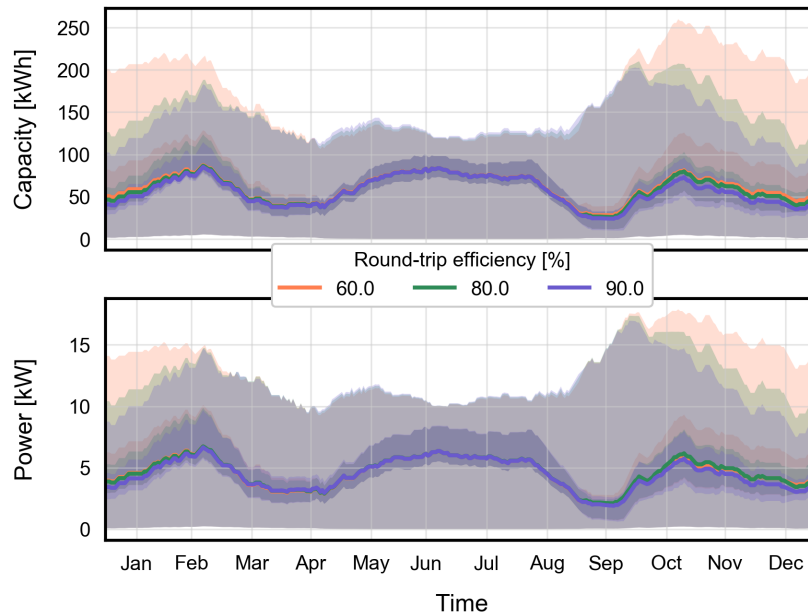

Figure D.2 – Temporal equivalent BESS performance indicator distribution for a rural building community located in the climatic zone of Geneva
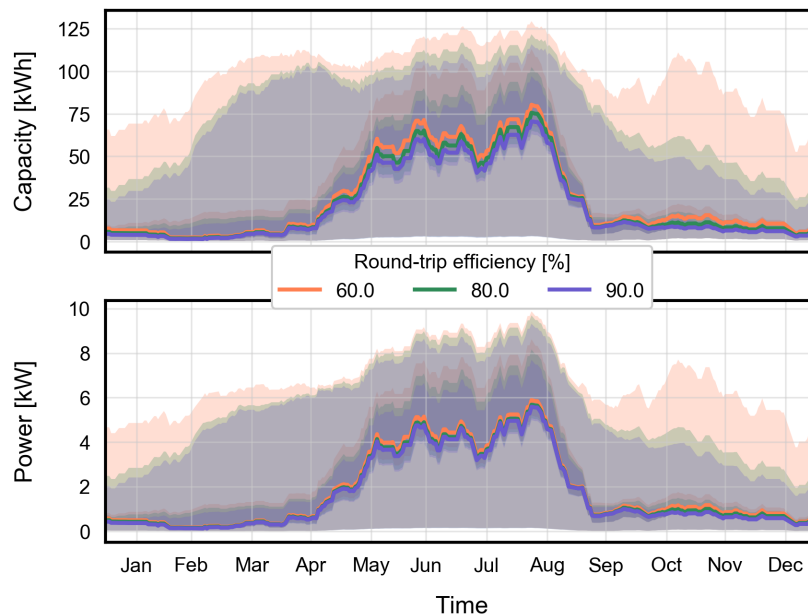

Figure D.3 – Temporal equivalent BESS performance indicator distribution for an urban building community located in the climatic zone of Geneva

Bibliography

[1] *Statistique globale suisse de l'énergie 2017*. Tech. rep. Bern, Switzerland: Bundesamt für Energie (BFE), July 2018. URL: 🔗.

[2] AEE Agence des énergies renouvelables et de l'efficacité énergétique. *Le tournant énergétique se réalise. Et nous y participons tous*. July 2013. URL: 🔗 (visited on 03/03/2019).

[3] *Climate Change 2014: Synthesis Report. Contribution of Working Groups I, II and III to the Fifth Assessment Report of the Intergovernmental Panel on Climate Change [Core Writing Team, R.K. Pachauri and L.A. Meyer (eds.)]* Tech. rep. Geneva, Switzerland: Intergovernmental Panel on Climate Change (IPCC), 2014. URL: 🔗.

[4] *Analyse des schweizerischen Energieverbrauchs 2000 - 2016 nach Verwendungszwecken*. Tech. rep. Bern, Switzerland: Bundesamt für Energie (BFE), Oct. 2017. URL: 🔗 (visited on 09/19/2018).

[5] Statistical Office of the European Communities. *Energy balance sheets: 2013 data*. Tech. rep. Luxembourg: Eurostat, 2015. URL: 🔗 (visited on 10/01/2018).

[6] Kesselring, P. and Winter, C. J. "World energy scenarios: a two-kilowatt society - plausible future or illusion". *Energy days 1994*. Villigen, Switzerland, Nov. 1994, pp. 103–116. URL: 🔗.

[7] *Contribution suisse à l'avenir énergétique: La recherche au Domaine des EPF*. 2008. URL: 🔗 (visited on 01/14/2019).

[8] Williams, Victoria and Noland, Robert B. "Comparing the CO2 emissions and contrail formation from short and long haul air traffic routes from London Heathrow". *Environmental Science & Policy* 9.5 (Aug. 2006), pp. 487–495. ISSN: 1462-9011. DOI: 10.1016/j.envsci.2005.10.004. URL: 🔗 (visited on 01/14/2019).

[9] *World Energy Balances 2018*. Paris, France: International Energy Agency (IEA), Sept. 2018. ISBN: 978-92-64-30156-6. URL: 🔗 (visited on 01/13/2019).

[10] *La stratégie énergétique 2050 après l'entrée en vigueur de la nouvelle loi sur l'énergie*. Jan. 2018. URL: 🔗 (visited on 01/14/2019).

[11] *Energy roadmap 2050*. 2012. URL: 🔗 (visited on 01/15/2019).

Bibliography

[12]   Marechal, François et al. "Energy in the perspective of the sustainable development: The 2000W society challenge". *Resources, Conservation and Recycling*. Sustainability and Renewable Resources 44.3 (June 2005), pp. 245–262. ISSN: 0921-3449. DOI: 10.1016/j.resconrec.2005.01.008. URL: ⬀.

[13]   Schulz, Thorsten F. et al. "Intermediate steps towards the 2000W society in Switzerland: An energy–economic scenario analysis". *Energy Policy* 36.4 (Apr. 2008), pp. 1303–1317. ISSN: 0301-4215. DOI: 10.1016/j.enpol.2007.12.006. URL: ⬀.

[14]   *Resource Flexibility*. Tech. rep. California Energy Commission, Dec. 2017. URL: ⬀ (visited on 05/10/2018).

[15]   *California ISO Open Access Same-time Information System (OASIS)*. URL: ⬀ (visited on 11/29/2019).

[16]   Burger, Bruno. *Power generation in Germany – assessment of 2017*. Freiburg, Germany, May 2018. URL: ⬀ (visited on 01/29/2019).

[17]   *Power System Flexibility for the Energy Transition: Part I - Overview for Policy Makers*. Tech. rep. Abu Dhabi: International Renewable Energy Agency (IRENA), Nov. 2018. URL: ⬀.

[18]   *ENTSO-E Transparency Platform*. URL: ⬀ (visited on 01/29/2019).

[19]   Sartori, Igor et al. "Net zero energy buildings: A consistent definition framework". *Energy and Buildings* 48 (2012), pp. 220–232. ISSN: 0378-7788. DOI: https://doi.org/10.1016/j.enbuild.2012.01.032. URL: ⬀.

[20]   Koller, M. et al. "Defining a degradation cost function for optimal control of a battery energy storage system". *2013 IEEE Grenoble Conference*. June 2013, pp. 1–6. DOI: 10.1109/PTC.2013.6652329.

[21]   Steffen, Bjarne. "Prospects for pumped-hydro storage in Germany". *Energy Policy* 45 (June 2012), pp. 420–429. ISSN: 0301-4215. DOI: 10.1016/j.enpol.2012.02.052. URL: ⬀.

[22]   Jentsch, Mareike et al. "Optimal Use of Power-to-Gas Energy Storage Systems in an 85% Renewable Energy Scenario". *Energy Procedia*. 8th International Renewable Energy Storage Conference and Exhibition (IRES 2013) 46 (Jan. 2014), pp. 254–261. ISSN: 1876-6102. DOI: 10.1016/j.egypro.2014.01.180. URL: ⬀.

[23]   O'Connell, Niamh et al. "Benefits and challenges of electrical demand response: A critical review". *Renewable and Sustainable Energy Reviews* 39 (Nov. 2014), pp. 686–699. ISSN: 1364-0321. DOI: 10.1016/j.rser.2014.07.098. URL: ⬀.

[24]   Morari, Manfred and H. Lee, Jay. "Model predictive control: past, present and future". *Computers & Chemical Engineering* 23.4 (May 1999), pp. 667–682. ISSN: 0098-1354. DOI: 10.1016/S0098-1354(98)00301-9. URL: ⬀ (visited on 02/25/2019).

[25]   Henze, Gregor P et al. "Experimental analysis of model-based predictive optimal control for active and passive building thermal storage inventory". *HVAC&R Research* 11.2 (2005), pp. 189–213.

[26]   Oldewurtel, F. et al. "Stochastic Model Predictive Control for Building Climate Control". *IEEE Transactions on Control Systems Technology* 22.3 (May 2014), pp. 1198–1205. ISSN: 1063-6536. DOI: 10.1109/TCST.2013.2272178.

[27]   Oldewurtel, F. et al. "Building control and storage management with dynamic tariffs for shaping demand response". *2011 2nd IEEE PES International Conference and Exhibition on Innovative Smart Grid Technologies.* Dec. 2011, pp. 1–8. DOI: 10.1109/ISGTEurope.2011.6162694.

[28]   Ashouri, Araz. "Simultaneous Design and Control of Energy Systems". Doctoral Thesis. ETH Zurich, 2014. DOI: 10.3929/ethz-a-010210627. URL: ☑ (visited on 01/14/2019).

[29]   SIA. *384/1 (2009): Installations de chauffage dans les bâtiments - Bases générales et performances requises.* Tech. rep. Zürich, Switzerland: Société suisse des ingénieurs et des architectes (SIA), Mar. 2009. URL: ☑.

[30]   SIA. *380/1 (2016): Besoins de chaleur pour le chauffage.* Tech. rep. Zürich, Switzerland: Société suisse des ingénieurs et des architectes (SIA), Dec. 2016. URL: ☑.

[31]   Girardin, Luc et al. "EnerGis: A geographical information based system for the evaluation of integrated energy conversion systems in urban areas". *Energy.* ECOS 2008 - 21st International Conference, on Efficiency, Cost, Optimization, Simulation and Environmental Impact of Energy Systems 35.2 (Feb. 2010), pp. 830–840. ISSN: 0360-5442. DOI: 10.1016/j.energy.2009.08.018. URL: ☑.

[32]   SIA. *2044 (2011): Bâtiments climatisés - Méthode de calcul standard pour la puissance requise et les besoins d'énergie.* Tech. rep. Zürich, Switzerland: Société suisse des ingénieurs et des architectes (SIA), Jan. 2011. URL: ☑.

[33]   SIA. *384/3 (2013): Installations de chauffage dans les bâtiments - Besoins en énergie.* Tech. rep. Zürich, Switzerland: Société suisse des ingénieurs et des architectes (SIA), Apr. 2013. URL: ☑.

[34]   SIA. *382/2 (2011): Bâtiments climatisés - Puissance requise et besoins d'énergie.* Tech. rep. Zürich, Switzerland: Société suisse des ingénieurs et des architectes (SIA), Jan. 2011. URL: ☑.

[35]   *Helion | Calculateur de devis.* URL: ☑ (visited on 02/07/2019).

[36]   *Wie viel Strom und Wärme kann mein Dach produzieren?* URL: ☑ (visited on 02/07/2019).

[37]   Bucher, Christof. *www.eigenverbrauchsrechner.ch Dokumentation.* URL: ☑ (visited on 02/24/2019).

[38]   Section Bâtiments et logements. *Registre fédéral des bâtiments et des logements - Catalogue des caractères Version 3.7.* Tech. rep. Neuchâtel: Office fédéral de la statistique (OFS), 2015. URL: ☑.

[39]   Stadler, Paul et al. "Model-based optimization of distributed and renewable energy systems in buildings". *Energy and Buildings* 120 (May 2016), pp. 103–113. ISSN: 0378-7788. DOI: 10.1016/j.enbuild.2016.03.051. URL: ☑.

[40] Merkel, Erik et al. "Modelling decentralised heat supply: An application and method-ological extension in TIMES". *Energy* 73 (Aug. 2014), pp. 592–605. ISSN: 0360-5442. DOI: 10.1016/j.energy.2014.06.060. URL: ⬀.

[41] Marnay, C. et al. "Optimal Technology Selection and Operation of Commercial-Building Microgrids". *IEEE Transactions on Power Systems* 23.3 (Aug. 2008), pp. 975–982. ISSN: 0885-8950. DOI: 10.1109/TPWRS.2008.922654.

[42] Crawley, Drury B. et al. "EnergyPlus: creating a new-generation building energy simulation program". *Energy and Buildings*. Special Issue: BUILDING SIMULATION'99 33.4 (Apr. 2001), pp. 319–331. ISSN: 0378-7788. DOI: 10.1016/S0378-7788(00)00114-6. URL: ⬀.

[43] Witzig, A. et al. "Simulation Tool for Architects". *CISBAT 2009 Proceedings, International Scientific Conference Renewables in a Changing Climate* (2009), pp. 677–682. URL: ⬀ (visited on 08/06/2018).

[44] Schütz, Thomas et al. "Optimal design of energy conversion units and envelopes for residential building retrofits using a comprehensive MILP model". *Applied Energy* 185.Part 1 (Jan. 2017), pp. 1–15. ISSN: 0306-2619. DOI: 10.1016/j.apenergy.2016.10.049. URL: ⬀.

[45] Bornatico, Raffaele et al. "Optimal sizing of a solar thermal building installation using particle swarm optimization". *Energy*. 23rd International Conference on Efficiency, Cost, Optimization, Simulation and Environmental Impact of Energy Systems, ECOS 2010 41.1 (May 2012), pp. 31–37. ISSN: 0360-5442. DOI: 10.1016/j.energy.2011.05.026. URL: ⬀.

[46] Weber, Céline et al. "Optimization of an SOFC-based decentralized polygeneration system for providing energy services in an office-building in Tōkyō". *Applied Thermal Engineering*. Process Integration, modelling and optimisation for energy saving and pollution reduction - PRES 2004 26.13 (Sept. 2006), pp. 1409–1419. ISSN: 1359-4311. DOI: 10.1016/j.applthermaleng.2005.05.031. URL: ⬀.

[47] Fazlollahi, Samira et al. "Methods for multi-objective investment and operating optimization of complex energy systems". *Energy*. The 24th International Conference on Efficiency, Cost, Optimization, Simulation and Environmental Impact of Energy, ECOS 2011 45.1 (Sept. 2012), pp. 12–22. ISSN: 0360-5442. DOI: 10.1016/j.energy.2012.02.046. URL: ⬀.

[48] Menon, Ramanunni P. et al. "Study of optimal design of polygeneration systems in optimal control strategies". *Energy* 55 (June 2013), pp. 134–141. ISSN: 0360-5442. DOI: 10.1016/j.energy.2013.03.070. URL: ⬀.

[49] Fux, Samuel F. et al. "Economic and environmental aspects of the component sizing for a stand-alone building energy system: A case study". *Renewable Energy* 55 (July 2013), pp. 438–447. ISSN: 0960-1481. DOI: 10.1016/j.renene.2012.12.034. URL: ⬀.

[50] Evins, Ralph. "A bi-level design and operation optimization process applied to an energy centre". *Journal of Building Performance Simulation* 9.3 (May 2016), pp. 255–271. ISSN: 1940-1493. DOI: 10.1080/19401493.2015.1045034. URL: ☑.

[51] Geidl, M. and Andersson, G. "A modeling and optimization approach for multiple energy carrier power flow". *2005 IEEE Russia Power Tech.* June 2005, pp. 1–7. DOI: 10.1109/PTC.2005.4524640.

[52] Bemporad, Alberto and Morari, Manfred. "Control of systems integrating logic, dynamics, and constraints". *Automatica* 35.3 (Mar. 1999), pp. 407–427. ISSN: 0005-1098. DOI: 10.1016/S0005-1098(98)00178-2. URL: ☑.

[53] Grossmann, Ignacio E. "Advances in mathematical programming models for enterprise-wide optimization". *Computers & Chemical Engineering.* FOCAPO 2012 47 (Dec. 2012), pp. 2–18. ISSN: 0098-1354. DOI: 10.1016/j.compchemeng.2012.06.038. URL: ☑.

[54] Ashouri, Araz et al. "Optimal design and operation of building services using mixed-integer linear programming techniques". *Energy* 59 (Sept. 2013), pp. 365–376. ISSN: 0360-5442. DOI: 10.1016/j.energy.2013.06.053. URL: ☑ (visited on 06/02/2017).

[55] Ashouri, Araz et al. "Sensitivity analysis for robust design of building energy systems". *Energy* 76 (Nov. 2014), pp. 264–275. ISSN: 0360-5442. DOI: 10.1016/j.energy.2014.07.095. URL: ☑.

[56] Steen, David et al. "Modeling of thermal storage systems in MILP distributed energy resource models". *Applied Energy* 137 (Jan. 2015), pp. 782–792. ISSN: 0306-2619. DOI: 10.1016/j.apenergy.2014.07.036. URL: ☑.

[57] Schütz, Thomas et al. "Optimal design of energy conversion units for residential buildings considering German market conditions". *Energy* 139 (Nov. 2017), pp. 895–915. ISSN: 0360-5442. DOI: 10.1016/j.energy.2017.08.024. URL: ☑.

[58] Fazlollahi, Samira et al. "A solid thermal storage model for the optimization of buildings operation strategy". *Energy* 88 (Aug. 2015), pp. 209–222. ISSN: 0360-5442. DOI: 10.1016/j.energy.2015.04.085. URL: ☑.

[59] Rager, Jakob Moritz Fabian. "Urban Energy System Design from the Heat Perspective using mathematical Programming including thermal Storage". PhD thesis. Lausanne: EPFL, 2015. DOI: 10.5075/epfl-thesis-6731.

[60] Wakui, Tetsuya and Yokoyama, Ryohei. "Optimal structural design of residential cogeneration systems with battery based on improved solution method for mixed-integer linear programming". *Energy* 84.Supplement C (May 2015), pp. 106–120. ISSN: 0360-5442. DOI: 10.1016/j.energy.2015.02.056. URL: ☑.

[61] Kayo, Genku and Ooka, Ryozo. "Building energy system optimizations with utilization of waste heat from cogenerations by means of genetic algorithm". *Energy and Buildings* 42.7 (July 2010), pp. 985–991. ISSN: 0378-7788. DOI: 10.1016/j.enbuild.2010.01.010. URL: ☑.

[62] Lauinger, D. et al. "A linear programming approach to the optimization of residential energy systems". *Journal of Energy Storage* 7 (Aug. 2016), pp. 24–37. ISSN: 2352-152X. DOI: 10.1016/j.est.2016.04.009. URL: ⤤ (visited on 03/05/2019).

[63] Wu, Raphael et al. "Multiobjective optimisation of energy systems and building envelope retrofit in a residential community". *Applied Energy* 190 (Mar. 2017), pp. 634–649. ISSN: 0306-2619. DOI: 10.1016/j.apenergy.2016.12.161. URL: ⤤ (visited on 03/20/2019).

[64] Maréchal, François and Kalitventzeff, Boris. "Process integration: Selection of the optimal utility system". *Computers & Chemical Engineering*. European Symposium on Computer Aided Process Engineering-8 22 (Mar. 1998), S149–S156. ISSN: 0098-1354. DOI: 10.1016/S0098-1354(98)00049-0. URL: ⤤ (visited on 03/20/2019).

[65] SIA. *2024 (2015): Données d'utilisation des locaux pour l'énergie et les installations du bâtiment.* Tech. rep. Zürich, Switzerland: Société suisse des ingénieurs et des architectes (SIA), Oct. 2015. URL: ⤤.

[66] SIA. *2028 (2008): Données climatiques pour la physique du bâtiment, l'énergie et les installations du bâtiment.* Tech. rep. Zürich, Switzerland: Société suisse des ingénieurs et des architectes (SIA), Jan. 2008. URL: ⤤.

[67] Fazlollahi, Samira et al. "Multi-objectives, multi-period optimization of district energy systems: I. Selection of typical operating periods". *Computers & Chemical Engineering* 65 (2014), pp. 54–66. URL: ⤤.

[68] Duffie, John A. and Beckman, William A. "Design of Photovoltaic Systems". *Solar Engineering of Thermal Processes.* John Wiley & Sons, Inc., 2013, pp. 745–773. ISBN: 978-1-118-67160-3. DOI: 10.1002/9781118671603.ch23. URL: ⤤.

[69] Fischer, David et al. "Model for electric load profiles with high time resolution for German households". *Energy and Buildings* 92 (Apr. 2015), pp. 170–179. ISSN: 0378-7788. DOI: 10.1016/j.enbuild.2015.01.058. URL: ⤤ (visited on 05/08/2019).

[70] Domínguez-Muñoz, Fernando et al. "Selection of typical demand days for CHP optimization". *Energy and Buildings* 43.11 (Nov. 2011), pp. 3036–3043. ISSN: 0378-7788. DOI: 10.1016/j.enbuild.2011.07.024. URL: ⤤.

[71] Kaufman, Leonard and Rousseeuw, Peter J. *Finding Groups in Data: An Introduction to Cluster Analysis.* John Wiley & Sons, Sept. 2009. ISBN: 978-0-470-31748-8.

[72] Borel, Lucien and Favrat, Daniel. *Thermodynamics and Energy Systems Analysis: From Energy to Exergy.* EPFL Press, June 2010. ISBN: 978-1-4398-3516-6.

[73] Bolliger, Raffaele. "Méthodologie de la synthèse des systèmes énergétiques industriels". PhD thesis. Lausanne, Switzerland: EPFL, 2010.

[74] Fux, Samuel F. et al. "EKF based self-adaptive thermal model for a passive house". *Energy and Buildings* 68, Part C (Jan. 2014), pp. 811–817. ISSN: 0378-7788. DOI: 10.1016/j.enbuild.2012.06.016. URL: ⤤ (visited on 06/02/2017).

[75]   Baeten, Brecht et al. "Reduction of heat pump induced peak electricity use and required generation capacity through thermal energy storage and demand response". *Applied Energy* 195 (June 2017), pp. 184–195. ISSN: 0306-2619. DOI: 10.1016/j.apenergy.2017.03.055. URL: [↗].

[76]   Turton, Richard et al. *Analysis, Synthesis and Design of Chemical Processes*. Pearson Education, Dec. 2008. ISBN: 978-0-13-245918-1.

[77]   Luthander, Rasmus et al. "Photovoltaic self-consumption in buildings: A review". *Applied Energy* 142 (Mar. 2015), pp. 80–94. ISSN: 0306-2619. DOI: 10.1016/j.apenergy.2014.12.028. URL: [↗].

[78]   De Coninck, Roel et al. "Modelling and simulation of a grid connected photovoltaic heat pump system with thermal energy storage using Modelica". *8th International Conference on System Simulation in Buildings*. Vol. 2010. 2010, pp. 1–21.

[79]   Verbruggen, B. and Driesen, J. "Grid Impact Indicators for Active Building Simulations". *IEEE Transactions on Sustainable Energy* 6.1 (Jan. 2015), pp. 43–50. ISSN: 1949-3029. DOI: 10.1109/TSTE.2014.2357475.

[80]   Mavrotas, George. "Effective implementation of the epsilon-constraint method in Multi-Objective Mathematical Programming problems". *Applied Mathematics and Computation* 213.2 (July 2009), pp. 455–465. ISSN: 0096-3003. DOI: 10.1016/j.amc.2009.03.037. URL: [↗].

[81]   Girardin, Luc. "A GIS-based Methodology for the Evaluation of Integrated Energy Systems in Urban Area". PhD thesis. Lausanne: EPFL, 2012. DOI: 10.5075/epfl-thesis-5287.

[82]   *Leclanché - Titanate industrial storage solution*. URL: [↗] (visited on 01/31/2019).

[83]   Moret, Stefano et al. "Robust Optimization for Strategic Energy Planning". *Informatica* 27.3 (Jan. 2016), pp. 625–648. ISSN: 0868-4952. URL: [↗] (visited on 05/22/2019).

[84]   Oldewurtel, Frauke et al. "Use of model predictive control and weather forecasts for energy efficient building climate control". *Energy and Buildings* 45 (Feb. 2012), pp. 15–27. ISSN: 0378-7788. DOI: 10.1016/j.enbuild.2011.09.022. URL: [↗] (visited on 05/22/2019).

[85]   Coninck, R. De et al. "Rule-based demand-side management of domestic hot water production with heat pumps in zero energy neighbourhoods". *Journal of Building Performance Simulation* 7.4 (July 2014), pp. 271–288. ISSN: 1940-1493. DOI: 10.1080/19401493.2013.801518. URL: [↗].

[86]   Bucher, Christof. "Analysis and Simulation of Distribution Grids with Photovoltaics". Doctoral Thesis. ETH Zurich, 2014. DOI: 10.3929/ethz-a-010204387. URL: [↗] (visited on 02/01/2019).

[87]   *Energyscope wiki*. URL: [↗] (visited on 03/04/2019).

[88] Stadler, Paul et al. "The Swiss Potential of Model Predictive Control for Building Energy Systems". *2017 7th IEEE PES International Conference and Exhibition on Innovative Smart Grid Technologies, Europe*. Turino, Italy, Sept. 2017.

[89] Stadler, Paul et al. "Contribution of model predictive control in the integration of renewable energy sources within the built environment". *Frontiers in Energy Research* 6 (2018). ISSN: 2296-598X. DOI: 10.3389/fenrg.2018.00022. URL: ☑ (visited on 03/20/2018).

[90] Heiple, Shem and Sailor, David J. "Using building energy simulation and geospatial modeling techniques to determine high resolution building sector energy consumption profiles". *Energy and Buildings* 40.8 (Jan. 2008), pp. 1426–1436. ISSN: 0378-7788. DOI: 10.1016/j.enbuild.2008.01.005. URL: ☑.

[91] Dascalaki, Elena G. et al. "Building typologies as a tool for assessing the energy performance of residential buildings – A case study for the Hellenic building stock". *Energy and Buildings* 43.12 (2011), pp. 3400–3409. ISSN: 0378-7788. DOI: https://doi.org/10.1016/j.enbuild.2011.09.002. URL: ☑.

[92] Ren, Hongbo et al. "Optimal option of distributed energy systems for building complexes in different climate zones in China". *Applied Energy* 91.1 (2012), pp. 156–165. ISSN: 0306-2619. DOI: https://doi.org/10.1016/j.apenergy.2011.08.044. URL: ☑.

[93] Lund, H. and Münster, E. "Modelling of energy systems with a high percentage of CHP and wind power". *Renewable Energy* 28.14 (2003), pp. 2179–2193. ISSN: 0960-1481. DOI: https://doi.org/10.1016/S0960-1481(03)00125-3. URL: ☑.

[94] Codina Gironès, Victor et al. "Strategic energy planning for large-scale energy systems: A modelling framework to aid decision-making". *Energy* 90.Part 1 (Oct. 2015), pp. 173–186. ISSN: 0360-5442. DOI: 10.1016/j.energy.2015.06.008. URL: ☑.

[95] Pensini, Alessandro et al. "Economic analysis of using excess renewable electricity to displace heating fuels". *Applied Energy* 131 (2014), pp. 530–543. ISSN: 0306-2619. DOI: https://doi.org/10.1016/j.apenergy.2014.04.111. URL: ☑.

[96] Schütz, Thomas et al. "Clustering algorithms for the selection of typical demand days for the optimal design of building energy systems". *Proceedings of ECOS 2016 - 29th International conference on efficiency, cost, optimization, simulation and environmental impact of energy systems*. Solvenia, June 2016.

[97] *Heating degree days - Trend in heating degree days in the EU-27*. Tech. rep. Denmark: European Environment Agency, 2012. URL: ☑ (visited on 12/01/2016).

[98] Shepard, Donald. "A Two-dimensional Interpolation Function for Irregularly-spaced Data". *Proceedings of the 1968 23rd ACM National Conference*. ACM '68. New York, NY, USA: ACM, 1968, pp. 517–524. DOI: 10.1145/800186.810616. URL: ☑.

[99] Lefèvre, Mireille et al. "Study of effective distances for interpolation schemes in meteorology". *European Geophysical Society, 27th General Assembly*. Nice, France: European Geophysical Society, Apr. 2002.

[100] Prognos AG et al. *Analyse des schweizerischen Energieverbrauchs 2000 - 2015 nach Verwendungszwecken*. Tech. rep. Bundesamt für Energie BFE, Oct. 2016. URL: ⬀ (visited on 10/01/2018).

[101] Burg, Vanessa et al. "Analyzing the potential of domestic biomass resources for the energy transition in Switzerland". *Biomass and Bioenergy* 111 (2018), pp. 60–69. ISSN: 0961-9534. DOI: https://doi.org/10.1016/j.biombioe.2018.02.007. URL: ⬀.

[102] Desthieux, Gilles et al. *Cadastre solaire du caton de Genève – Phase 2 : Analyse du potentiel de production énergétique par les panneaux solaires thermique et PV*. Tech. rep. Geneva, Switzerland: HEPIA, Oct. 2014. URL: ⬀ (visited on 11/27/2018).

[103] Klauser, Daniel. *Solarpotentialanalyse für Sonnendach.ch - Schlussbericht*. Tech. rep. Bern, Switzerland: Bundesamt für Energie (BFE), Feb. 2016. URL: ⬀ (visited on 11/23/2018).

[104] SIA. *2040 (2017): La voie SIA vers l'efficacité énergétique*. Tech. rep. Zürich, Switzerland: Société suisse des ingénieurs et des architectes (SIA), May 2017. URL: ⬀.

[105] Schlecht, Ingmar and Weigt, Hannes. *Swissmod - A Model of the Swiss Electricity Market*. SSRN Scholarly Paper ID 2446807. Rochester, NY: Social Science Research Network, June 2014. URL: ⬀ (visited on 05/09/2019).

[106] Borghetti, A. et al. "Short-Term Scheduling and Control of Active Distribution Systems With High Penetration of Renewable Resources". *IEEE Systems Journal* 4.3 (Sept. 2010), pp. 313–322. ISSN: 1932-8184. DOI: 10.1109/JSYST.2010.2059171.

[107] Mehleri, Eugenia D. et al. "A mathematical programming approach for optimal design of distributed energy systems at the neighbourhood level". *Energy*. Integration and Energy System Engineering, European Symposium on Computer-Aided Process Engineering 2011 44.1 (Aug. 2012), pp. 96–104. ISSN: 0360-5442. DOI: 10.1016/j.energy.2012.02.009. URL: ⬀.

[108] Omu, Akomeno et al. "Distributed energy resource system optimisation using mixed integer linear programming". *Energy Policy* 61 (Oct. 2013), pp. 249–266. ISSN: 0301-4215. DOI: 10.1016/j.enpol.2013.05.009. URL: ⬀.

[109] Yang, Yun et al. "Optimal design of distributed energy resource systems coupled with energy distribution networks". *Energy* 85 (2015), pp. 433–448. ISSN: 0360-5442. DOI: https://doi.org/10.1016/j.energy.2015.03.101. URL: ⬀.

[110] Orehounig, Kristina et al. "Integration of decentralized energy systems in neighbourhoods using the energy hub approach". *Applied Energy* 154 (Sept. 2015), pp. 277–289. ISSN: 0306-2619. DOI: 10.1016/j.apenergy.2015.04.114. URL: ⬀.

[111] Ondeck, Abigail D. et al. "Optimal operation of a residential district-level combined photovoltaic/natural gas power and cooling system". *Applied Energy* 156 (Oct. 2015), pp. 593–606. ISSN: 0306-2619. DOI: 10.1016/j.apenergy.2015.06.045. URL: ⬀ (visited on 11/05/2018).

[112] Morvaj, Boran et al. "Optimization framework for distributed energy systems with integrated electrical grid constraints". *Applied Energy* 171.Supplement C (June 2016), pp. 296–313. ISSN: 0306-2619. DOI: 10.1016/j.apenergy.2016.03.090. URL: [↗].

[113] Schütz, Thomas et al. "Optimal design of decentralized energy conversion systems for smart microgrids using decomposition methods". *Energy* 156 (Aug. 2018), pp. 250–263. ISSN: 0360-5442. DOI: 10.1016/j.energy.2018.05.050. URL: [↗].

[114] Harb, Hassan et al. "Decentralized scheduling strategy of heating systems for balancing the residual load". *Building and Environment* 86 (Apr. 2015), pp. 132–140. ISSN: 0360-1323. DOI: 10.1016/j.buildenv.2014.12.015. URL: [↗].

[115] Gabrielli, Paolo et al. "Optimal design of multi-energy systems with seasonal storage". *Applied Energy* 219 (June 2018), pp. 408–424. ISSN: 0306-2619. DOI: 10.1016/j.apenergy.2017.07.142. URL: [↗].

[116] Nick, M. et al. "Optimal Planning of Distributed Energy Storage Systems in Active Distribution Networks Embedding Grid Reconfiguration". *IEEE Transactions on Power Systems* PP.99 (2017), pp. 1–1. ISSN: 0885-8950. DOI: 10.1109/TPWRS.2017.2734942.

[117] Kefayat, M. et al. "A hybrid of ant colony optimization and artificial bee colony algorithm for probabilistic optimal placement and sizing of distributed energy resources". *Energy Conversion and Management* 92 (Mar. 2015), pp. 149–161. ISSN: 0196-8904. DOI: 10.1016/j.enconman.2014.12.037. URL: [↗].

[118] Sossan, F. et al. "Large scale deployment of PV units in existing distribution networks: Optimization of the installation layout". *2016 Power Systems Computation Conference (PSCC)*. June 2016, pp. 1–6. DOI: 10.1109/PSCC.2016.7541023.

[119] Halu, Arda et al. "Data-driven modeling of solar-powered urban microgrids". *Science Advances* 2.1 (Jan. 2016), e1500700. ISSN: 2375-2548. DOI: 10.1126/sciadv.1500700. URL: [↗] (visited on 04/18/2018).

[120] Harb, Hassan et al. "MIP approach for designing heating systems in residential buildings and neighbourhoods". *Journal of Building Performance Simulation* 9.3 (May 2016), pp. 316–330. ISSN: 1940-1493. DOI: 10.1080/19401493.2015.1051113. URL: [↗].

[121] Weber, C. and Shah, N. "Optimisation based design of a district energy system for an eco-town in the United Kingdom". *Energy* 36.2 (Feb. 2011), pp. 1292–1308. ISSN: 0360-5442. DOI: 10.1016/j.energy.2010.11.014. URL: [↗] (visited on 02/15/2019).

[122] Schiefelbein, Jan et al. "Design of an optimization algorithm for the distribution of thermal energy systems and local heating networks within a city district". *Proceedings of ECOS*. 2015.

[123] Fux, Samuel F. "Optimal energy management and component sizing of a stand-alone building energy system". Doctoral Thesis. ETH Zurich, 2013. DOI: 10.3929/ethz-a-009928622. URL: [↗] (visited on 01/14/2019).

[124] Voll, Philip et al. "The optimum is not enough: A near-optimal solution paradigm for energy systems synthesis". *Energy* 82 (Mar. 2015), pp. 446–456. ISSN: 0360-5442. DOI: 10.1016/j.energy.2015.01.055. URL: ⬀ (visited on 03/11/2019).

[125] Ondeck, Abigail et al. "A multi-scale framework for simultaneous optimization of the design and operating strategy of residential CHP systems". *Applied Energy* 205 (Nov. 2017), pp. 1495–1511. ISSN: 0306-2619. DOI: 10.1016/j.apenergy.2017.08.082. URL: ⬀ (visited on 03/13/2019).

[126] Nick, M. et al. "Optimal Planning of Distributed Energy Storage Systems in Active Distribution Networks Embedding Grid Reconfiguration". *IEEE Transactions on Power Systems* 33.2 (Mar. 2018), pp. 1577–1590. ISSN: 0885-8950. DOI: 10.1109/TPWRS.2017.2734942.

[127] Chinese, Damiana. "Optimal size and layout planning for district heating and cooling networks with distributed generation options". *International Journal of Energy Sector Management* 2.3 (2008), p. 385.

[128] Henchoz, Samuel et al. "Performance and profitability perspectives of a CO2 based district energy network in Geneva's City Centre". *Energy* 85 (June 2015), pp. 221–235. ISSN: 0360-5442. DOI: 10.1016/j.energy.2015.03.079. URL: ⬀.

[129] Deml, S. et al. "The role of aggregation in power system simulation". *2015 IEEE Eindhoven PowerTech*. June 2015, pp. 1–6. DOI: 10.1109/PTC.2015.7232755.

[130] Oldewurtel, F. et al. "Towards a standardized building assessment for demand response". *52nd IEEE Conference on Decision and Control*. Dec. 2013, pp. 7083–7088. DOI: 10.1109/CDC.2013.6761012.

[131] Ulbig, Andreas and Andersson, Göran. "Analyzing operational flexibility of electric power systems". *International Journal of Electrical Power & Energy Systems*. The Special Issue for 18th Power Systems Computation Conference. 72.Supplement C (Nov. 2015), pp. 155–164. ISSN: 0142-0615. DOI: 10.1016/j.ijepes.2015.02.028. URL: ⬀.

[132] Heussen, K. et al. "Energy storage in power system operation: The power nodes modeling framework". *2010 IEEE PES Innovative Smart Grid Technologies Conference Europe (ISGT Europe)*. Oct. 2010, pp. 1–8. DOI: 10.1109/ISGTEUROPE.2010.5638865.

[133] Heussen, K. et al. "Unified System-Level Modeling of Intermittent Renewable Energy Sources and Energy Storage for Power System Operation". *IEEE Systems Journal* 6.1 (Mar. 2012), pp. 140–151. ISSN: 1932-8184. DOI: 10.1109/JSYST.2011.2163020.

[134] Namor, E. et al. "Control of Battery Storage Systems for the Simultaneous Provision of Multiple Services". *IEEE Transactions on Smart Grid* (2018), pp. 1–1. ISSN: 1949-3053. DOI: 10.1109/TSG.2018.2810781.

[135] *Power System Flexibility for the Energy Transition: Part II - IRENA FLEXTOOL Methodology*. Tech. rep. Abu Dhabi: International Renewable Energy Agency (IRENA), Nov. 2018. URL: ⬀.

Bibliography

[136] Sturzenegger, David et al. "Model Predictive Control of a Swiss Office Building". *Clima 2013 : 11th REHVA World Congress and 8th International Conference "Energy Efficient, Smart and Healthy Buildings"*. Prague, Czech Republic, June 2013, pp. 3227–3236.

[137] De Coninck, Roel and Helsen, Lieve. "Practical implementation and evaluation of model predictive control for an office building in Brussels". *Energy and Buildings* 111 (Jan. 2016), pp. 290–298. ISSN: 0378-7788. DOI: 10.1016/j.enbuild.2015.11.014. URL: ⬏.

[138] Blum, D. H. et al. "Opportunity Cost Quantification for Ancillary Services Provided by Heating, Ventilating, and Air-Conditioning Systems". *IEEE Transactions on Smart Grid* 8.3 (May 2017), pp. 1264–1273. ISSN: 1949-3053. DOI: 10.1109/TSG.2016.2582207.

[139] Good, N. et al. "Optimization Under Uncertainty of Thermal Storage-Based Flexible Demand Response With Quantification of Residential Users #x2019; Discomfort". *IEEE Transactions on Smart Grid* 6.5 (Sept. 2015), pp. 2333–2342. ISSN: 1949-3053. DOI: 10.1109/TSG.2015.2399974.

[140] Sossan, Fabrizio. "Equivalent electricity storage capacity of domestic thermostatically controlled loads". *Energy* 122 (Mar. 2017), pp. 767–778. ISSN: 0360-5442. DOI: 10.1016/j.energy.2016.12.096. URL: ⬏.

[141] Stinner, Sebastian et al. "Quantifying the operational flexibility of building energy systems with thermal energy storages". *Applied Energy* 181 (Nov. 2016), pp. 140–154. ISSN: 0306-2619. DOI: 10.1016/j.apenergy.2016.08.055. URL: ⬏.

[142] Lutz, O. et al. "Dynamic tariff design for a robust smart grid concept: An analysis of global vs. local incentives". *2017 IEEE PES Innovative Smart Grid Technologies Conference Europe (ISGT-Europe)*. Sept. 2017, pp. 1–6. DOI: 10.1109/ISGTEurope.2017.8260143.

[143] Pertsinidis, A. et al. "Parametric optimization of MILP programs and a framework for the parametric optimization of MINLPs". *Computers & Chemical Engineering*. European Symposium on Computer Aided Process Engineering-8 22 (Mar. 1998), S205–S212. ISSN: 0098-1354. DOI: 10.1016/S0098-1354(98)00056-8. URL: ⬏ (visited on 03/18/2019).

[144] *Hoval Wärmepumpen Dimensionierungshilfen*. Tech. rep. Feldmeilen, Schweiz: Hoval, 2014.

[145] SIA. *385/2 (2015): Installations d'eau chaude sanitaire dans les bâtiments - Besoins en eau chaude, exigences globales et dimensionnement*. Tech. rep. Zürich, Switzerland: Société suisse des ingénieurs et des architectes (SIA), Jan. 2015. URL: ⬏.

[146] Perch-Nielsen, Sabline et al. *Preise von Luft/Wasser Wärmepumpen - Analyse der Preise von Luft/Wasser Wärmepumpen und der Qualität ihrer Installation*. Tech. rep. Bern, Switzerland: Bundesamt für Energie (BFE), Dec. 2015. URL: ⬏ (visited on 12/20/2018).

[147] Arnold, Michael et al. *PV-Preisumfrage 2015 - Resultate*. Tech. rep. Basel, Switzerland: Energie Zukunft Schweiz, June 2016. URL: ⬏ (visited on 12/20/2018).

[148]   Duffie, John A. and Beckman, William A. "Flat-Plate Collectors". *Solar Engineering of Thermal Processes.* John Wiley & Sons, Inc., 2013, pp. 236–321. ISBN: 978-1-118-67160-3. DOI: 10.1002/9781118671603.ch6. URL: ☑.

[149]   HSR Hochschule für Technik. *SPF Institute für Solartechnik.* URL: ☑ (visited on 02/07/2019).

[150]   *Renewable Energy Cost Analysis - Hydropower.* Tech. rep. Abu Dhabi: International Renewable Energy Agency (IRENA), June 2012. URL: ☑.

[151]   *Tesla Powerwall.* URL: ☑ (visited on 03/17/2019).

Paul Stadler

Rue du Simplon 39
CH-1800 Vevey
Switzerland
📞 *+41 (0) 76 480 78 04*
✉ *paul.stadler@windowslive.ch*
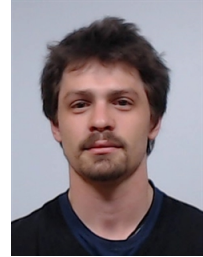
Education

2014–2019 **PhD Energy**, *École Polytechnique Fédérale de Lausanne (EPFL)*, Switzerland.
Thesis: "Model-based sizing of building energy systems with renewable sources"
Prof. François Maréchal

2009–2014 **MSc Mechanical Engineering**, *École Polytechnique Fédérale de Lausanne (EPFL)*, Switzerland, GPA 5.5/6.0.
Focus on thermal energy system and process design
Thesis: "Assessment of energy requirements of commercial and industrial facilities in Luxembourg"
Prof. François Maréchal

Experience

2014–Present **Research and teaching assistant**, *IPESE group, EPFL*, Switzerland.
Research on the integration of renewable energy sources in the national building stock
Research projects:
- NRP70 (commelec): Development of a holisitic modelling framework to optimally size distributed energy systems in buildings (W2)
- SCCER-FURIES (Swiss Competence Centre for Energy Research - Future Swiss Electrical Infrastructure): Contribution to the national assessment of multi-energy systems for the built environment

Teaching:
- Assistance to master courses: preparation of lectures and exercise sessions
- Student supervision: semester and master projects

2014 **Intern**, *CRP Henri Tudor*, Esch-sur-Alzette, Luxembourg.
Development of a national database comprising thermal energy requirements of industrial processes within the context of the luxembourgish *Optiheat* research project

Miscellaneous

2009–2014 **Sales employee**, *Alimentana-Sista Holding SA*, Vevey, Switzerland.
Customer service and stock maintenance in a local convenience store (part-time employment)

Languages

Mothertongue German
Fluent French, English   *written and spoken*

Publications

Journal articles

Paul Stadler, Araz Ashouri, and François Maréchal. Model-based optimization of distributed and renewable energy systems in buildings. *Energy and Buildings*, 120:103–113, May 2016.

Paul Stadler, Luc Girardin, Araz Ashouri, and Francois Maréchal. Contribution of model predictive control in the integration of renewable energy sources within the built environment. *Frontiers in Energy Research*, 6, 2018.

Conference proceedings

Araz Ashouri, Paul Stadler, and François Maréchal. Day-ahead promised load as alternative to real-time pricing. In *2015 IEEE International Conference on Smart Grid Communications (SmartGridComm)*, pages 551–556, November 2015.

Paul Stadler, Araz Ashouri, and François Maréchal. Distributed model predictive control of energy systems in microgrids. In *2016 Annual IEEE Systems Conference (SysCon)*, pages 1–6, April 2016.

Paul Stadler, Luc Girardin, and François Maréchal. The Swiss Potential of Model Predictive Control for Building Energy Systems. In *2017 7th IEEE PES International Conference and Exhibition on Innovative Smart Grid Technologies, Europe*, Turino, Italy, September 2017.

Raluca Suciu, Paul Stadler, Araz Ashouri, and François Maréchal. Towards energy-autonomous cities using CO2 networks and Power to Gas storage. In *Proceedings of ECOS 2016*, 2016.

Raluca Suciu, Paul Stadler, Luc Girardin, and François Maréchal. Multi-period multi-time optimisation of CO2 based district energy systems. In *Computer Aided Chemical Engineering*, volume 43 of *28 European Symposium on Computer Aided Process Engineering*, pages 1057–1062. Elsevier, January 2018.

Raluca-Ancuta Suciu, Paul Stadler, Luc Girardin, and François Maréchal. Method for the systematic integration of multi-energy networks and low carbon resources in cities. 2018.